ELIASHBERG THEORY

AND THE HIGH T_c OXIDES

By

Frank Marsiglio, B.A.Sc., M.Sc.

A Thesis

Submitted to the Faculty of Graduate Studies

in Partial Fulfilment of the Requirements

for the Degree

Doctor of Philosophy

McMaster University

March 1988

DOCTOR OF PHILOSOPHY(1987)   McMASTER UNIVERSITY
(PHYSICS)   Hamilton, Ontario

TITLE: Eliashberg theory and the high T_c oxides

AUTHOR: Frank Marsiglio; B.A.Sc. (University of Toronto)
 M.Sc. (McMaster University)

SUPERVISOR: Dr. J.P. Carbotte

NUMBER OF PAGES: viii, 188

ABSTRACT

The Eliashberg theory of superconductivity has been very successful in accounting for properties of conventional materials. The price for this success has been a lack of understanding of exactly what features of the input parameters affect the superconducting properties in significant ways. The first part of this thesis is concerned with the identification of an important parameter in the study of thermodynamic, critical magnetic field, and electromagnetic properties of a superconductor. The Bardeen-Cooper-Schreiffer (BCS) theory of superconductivity produces laws of corresponding states, i.e., various properties are predicted to have universal values. We have studied the deviations from BCS theory due to retardation effects, which are embodied in Eliashberg theory. These deviations, or corrections to BCS, can be well understood and characterized by a single simple parameter, $T_c/\omega_{\ln}$, to be defined later. Attention has been focussed on reproducing numerical (theoretical) results, since for most conventional superconducting materials, experiment agrees with theory at the 10% level.

The second half of the thesis has been largely motivated by the recent discoveries of the high-T_c oxide materials. We have applied Eliashberg theory almost entirely in an inverse manner. That is, with little knowledge of the microscopic parameters for these new materials, we have investigated the relationships between various macroscopically observable properties, based on model spectra. The model spectra have been of three general types, the conventional category, spectra based on a combined phonon-exciton mechanism, and thirdly those based on relatively low frequency exchange bosons. We have called this latter category the very strong coupling regime. It was

hoped that measured properties could uniquely specify the type of spectrum responsible for the superconductivity in the high-T_c oxides. At this point in time this goal has not really been achieved. Too many uncertainties exist in the experimental properties, a situation which has been aggravated by a lack of single crystal data. Moreover, various kinds of measurements on the same property often give very different results. At the same time the theory needs to be improved upon. For example, anisotropy ought to be incorporated into our results, since the single crystals are displaying large anisotropies. Nonetheless, some interesting signatures for the various spectral regimes have been obtained, and these are presented in the latter half of the thesis.

ACKNOWLEDGEMENTS

I wish to thank the pleasant secretarial staff, Devi Symons, Jackie Collin, Jane Hammingh, Sandy Raiser, and Helen Kennelly for their assistance. Sadly, Helen passed away this past year.

I found conversations with the faculty members stimulating, and in particular, Rajat Bhaduri has helped maintain my interest in high energy physics, through his enthusiasm. I have also benefitted from discussions with Tom Timusk, especially this past year, in high-T_c work.

Many students and post-doctoral fellows have been much appreciated. Doug Bonn, Bruce Gaulin, Karen Hughes, and Margaret St. Peters have often provided interesting discussions. Walter Stephan, Mike Coombes and Jeff Blezius were helpful in my progress. Jeff and Mike also wrote programs which were used in this thesis. More recently, Richard Akis and Peter Williams have been very helpful. Much of the work on the high-T_c oxides has been done in collaboration with Richard, and Peter has helped in many ways, one of which was a suggestion which led to the calculations in Appendix E. Past students, Johanna Daams and Boža Mitrović, wrote many of the programs which have been used in this thesis. Ewald Schachinger has also contributed in this regard. Ewald's visits have always been stimulating and fruitful in collaborative efforts. Finally a very enjoyable journey with Michael Schossmann through the complex plane resulted in the latter half of Appendix A, and he has also helped in many other ways.

I wish to thank my two office mates, Derek Leinweber and Elisabeth Nicol, who have made the past several years very pleasant for me. Derek has been helpful with computers, and in particular gave me a nice curve fitting program to help out in Chapter 2. Elisabeth has been most helpful with regard to discussions, and many fine points were ironed out over lengthy conversations. She is also largely responsible for the final look of this thesis, and has helped in the proofreading. I also wish to thank Ray Nogami, who typed the bulk of the thesis.

The high-T_c work has also benefitted from correspondence with Werner Weber, who graciously supplied several spectral functions for us to work with, and Steve Kivelson, who helped me understand the asymptotic limit results.

Jules Carbotte has been fantastic as a supervisor and friend. All of the work of this thesis has been done in collaboration with him, and many a time his enthusiasm and ideas have been very helpful to my progress.

Finally, I wish to thank my parents, my wife, Mary, my children, Michael and Julia, and our Lord, for having helped me all along the way.

Table of Contents

Chapter 1

Introduction

The phenomenon of superconductivity has recently re-emerged as a topic of intense interest following the initial discovery of a "high-T_c" material by Bednorz and Müller,[1] early in 1986. Within a year, subsequent discoveries followed,[2,3,4,5] and by February, 1987, T_c, the critical temperature at which a material begins to superconduct, had attained values close to 100 K. Since then, reports and rumours have abounded, with claims of $T_c \approx 155 K$,[6] 240 K,[7,8,9] and room temperature.[10] The past year has seen intense efforts worldwide in an attempt to both produce materials with even higher T_c, and to understand the mechanism at play in these new materials. Innumerable theories[11] have been advanced in efforts to explain both the normal state and superconducting state properties in these oxides, although success has been hampered on the one hand by lack of sophistication in these theories, and on the other hand by the presence of conflicting experimental data. Added to this is the nuisance that most experiments up to the time of this writing

have been performed on polycrystalline samples of varying quality, and this fact has also contributed to the confusion present. At the time of this writing, single crystals have been grown, and experiments are being redone. It is already clear, for example, that the 90 K material, $YBa_2Cu_3O_{7-y}$, is quasi-two-dimensional. (The "y" in the material formula indicates that the number of oxygen atoms present is slightly less than 7.)

As far as conventional materials are concerned, the microscopic theory of superconductivity, discovered by Bardeen, Cooper, and Schrieffer[12] (BCS) in 1957, describes quite well the features of the superconducting state. The BCS theory recognized that electrons were attracted to one another through the exchange of phonons, and in the presence of this attraction, which they modelled through a potential, the energy of the normal state could be lowered by requiring the electrons in the Fermi sea to "condense" into a new state. Physically, the origin of this attraction can be seen most simply from a real space picture (although it should be emphasized that the pairing occurs in momentum space). Fig. 1.1 shows an electron propagating through a lattice of ions. The ions in the immediate vicinity of the electron are polarized (due to simple Coulomb forces). Moreover, the time scale on which the electron moves is roughly determined by the Fermi velocity, v_F, whereas, the time scale for the ion is determined by the speed of sound. The Bohm-Staver[13] relation illustrates that the latter is typically a percent of the former. Hence, a region of positive enhanced charge remains long after the electron has moved on, and serves as an attractive center for a second electron. The dynamics of this interaction was mimicked to a small extent by an attractive potential which acted on electrons whose energies were within $\hbar\omega_D$ (a typical phonon energy) of the Fermi surface. More precisely, it is the

quasiparticles of Landau's theory of the normal Fermi liquid which undergo condensation. These quasiparticles were considered to already include, for example, small correlation effects which were present in the normal state. These effects, which can be quite large with respect to the attractive effects discussed above, were assumed to undergo no change as the material became superconducting. Hence, the subtle difference between the two states was deemed to lie in the pairing correlations that arise from phonon exchange. Moreover, the Landau picture assumes that the inverse life-time of the quasiparticles is much smaller than the energy of the quasiparticle, so that a one-to-one correspondence with the free electron gas excitation spectrum is maintained.

BCS theory enjoyed remarkable success, as far as a qualitative description of the superconducting state was concerned. However, it became clear that quantitative discrepancies with experimental results existed, especially for the "bad actors"[14], Pb and Hg. In the meantime, Eliashberg[15] had extended Migdal's[16] earlier work on the normal state electron-phonon interaction to the superconducting state. In both these works a formal Green's function approach[17,18] was employed; the electron self-energy in the superconducting state is calculated by summing an infinite set of diagrams arising from the electron-phonon interaction. These are illustrated in Fig. 1.2. Proper accounts of the retarded nature of the interacton is considered through use of phonon propagators, although the phonon self-energy is generally not calculated from first principles. Rather, the phonon spectral function is taken from experiment. The important function in Eliashberg theory is, however, $\alpha^2 F(\omega)$, which can either be calculated from first principles (after fitting the phonon spectral function

Figure 1.1   An electron propagates through a lattice of ions and polarizes
the ions around it. This results in a net positive region of space (the original
electron has long since departed from the vicinity) to which a second electron
is attracted. The net effect is a phonon-induced electron-electron attraction.
(Note that this is a real space picture and hence not to be taken too literally.)
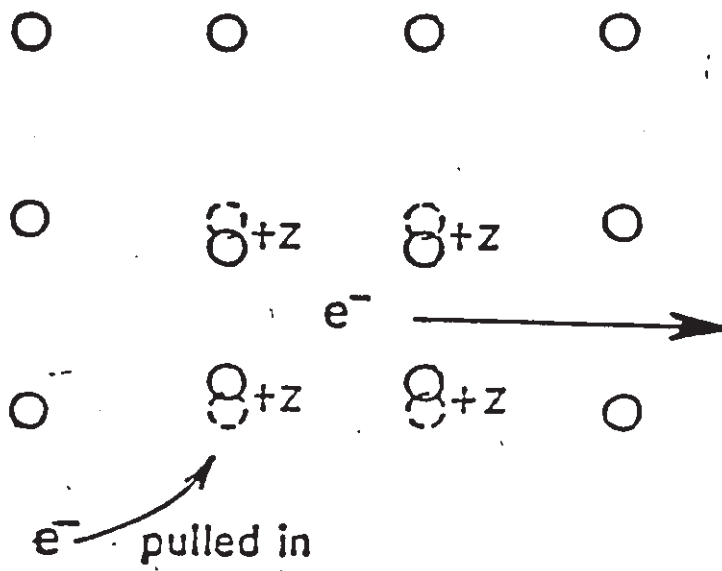
to experiment) or measured in tunneling experiments, as will be described later. In principle, $\alpha^2 F(\omega)$ is also dependent on the wavevectors of the electrons engaged in the exchange of a phonon, although this dependence is usually weak and has been ignored in the remainder of this thesis. Sophisticated arguments to justify this procedure in the case of phonon exchange have been given in an excellent review by Allen and Mitrović.[19]

A direct Coulomb interaction between electrons will lead to a repulsion which will tend to offset the phonon mediated attraction to some extent. This interaction is practically instantaneous, and fortunately can be modelled fairly well by use of a single parameter, μ^*. This parameter is often treated phenomenologically as it is difficult to calculate. Coulomb interactions also enter through screening processes, but are incorporated into the theory either through use of experimental results (for $\alpha^2 F(\omega)$) in which they are already contained, or through band structure calculations.

The important point of the preceding paragraphs is that the microsopic parameters which enter into the simplest theory of Eliashberg are $\alpha^2 F(\omega)$ and μ^*. We will not discuss further origins of the theory as excellent reviews exist on this subject.[19-22] Later the basic equations will simply be utilized. Unfortunately the equations require numerical solutions. This would not be so unmanageable except that the independent variables are effectively infinite in number. In practice $\alpha^2 F(\omega)$ is described by a number of bins (say ~ 100), but this number of variables is still too large. The systematics of what does matter can be understood a little more clearly in one of two ways.

One approach is to identify some parameter which will in general be a functional of $\alpha^2 F(\omega)$, which contains the essence of why one $\alpha^2 F(\omega)$ is

Figure 1.2   Schematic illustration of the electron self-energy due to vir-
tual phonon exchange. The double line indicates that the fully renormalized
Green's function is to be used; the single line is the normal state one electron
Green's function. The self-energy is used to calculate the former and hence
the problem is a self-consistent one. Note that phonon (wavy) lines never
cross one another – these diagrams would correspond to vertex corrections
and are small as is assured by Migdal's theorem.
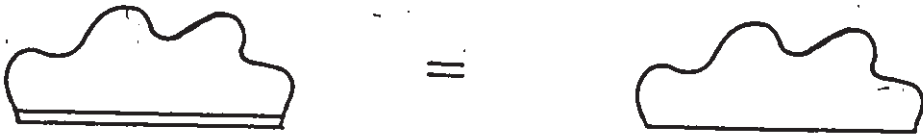
different from another, and then study various superconducting properties as a function of this parameter. This has long been the goal of many theorists in the field of superconductivity, more in the context of a T_c-equation, in terms of some parameter, usually the mass-renormalization parameter, $\lambda (\equiv \int_0^\infty \frac{2}{\nu} \alpha^2 F(\nu) \, d\nu)$. We concentrate instead on properties which are given by numbers within BCS theory, such as $\frac{2\Delta_0}{k_B T_c}$ (twice the ratio of the gap edge to the critical temperature). This has an advantage in that one can use a strong-coupling parameter which is zero in the BCS limit, and expand any unknown in terms of this parameter. These kinds of calculations will be described in Chapter 2.

Another approach follows the standard procedure that one carries out when faced with a complicated function: take a derivative. Let us write $\alpha^2 F(\omega) \equiv \frac{1}{N} \sum_{i=1}^{N} a_i \delta(\omega - \omega_i)$. Here N is some large number such that the function is well represented. The index i enumerates the bins and ω_i the bin frequencies, in monotonically increasing order, and the a_i represent the coupling strength at each frequency ω_i. The a_i represent the independent variables in the theory, so that, for example, $T_c = f(a_1, a_2, \ldots, a_N)$. The quantities of interest then become the partial derviatives, $\frac{\partial T_c}{\partial a_i}$, $i = 1, \ldots, N$. The partial derivatives are more useful than the total derivative, since it is useful to ask how T_c changes when the coupling to the phonons at one particular frequency is increased. The more elegant mathematical representation of this compilation of partial derivatives is the functional derivative, which is defined

$$\frac{\delta Q}{\delta \alpha^2 F(\Omega)} = \lim_{\epsilon \to 0} \frac{Q\left[\alpha^2 F(\omega) + \epsilon \delta(\omega - \Omega)\right] - Q\left[\alpha^2 F(\omega)\right]}{\epsilon} \qquad (1.1)$$

where Q is any property that is a functional (denoted by square brackets) of $\alpha^2 F(\omega)$. Note that (i) the derivative is a function of Ω, the frequency at which

the coupling has been perturbed, and (ii) the dimensions of the derivative are $[Q/\Omega]$, and not simply $[Q]$. It will be seen also in Chapter 2 that the functional derivative can yield very useful information about a particular property.

Chapter 2 deals mainly with properties of superconductors for conventional materials. The recent discoveries of high-T_c materials now raise the questions; (1) can these materials be described simply according to the results of Chapter 2, (2) if not, can they be described within Eliashberg theory at all, and (3) if the phonon mechanism fails, is it possible to describe them with the Eliashberg-BCS framework using perhaps an alternative mechanism? These questions can be answered in part, as will be seen in Chapter 3. Unfortunately, however, there are limitations to the conclusions one can present. Modifications of the theory to incorporate various effects such as anisotropy and strong energy dependence are possible but have been ignored in this thesis. These modifications have been investigated previously, though not in the context of these new materials. The other limitation arises from the discrepancies and uncertainties which exist in the experimental literature at the present time. Single crystal data may improve upon this situation in the future.

A summary is provided in Chapter 4.

Five appendices are included. The first describes an exact procedure for analytic continuation of the gap function. The second outlines the derivations used in obtaining strong coupling corrections. The third lists sources of spectral functions used in Table 1 and in the figures in Chapter 2. The fourth briefly describes the functional derivative of the specific heat jump, and the final appendix illustrates a method for solving asymptotic limits.

Chapter 2

Strong Coupling Effects

2.1 SUPERCONDUCTING PARAMETERS

The Eliashberg equations have generally been found to be accurate at the 10% level[23,24] for most conventional superconductors. There is no question that for this class of superconductors, some of whose elements are listed in Table 1, Eliashberg theory is a valid and accurate description. It is not the point of this chapter to improve on this theory. Rather we would like to improve a feature of the theory, namely that it is entirely numerical. One generally overcomes this difficulty by solving everything analytically, but this is easier said than done. The Eliashberg equations are complicated and non-linear and thus far have not been solved even in linear form, and even for the simplest model spectrum, $\alpha^2 F(\nu) = A\delta(\nu - \nu_E)$. (Wu[25] and coworkers have actually obtained an exact series solution for T_c, provided that $\lambda > \Lambda$, where Λ is a material dependent parameter; however, the solution suffers from the fact

that the coefficients require numerical evaluation for a practical calculation.) Approximate solutions for T_c and other superconducting properties abound in the literature. These share the common feature that one or two simple functionals of $\alpha^2 F(\nu)$ are deemed to be important and approximate solutions are found which depend only on these functionals. Some of the most widely used functionals are, for example,

$$\lambda \equiv 2 \int_0^\infty \frac{d\nu}{\nu} \alpha^2 F(\nu) \, , \tag{2.1}$$

$$\langle \omega^n \rangle \equiv \frac{2}{\lambda} \int_0^\infty \frac{d\nu}{\nu} \alpha^2 F(\nu) \nu^n \, , \tag{2.2}$$

$$\omega_{\ln} \equiv \exp\left\{ \frac{2}{\lambda} \int_0^\infty \frac{d\nu}{\nu} \alpha^2 F(\nu) \ln \nu \right\} \, , \tag{2.3}$$

$$A = \int_0^\infty d\nu \, \alpha^2 F(\nu) \, . \tag{2.4}$$

It has become standard practice in the literature to weight averages with $\frac{2}{\lambda\nu}$. This has the advantage that averages are then automatically renormalized since

$$\int_0^\infty d\nu \, \frac{2}{\lambda\nu} \alpha^2 F(\nu) = 1 \, . \tag{2.5}$$

Equation (2.3) defines the Allen-Dynes[26] parameter $\omega_{\ln}$, which will be used extensively in this chapter. Eq. (2.4) defines the area under $\alpha^2 F(\nu)$ which gives a measure of the strength of the electron-phonon interaction. If the coupling was absent only the phonon spectral distribution, $F(\nu)$, would remain and the resulting integral is normalized to the number of phonon modes in the system. One more functional should be mentioned as well, the first moment of $\alpha^2 F(\nu)$:

$$\bar{\omega} \equiv \frac{\lambda \langle \omega^2 \rangle}{2} = \int_0^\infty d\nu \, \alpha^2 F(\nu) \nu \, . \tag{2.6}$$

The importance of this parameter is seen from the definition of $\alpha^2 F(\nu)$:[21]

$$\alpha^2 F(\nu) = N(0) \sum_\sigma \int \frac{d\Omega_k}{4\pi} \int \frac{d\Omega_{k'}}{4\pi} \left| g(\vec{k}, \vec{k}'; \sigma) \right|^2 \delta(\nu - \omega(\vec{q}, \sigma)) , \qquad (2.7)$$

where

$$g(\vec{k}, \vec{k}'; \sigma) \equiv -i\vec{\epsilon}(\vec{q}, \sigma) \cdot (\vec{k}' - \vec{k}) \left[\frac{1}{2MN\omega(\vec{q}, \sigma)} \right]^{1/2} V(\vec{k}' - \vec{k}) , \qquad (2.8)$$

in the case of plane waves. We have used $\hbar \equiv 1$ and will use $k_B \equiv 1$ for the remainder of this thesis. Here, $\vec{k} - \vec{k}' = \pm \vec{q} + \vec{G}$, where $\vec{G}$ is a reciprocal lattice vector, $\vec{k}$ ($\vec{k}'$) is the initial (final) momentum of the electron, and $\vec{q}$ is the phonon wave vector. N is the total number of ions, M the mass of the ions, and $\vec{\epsilon}(\vec{q}, \sigma)$ is the polarization unit vector of the mode $(\vec{q}, \sigma)$. In Eq. (2.7) $N(0)$ is the single spin density of electron states at the Fermi surface. σ is the phonon branch index. Finally, $V(\vec{k}' - \vec{k})$ is the Fourier transform of the effective potential of a single ion seen by an electron. Fig. 2.1 illustrates the process encompassed in Eqs. (2.7–2.8) diagrammatically. An electron with wave vector $\vec{k}$ emits a virtual phonon with wave vector $\vec{q}$ and branch index σ and scatters off with wave vector $\vec{k}'$. The coupling strength of this process is given by $g(\vec{k}, \vec{k}'; \sigma)$. A similar virtual absorption occurs on the other side. Hence $g(\vec{k}, \vec{k}'; \sigma)$ occurs twice in Eq. (2.7), and is the reason for the notation $\alpha^2 F(\nu)$, sometimes written $\alpha^2(\nu) F(\nu)$.

What is clear from Eqs. (2.6–2.8) is that $\bar{\omega}$ is independent of the phonon spectrum. Without knowing how hard or soft the spectrum is, $\bar{\omega}$ gives an indication of the strength of the electron-ion potential. Even more useful in this regard is the McMillan-Hopfield parameter,[21] $\eta \equiv 2M\bar{\omega}$, which removes the ion mass dependence as well. Note that $\bar{\omega}$ is not an average phonon frequency, as it has units of [energy]^2.

Figure 2.1   Virtual exchange of a phonon between two electron states. See text for explanation.
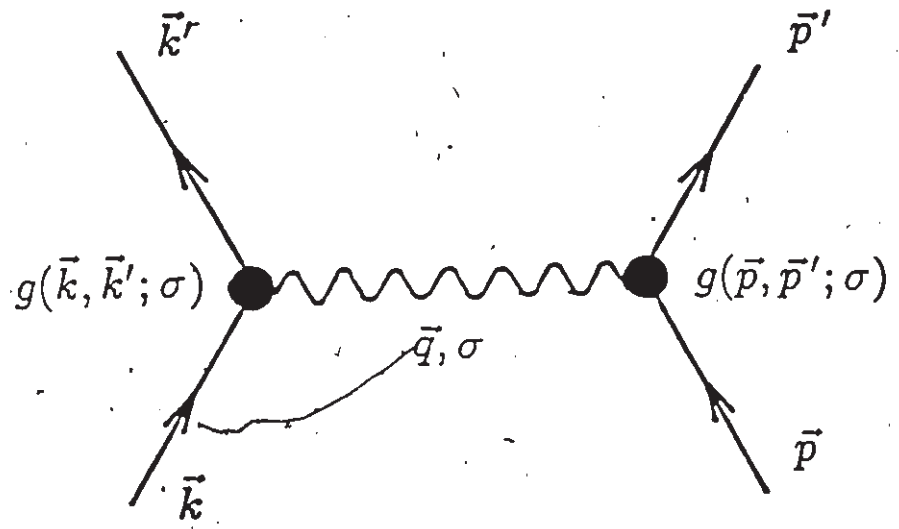
Clearly, a vast number of parameters are available for use in describing macroscopic superconducting properties. Which parameter(s) is (are) most useful? There is no definitive answer to this question; however, in this thesis we will describe two approaches to a solution of this problem. In the first, a strong coupling parameter,[24] T_c/ω_{ln}, is identified, and formulas for various properties, such as the gap ratio, $\frac{2\Delta_0}{k_B T_c}$ (to be defined later), are derived in terms of this parameter. In the end, two constants are fitted to numerical data. The success of this approach is demonstrated by the fact that a simple formula does indeed describe the trend for $\frac{2\Delta_0}{k_B T_c}$ (and other properties) for many materials as a function of T_c/ω_{ln}, regardless of the shape of their spectral functions, $\alpha^2 F(\nu)$, and their values of μ^*. Thus, $\frac{2\Delta_0}{k_B T_c}$ is an almost universal function of T_c/ω_{ln}.

The second approach focuses on lower and upper limits for superconducting properties imposed by Eliashberg theory itself. The critical temperature, T_c , is the obvious property to study in this respect. Allen and Dynes[26] made it clear that Eliashberg theory imposes no limitations on T_c; the limitations exist on the microscopic functions which enter Eliashberg theory. However limitations may exist when T_c is referenced to a microscopic parameter (with dimensions of energy, of course). Allen and Dynes discovered the limitation,

$$\frac{T_c}{\bar{\omega}^{1/2}} \le 0.258 \; . \tag{2.9}$$

This is useful because the electron-phonon interaction strength cannot physically exceed a certain value so that Eq. (2.9) is a limitation on T_c . The equality occurs in the limit that the phonon frequencies go to zero ($\lambda \to \infty$).

Leavens[27] derived the result,

$$\frac{T_c}{A} \leq 0.231 \tag{2.10}$$

Here the equality occurs for $\lambda = 1.14$, a much more physical regime. A little later, Leavens[28] was able to derive what the most useful parameter for T_c was, from amongst the infinite parameters:

$$\omega(n) \equiv \left[\frac{\lambda}{2}\langle\omega^{n+1}\rangle\right]^{1/_{n+1}} . \tag{2.11}$$

It turned out that most were useless, that is, inequalities of the form $\frac{T_c}{\omega(n)} < \infty$ were derived. However, for $\lambda \leq 2.5$ (the conventional regime), Eq. (2.10) imposed a more severe limitation than Eq. (2.9). For large λ, the opposite is true. Moreover, it still remains that the parameter λ itself is useful when λ is small, i.e., in the weak coupling regime. This is true in spite of the fact that T_c can be shown to be independent of λ.[26] These results are true for $\mu^* = 0$, and are readily generalized for non-zero μ^*. The fact that Eq. (2.10) holds in the physical regime is motivation to seek a simple T_c equation. Indeed, Leavens and Carbotte[29] had (earlier) found the semiempirical formula

$$T_c \doteq 0.148\,A \qquad 1.2 \leq \lambda \leq 2.5 , \quad 0.1 \leq \mu^* \leq 0.15 , \tag{2.12}$$

gave quite accurate values of T_c. Since $T_c \leq (0.16 - 0.176)\,A$ [28] for this regime of μ^*, it can be noted that in nature materials with a given area under $\alpha^2 F(\nu)$ achieve near optimum values of T_c.

2.2 STRONG COUPLING CORRECTIONS
(i) Introduction

The result of a BCS-type analysis[12] was that many superconducting properties were described by universal constants. Amongst these, for example, are $\frac{2\Delta_0}{k_B T_c}$, where Δ_0 is the zero-temperature gap edge defined as the energy above which the quasiparticle density of states, $N(\omega)$, is non-zero; the normalized specific heat jump, $\frac{\Delta C(T_c)}{\gamma_0 T_c}$, where $\Delta C(T_c) \equiv -\frac{T d^2 \Delta F}{dT^2}\Big|_{T_c}$ is the specific heat jump which occurs at T_c, and $\gamma_0 \equiv \frac{2}{3}\pi^2 N(0)(1+\lambda)$ is the Sommerfeld constant. For T_c small compared to a typical phonon frequency, $\gamma_0 T_c$ is the normal state specific heat. Otherwise, there are corrections (beyond the $(1+\lambda)$ renormalization) due to the electron-phonon interaction. The reduced critical magnetic field is $h_c(0) \equiv \frac{H_c(0)}{T_c |H_c'(T_c)|}$, where $H_c(T)$ is the critical magnetic field above which superconductivity is destroyed for type I superconductors. Many superconductors are type II, the difference being that a perfect Meissner-Ochsenfeld effect (perfect diamagnetism or flux expulsion) occurs only up to an applied field, H_{c1}, beyond which a mixed state occurs in which flux penetrates the material in filaments. This continues to occur up to an upper critical field, $H_{c2}(T)$, beyond which the superconductivity is destroyed. We will present results involving the upper critical field as well as electromagnetic properties.

It is of interest to know what the effect of strong coupling is on the values of these superconducting ratios. Strong coupling is perhaps somewhat of a misnomer, that we will continue to use nonetheless. The term "strong coupling" can be used within BCS theory for the case that $N(0)V$ (V is the model potential uesd by BCS: $N(0)V \approx \lambda - \mu^*$) is not small (weak coupling).

These kinds of corrections to weak coupling BCS theory have been investigated by Swihart,[30] for example. It was found that in the limit $N(0)V \to \infty$, $\frac{2\Delta_0}{k_B T_c} = 4$, and no higher. Also investigated were various nonseparable forms for the attractive (and repulsive) potential which presumably included some retardation effects. These latter effects are fully incorporated into Eliashberg theory. Also included, however, are lifetime effects due to damping from phonon emission. We will not present a derivation of these equations here; excellent reviews[19,20] already exist for this purpose. The equations are:[31]

$$\Delta(i\omega_n)Z(i\omega_n) = \pi T \sum_{m=-\infty}^{\infty} \left[\lambda(i\omega_n - i\omega_n) - \mu^*(\omega_c)\theta(\omega_c - |\omega_m|)\right] \frac{\Delta(i\omega_m)}{\sqrt{\omega_m^2 + \Delta^2(i\omega_m)}}$$

(2.13)

and

$$Z(i\omega_n) = 1 + \frac{\pi T}{\omega_n} \sum_{m=-\infty}^{\infty} \lambda(i\omega_m - i\omega_n) \frac{\omega_m}{\sqrt{\omega_m^2 + \Delta^2(i\omega_m)}} .$$

(2.14)

The $\Delta(i\omega_n)$ are the Matsubara gaps defined at the Matsubara frequencies, $i\omega_n \equiv i\pi T(2n-1)$, $n = 0, \pm 1, \pm 2, \ldots$, Similarly, $Z(i\omega_n)$ are the renormalization factors. The electron-phonon spectral density, $\alpha^2 F(\nu)$, appears through the relation,

$$\lambda(z) \equiv \int_0^{\infty} \frac{2\nu \, d\nu \, \alpha^2 F(\nu)}{\nu^2 - z^2}$$

(2.15)

and $\mu^*(\omega_c)$ is the Coulomb pseudopotential with cutoff ω_c. The value of this cutoff is typically 5–10 times the maximum phonon frequency. Physically, the cutoff for the Coulomb interaction should be of order the Fermi energy, E_F, but as Morel and Anderson[32] first showed, this cutoff can be scaled down to ω_c, with a result that the potential is renormalized:

$$\mu^*(\omega_c) = \frac{\mu(E_F)}{1 + \mu(E_F)\ln(\frac{E_F}{\omega_c})} .$$

(2.16)

These equations have been written in the isotropic limit, often referred to as the "dirty" limit. This latter name is perhaps not so appropriate; when impurities are introduced into a material the anisotropy that is present will be washed out so that the isotropic equations are applicable. This assumes, however, that the "dirt" effects are incorporated into the spectral function; otherwise corrections to the equations in order to account for the impurities are required. However, T_c , the gaps, and for example the free energy difference remain unaffected. Electromagnetic properties and upper critical fields do depend on impurity concentration. Eqs. (2.13–2.14) are the Eliashberg equations written on the imaginary axis. Most of the computations in this thesis were done using this formulation. Note that all quantities involved are real, and simple summations are required for iteration. This will contrast remarkably with the "real axis" Eliashberg equations, about which we will have more to say later.

The disadvantage of the imaginary axis formulation is that the terms in the equations do not represent physical quantities. Generally, an analytic continuation to the real axis is required for this purpose. Although the quantities in Eqs. (2.13–2.14) are all real, upon analytic continuation the gap attains an imaginary part and lifetime effects become somewhat more apparent. The retardation effects can be seen through Eq. (2.15). Note that if a typical phonon frequency satisfies $\nu \gg \nu_m$, where $i\nu_m \equiv i2\pi T m$ is a Matsubara boson frequency, for values of "m" which are relevant to superconductivity through Eq. (2.13), then a good approximation would be $\lambda(i\nu_m) \approx \lambda(0)$ defined in Eq. (2.1). A cutoff is also required for convergence. This is the "renormalized BCS" approximation often referred to as the $\lambda^{\theta\theta}$ model.[19] Retardation effects have been disregarded to the extent that the frequency (and hence response

time) of the phonon is considered high compared to superconductivity energy scales. Note that retardation is subtly included through the required cutoff, however; *i.e.*, the response is not instantaneous. Upon evaluating Eq. (2.14) (with care — see, for example, Ref. 33) one obtains $Z_n (\equiv Z(i\omega_n)) \approx 1 + \lambda$ which is simply the zero temperature mass renormalization. Eq. (2.14) then, which exists even in the normal state, describes the renormalization of the electron propagator due to the electron-phonon interaction. The renormalization is affected slightly by the fact that the electrons are not in the normal state, *i.e.*, the order parameter $(\Delta_n \equiv \Delta(i\omega_n))$ is non-zero. A non-trivial solution to Eq. (2.13), (it is coupled to Eq. (2.14)), gives the superconducting order parameters, Δ_n. This equation can be looked upon as describing an "anomalous renormalization" of the electrons, one which changes their state from normal to superconducting. Applications of the $\lambda^{\theta\theta}$ model show that the order parameter is independent of the Matsubara frequency (except for a cutoff). Eq. (2.13) becomes:

$$\frac{1+\lambda}{\lambda - \mu^*} = \pi T \sum_{m=-N_c+1}^{N_c} \frac{1}{\sqrt{\omega_m^2 + \Delta_0^2(T)}} \quad (2.17)$$

Here $\Delta_0(T)$ is the gap or order parameter (since analytic continuation of a constant is a constant), which remains a function of temperature. The T_c equation is defined by linearization of Eq. (2.17); the zero-temperature gap is defined through the prescription[17] for $T \to 0$:

$$\omega_m \to \omega \qquad \pi T \sum_m \to \int \frac{d\omega}{2} \, . \quad (2.18)$$

The cutoff N_c is given by $N_c = \left[\frac{\omega_c}{2\pi T} + \frac{1}{2}\right]$, where the square brackets indicate "nearest integer". These sums and integrals can be easily performed, with

the result that:

$$T_c = 1.13\,\omega_c \exp\left(-\frac{1+\lambda}{\lambda - \mu^*}\right) \tag{2.19a}$$

$$\Delta_0 = 2\,\omega_c \exp\left(-\frac{1+\lambda}{\lambda - \mu^*}\right) \tag{2.19b}$$

An obvious consequence is

$$\frac{2\Delta_0}{k_B T_c} = 3.53 . \tag{2.20}$$

Note that both T_c and Δ_0 give a measure of the strength of the superconductivity in the material. Also note that the expressions for T_c and Δ_0 are nonanalytic in λ at $\lambda = 0$. This illustrates that no finite perturbation theory could have produced these results; an infinite sum of Feynman diagrams is required. The cutoff frequency occurs as a prefactor in both expressions. It is generally of order the Debye frequency of a material, and serves to set the energy scale for the superconducting parameters, T_c and Δ_0.

Eq. (2.20) was one of the first predictions[12] of BCS theory. Measurements[34] on Al and Sn provided experimental verification of this prediction. However, it became readily apparent that several superconductors had gap ratios that exceeded 3.53 by 30 % or more. Pb ang Hg were prominent in this respect, and became known as "bad actors"[14] This disagreement remained unresolved until full strong coupling predictions were provided[35] for Pb. Similar statements can be made for other properties: $\frac{\Delta C}{\gamma_0 T_c} = 1.43$, $h_c(0) = 0.576$, $\frac{\gamma_0 T_c^2}{H_c^2(0)} = 0.168$ all give universal "BCS constants" for some thermodynamic properties. Additional constants will be given for critical magnetic field and electromagnetic properties as we go along.

(ii) Thermodynamic Properties

Geilikman and Kresin[36] first derived an approximate expression for $\frac{2\Delta_0}{k_B T_c}$ of the form

$$\frac{2\Delta_0}{k_B T_c} = 3.53\left[1 + 5.3\left(\frac{T_c}{\tilde{\omega}}\right)^2 \ln\left(\frac{\tilde{\omega}}{T_c}\right)\right] \tag{2.21}$$

in which $\tilde{\omega}$ is some phonon energy which is not sharply specified in the theory and remains uncertain. The approximations used were to some extent uncontrolled so that the range of validity of Eq. (2.21) is not known.

Mitrović et al.,[24] using an entirely different approach, presented a new derivation of an expression similar in form to Eq. (2.21), starting from the real axis equations (see Appendix A). They included strong coupling corrections in the Z-channel (Eq. (A3)), but omitted contributions from the Δ-channel (Eq. (A2)). The result was a formula, similar to Eq. (2.21):

$$\frac{2\Delta_0}{k_B T_c} = 3.53\left[1 + \alpha\left(\frac{\Delta_0}{\bar{\Omega}}\right)^2 \ln\left(\frac{\bar{\Omega}}{\Delta_0 \beta}\right)\right] \tag{2.22}$$

Here $\bar{\Omega}$ is some suitably defined average phonon frequency. Mitrović et al.[24] made the choice $\bar{\Omega} = \omega_{\ln}$. α and β are constants which they determined semi-phenomenologically from numerical solutions to the Eliashberg equations, for many known superconductors. Efficient solution was possible by solving on the imaginary axis, and analytically continuing to the real axis by use of Padé approximants, a technique first described by Vidberg and Serene.[37] The gap edge is defined by:

$$\text{Re}\Delta(\omega = \Delta_0) = \Delta_0 \ . \tag{2.23}$$

At zero temperature, this definition coincides with the qualitative definition given earlier, i.e., the energy above which $N(\omega)$ is non-zero. This method of solution is reviewed in Appendix A, along with an exact method used for

extracting more detailed information than the gap edge. The final equation is given by Eq. 23 of Ref. 24:

$$\frac{2\Delta_0}{k_B T_c} = 3.53\left(1 + 12.5\left(\frac{T_c}{\omega_{\ln}}\right)^2 \ln\frac{\omega_{\ln}}{2T_c}\right) .$$

(2.24)

These Geilikman-Kresin[36,38] type formulas were derived in a subsequent paper[39] for various thermodynamic ratios. We should also note that in the Russian literature, the original work[36] was followed up by Masharov[40] and Kresin and Parkhomenko,[41] in discussing thermodynamic and critical magnetic field properties.

As our starting point, we used the Eliashberg equations on the imaginary axis, given in Eqs. (2.13) and (2.14). We ignore μ^* from the start. (It can be kept, as in Ref. 39, and retained as an extra parameter; however the benefits are minimal, at the cost of an extra parameter. Note, moreover, that in the strong coupling parameter, $T_c/\omega_{\ln}$, the T_c is to be regarded as coming from experiment. It contains, therefore, some effect of μ^* already.) The model we use is a step-function approximation on the imaginary axis:

$$\Delta(\omega_n) = \begin{cases} \Delta_0(T) & |\omega_n| < \omega_0 \\ 0 & |\omega_n| > \omega_0 \end{cases}$$

(2.25a)

$$Z(\omega_n) = \begin{cases} Z_0(T) & |\omega_n| < \omega_0 \\ 1 & |\omega_n| > \omega_0 \end{cases}$$

(2.25b)

Here, ω_0 represents roughly a few times the maximum phonon frequency in the system. Note that, for self-consistency we would require $\lambda(i\omega_n - i\omega_m)$ to be independent of n. This would reduce to the $\lambda^{\theta\theta}$ approximation. Instead, we evaluate Eqs. (2.13) and (2.14) at $n = 1$. Thus, Δ_1 is the constant gap in Eq. (2.25a). The procedure is outlined in Appendix B. Essential to the approximations used is the requirement, $\frac{T_c}{\omega_{\ln}} \ll 1$. We have also assumed that ω_0 is sufficiently large that $\frac{\omega_n}{\omega_0} \ll 1$. Expansions near T_c and at $T = 0$

are required. In order to calculate thermodynamic properties, the Bardeen-Stephen[42] formula for the free energy difference $(F_S - F_N)$ is required:

$$\frac{\Delta F}{N(0)} = -\pi T \sum_{m=-\infty}^{\infty} \left[\sqrt{\omega_n^2 + \Delta_n^2} - |\omega_n| \right] \left[Z_S(n) - Z_N(n) \frac{\omega_n}{\sqrt{\omega_n^2 + \Delta_n^2}} \right] \qquad (2.26)$$

Technical Remarks Regarding Table 1:

1) References for the spectra used can be found in Appendix C.

2) T_c is defined. A value for μ^* is then calculated with a cutoff of 6 times the maximum phonon frequency in the spectrum. Two values are obtained depending on whether the Z-channel is summed exactly ($H_{c2}(T)$ calculations) or summed approximately (thermodynamic calculations). This discrepancy has since been removed; the changes in the calculated properties are no more than $\sim 1\%$.

3) We have investigated the dependence of properties on the T_c value used. It is very weak.

4) Note that:

$$h_c(0) = \left(4\pi \, \frac{\gamma T_c^2}{H_c^2(0)} \, \frac{\Delta C(T_c)}{\gamma_o T_c} \right)^{-1/2} .$$

5) Extrapolated values near T_c were obtained through fits to cubic polynomials. Values for $T = 0$ were obtained from $t = 0.1$ values *for properties which behave exponentially at low temperatures, e.g. the gap edge*. Otherwise they were obtained from quadratic fits, *e.g.* $H_c(0)$.

6) Note that $y_i(T) = \lambda_i^{-2}(T)$. Also

$$\frac{y_L(0)}{T_c \, | \, y_L'(T_c) \, |} = \frac{\xi(0)}{\xi(T_c)} \frac{y_l(0)}{T_c \, | \, y_l'(T_c) \, |}$$

7) We have used $t^+ = 100$ meV to represent the dirty limit. In fact there is still some impurity dependence at this value, but it is small.

8) Note that $k(0) = h_{c2}(0)/h_c(0)$.

9) We have used a sharp cutoff on the imaginary axis. To be completely accurate we should use the same cutoff *on the real axis* as was used in the inversion process, or use the appropriately smeared cutoff on the imaginary axis. For our purposes this is of no consequence.

Table 1 Superconducting Properties of Conventional Materials (Part 1)

Material	T_c (meV)	$\mu^*(N=6)$	λ	ω_{ln} (meV)	Area (meV)	ω_{max} (meV)	T_c/ω_{ln}
Al	0.1017	0.147	0.43	25.50	5.74	41.4	0.004
V	0.4621	0.223	0.80	14.78	6.76	33.1	0.031
Ta	0.3862	0.121	0.69	11.06	4.18	20.9	0.035
Sn	0.3233	0.116	0.72	8.40	3.42	18.8	0.038
Tl	0.2034	0.132	0.80	4.45	2.00	10.9	0.046
$Tl_{0.9}Bi_{0.1}$	0.1983	0.113	0.78	4.15	1.86	10.5	0.048
In	0.2931	0.116	0.81	5.83	2.74	15.8	0.050
Nb (Butler)	0.7931	0.373	1.22	13.88	9.35	26.9	0.057
Nb (Arnold)	0.7931	0.186	1.01	12.83	7.25	28.3	0.062
V_3Si-1	1.4741	0.142	1.00	21.11	11.80	49.3	0.070
V_3Si (Kihl.)	1.4132	0.139	1.00	19.88	10.76	44.5	0.071
Nb (Rowell)	0.7931	0.118	0.98	10.69	6.29	28.5	0.074
Mo	0.7586	0.071	0.90	9.95	5.47	33.0	0.076
$Pb_{0.4}Tl_{0.6}$	0.3966	0.115	1.15	4.17	2.74	11.0	0.095
La	0.4340	0.040	0.98	4.37	2.56	15.0	0.099
V_3Ga	1.2931	0.090	1.14	12.54	8.56	37.0	0.103
Nb_3Al (2)	1.2070	0.082	1.20	10.66	7.51	35.7	0.113
Nb_3Ge (2)	1.7240	0.238	1.60	15.17	13.34	31.3	0.114
$Pb_{0.6}Tl_{0.4}$	0.5086	0.125	1.38	4.27	3.35	10.9	0.119
Pb	0.6198	0.144	1.55	4.83	4.03	11.0	0.128
Nb_3Al (3)	1.6121	0.225	1.70	12.52	12.72	35.7	0.129
$Pb_{0.8}Tl_{0.2}$	0.5862	0.121	1.53	4.32	3.71	10.9	0.136
Hg	0.3612	0.124	1.62	2.47	2.64	14.3	0.146
Nb_3Sn	1.5603	0.156	1.70	10.68	10.69	28.7	0.146
$Pb_{0.9}Bi_{0.1}$	0.6595	0.105	1.66	4.33	3.98	9.9	0.152
Nb_3Al (1)	1.4138	0.127	1.70	9.06	9.32	35.7	0.156
Nb_3Ge (1)	1.7240	0.088	1.60	10.80	10.33	34.3	0.160
$Pb_{0.8}Bi_{0.2}$	0.6853	0.111	1.88	3.99	4.21	11.0	0.172
$Pb_{0.7}Bi_{0.3}$	0.7284	0.109	2.01	4.01	4.46	10.4	0.182
$Pb_{0.65}Bi_{0.35}$	0.7716	0.091	2.13	3.85	4.60	10.1	0.200
$Pb_{0.5}Bi_{0.5}$	0.6026	0.136	3.00	1.88	4.30	13.1	0.320
Ga	0.7379	0.174	2.25	3.04	6.15	27.0	0.243
$Pb_{0.75}Bi_{0.25}$	0.5957	0.136	2.76	2.07	4.20	10.4	0.288
Bi	0.5267	0.091	2.45	1.64	3.53	14.0	0.320

Table 1 Superconducting Properties (Part 2)

Material	T_c/ω_{ln}	$\frac{2\Delta_s}{k_B T_c}$	$\frac{\gamma T_c^2}{H_c^2(0)}$	$\frac{\Delta C(T_c)}{\gamma_s T_c}$	$h_c(0)$
Al	0.004	3.535	0.168	1.43	0.576
V	0.031	3.675	0.162	1.63	0.550
Ta	0.035	3.673	0.162	1.63	0.550
Sn	0.038	3.705	0.160	1.68	0.544
Tl	0.046	3.753	0.158	1.74	0.538
$Tl_{0.9}Bi_{0.1}$	0.048	3.769	0.157	1.76	0.536
In	0.050	3.791	0.156	1.79	0.533
Nb (Butler)	0.057	3.876	0.153	1.94	0.517
Nb (Arnold)	0.062	3.883	0.153	1.92	0.521
V_3Si_1	0.070	3.933	0.150	1.99	0.515
V_3Si (Kihl.)	0.071	3.935	0.150	2.02	0.512
Nb (Rowell)	0.074	3.964	0.150	1.97	0.518
Mo	0.076	3.968	0.150	1.98	0.518
$Pb_{0.4}Tl_{0.6}$	0.095	4.134	0.144	2.24	0.497
La	0.099	4.104	0.145	2.14	0.506
V_3Ga	0.103	4.179	0.143	2.24	0.499
Nb_3Al (2)	0.113	4.248	0.141	2.33	0.492
Nb_3Ge (2)	0.114	4.364	0.137	2.61	0.471
$Pb_{0.6}Tl_{0.4}$	0.119	4.352	0.137	2.52	0.479
Pb	0.128	4.497	0.132	2.77	0.466
Nb_3Al (3)	0.129	4.461	0.137	2.54	0.479
$Pb_{0.8}Tl_{0.2}$	0.136	4.505	0.134	2.69	0.470
Hg	0.146	4.591	0.134	2.49	0.488
Nb_3Sn	0.146	4.567	0.134	2.64	0.474
$Pb_{0.9}Bi_{0.1}$	0.152	4.674	0.130	2.86	0.463
Nb_3Al (1)	0.156	4.617	0.134	2.61	0.477
Nb_3Ge (1)	0.160	4.601	0.134	2.59	0.479
$Pb_{0.8}Bi_{0.2}$	0.172	4.843	0.127	2.92	0.462
$Pb_{0.7}Bi_{0.3}$	0.182	4.968	0.125	3.01	0.460
$Pb_{0.65}Bi_{0.35}$	0.200	5.081	0.125	2.98	0.462
$Pb_{0.5}Bi_{0.5}$	0.320	5.194	0.147	2.16	0.500
Ga	0.243	4.722	0.150	2.04	0.509
$Pb_{0.75}Bi_{0.25}$	0.288	5.119	0.143	2.27	0.494
Bi	0.320	4.916	0.153	2.03	0.506

Table 1 Superconducting Properties (Part 3)

Material	T_c/ω_{ln}	$\dfrac{\xi(0,t^+=0)}{\xi(T_c,t^+=0)}$	$\dfrac{v_l(0)}{T_c|v_l'(T_c)|}$	$\dfrac{v_L(0)}{T_c|v_L'(T_c)|}$
Al	0.004	1.330	0.376	0.500
V	0.031	1.293	0.351	0.454
Ta	0.035	1.292	0.352	0.454
Sn	0.038	1.286	0.346	0.445
Tl	0.046	1.278	0.340	0.434
$Tl_{0.9}Bi_{0.1}$	0.048	1.277	0.338	0.431
In	0.050	1.273	0.334	0.425
Nb (Butler)	0.057	1.261	0.321	0.405
Nb (Arnold)	0.062	1.260	0.322	0.406
$V_3Si.1$	0.070	1.253	0.315	0.395
V_3Si (Kihl.)	0.071	1.251	0.314	0.393
Nb (Rowell)	0.074	1.255	0.317	0.397
Mo	0.076	1.254	0.315	0.395
$Pb_{0.4}Tl_{0.6}$	0.095	1.233	0.294	0.363
La	0.099	1.244	0.301	0.374
V_3Ga	0.103	1.234	0.294	0.363
Nb_3Al (2)	0.113	1.228	0.286	0.352
Nb_3Ge (2)	0.114	1.211	0.271	0.328
$Pb_{0.6}Tl_{0.4}$	0.119	1.215	0.274	0.333
Pb	0.128	1.195	0.260	0.310
Nb_3Al (3)	0.129	1.219	0.269	0.328
$Pb_{0.8}Tl_{0.2}$	0.136	1.204	0.262	0.316
Hg	0.146	1.215	0.269	0.326
Nb_3Sn	0.146	1.214	0.262	0.318
$Pb_{0.9}Bi_{0.1}$	0.152	1.193	0.253	0.302
Nb_3Al (1)	0.156	1.217	0.262	0.318
Nb_3Ge (1)	0.160	1.218	0.262	0.320
$Pb_{0.8}Bi_{0.2}$	0.172	1.193	0.245	0.293
$Pb_{0.7}Bi_{0.3}$	0.182	1.186	0.239	0.284
$Pb_{0.65}Bi_{0.35}$	0.200	1.194	0.237	0.283
$Pb_{0.5}Bi_{0.5}$	0.320	1.359	0.250	0.340
Ga	0.243	1.342	0.274	0.368
$Pb_{0.75}Bi_{0.25}$	0.288	1.326	0.252	0.333
Bi	0.320	1.380	0.265	0.366

Table 1 Superconducting Properties (Part 4).

Material	T_c/ω_{ln}	$\mu^*(N=6)$	$h_{c2}(0,0)$	$h_{c2}(0,100)$	$k(0,0)$	$k(0,100)$
Al	0.004	0.000	0.727	0.690	1.26	1.20
V	0.031	0.219	0.725	0.667	1.32	1.21
Ta	0.035	0.119	0.725	0.666	1.32	1.21
Sn	0.038	0.114	0.725	0.662	1.33	1.22
Tl	0.046	0.130	0.726	0.658	1.35	1.22
$Tl_{0.9}Bi_{0.1}$	0.048	0.112	0.727	0.659	1.36	1.23
In	0.050	0.114	0.727	0.657	1.36	1.23
Nb (Butler)	0.057	0.363	0.724	0.648	1.40	1.25
Nb (Arnold)	0.062	0.182	0.728	0.652	1.40	1.25
V_3Si_1	0.070	0.140	0.729	0.651	1.42	1.26
V_3Si (Kihl.)	0.071	0.136	0.727	0.646	1.42	1.26
Nb (Rowell)	0.074	0.116	0.737	0.659	1.42	1.27
Mo	0.076	0.069	0.737	0.659	1.42	1.27
$Pb_{0.4}Tl_{0.6}$	0.095	0.112	0.739	0.647	1.49	1.30
La	0.099	0.039	0.743	0.657	1.47	1.30
V_3Ga	0.103	0.088	0.746	0.658	1.50	1.32
Nb_3Al (2)	0.113	0.080	0.748	0.656	1.52	1.33
Nb_3Ge (2)	0.114	0.231	0.743	0.643	1.58	1.36
$Pb_{0.6}Tl_{0.4}$	0.119	0.122	0.750	0.649	1.57	1.35
Pb	0.128	0.139	0.756	0.643	1.62	1.38
Nb_3Al (3)	0.129	0.219	0.760	0.664	1.59	1.39
$Pb_{0.8}Tl_{0.2}$	0.136	0.118	0.760	0.652	1.62	1.39
Hg	0.146	0.123	0.791	0.690	1.62	1.41
Nb_3Sn	0.146	0.151	0.769	0.670	1.62	1.41
$Pb_{0.9}Bi_{0.1}$	0.152	0.101	0.777	0.661	1.68	1.43
Nb_3Al (1)	0.156	0.124	0.777	0.679	1.63	1.42
Nb_3Ge (1)	0.160	0.085	0.774	0.679	1.62	1.42
$Pb_{0.8}Bi_{0.2}$	0.172	0.108	0.796	0.679	1.72	1.47
$Pb_{0.7}Bi_{0.3}$	0.182	0.105	0.813	0.691	1.77	1.50
$Pb_{0.65}Bi_{0.35}$	0.200	0.087	0.827	0.709	1.79	1.53
$Pb_{0.5}Bi_{0.5}$	0.320	0.133	0.800	0.793	1.60	1.59
Ga	0.243	0.171	0.763	0.745	1.50	1.46
$Pb_{0.75}Bi_{0.25}$	0.288	0.132	0.803	0.774	1.62	1.57
Bi	0.320	0.089	0.762	0.767	1.51	1.52

Table 1 Superconducting Properties of Einstein Spectra (Part 1)

λ	ω_{ln} (meV)	ω_c (meV)	T_c (meV)	T_c/ω_{ln}	$\frac{2\Delta_0}{k_B T_c}$	$\frac{\Delta C(T_c)}{\gamma_\bullet T_c}$	$\frac{\gamma T_c^2}{H_c^2(0)}$	$h_c(0)$
0.4	20.0	150	0.4767	0.024	3.58	1.49	0.166	0.566
0.6	13.3	150	0.7526	0.056	3.75	1.76	0.158	0.536
0.8	10.0	150	0.8768	0.088	3.98	2.15	0.147	0.501
1.0	8.0	120	0.9213	0.115	4.24	2.56	0.138	0.474
1.2	6.7	120	0.9258	0.139	4.48	2.89	0.131	0.459
1.4	5.7	120	0.9135	0.160	4.71	3.11	0.126	0.451
1.6	5.0	120	0.8939	0.179	4.92	3.26	0.122	0.448
1.8	4.4	120	0.8714	0.196	5.11	3.34	0.119	0.447
2.0	4.0	120	0.8483	0.212	5.29	3.38	0.117	0.449

Superconducting Properties of Einstein Spectra (Part 2)

| λ	$\frac{\xi(0,t^+=0)}{\xi(T_c,t^+=0)}$	$\frac{y_I(0)}{T_c\|y_I'(T_c)\|}$	$\frac{y_L(0)}{T_c\|y_L'(T_c)\|}$	$h_{c2}(0,0)$	$h_{c2}(0,100)$	$k(0,0)$	$k(0,100)$
0.4	1.311	0.368	0.482	0.726	0.678	1.28	1.20
0.6	1.277	0.339	0.432	0.723	0.655	1.35	1.22
0.8	1.240	0.304	0.378	0.722	0.636	1.44	1.27
1.0	1.210	0.276	0.334	0.731	0.629	1.54	1.33
1.2	1.188	0.257	0.305	0.749	0.634	1.63	1.38
1.4	1.173	0.244	0.286	0.773	0.647	1.71	1.43
1.6	1.164	0.235	0.273	0.799	0.665	1.78	1.49
1.8	1.159	0.228	0.264	0.825	0.686	1.85	1.54
2.0	1.158	0.223	0.259	0.851	0.709	1.89	1.58
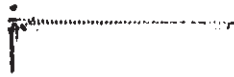
Figure 2.2 Specific heat jump ratio $f \equiv \Delta C(T_c)/\gamma_0 T_c$ vs. $T_c/\omega_{\ln}$. The dots represent the accurate results from the full numerical solutions of the Eliashberg equations. Experiment tends to agree to within 10%. In increasing order of $T_c/\omega_{\ln}$, the dots correspond to the following systems: Al, V, Ta, Sn, Tl, $Tl_{0.9}Bi_{0.1}$, In, Nb (Butler), Nb (Arnold), V_3Si-1, V_3Si (Kihl.), Nb (Rowell), Mo, $Pb_{0.4}Tl_{0.6}$, La, V_3Ga, Nb_3Al (2), Nb_3Ge (2), $Pb_{0.6}Tl_{0.4}$, Pb, Nb_3Al (3), $Pb_{0.8}Tl_{0.2}$, Hg, Nb_3Sn, $Pb_{0.9}Bi_{0.1}$, Nb_3Al (1), Nb_3Ge (1), $Pb_{0.8}Bi_{0.2}$, $Pb_{0.7}Bi_{0.3}$, and $Pb_{0.65}Bi_{0.35}$. The drawn curve corresponds to $\frac{\Delta C(T_c)}{\gamma_0 T_c} = 1.43(1 + 53(\frac{T_c}{\omega_{\ln}})^2 \ln \frac{\omega_{\ln}}{3T_c})$. See Appendix C for origin of spectral functions.
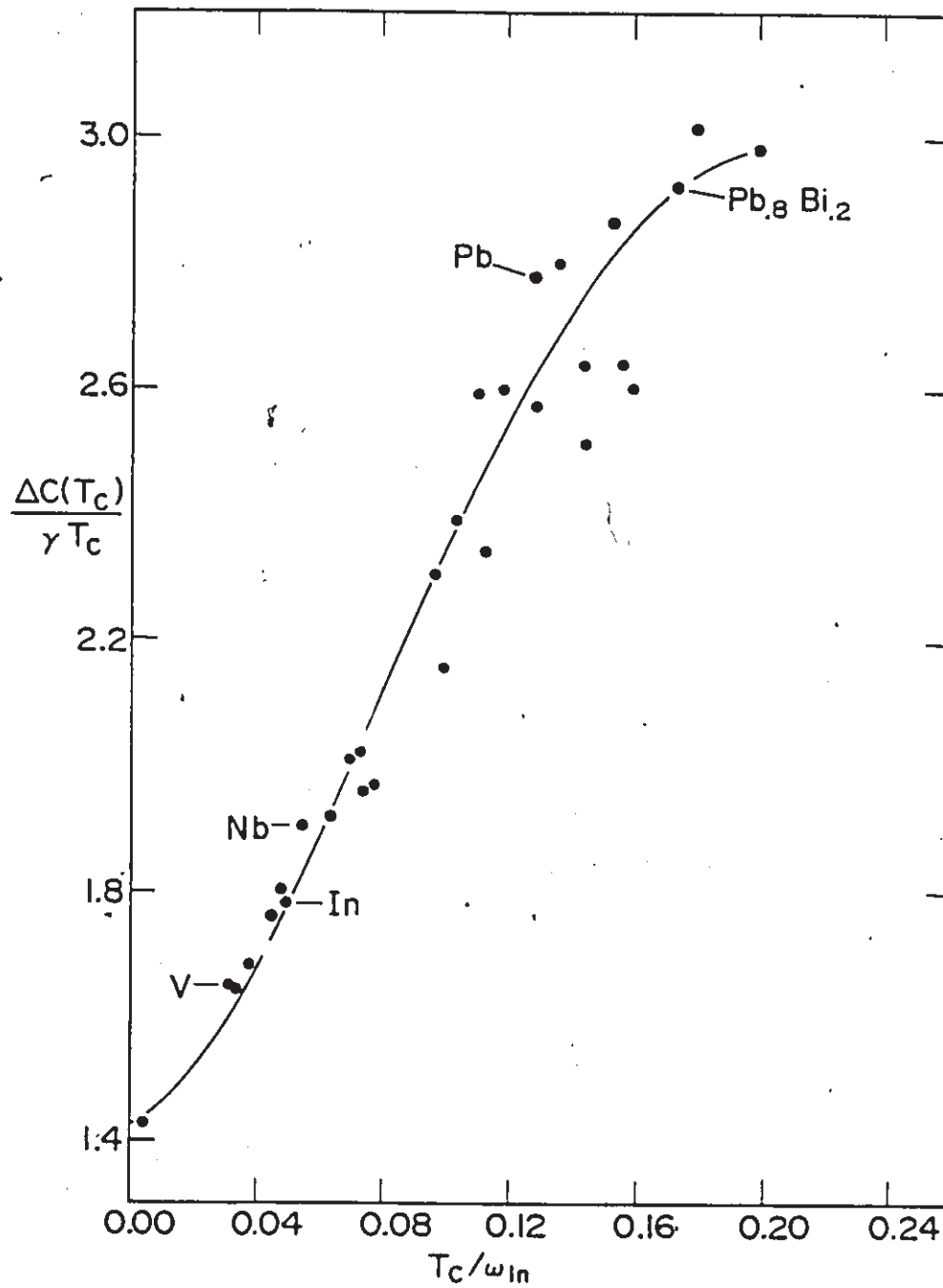
along with the thermodynamic formulas:

$$\Delta C(T) = -\frac{T d^2 \Delta F}{dT^2} \qquad (2.27)$$

and

$$H_c(T) = [-8\pi \Delta F]^{1/2} \qquad (2.28)$$

From Appendix B, for T near T_c, we obtain the expression ($t \equiv T/T_c$):

$$\frac{\Delta C(T)}{\gamma_0 T_c} = f + (1-t)g \qquad (2.29)$$

where

$$f \equiv \frac{\Delta C(T_c)}{\gamma_0 T_c} = 1.43 \left(1 + 53 \left(\frac{T_c}{\omega_{\ln}} \right)^2 \ln \left(\frac{\omega_{\ln}}{3T_c} \right) \right) \qquad (2.30)$$

and

$$g = -3.77 \left(1 + 117 \left(\frac{T_c}{\omega_{\ln}} \right)^2 \ln \left(\frac{\omega_{\ln}}{2.9 T_c} \right) \right) . \qquad (2.31)$$

The form of these expressions has been derived and is similar to that used previously.[36,40,41] In addition, we have specified an average phonon frequency, $\omega_{\ln}$, and fitted coefficients to numerical data. The data are listed in Table 1. The derived expressions are plotted in Fig. (2.2) and (2.3) along with the numerical data. Experimental data have been omitted, although the Eliashberg theory results are generally accurate to within 10 %. The origin of the spectral functions used in these calculations is described in Appendix C. Note that there is some scatter, especially amongst the A15 compounds and Hg. In the case of Hg, there is a very low frequency peak in the $\alpha^2 F(\nu)$ spectrum, so that the assumption $\nu \gg T_c$ for all important ν has broken down. Also note that the results from amorphous materials have not been plotted. They are not well described by these formulas at all. They are included in Table 1: it is seen that their values for $\frac{T_c}{\omega_{\ln}}$ are near 0.3 . This value is beyond the limit

Figure 2.3   Plot of g (see Eq. (2.29) in text) vs. $T_c/\omega_{\ln}$ for a selected number of systems. Dots correspond to the results extracted from numerical solutions for $D(t) \equiv \frac{H_c(T)}{H_c(0)} - (1-t^2)$ vs. t, using the Eliashberg equations. In increasing order of $T_c/\omega_{\ln}$, the dots correspond to Tl, In, Nb_3Al (2), Nb_3Al (3), Nb_3Sn, $Pb_{0.9}Bi_{0.1}$, Nb_3Al (1), $Pb_{0.8}Bi_{0.2}$, $Pb_{0.7}Bi_{0.3}$, and $Pb_{0.65}Bi_{0.35}$. The drawn curve corresponds to $g = -3.77\left(1 + 117\left(\frac{T_c}{\omega_{\ln}}\right)^2 \ln\left(\frac{\omega_{\ln}}{2.9T_c}\right)\right)$. The fit is remarkably good, considering the constraints on the coefficients.
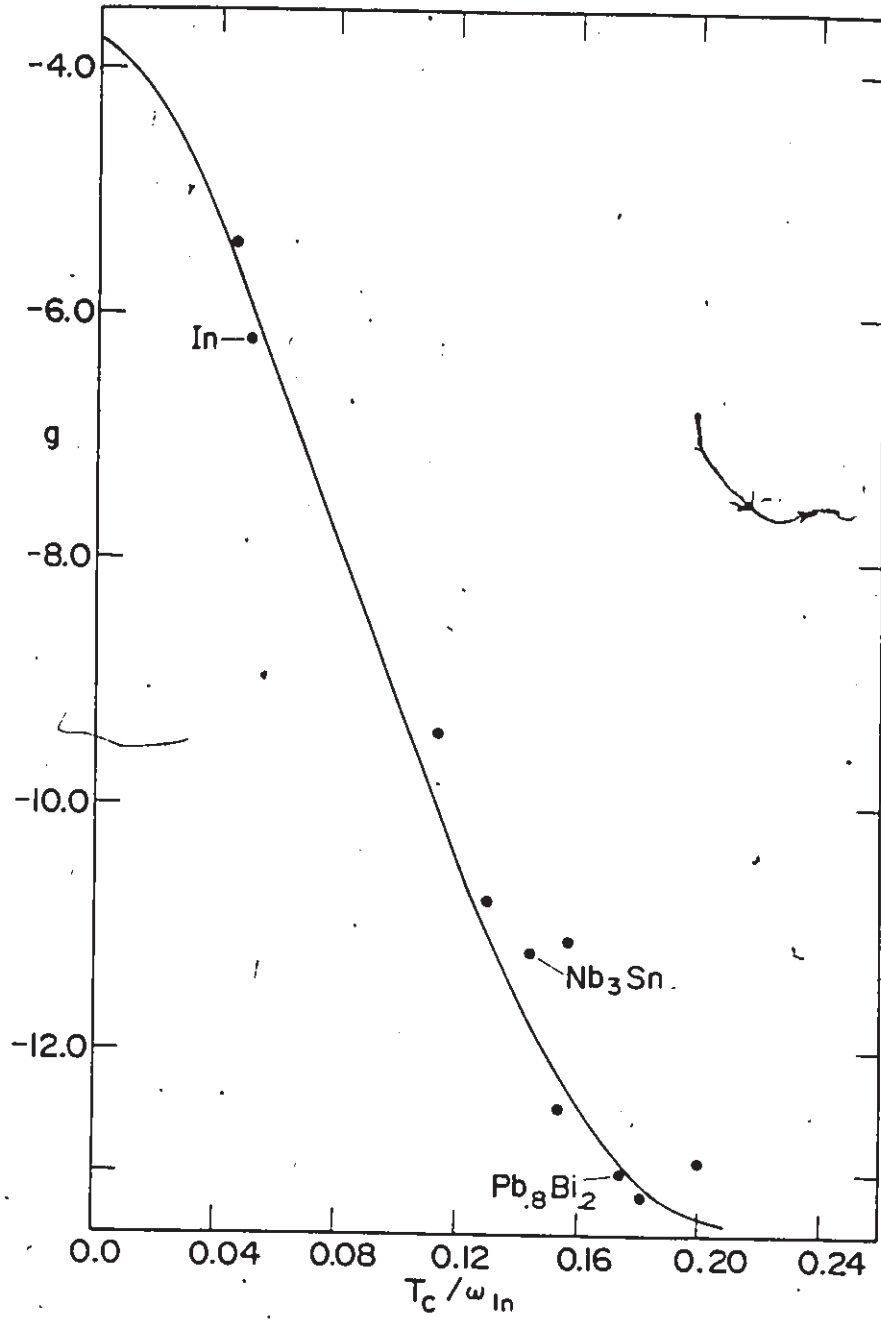
of validity of formulas (2.30) and (2.31) (and others to be presented later). More importantly however, the spectral shapes of $\alpha^2 F(\nu)$ for these materials is such that they are not well described by an Einstein spectrum with frequency $\nu_E = \omega_{\ln}$ of the material. The opposite tends to be true for the crystalline materials. Coombes and Carbotte[43,44] have analysed shape dependence in detail. Some of the scatter is also due to variations in μ^*. In any event, the point of these expressions is to describe the general trend of superconducting properties as a function of strong coupling. The result is a continual increase from 0 (BCS) to 0.20 . Note that there are signs of saturation, and in fact, later it will be seen that as the coupling is increased further, $\frac{\Delta C(T_c)}{\gamma_0 T_c}$ will decrease to values below 1.43 .

The physical reason behind the increase can be traced to the gap opening up more rapidly just below T_c as the coupling strength is increased. The specific heat jump, which is a measure of steepness of the ascent of the gap, will increase as well. The subsequent decline alluded to in the previous paragraph is not physical; it is a result of having used γ_0 instead of the Grimvall[45] $\gamma(T_c)$ (see ahead, Eq. (2.54)). More will be said about this choice later in the thesis.

A calculation of other thermodynamic properties requires a knowledge of strong coupling corrections at zero temperature. The procedure is similar to that near T_c , and is also outlined in Appendix B. The result for the gap ratio is readily obtained:

$$\frac{2\Delta_0}{k_B T_C} = 3.53\left[1 + 12.5\left(\frac{T_c}{\omega_{\ln}}\right)^2 \ln\left(\frac{\omega_{\ln}}{2T_c}\right)\right] . \qquad (2.32)$$

We have use the same fit as Mitrović *et al.*[24] This result is plotted in Fig. (2.4). along with numerical data. Note that data from more A15 compounds have

Figure 2.4   The ratio $\frac{2\Delta_0}{k_B T_c}$ vs. $T_c/\omega_{\ln}$. Most of the points have been repro-
duced from Ref. 24. We have also included some numerical solutions of A15
compounds. See Fig. 2.2 for identification of materials. The curve corresponds
to $\frac{2\Delta_0}{k_B T_C} = 3.53 \left[1 + 12.5 \left(\frac{T_c}{\omega_{\ln}} \right)^2 \ln \left(\frac{\omega_{\ln}}{2T_c} \right) \right]$.
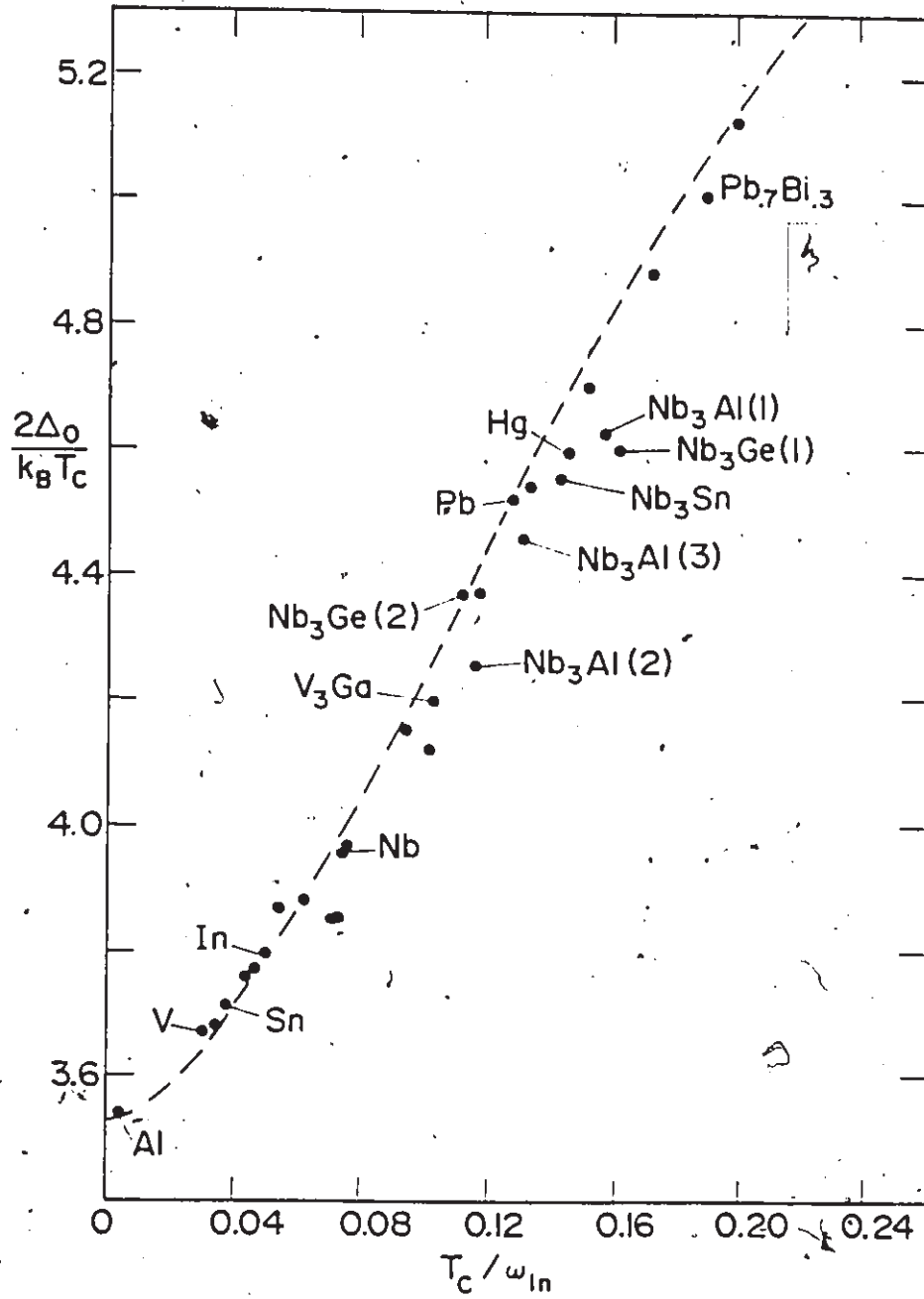
been included, and has increased the amount of scatter slightly. However, overall, the fit is very good and the trend is well described by Eq. (2.32). The shape dependence of $\frac{2\Delta_0}{k_B T_c}$ has been studied by Coombes and Carbotte[43] and more recently in Ref. 46 . In Ref. 44 it was noted that shape dependence was much more prominent for $\frac{\Delta C}{\gamma_0 T_c}$ than for $\frac{2\Delta_0}{k_B T_C}$. This conclusion is supported by the increased amount of scatter in Fig. (2.2) relative to Fig. (2.4). Also note that the trend shows no sign of saturation, as was the case for $\frac{\Delta C}{\gamma T_c}$. It will be seen later, in fact, that $\frac{2\Delta_0}{k_B T_c}$ saturates only in the limit of $\frac{T_c}{\omega_{ln}} \to \infty$. We should also add that amorphous compounds have once again been excluded, as they are not well described by Eq. (2.32) for the same reasons given earlier. The enhancement of $\frac{2\Delta_0}{k_B T_c}$ with increased coupling can be understood by the following simple argument: as the coupling strength increases both T_c and Δ_0 increase. However, the detrimental effect of thermal phonons is also felt more strongly by T_c , whereas Δ_0 is unaffected since it is a zero temperature property.[20] The result is a larger increase of Δ_0 compared to T_c .

Also derived in Appendix B are expressions for two more commonly used ratios:
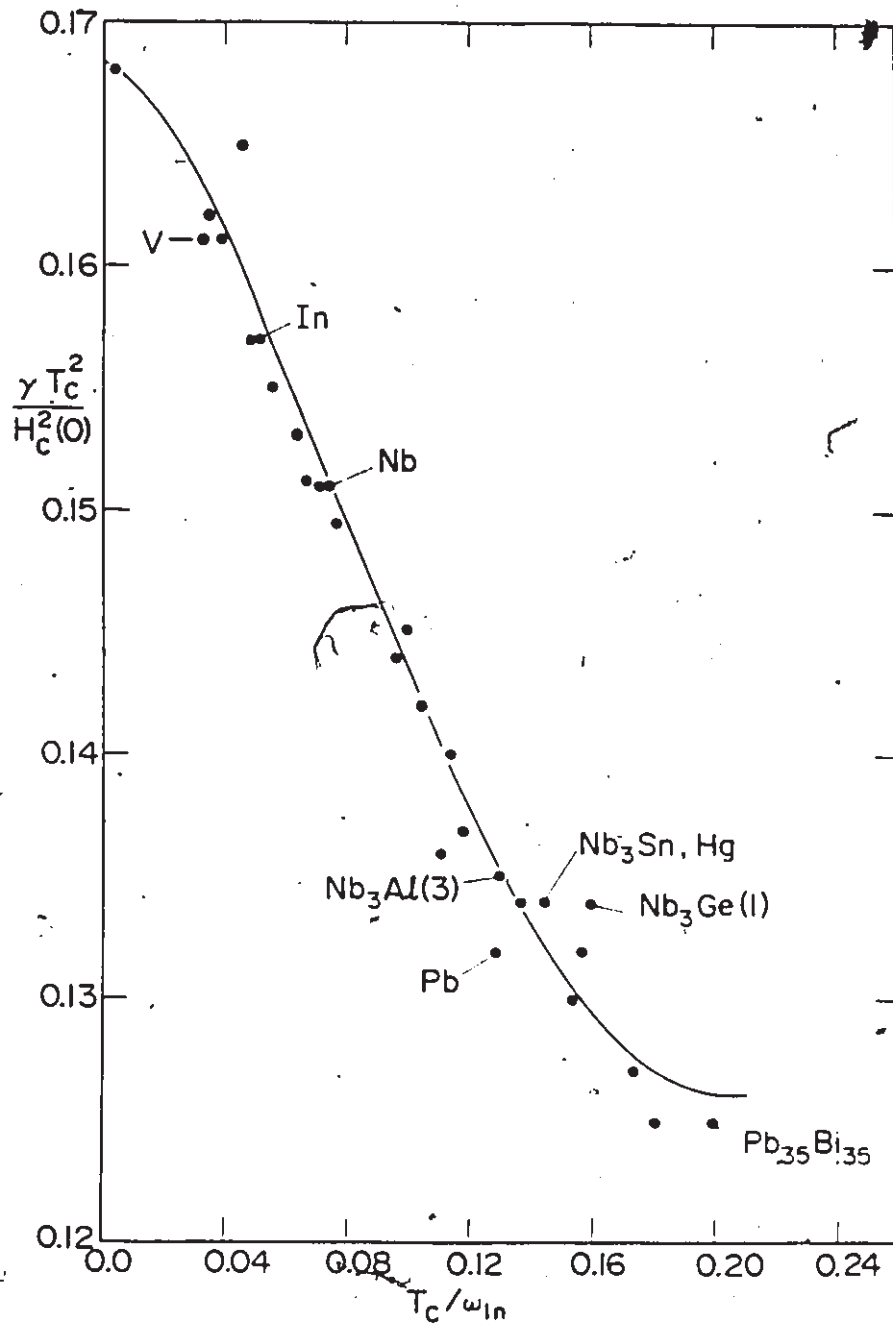
$$\frac{\gamma_0 T_c^2}{H_c^2(0)} = 0.168\left(1 - 12.2\left(\frac{T_c}{\omega_{ln}}\right)^2 \ln\left(\frac{\omega_{ln}}{3T_c}\right)\right) \qquad (2.33)$$

and

$$h_c(0) = 0.576\left(1 - 13.4\left(\frac{T_c}{\omega_{ln}}\right)^2 \ln\left(\frac{\omega_{ln}}{3.5T_c}\right)\right) \qquad (2.34)$$

These expressions, along with numerical data, are plotted in figures (2.5) and (2.6). The first ratio is rather well described by Eq. (2.33). The second exhibits considerably more scatter. Both show indications of saturation. The important point, however, is that the trend for realistic spectral shapes is

Figure 2.5 The ratio $\frac{\gamma_0 T_c^2}{H_c^2(0)}$ vs. $T_c/\omega_{\ln}$. See Fig. 2.2 for identification of materials. The curve corresponds to $\frac{\gamma_0 T_c^2}{H_c^2(0)} = 0.168\left(1 - 12.2\left(\frac{T_c}{\omega_{\ln}}\right)^2 \ln\left(\frac{\omega_{\ln}}{3T_c}\right)\right)$.

Figure showing $\frac{\gamma T_c^2}{H_c^2(0)}$ versus T_c/ω_{ln}. Labeled data points: V, In, Nb, Nb$_3$Al(3), Nb$_3$Sn, Hg, Nb$_3$Ge(1), Pb, Pb$_{.35}$Bi$_{.35}$.

well described by these formulas. Note, moreover, that the deviation from BCS behaviour is relatively small ($\sim 20\%$) in $h_c(0)$, as compared to, say $\frac{2\Delta_0}{k_B T_c}$.

(iii) Electromagnetic properties

Electromagnetic properties were first discussed (within BCS theory) in Ref. 12 . Nam[47] later extended many of the calculations to the strong coupling form. General derivations are provided in Ref. 47 and hence will be omitted here. More recently, Blezius and Carbotte[48] have studied electromagnetic properties of strong coupling superconductors with impurities through functional derivative and optimum spectrum techniques. We wish to include here strong coupling formulas of the type discussed in the previous section.

Within linear response theory, the current density is written in the form:

$$J_\mu(\vec{q}, \omega) = -K_{\mu\nu}(\vec{q}, \omega) A^\nu(\vec{q}, \omega) . \tag{2.35}$$

$A^\nu(\vec{q}, \omega)$ is a vector potential component, and $K_{\mu\nu}(\vec{q}, \omega)$ is the tensor kernel. The properties discussed here are expressible in terms of $K_{\mu\nu}(\vec{q}, \omega)$. For example, the frequency dependent penetration depth is given, for the case of specular reflection, by the expression[49,47]

$$\lambda(T, \omega) = \frac{2}{\pi} \int_0^\infty dq \frac{1}{q^2 + \frac{K(q,\omega)}{4\pi}} . \tag{2.36}$$

What is often quoted as the penetration depth is the zero frequency limit of this expression, $\lambda(T) = \lim_{\omega \to 0} \lambda(T, \omega)$. Moreover, simple expressions are possible in limiting cases. In a superconductor which is dirty, the mean free path (ℓ) of the electron is greatly reduced due to the increased scattering probability so that the response to an external field is local. A local response

Figure 2.6 . The ratio $h_c(0)$ vs. $T_c/\omega_{\ln}$. See Fig. 2.2 for identification of materials. The curve corresponds to $h_c(0) = 0.576\left(1 - 13.4\left(\frac{T_c}{\omega_{\ln}}\right)^2 \ln\left(\frac{\omega_{\ln}}{3.5T_c}\right)\right)$.
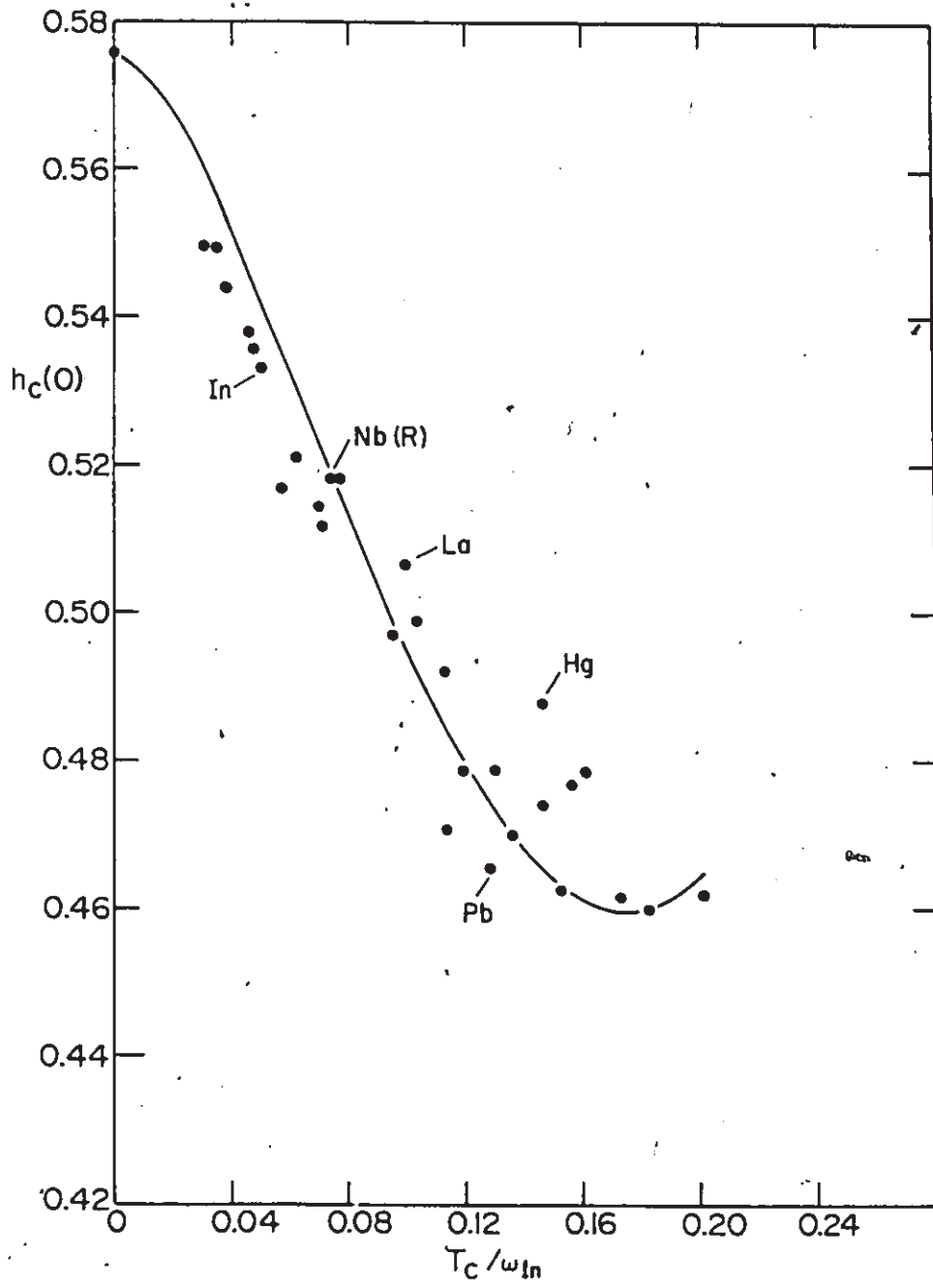
implies that $\vec{q}$ is null; *i.e.* the integration in Eq. (2.36) is important near $q = 0$. $K(q, 0)$ can be expanded near $q = 0$ with the result:[47]

$$\lambda_\ell(T) = \left[4\pi\sigma_N T \sum_{n=1}^\infty \frac{\Delta_n^2}{\omega_n^2 + \Delta_n^2} \right]^{-\frac{1}{2}} . \tag{2.37}$$

In Eq. (2.37) the subscript "ℓ" indicates the local limit. The normal state conductivity, σ_N, is given by $\sigma_N = \frac{2}{3} N(0)e^2 v_F^2 \tau_N$, where τ_N is the lifetime due to normal impurities and v_F is the Fermi velocity. The local limit is generally characterized by $\xi(0) \gg \ell$, where $\xi(0)$ is the zero temperature coherence distance, to be defined later. $\xi(0)$ is roughly the distance over which electrons pair.

When non-local effects become important, one must use either the Pippard (extreme type I) or London (extreme type II) limits. The Pippard limit is characterized by $\lambda \ll \xi(0)$ and is determined through Eq. (2.36) where most of contribution comes from the region $q \to \infty$. The result is:[47]

$$\lambda_P(T) = \frac{4}{3\sqrt{3}} \left[\frac{3\pi^2}{v_F} \frac{n}{m} e^2 T \sum_{n=1}^\infty \frac{\Delta_n^2}{\omega_n^2 + \Delta_n^2} \right]^{-\frac{1}{3}} . \tag{2.38}$$

For the London limit, $\lambda \gg \xi(0)$, and again we use $q \to 0$ to obtain:[47]

$$\lambda_L(T) = \left[\frac{4}{3}\pi N(0)e^2 v_F^2 \, T \sum_{n=1}^\infty \frac{\Delta_n^2}{Z_n(\omega_n^2 + \Delta_n^2)^{3/2}} \right]^{-\frac{1}{2}} . \tag{2.39}$$
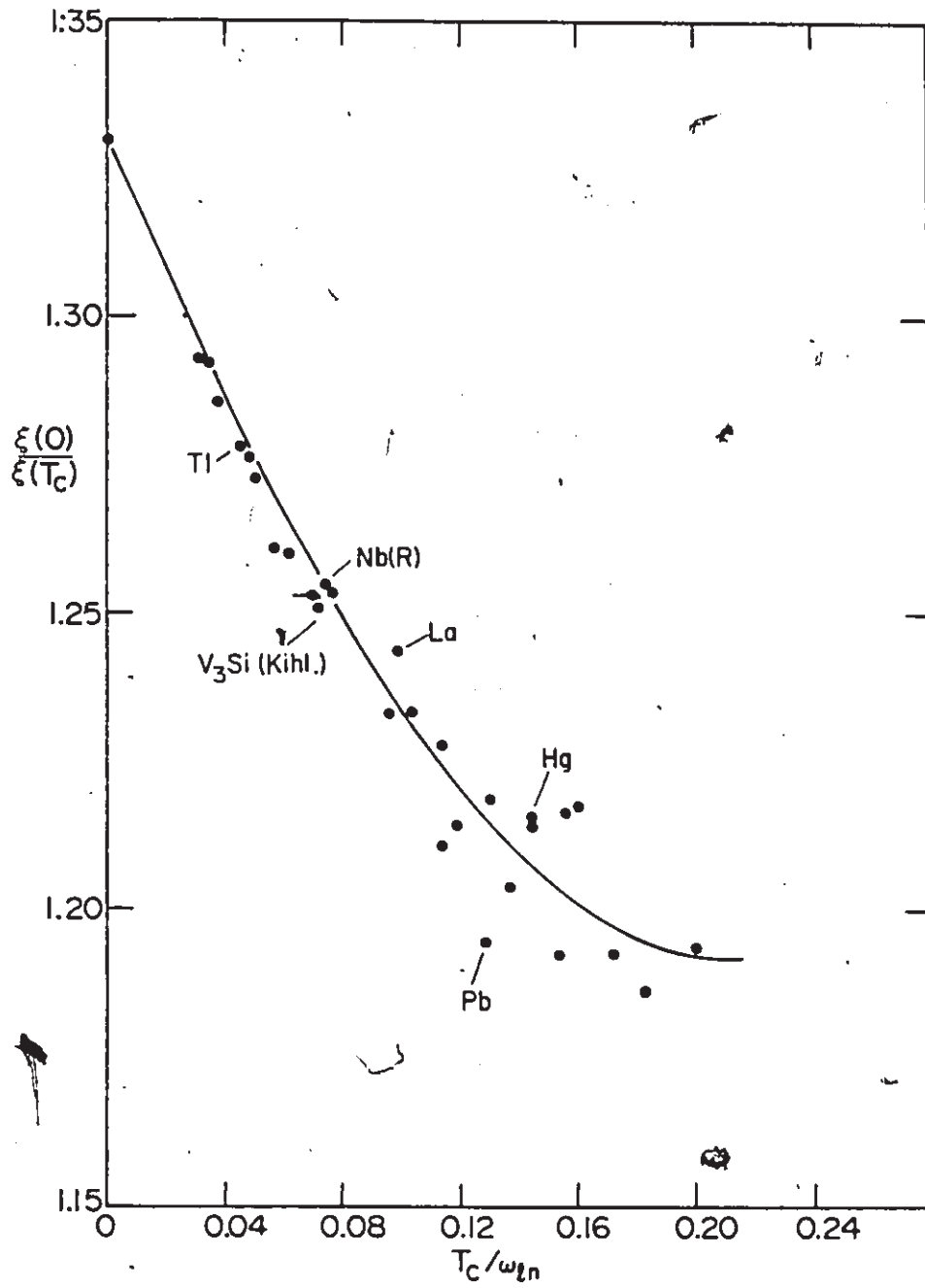
One more useful quantity is the electromagnetic coherence length, which is defined by:[50]

$$\lim_{q \to \infty} \frac{q K(q, 0)}{K(0, 0)} = \frac{3\pi}{4\xi(T)} \tag{2.40}$$

with the result:[47]

$$\xi(T) = \frac{v_F}{2} \frac{\sum_{n=1}^\infty \frac{\Delta_n^2}{Z_n(\omega_n^2 + \Delta_n^2)^{3/2}}}{\sum_{n=1}^\infty \frac{\Delta_n^2}{\omega_n^2 + \Delta_n^2}} . \tag{2.41}$$

Figure 2.7   The ratio $\frac{\xi(0)}{\xi(T_c)}$ vs. $T_c/\omega_{\ln}$. See Fig. 2.2 for identification of materials. The curve corresponds to $\frac{\xi(0)}{\xi(T_c)} = 1.33\left(1 - 0.83\frac{T_c}{\omega_{\ln}} - 0.75\left(\frac{T_c}{\omega_{\ln}}\right)^2 \ln\frac{\omega_{\ln}}{40T_c}\right)$.

Reductions of these equations within BCS theory or the $\lambda^{\theta\theta}$ model are straightforward and will not be presented here. The strong coupling corrections to Z_n and Δ_n are given in Appendix B and it is straightforward to calculate the strong coupling corrections to the quantities presented here. We note, moreover, that useful ratios are $\frac{\xi(0)'}{\xi(T_c)}$, and $\frac{y_i(0)}{T_c|y_i'(T_c)|}$, $i = \ell, L$. Here $y_i(T) \equiv \lambda_i^{-2}(T)$. This form is useful since $\lambda_i(T)$ diverges near T_c. These latter ratios have been defined in analogy to the reduced critical magnetic field, $h_c(0)$. Moreover, the experimentally accessible muon spin relaxation rate is proportional to $y_i(T)$. The Pippard ratio has been omitted since the appropriate quantity to define in this case would be $z_p(T) \equiv \lambda_P^{-3}(T)$, and one can easily show that

$$\frac{z_p(0)}{T_c|z_p'(T_c)|} = \frac{y_\ell(0)}{T_c|y_\ell'(T_c)|} . \qquad (2.42)$$

The numerical data for the three ratios is presented in Figs. (2.7–2.9). Note that it is apparent in all three cases, that the corrections from BCS are negative and seem to deviate linearly. We have thus allowed ourselves the freedom of another parameter so that a linear term is also presented in the fits to the data. In Fig. (2.8) we also show a curve obtained from an Einstein spectrum with $\mu^* = 0$. It appears to display no linear term, and so is consistent with our general derivations in Appendix B, which, after all, were modelled after such a spectrum. The effect of a realistic shape and/or finite μ^*, has been to produce a linear behaviour, so we have (phenomenologically) included it. The expressions we have obtained are:

$$\frac{\xi(0)}{\xi(T_c)} = 1.33\left(1 - 0.83\frac{T_c}{\omega_{\ln}} - 0.75\left(\frac{T_c}{\omega_{\ln}}\right)^2 \ln\frac{\omega_{\ln}}{40T_c}\right), \qquad (2.43)$$

$$\frac{y_\ell(0)}{T_c|y_\ell'(T_c)|} = 0.376\left(1 - 1.5\frac{T_c}{\omega_{\ln}} - 7.6\left(\frac{T_c}{\omega_{\ln}}\right)^2 \ln\frac{\omega_{\ln}}{4T_c}\right); \qquad (2.45)$$

and

Figure 2.8 The ratio $\frac{\gamma_i(0)}{T_c|\nu_i'(T_c)|}$ vs. $T_c/\omega_{\ln}$. See Fig. 2.2 for identification of materials. Note that Ga has also been included and deviates substantially from the trend. The solid curve corresponds to $\frac{\gamma_i(0)}{T_c|\nu_i'(T_c)|} = 0.376\left(1 - 1.5\frac{T_c}{\omega_{\ln}} - 7.6\left(\frac{T_c}{\omega_{\ln}}\right)^2 \ln\frac{\omega_{\ln}}{4T_c}\right)$. Note that a linear term has been required for an accurate fit. The dashed curve corresponds to a series of Einstein spectra with μ^*, the model spectra upon which our derivations are based. The trend is quite similar to that of the real materials. Note, however, that the initial decrease from BCS is more quadratic, and hence no linear term would be required. Thus, it appears that the effect of the realistic shapes used has been to produce a linear correction below the BCS value.
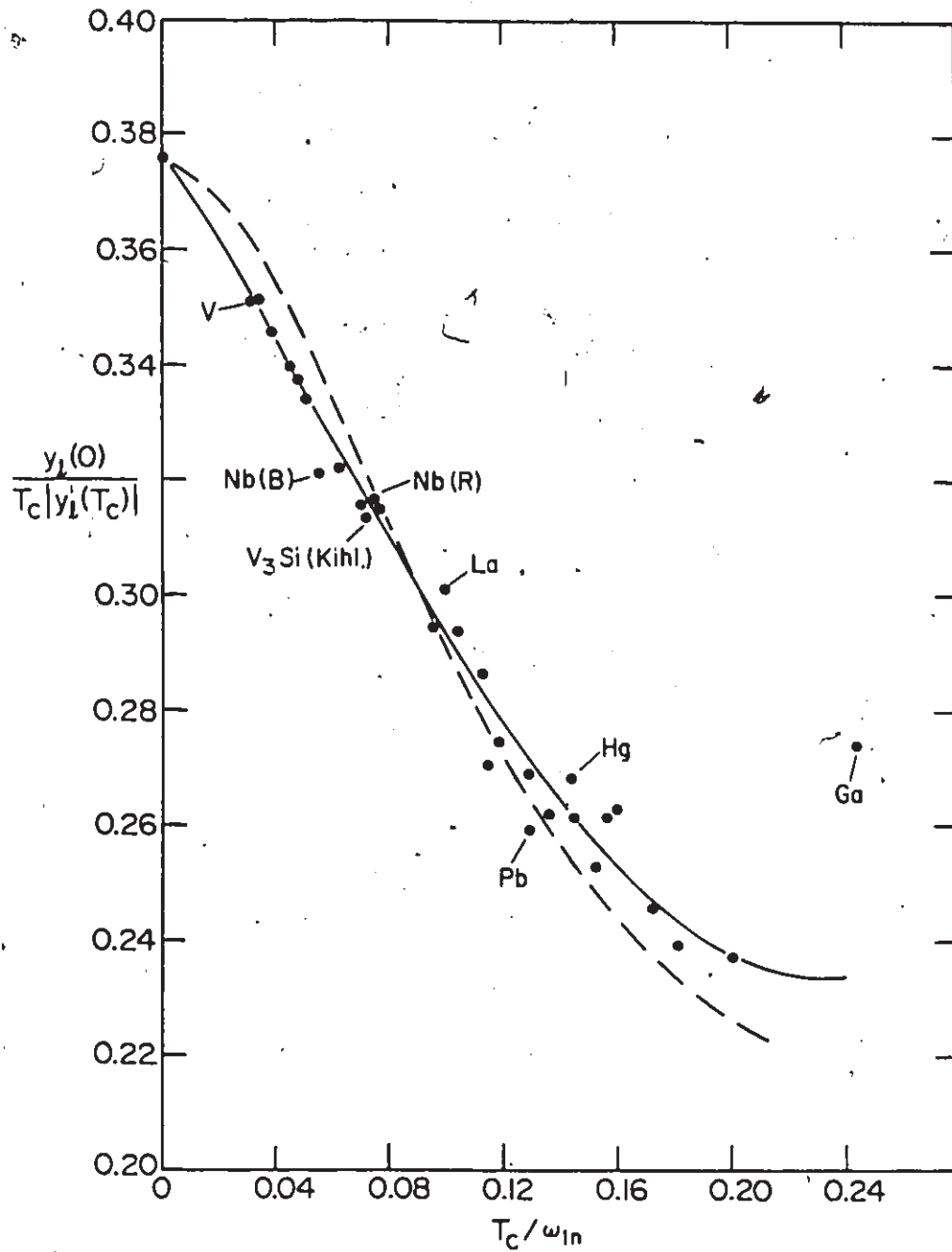
$$\frac{y_L(0)}{T_c|y_L'(T_c)|} = 0.5\left(1 - 2\frac{T_c}{\omega_{\ln}} - 11\left(\frac{T_c}{\omega_{\ln}}\right)^2 \ln\frac{\omega_{\ln}}{4.5T_c}\right) \qquad (2.45)$$

Once again, there is some scatter in the data, although the general trend is well described by the formulas. Note moreover, that the exact relation:[50]

$$\frac{y_L(0)}{T_c|y_L'(T_c)|} = \frac{\xi(0)}{\xi(T_c)}\frac{y_\ell(0)}{T_c|y_\ell'(T_c)|} \qquad (2.46)$$

is not observed by the relations (2.43–2.45) to lowest order in $T_c/\omega_{\ln}$, so that the full expressions must be used.

The discussion so far has focussed on the clean limit; i.e. no impurities are present. To include normal (i.e. non-magnetic) impurities, the terms $\pi t^+ \frac{\Delta_n}{\sqrt{\omega_n^2+\Delta_n^2}}$ and $\frac{\pi t^+}{\sqrt{\omega_n^2+\Delta_n^2}}$ must be added on the right-hand-side of equations (2.13) and (2.14), respectively. $t^+ = \frac{1}{2\pi\tau_N}$, where τ_N is the lifetime defined earlier. It is then easy to show that the solution Δ_n is in fact independent of impurities. This is in accordance with Anderson's theorem,[51] which states that T_c is unaffected by normal impurities. The impurity dependence is contained in Z_n. Thus, for example, the local penetration depth remains the same in the dirty limit ($t^+ \to \infty$). This is expected since the dirty limit assumption ($\ell \ll \xi(0)$) is already built in. In the dirty limit, $Z_n \approx \frac{\pi t^+}{\sqrt{\omega_n^2+\Delta_n^2}}$, so that the London penetration depth becomes equal to the local penetration depth. The coherence distance becomes especially simple: $\xi(T) \approx \frac{v_F}{2\pi t^+} = v_F\tau_N = \ell$, the mean free path of the electron. Thus, as expected, the distance over which an electron can carry information about an external field becomes limited by its mean free path in the dirty limit. Note that this coherence distance contrasts with the Ginzburg-Landau coherence distance, which, as all coherence distances associated with critical phenomena do, diverges at $T = T_c$.

Figure 2.9   The ratio $\frac{\nu_L(0)}{T_c|\nu'_L(T_c)|}$ vs. $T_c/\omega_{\ln}$. See Fig. 2.2 for identification of materials. The solid curve corresponds to $\frac{\nu_L(0)}{T_c|\nu'_L(T_c)|} = 0.5\left(1 - 2\frac{T_c}{\omega_{\ln}} - 11\left(\frac{T_c}{\omega_{\ln}}\right)^2 \ln\frac{\omega_{\ln}}{4.5T_c}\right).$
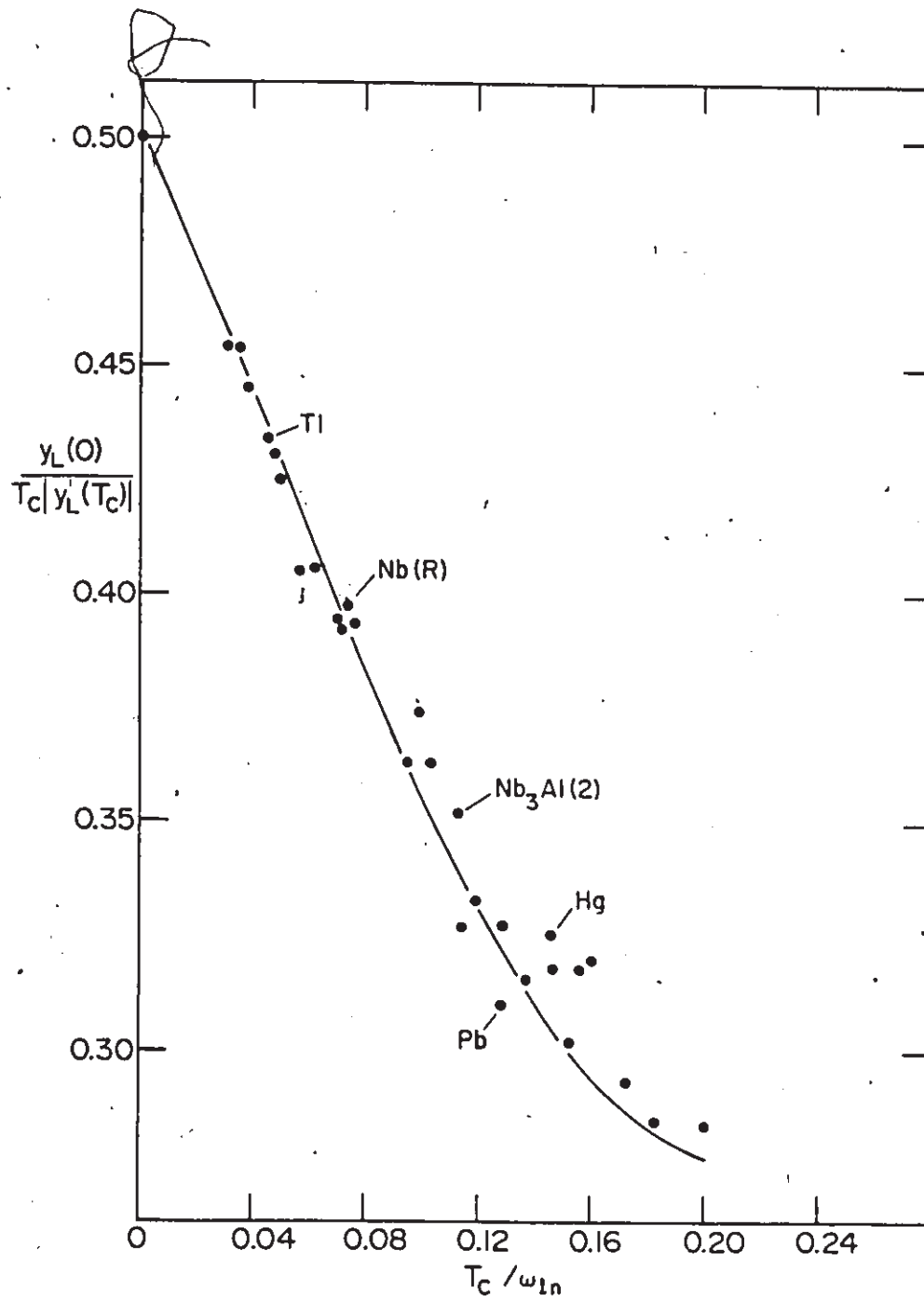
Finally the Pippard limit remains the same, although anomalous, due to the exponent $-\frac{1}{3}$ rather than $-\frac{1}{2}$.

(iv) Upper Critical Magnetic Field

Type II superconductors are of special interest since they are the most technologically useful. Even in the mixed phase, *i.e.* with both normal and superconducting material present, they are capable of carrying supercurrents while supporting high magnetic fields. A study of the upper critical magnetic field as a function of temperature amounts to a study along the phase boundary between the normal and mixed superconducting phase in the H-T plane. The first theoretical descriptions were based on the Ginzburg-Landau-Abrikosov-Gorkov[52-54] (GLAG) theory. Werthamer and co-workers[55-57] developed a set of equations which determined $H_{c2}(T, t^+)$ for all temperatures and all impurity concentrations, and included Pauli spin paramagnetism and electron spin-orbit scattering. These equations were cast at the level of BCS theory, as far as the electron-phonon interaction was concerned. Later, Werthamer and McMillan[58] generalized this approach to Eliashberg theory. Recently Schossmann and Schachinger[59] have formulated a strong coupling theory valid for any impurity concentration. We will neglect Pauli limiting here. The equations, formulated on the imaginary axis, are:[59]

$$\tilde{\Delta}(i\omega_n) = \pi T \sum_{m=-\infty}^{\infty} \left[\lambda(i\omega_n - i\omega_m) - \mu^*\theta(\omega_c - |\omega_m|) \right] \frac{\tilde{\Delta}(i\omega_m)}{\chi^{-1}(i\tilde{\omega}_m) - \pi t_+} \quad (2.47a)$$

$$\bar{\omega}(i\omega_n) = \omega_n + \pi T \left(\lambda(0) + 2\sum_{m=1}^{n-1} \lambda(i\nu_m) \right) + \pi t^+ \text{sgn}\,\omega_n \quad (2.47b)$$

with

$$\chi(\tilde{\omega}_n) = \frac{2}{\sqrt{\alpha}} \int_0^{\infty} dq\, e^{-q^2} \tan^{-1}\left[\frac{q\sqrt{\alpha}}{|\tilde{\omega}_n|} \right] \quad (2.47c)$$

Figure 2.10   The reduced quantity $h_{c2}(0, t^+ = 100\,\text{meV})$ vs. $T_c/\omega_{\ln}$. See Fig. 2.2 for identification of materials. Two curves are drawn: the solid one corresponds to $h_{c2}(0, 100) = 0.69\left(1 - 1.5\frac{T_c}{\omega_{\ln}} + 2.0\left(\frac{T_c}{\omega_{\ln}}\right)^2 \ln\frac{\omega_{\ln}}{0.8T_c}\right)$. The dotted curve corresponds to $h_{c2}(0, 100) = 0.69\left(1 - \frac{T_c}{\omega_{\ln}} - 3.2\left(\frac{T_c}{\omega_{\ln}}\right)^2 \ln\frac{\omega_{\ln}}{30T_c}\right)$. More-over, the data corresponding to Einstein spectra differs significantly from either of these two curves. Note that the corrections from BCS are very small. Also, the variation in possible parameters used in the fits indicates that the scatter in the data is much too large to be described by a single curve. It is clear, however, that there is a small decrease initially, followed by corrections which are positive with respect to the BCS value.
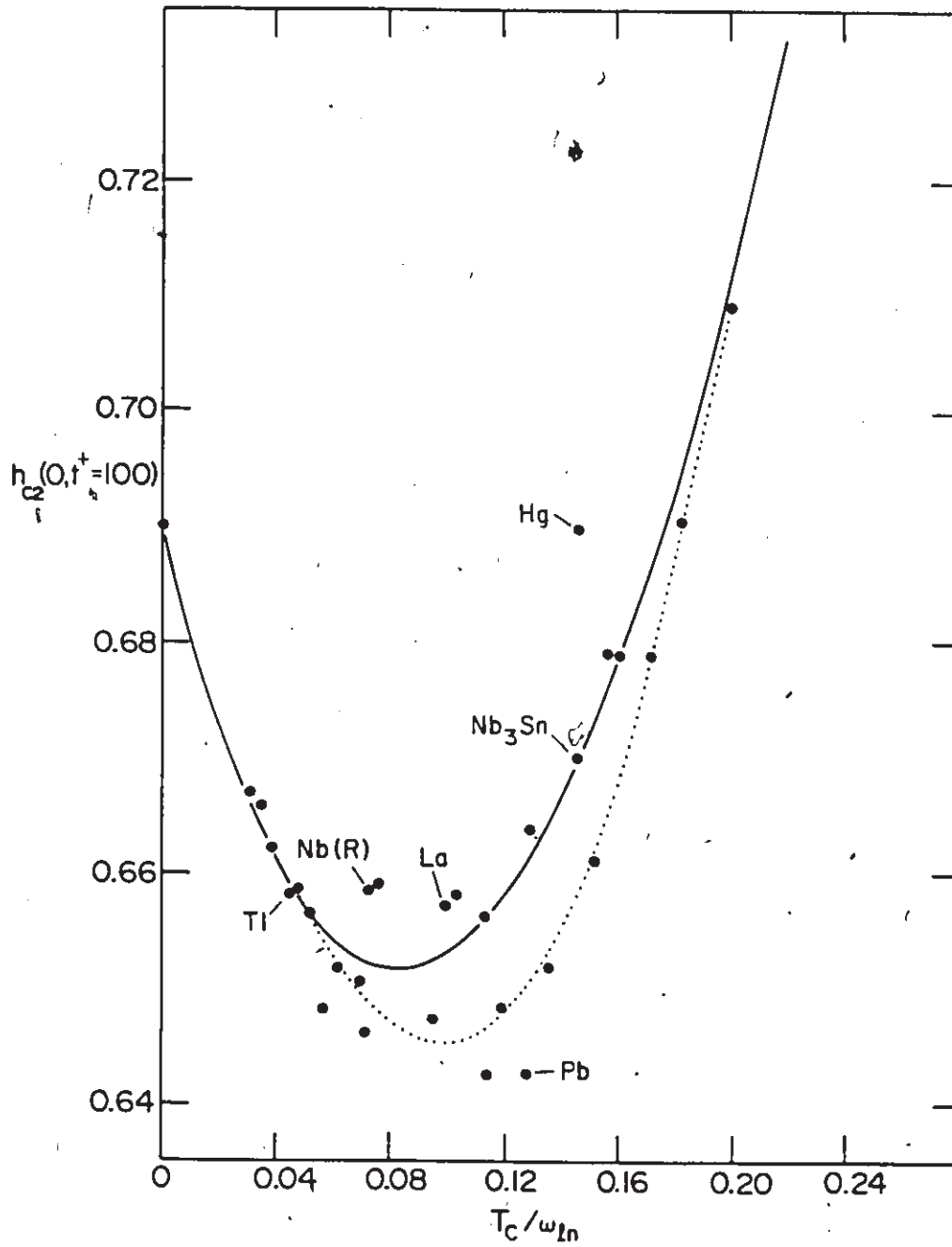
where $\alpha(t) \equiv e v_F^2 H_{c2}(T)$. The tildes indicate that the gaps and frequencies are renormalized quantities. It is perhaps useful to illustrate the dirty limit of these equations, first derived by Rainer and Bergmann.[31] Equation (2.47b) becomes dominated by the impurity term, which becomes large, so that the inverse tangent function in Eq. (2.47c) can be expanded so that $\chi(\tilde{\omega}_n) \approx \frac{1}{|\tilde{\omega}_n|} - \frac{1}{3}\frac{\alpha}{|\tilde{\omega}_n|^3}$. Upon substitution into Eq. (2.47a), we obtain,

$$\tilde{\Delta}_n = \pi T \sum_{m=-\infty}^{\infty} \left[\lambda(i\omega_m - i\omega_n) - \mu^* \theta(\omega_c - |\omega_m|) \right] \frac{\tilde{\Delta}_m}{|\tilde{\omega}_{0m}| + \rho} \qquad (2.48)$$

where the subscript "0" signifies that the impurity term is absent in Eq. (2.47b) and $\rho \equiv \frac{1}{3}\frac{ev_F^2}{\pi t^+} H_{c2}(T)$. Eq. (2.48) is in general a T_c equation with a pair-breaking effect (caused by ρ) present. Maki[60] has enumerated possible pair-breaking mechanisms. In the limit $\rho \to 0$, we recover the standard T_c equation obtained by linearizing Eq. (2.13). Eq. (2.48) is valid for all temperatures. It is customary to present results for the reduced upper critical field, $h_{c2}(0, t^+) \equiv \frac{H_{c2}(0, t^+)}{T_c|H'_{c2}(T_c, t^+)|}$. Strong coupling corrections are derived in Appendix B. We find, for the dirty limit ($t^+ \to \infty$), that there is considerable scatter in the numerical data (see Fig. 2.10). We have included curves which correspond to two very different sets of parameters, and neither do a very good job of describing the data (although they do describe the trend). Moreover, the curve corresponding to an Einstein model (with $\mu^* = 0$) differs significantly from the drawn curves. In a sense this failure is not too surprising, because the deviations from BCS being described are less than 7% in most cases. Formulas of this type are not expected to be better than 10% usually. Moreover, note that in the modest strong coupling regime the correction is negative, but then becomes postive as $T_c/\omega_{\ln}$ exceeds about 0.2 .

Figure 2.11   The reduced ratio $h_{c2}(0, t^+ = 0)$ vs. $T_c/\omega_{\ln}$. See Fig. 2.2 for identification of materials. The curve corresponds to $h_{c2}(0,0) = 0.727\left(1 - 2.7\left(\frac{T_c}{\omega_{\ln}}\right)^2 \ln\frac{\omega_{\ln}}{20 T_c}\right)$. Note that there is a very tiny initial decrease from BCS as $T_c/\omega_{\ln}$ is increased above 0.
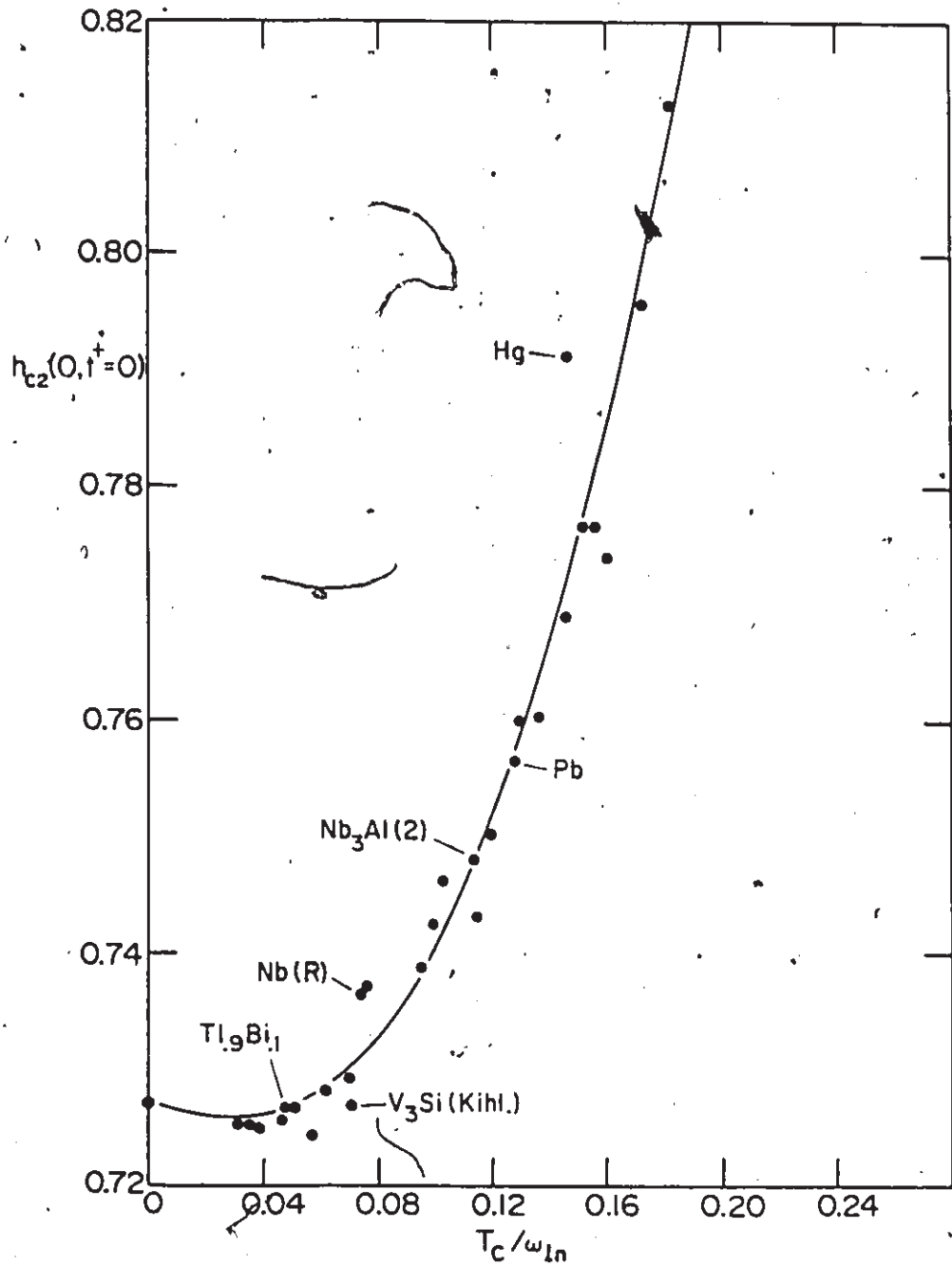
This is the first case of such behaviour encountered so far, and can be ascribed to the non-universal behaviour of the functional derivative[61] of $h_{c2}(0, \infty)$.

The situation is far better in the clean limit, as Fig. (2.11) illustrates. Here again the correction actually changes sign; however, the initial decrease in $h_{c2}(0, t^+ = 0)$ is sufficiently small (the functional derivative is almost universal) that the data follow a specific trend, which is well described by the expression:

$$h_{c2}(0, t^+ = 0) = 0.727\left(1 - 2.7\left(\frac{T_c}{\omega_{\ln}}\right)^2 \ln \frac{\omega_{\ln}}{20T_c}\right) \qquad (2.49)$$

Note that a linear term is not required for a good fit. Also, the trend is such that as $T_c/\omega_{\ln}$ increases beyond 0.2, $h_{c2}(0,0)$ is increasing. Hence, the deviations from the trend when amorphous materials (see Table 1) are used are quite large.

It is also useful to study the behaviour of the Ginzburg-Landau parameter $K_1(T, t^+) \equiv \frac{1}{\sqrt{2}}\frac{H_{c2}(T,t^+)}{H_c(T)}$, which is a measure of how strongly a type-II superconductor deviates from type-I superconductivity. In Fig. (2.12) the ratio $k(0, t^+ = 100\,\text{meV}) \equiv \frac{K_1(0, t^+=100)}{K_1(T_c, t^+=100)}$ is plotted versus $T_c/\omega_{\ln}$ for material spectra. We have also found that the curve

$$k(0, t^+ = 100) = 1.2\left(1 + 2.3\left(\frac{T_c}{\omega_{\ln}}\right)^2 \ln \frac{\omega_{\ln}}{0.2T_c}\right) \qquad (2.50)$$

describes the numerical data quite well. Note that although $k(0, 100)$ is obtained through $h_{c2}(0, 100)$, the inaccuracies present in Fig. (2.10) do not appear in Fig. (2.12). Also, we have found no need for a linear term in fitting the data in Fig. (2.12). The clean limit values of $h_c(0)$ derived in section (ii) of this chapter have been used, since it is easily shown that $h_c(0)$ is independent

Figure 2.12 The ratio $k(0, t^+ = 100\,\text{meV})$ vs. $T_c/\omega_{\ln}$. See Fig. 2.2 for identification of materials. The curve corresponds to $k(0, 100) = 1.2\left(1 + 2.3\left(\frac{T_c}{\omega_{\ln}}\right)^2 \ln\frac{\omega_{\ln}}{0.2T_c}\right)$. Note that a linear term is not needed for a good fit.
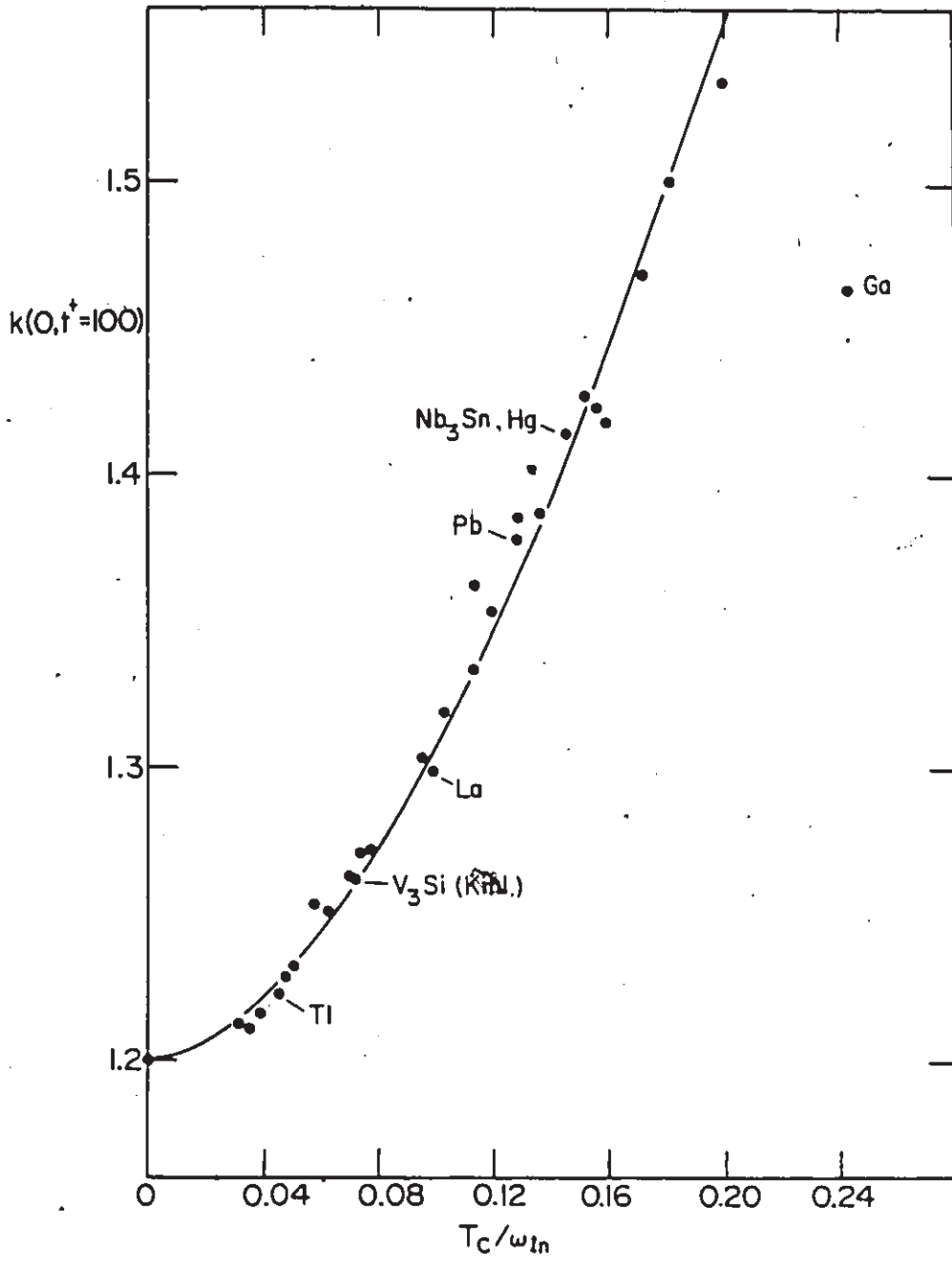
of impurity concentration. In Fig. (2.13) the numerical data for $k(0, t^+ = 0)$ have been plotted as a function of $T_c/\omega_{\ln}$. The expression

$$k(0, t^+ = 0) \doteq 1.26 \left(1 + 12 \left(\frac{T_c}{\omega_{\ln}} \right)^2 \ln \frac{\omega_{\ln}}{2T_c} \right) \qquad (2.51)$$

describes the data quite well, and, though not shown, the result for an Einstein mode is well described by Eq. (2.51) as well. This was also true for the dirty limit.

(v) Application of Strong Coupling Formulas

We conclude this section with some brief remarks about a straightforward application of the formulas derived in the previous sections. More will be said in Chapter 3. The most compelling evidence in favour of the Eliashberg theory of superconductivity is perhaps the inversion accomplished through the measurement of the current-voltage (I-V) characteristic in a tunnelling junction.[62,63] The idea is the following. A trial $\alpha^2 F(\omega)$ is assumed, and the tunnelling density of states $\frac{N(\omega)}{N(0)}$ calculated. It will in general disagree with the measured density of states. Hence, $\alpha^2 F(\omega)$ is adjusted in an iterative fashion until agreement is reached. This procedure is usually a very reliable determination of the microscopic function, $\alpha^2 F(\omega)$. The Coulomb pseudopotential μ^* is then obtained by some requirement, for instance, that the measured gap edge is obtained theoretically. In this fashion the microscopic parameters from which all superconducting properties can be calculated are known. This procedure may seem circular, except that the experimentally measured (I-V) characteristic is used only up to a frequency which is the maximum phonon frequency ($\omega_{\max}$) in the spectral function. However, once $\alpha^2 F(\omega)$ has been determined in this way, $\frac{N(\omega)}{N(0)}$ can be calculated beyond $\omega_{\max}$ and compared with experiment. The agreement for Pb, for instance, is

Figure 2.13 The ratio $k(0, t^+ = 0)$ vs. $T_c/\omega_{\ln}$. See Fig. 2.2 for identification of materials. The curve corresponds to $k(0,0) = 1.26\left(1 + 12\left(\frac{T_c}{\omega_{\ln}}\right)^2 \ln \frac{\omega_{\ln}}{2T_c}\right)$.
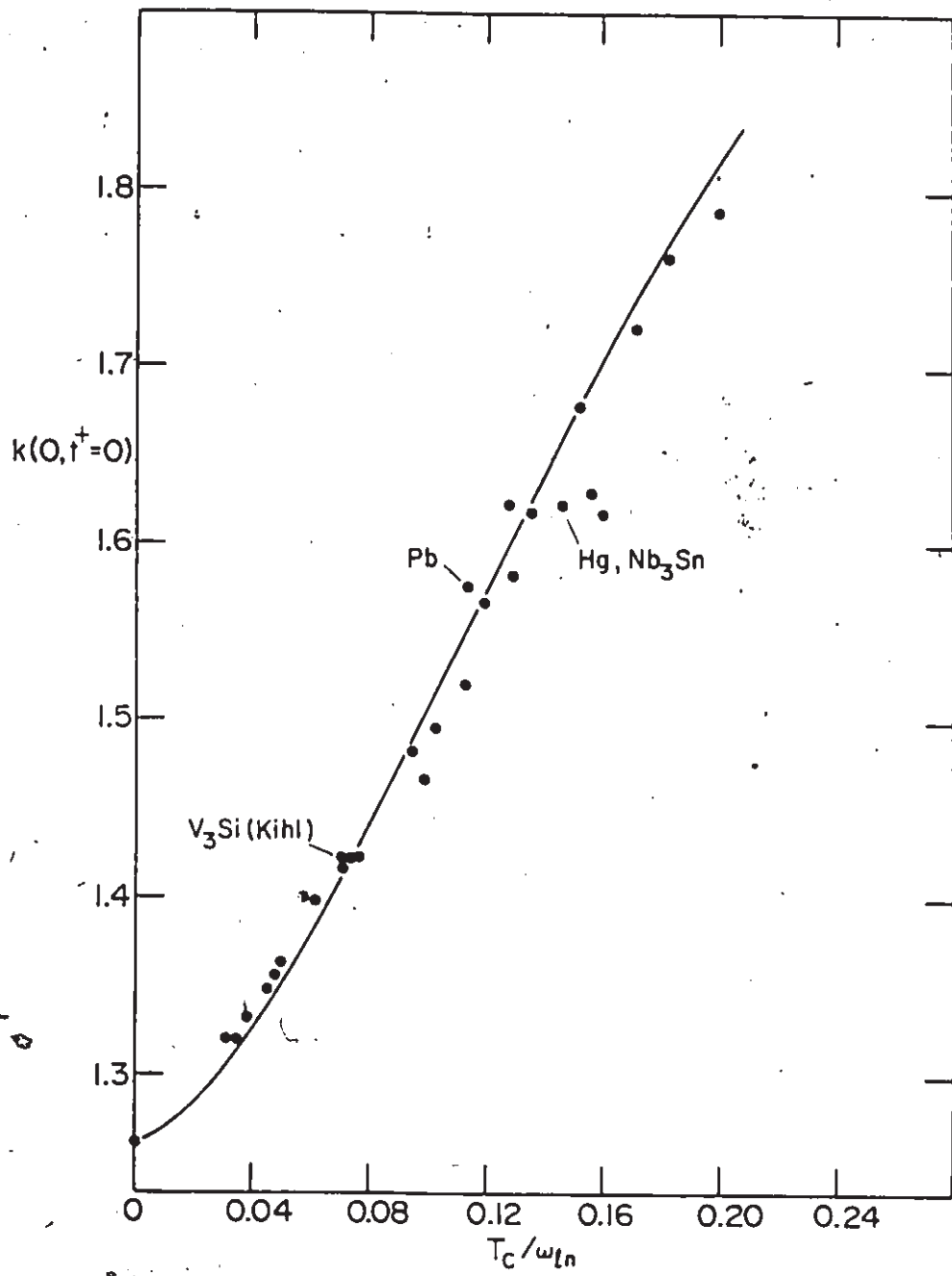
excellent.[62] That it is phonons which are mediating the interaction is supported upon comparison with measured phonon density of states obtained through neutron scattering experiments. We should also add that theoretical calculations[64-69] of $\alpha^2 F(\omega)$ are possible, and these generally agree fairly well with the measured functions, where comparison is possible.

Unfortunately, however, tunnelling junctions are sometimes difficult to fabricate, and hence for some materials an $\alpha^2 F(\omega)$ spectrum does not exist. Moreover, for the same reason, the gap edge is unknown as well. Hence, over the years many formulas[70-73] have been developed, which estimate the gap edge given thermodynamic properties, since these are often more easily measured. The formulas in the previous section allow much more accurate determinations. The parameter T_c/ω_{ln} is still unknown, but can be determined through one measurement, for example, of the specific heat jump, from Eq. (2.30). Eq. (2.32) then allows for an accurate determination of the gap ratio, $\frac{2\Delta_0}{k_B T_c}$. In Fig. (2.14) we plot $\frac{\Delta C}{\gamma_0 T_c}$ versus $\frac{2\Delta_0}{k_B T_c}$ for many crystalline spectra. The solid curve is determined through equations (2.30) and (2.32). Once again, amorphous materials tend to ruin the simple relation somewhat. What is clear however, is that with little error, the specific heat jump of a material uniquely determines the gap ratio, provided the material is crystalline, and has a value of $\frac{T_c}{\omega_{ln}} \lesssim 0.2$. A relaxation of this latter condition will cause some problems as will be seen later in Chapter 3. Similar remarks hold for the other properties discussed (with the exception of $h_{c2}(0, \infty)$). In particular a plot of $k(0,0)$ versus $\frac{2\Delta_0}{k_B T_c}$ is shown in Fig. (2.15). In this case the coefficient in the logarithm was fitted to 2, the same number as that used for $\frac{2\Delta_0}{k_B T_c}$ (see Eqs. 2.32 and 2.51).
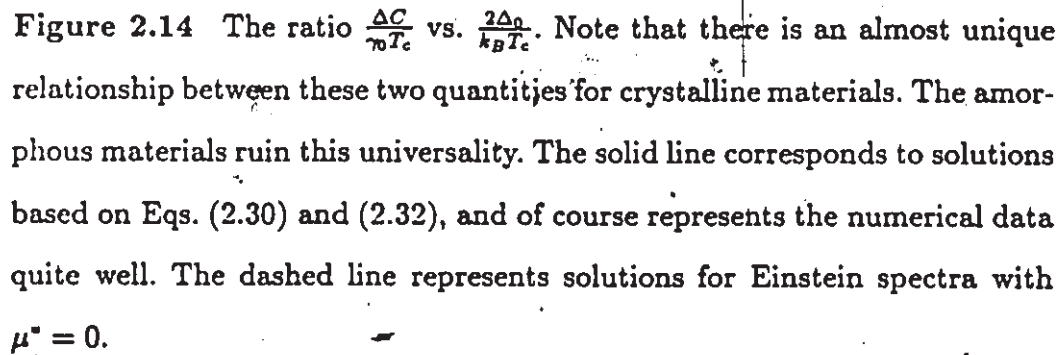
Figure 2.14   The ratio $\frac{\Delta C}{\gamma_0 T_c}$ vs. $\frac{2\Delta_0}{k_B T_c}$. Note that there is an almost unique relationship between these two quantities for crystalline materials. The amorphous materials ruin this universality. The solid line corresponds to solutions based on Eqs. (2.30) and (2.32), and of course represents the numerical data quite well. The dashed line represents solutions for Einstein spectra with $\mu^* = 0$.
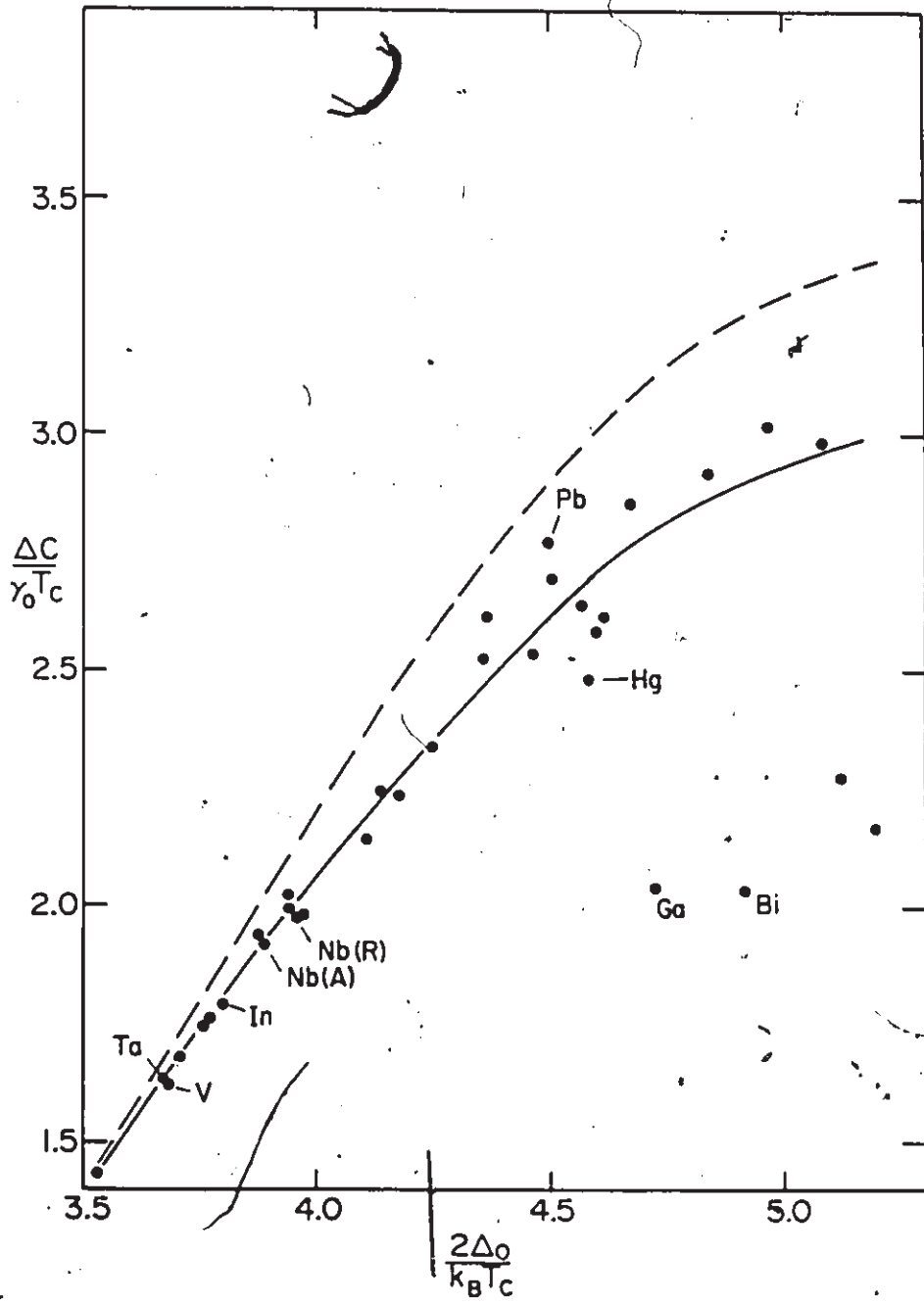
In this case, then, it is easy to derive the identity:

$$\frac{2\Delta_0}{k_B T_c} = 2.9\, k(0,0) - 0.15 \qquad\qquad (2.52)$$

which is also illustrated in Fig. (2.15). The agreement with numerical data of known materials is excellent. In Ref. 73 a similar type of analysis has allowed improvement of the Toxen[70] relation.

2.3 FUNCTIONAL DERIVATIVES AND OPTIMUM SPECTRUM ANALYSIS

(i) General Remarks

Does coupling to all phonon modes enhance T_c? This important question was first answered by Bergmann and Rainer[74] through a functional derivative calculation. They calculated $\frac{\delta T_c}{\delta \alpha^2 F(\Omega)}$ and found a positive definite curve which peaked at a frequency $\Omega^* \approx 7 T_c$ and fell to zero as $\Omega \to 0$ and $\Omega \to \infty$. Furthermore, they were able to prove that (for $\mu^* = 0$) $\frac{\delta T_c}{\delta \alpha^2 F(\Omega)}$ is always positive definite (regardless of what base spectrum one starts with). Hence, within linear response, since the change in T_c due to a small change in $\alpha^2 F(\omega)$ is given by

$$\Delta T_c = \int_0^\infty d\Omega\, \frac{\delta T_c}{\delta \alpha^2 F(\Omega)} \Delta \alpha^2 F(\Omega)\,, \qquad\qquad (2.53)$$

then T_c is always enhanced by additional coupling to any phonon mode. This important result also indicated that T_c could grow without bound, since increased coupling would always increase T_c. This will be shown more clearly later on. The limitation on T_c would have to come from lattice instability, for example, and not the theory of superconductivity.

Functional derviatives of other superconducting properties were calculated by Rainer and Bergmann,[31] by Carbotte and coworkers,[75-85,33,48,61]

Figure 2.15   The ratio $k(0, t^+ = 0)$ vs. $\frac{2\Delta_0}{k_B T_c}$. Eqs. (2.32) and (2.51) suggest that $\frac{2\Delta_0}{k_B T_c} = 2.9 k(0,0) - 0.15$. This curve is drawn with a solid line and describes the data extremely well.
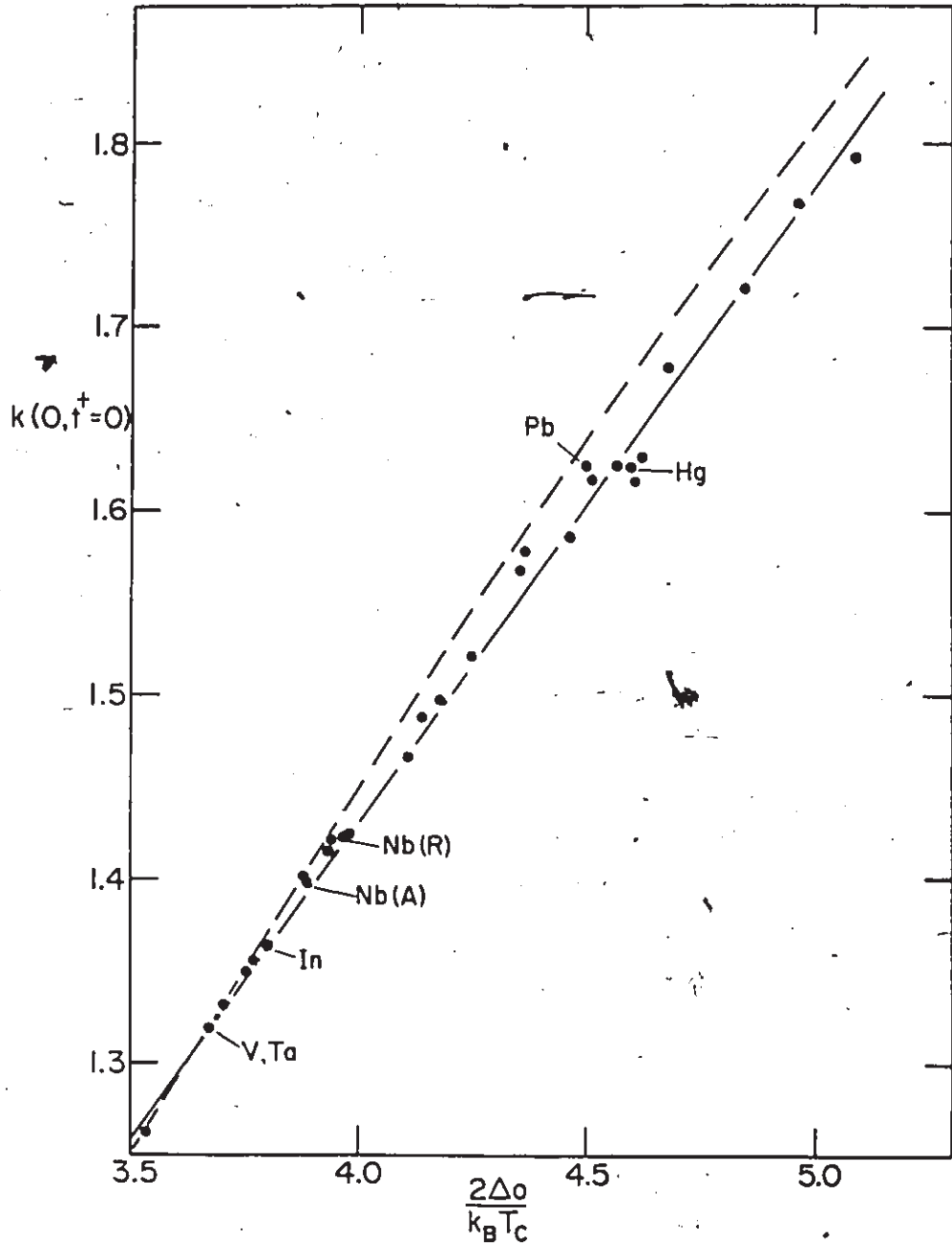
and by Sachdev *et al.* .[86] It is difficult to make general statements about these results. In all cases functional derivatives tend towards zero as the frequency becomes larger. Similarly, one would expect that as $\Omega \to 0$, $\frac{\delta Q}{\delta \alpha^2 F(\Omega)} \to 0$, where Q is any property. This can be looked upon as a consequence of Anderson's theorem,[51] since low frequency phonons behave like static impurities. There are, however, several exceptions to this rule. First, when anisotropy is included $\lim_{\Omega \to 0} \frac{\delta Q}{\delta \alpha^2 F(\Omega)} = \pm \infty$. This is due to the fact that anisotropy affects all superconducting properties. It is also well known that addition of impurities washes out anisotropy. Hence, adding zero frequency phonons (which is like adding impurities) causes a change in Q so that $\lim_{\Omega \to 0} \frac{\delta Q}{\delta \alpha^2 F(\Omega)} \neq 0$. In fact the behaviour at low frequency will in general be $\frac{\delta Q}{\delta \alpha^2 F(\Omega)} \sim \frac{1}{\Omega}$. The response calculated through a formula like Eq. (2.53) is not infinite however, since in physical systems, $\Delta \alpha^2 F(\Omega) \sim \Omega^n$ where $n = 2\,(1)$ for crystalline (amorphous) materials. A second exception arises because Anderson's theorem is not applicable to many superconducting properties (transport properties and upper critical magnetic fields). Many of these properties depend on impurity concentration so that for the same reason as above, $\frac{\delta Q}{\delta \alpha^2 F(\Omega)} \sim \frac{1}{\Omega}$ as $\Omega \to 0$. (Note however, that in the dirty limit, the functional derivatives will tend to zero once again, since adding dirt to an infinitely dirty material changes nothing.) Finally, the zero frequency behaviour can be introduced artificially, by defining a non-physical quantity. This can be exemplified by considering the specific heat jump, $\frac{\Delta C(T_c)}{\gamma_0 T_c}$. The denominator, $\gamma_0 T_c$ is often taken to be the normal state specific heat. However, Grimvall has shown that[45]

$$\gamma(T) = \gamma_B \left(1 + \int_0^\infty 2\frac{d\nu}{\nu} \alpha^2 F(\nu) Z\left(\frac{T}{\nu}\right) \right) \qquad (2.54)$$

Figure 2.16   Plot of the functional derivative of the specific heat difference, $\frac{\delta \frac{\Delta C(T)}{\gamma(T_c)T_c}}{\delta \alpha^2 F(\omega)}$ vs. ω/T_c for Pb, for various reduced temperatures. Note that as $\omega \rightarrow 0$, the derivative approaches zero as well, in contrast to the situation when γ_0 is used instead of $\gamma(T_c)$.
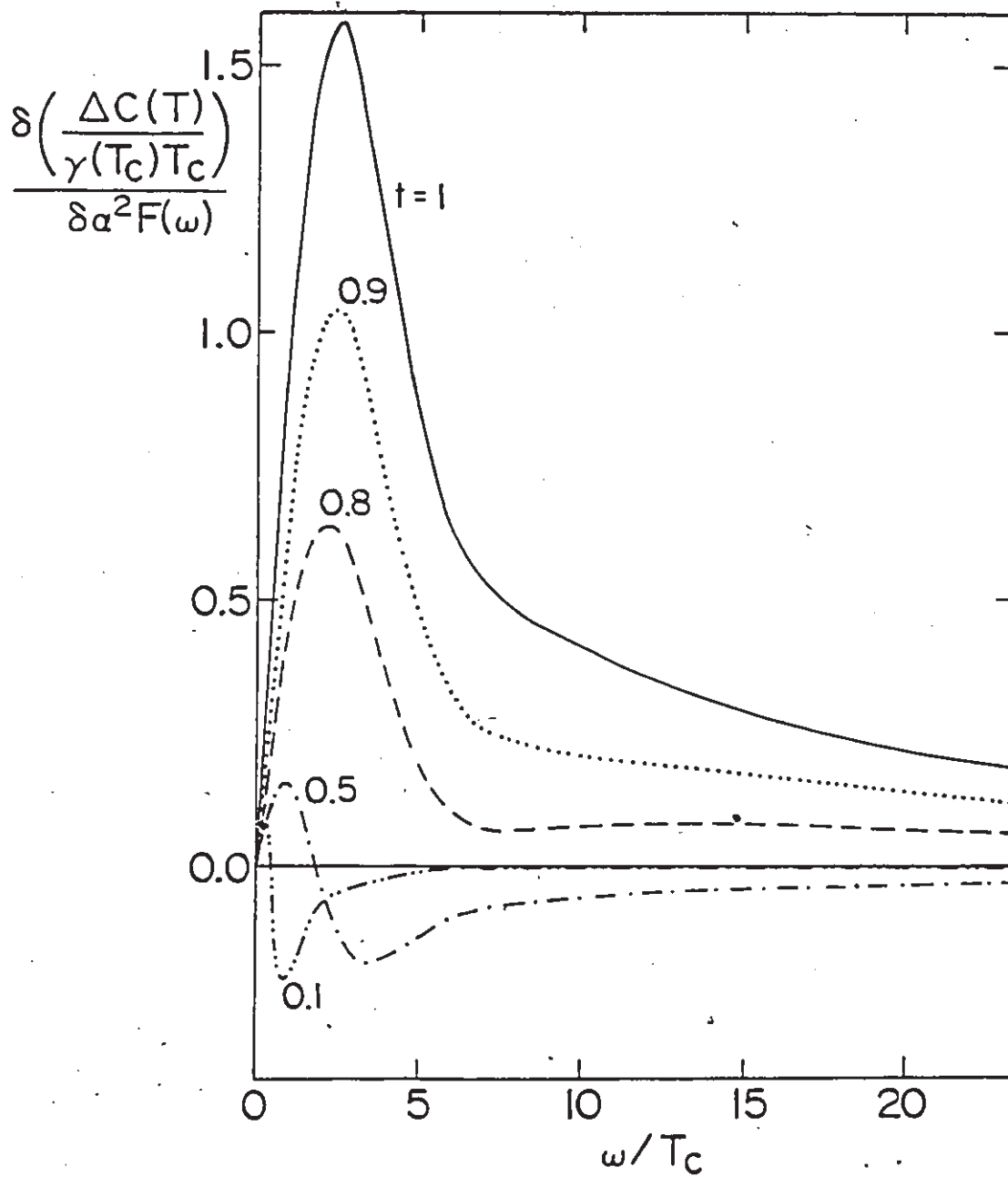
where

$$\gamma_B \equiv \frac{\gamma_0}{1+\lambda} = \frac{2}{3}\pi^2 N(0) \qquad (2.55)$$

is the band density of states. The universal function $Z\left(\frac{T}{\nu}\right)$ can be approximated by[87]

$$Z(x) \approx \Phi(9x^2) \quad , \quad \Phi(u) = \frac{1 + 2.6u + 16u^2}{1 + 65u^3} - 1.6\frac{u^3 + 4.1u^2}{u^4 + 9(u^3 + 1)} \cdot \qquad (2.56)$$

It is easy to show that $\lim_{\Omega\to 0}\frac{\delta\gamma(T)}{\delta\alpha^2 F(\Omega)} = 0$ whereas $\lim_{\Omega\to 0}\frac{\delta m}{\delta\alpha^2 F(\Omega)} \approx \frac{1}{\Omega}$. Hence $\frac{\delta\frac{\Delta C(T_c)}{\gamma(T_c)T_c}}{\delta\alpha^2 F(\Omega)}$, as illustrated in Fig. (2.16), goes to zero as $\Omega \to 0$, whereas the analogue calculated in Ref. 88, though similar in all other respects has the property: $\lim_{\Omega\to 0}\frac{\delta\frac{\Delta C(T_c)}{\gamma_0 T_c}}{\delta\alpha^2 F(\Omega)} = -\frac{a}{\Omega}$, where "$a$" is some constant. Some details of these calculations are included in Appendix D.

To illustrate the second exception,[61] Fig. (2.17) shows for two materials, Nb_3Sn and Nb, the derivative $\delta h_{c2}(0, t^+)$ where we adopt the notation[31] $\delta Q \equiv \frac{T_c}{Q}\frac{\delta Q}{\delta\alpha^2 F(\Omega)}$. Note that as the impurity concentration increases, the singularity near the origin is pushed into the origin. In Ref. 31, where the dirty limit is taken analytically, they find $\lim_{\Omega\to 0}\delta h_{c2}(0, \infty) = 0$.

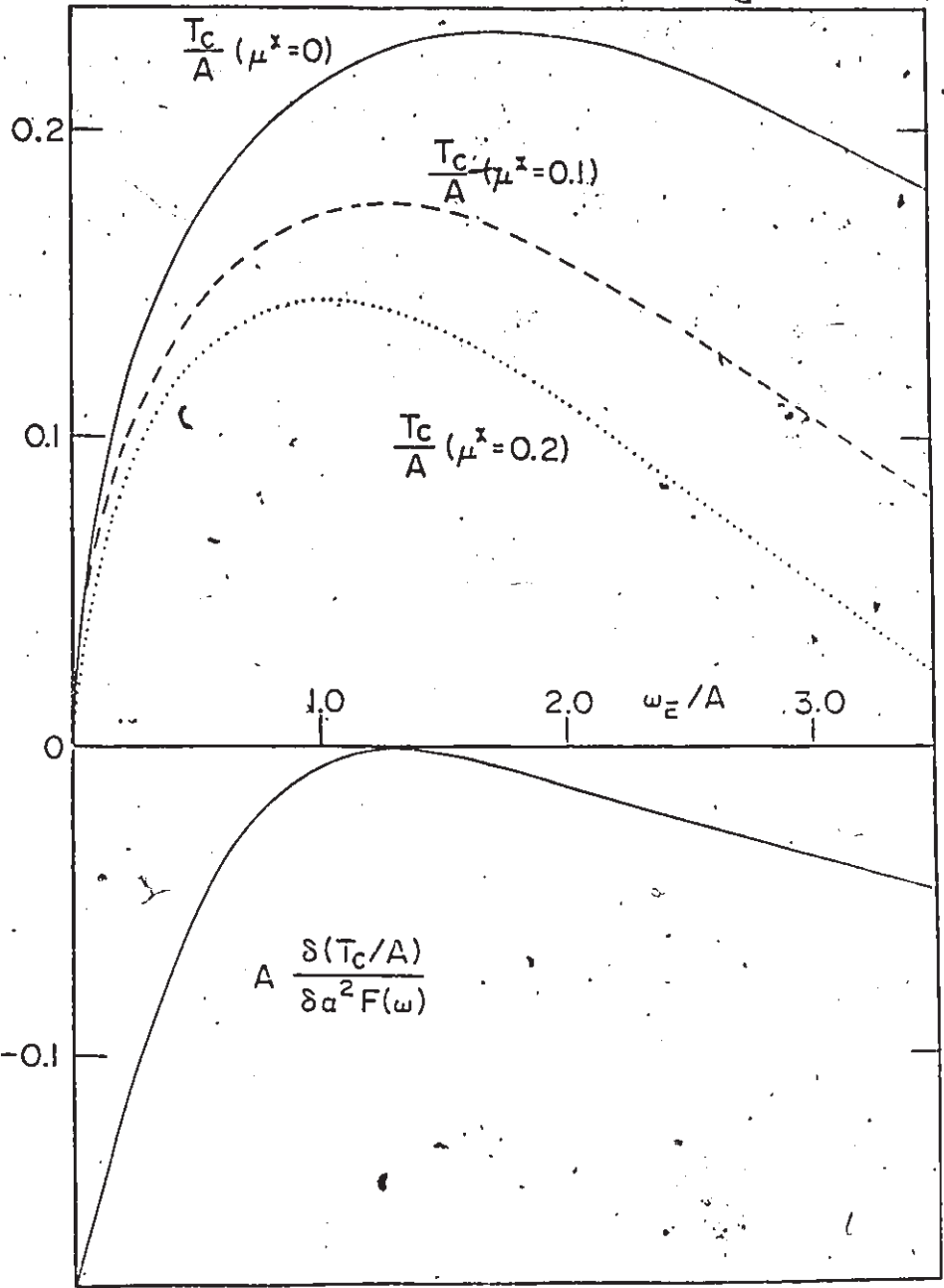## (ii) Relation to Strong-Coupling Corrections

Functional derivative calculations can aid in understanding why the strong coupling correction formulas of section 2 work well, but sometimes fail. Critical to the success of these formulas is that the functional derivative of a property has a simple, almost universal shape, as a function of $\frac{\Omega}{T_c}$, i.e. the shape does not depend strongly on what base spectrum is used. $\lambda^{\theta\theta}$ model calculations[80,83] have indicated that functional derivatives of some properties such as δT_c and $\delta\left(\frac{\Delta C}{\gamma_0 T_c}\right)$ are indeed well described by universal functions

Figure 2.17   Normalized functional derivative, $\delta h_{c2}(0, t^+)$, for $t^+ = 0.0$, 10.0, and 100.0 meV for (a) Nb_3Sn and (b) Nb. Note that the low frequency node approaches $\omega = 0$ as t^+ increases. In the extreme dirty limit of Rainer and Bergmann the curve goes to zero from above at $\omega = 0$.
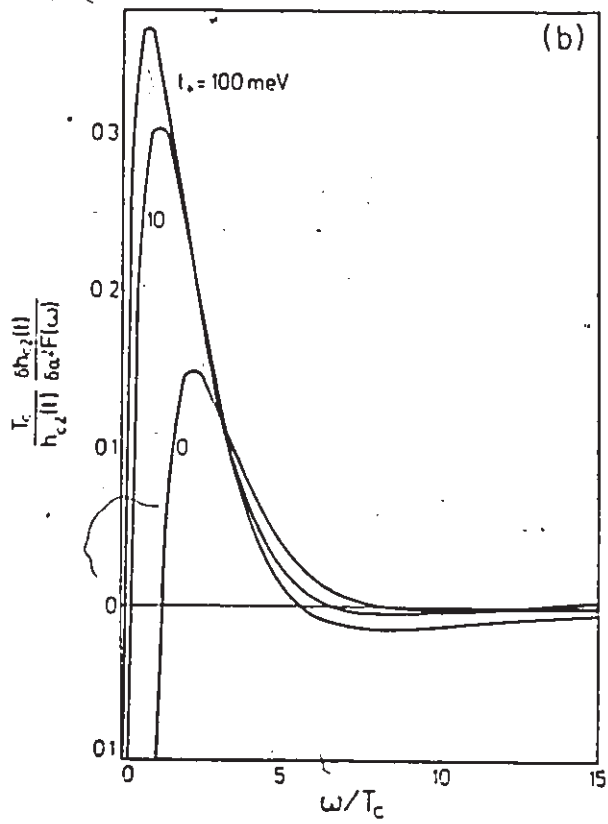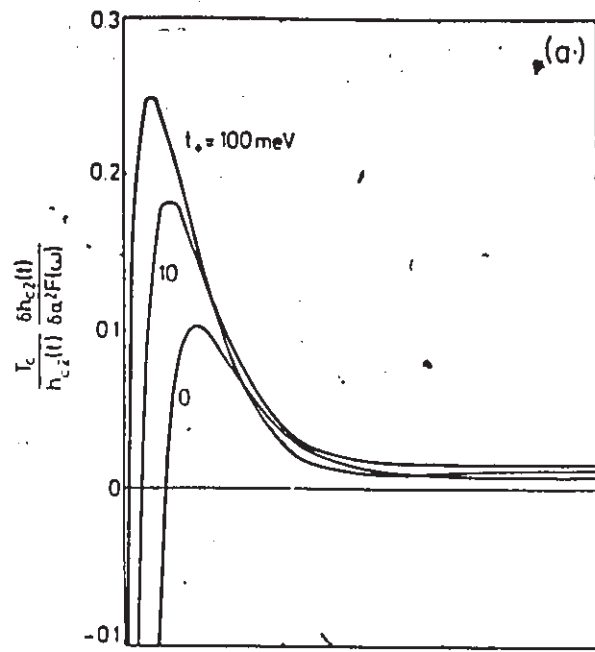
of $\frac{\Omega}{T_c}$. This results in the following simple picture. Imagine a spectrum described by an Einstein mode with frequency such that $\frac{\Omega_E}{T_c} \gtrsim 20$. This corresponds to the BCS limit $\left(\frac{T_c}{\Omega_E} \lesssim 0.05\right)$. With reference to Fig. (2.16) for the specific heat jump functional derivative, for example, we note that if we could reduce Ω_E with fixed area, we would find ourselves in a region where the functional derivative is larger (keep T_c fixed, to first order) so that the change in $\frac{\Delta C(T_c)}{\gamma_0 T_c}$ described by a formula like Eq. (2.53) is positive, and $\frac{\Delta C(T_c)}{\gamma_0 T_c}$ increases. Now one would calculate a functional derivative for this new spectrum. However, by hypothesis, the derivative is universal. The process can be repeated, with the effect that as $\frac{\Omega_E}{T_c}$ decreases $\left(\frac{T_c}{\omega_{1n}} \text{ increases}\right)$, $\frac{\Delta C(T_c)}{\gamma_0 T_c}$ increases in a somewhat smooth fashion. A breakdown will inevitably occur as we lower Ω_E since we will encounter the peak area, which is sensitive to details. However, a breakdown can occur for another reason. In Fig. (2.17), $\delta h_{c2}(0, t^+)$ is plotted for two different materials. The non-universality in the dirty limit is readily apparent. For Nb (a relatively weak coupler), the high frequency region of $\delta h_{c2}(0, 100\,\text{meV})$ is negative; for Nb$_3$Sn, however, it is positive. Hence, as Ω_E is lowered, we expect $h_{c2}(0, 100)$ to decrease. This indeed occurs $\left(\text{see Fig. 2.10 as } \frac{T_c}{\omega_{1n}} \text{ increases from 0}\right)$. However, at the same time the functional derivative is itself undergoing a significant change; it is beginning to change sign. Thus, at some point as Ω_E is lowered further, $h_{c2}(0, 100)$ should increase. This will continue to occur as Ω_E enters the peak region in the functional derivative. These statements are borne out by Fig. (2.10). However, since the functional derivative itself is dependent on the base spectrum used, we do not expect to see as smooth a trend, which is also the case.

Figure 2.18   Plot of T_c/A vs. ω_E/A for Einstein spectra located at frequency ω_E with weight A, for various μ^*. The curves are universal and all exhibit a maximum, indicating that an optimum spectrum exists. Also drawn is the functional derivative of T_c/A for the optimum Einstein spectrum for $\mu^* = 0.1$, with $\omega_E^* = 1.3$. Note that it is non-positive definite, obtaining a maximum value (0.0) at the location of the optimum spectrum. Clearly, T_c/A cannot be enhanced.

$\frac{T_c}{A} \ (\mu^x=0)$

0.2

$\frac{T_c}{A} \ (\mu^x=0.1)$

0.1

$\frac{T_c}{A} \ (\mu^x=0.2)$

1.0   2.0 ω_E/A 3.0

0

$A \ \dfrac{\delta(T_c/A)}{\delta a^2 F(\omega)}$

-0.1

(iii) Optimum Spectrum Analysis

The concept of an optimum spectrum began with Leavens.[27] He noted that for an Einstein spectrum, the T_c equation could be scaled such that

$$\frac{T_c}{A} = f\left(\frac{\nu_E}{A}\right), \tag{2.57}$$

where $f\left(\frac{\nu_E}{A}\right)$ is a universal function. Hence, for a given area, ν_E' could be adjusted so that T_c was maximized. Another way of saying this is that the Einstein mode was moved to a frequency at which the maximum of its functional derivative occurred. If the mode were anywhere else, T_c could be increased by moving it towards the peak. In Fig. (2.18) we have illustrated[46] the universal function $f\left(\frac{\nu_E}{A}\right)$ for various μ^*. To optimize $\frac{T_c}{A}$ (for say, $\mu^* = 0.1$) we could move an Einstein peak towards a value, $\frac{\nu_E^*}{A} \approx 1.3$, where $f\left(\frac{\nu_E}{A}\right)$ peaks. Also illustrated is $\delta\left(\frac{T_c}{A}\right)$ for this particular spectrum. It is non-postive definite. This is proof that we have achieved the optimum value for $\frac{T_c}{A}$.

This work has been extended to electromagnetic properties and thermodynamic properties by Blezius and Carbotte,[48] upper critical magnetic fields by Schossman *et al.* [89] and R. Akis *et al.* ,[90] and to $\frac{2\Delta_0}{k_B T_c}$ by Carbotte *et al.* .[91] The specific heat jump is interesting to study because $\frac{\Delta C(T_c)}{\gamma_0 T_c}$ does indeed have a maximum at finite frequency. We had noted already that Fig. (2.2) seemed to indicate that $\frac{\Delta C(T_c)}{\gamma_0 T_c}$ was saturating. In fact it is easy to show that as $\frac{T_c}{\omega_{1n}}$ increases, $\frac{\Delta C(T_c)}{\gamma_0 T_c}$ decreases from its optimum value and falls below the BCS value. In fact, as $\frac{T_c}{\omega_{1n}}(\lambda) \to \infty$, $\frac{\Delta C(T_c)}{\gamma_0 T_c} \propto \frac{1}{\lambda}$.[92] Moreover, the maximum value[88] is between 3 and 4, depending on μ^*. We should emphasize that such behaviour occurs only because γ_0 and not $\gamma(T_c)$ has been used in the ratio.

Figure 2.19   The functional derivative of the gap Δ_0 to critical temperature ratio, $\frac{2\Delta_0}{k_B T_c}$, for three delta function based spectrum labelled by normalized Eliashberg frequency ω_E/T_c. The upper curve for which $\omega_E/T_c = 4.7$ is characteristic of results found for real materials. As the Einstein frequency of the base spectrum is lowered towards zero, however, the curves distort in shape and become negative for much of the frequency range except for a positive peak at ever lower value of ω/T_c. The progression is for the functional derivative curve to become negative definite for $\omega_E/T_c = 0$ with maximum exactly at $\omega/T_c = 0$.
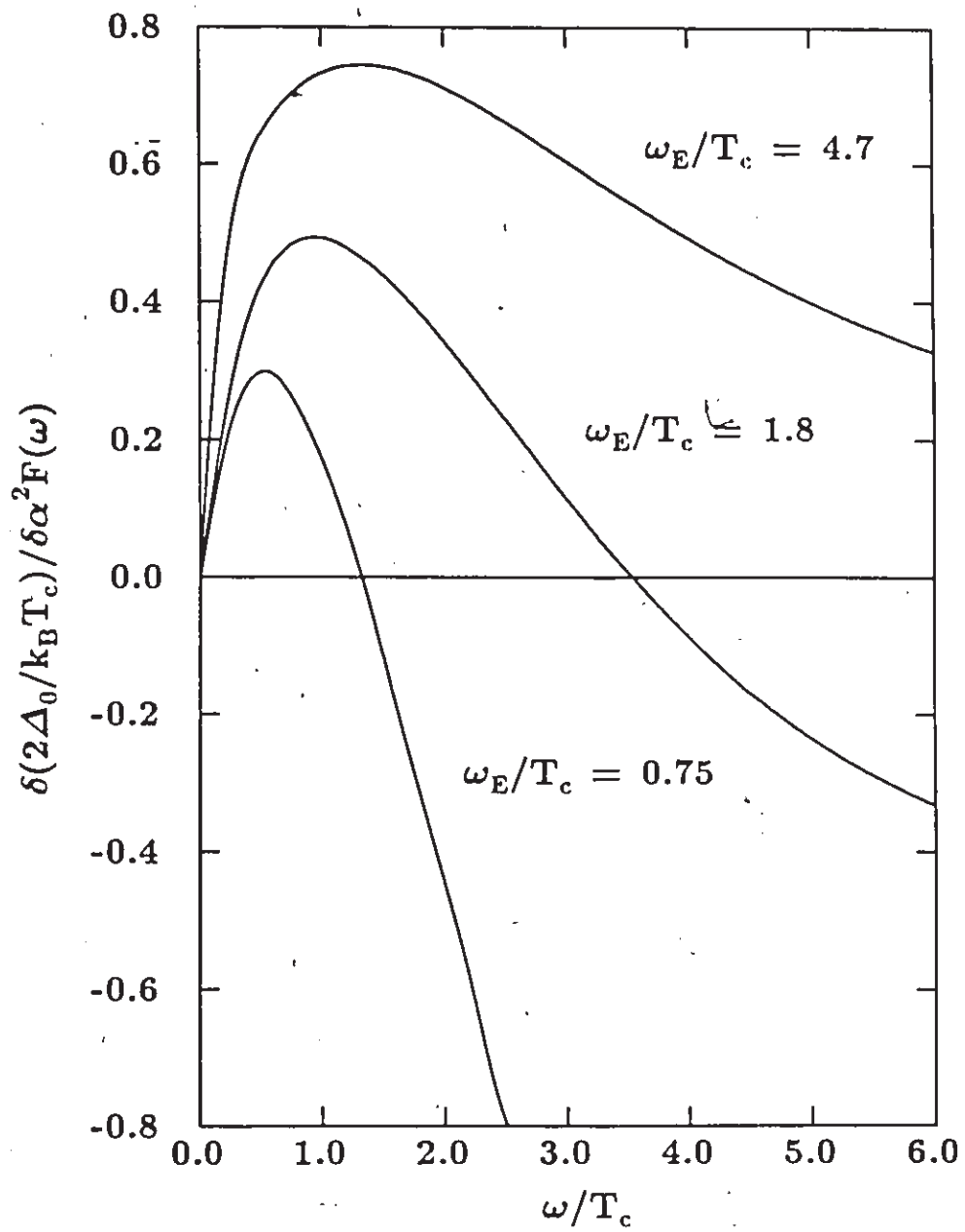
However, this form is the most useful since it is the one used in experimental analysis. The gap ratio $\frac{2\Delta_0}{k_B T_c}$ is of interest for the opposite reason. Upon lowering the frequency of the Einstein mode to the frequency of the maximum of its functional derivative, one finds, upon calculating the functional derivative of the new spectrum, that the peak has shifted to a lower frequency. This will continue to occur and in fact one must approach the limit $\frac{T_c}{\omega_{ln}}(\lambda) \to \infty$ in order to find the optimum $\frac{2\Delta_0}{k_B T_c}$. For $\mu^* = 0$, we find numerically[93] that the maximum value is about 12.8 . A sequence of functional derviatives for several Einstein modes is shown in Fig. (2.19). Note that the magnitude of the peak in the functional derivative is decreasing as the mode frequency is lowered, and will approach zero only as the frequency at which the peak occurs approaches zero.

(iv) A T_c Equation

In this final section we provide a suggestion for yet another T_c equation to add to the large list of existing formulas. Our motivation comes from the strong coupling corrections derived in section 2. It is clear there that $\frac{T_c}{\omega_{ln}}$ is an effective strong coupling parameter because it has minimized the scatter of data due to different spectral shapes. Hence, in analogy to those ratios, we can study the "ratio" $\frac{T_c}{A}$ as a function of $\frac{T_c}{\omega_{ln}}$. Demanding consistency, we can then solve for T_c in terms of A and ω_{ln}. Note that we bypass the usual parameter λ, in favour of these two. Of course in the case of an Einstein mode they are related, $\lambda = \frac{2A}{\omega_{ln}}$. For our purposes we fix ourselves at $\mu^* = 0.1$, and consider several material spectra. As first shown by Coombes and Carbotte,[43] under the transformation $\alpha^2 F(\nu) \to \alpha^2 F(\gamma\nu)$, $T_c \to \frac{T_c}{\gamma}$, $\omega_{ln} \to \frac{\omega_{ln}}{\gamma}$ and $A \to \frac{A}{\gamma}$.

Figure 2.20　Plot of T_c/A vs. T_c/ω_{ln}. The solid curve represents an Einstein spectrum with $\mu^* = 0.1$. Also illustrated are curves for various real spectra: Pb (- - - -), Nb ($\cdots$), V(– · – ·) and Nb$_3$Sn and Nb$_3$Al (– ·· – ··). Note that the curves describing spectra corresponding to realistic shapes practically form a universal curve. Eq. (2.61) fits the center of the band quite well.
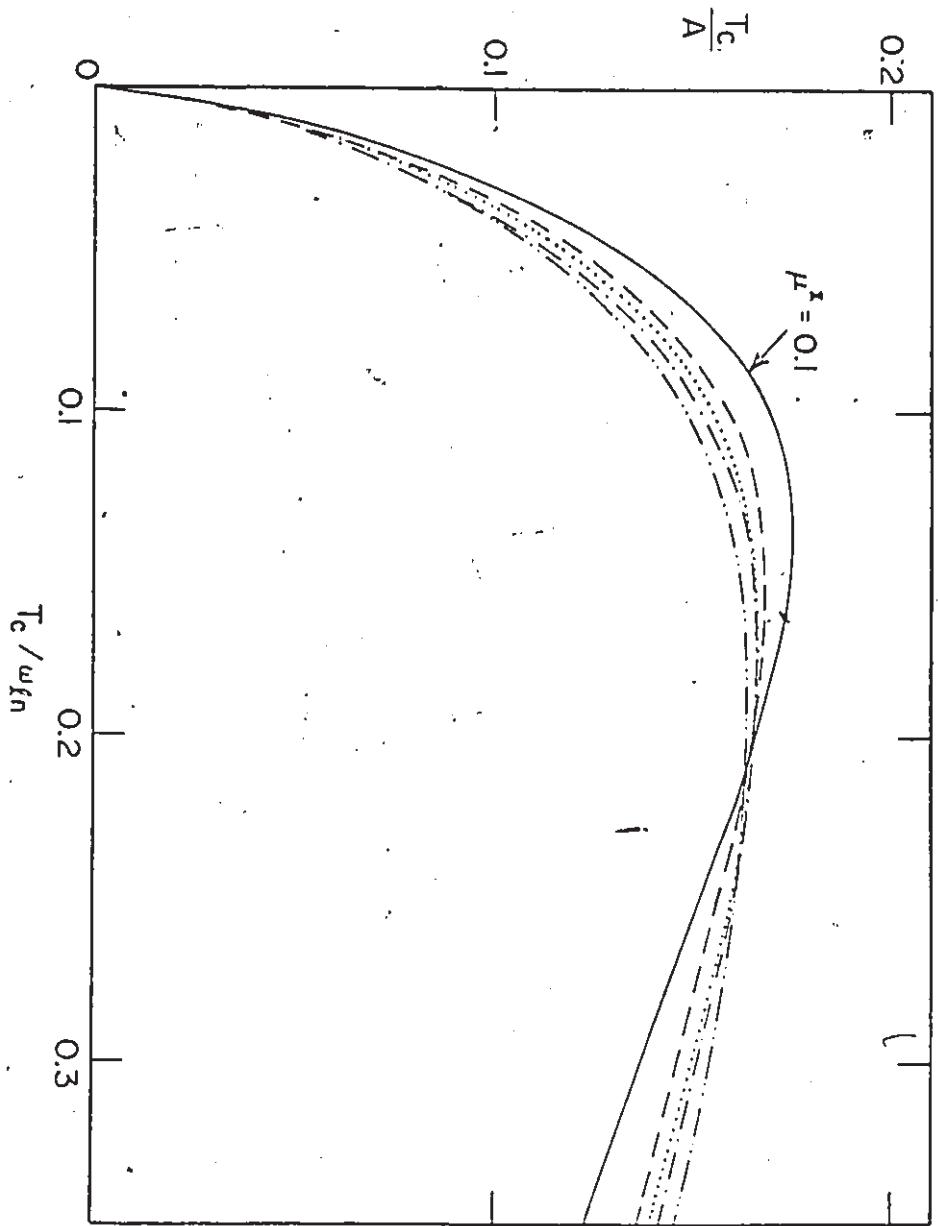
This enables us to plot curves for various spectral shapes over a whole range of $\frac{T_c}{\omega_{\ln}}$. These are illustrated in Fig. (2.20).[46] If we exclude the Einstein spectrum as well as the amorphous materials, then as anticipated the various curves tend to form a rather tight band so that $\frac{T_c}{A}$ is an almost universal function of $\frac{T_c}{\omega_{\ln}}$. What functional form should we attempt to fit? A motivation comes from the exact T_c equation. In Eq. (2.48), with $\rho = 0$, the transformation $\bar{\Delta}_m \equiv \frac{\Delta_m}{|\bar{\omega}_m|}$ yields the set of equations $\sum_{m=1}^{\infty} K_{nm}\bar{\Delta}_m = 0$, where

$$K_{nm} = \lambda(i\omega_m - i\omega_n) + \lambda(i\omega_m + i\omega_n) - 2\mu^* - \delta_{nm}\left[(2m-1) + \lambda(0) + 2\sum_{m'=1}^{m-1} \lambda(i2\pi T_{m'})\right].$$
(2.58)

The solution is $\det(K_{nm}) = 0$. Using a trial vector,[26] $\bar{\Delta}_m = \delta_{m1}$, we find

$$1 + 2\mu^* = \frac{2A\nu_E}{\nu_E^2 + (2\pi T_c)^2}$$
(2.59)

for an Einstein spectrum, which can be rewritten

$$\frac{T_c}{A} = a(\mu^*)\frac{\frac{T_c}{\omega_{\ln}}}{b^2 + \left(\frac{T_c}{\omega_{\ln}}\right)^2}.$$
(2.60)

A fit for $a(\mu^*)$ and b^2 tended to reproduce the curve in Fig. (2.20) obtained from an Einstein spectrum, which differs considerably from the band of curves corresponding to material spectra. The form,

$$\frac{T_c}{A} = \frac{0.053\left(\frac{T_c}{\omega_{\ln}}\right)^{1/2}}{\left(\frac{T_c}{\omega_{\ln}}\right)^2 + 0.10}$$
(2.61)

fits remarkably well, however. Given $\omega_{\ln}$ and A one can determine T_c on a pocket calculator from the simple equation:

$$y^5 + 0.1025y - 0.53\frac{A}{\omega_{\ln}} = 0,$$
(2.62)

where $y = \left(\frac{T_c}{\omega_{ln}}\right)^{1/2}$. We have restricted ourselves to $\mu^* = 0.1$. The fitted
coefficients would require some simple μ^* dependence in order to remove
this restriction. We have adopted a simpler approach for the purposes of
comparison. In practice, T_c and $\alpha^2 F(\nu)$ are given; μ^* is then calculated
for consistency. To test Eq. (2.61) we have regarded T_c , $\mu^* \equiv 0.1$, and
$B\alpha^2 F(\nu)$ as given for any material. The parameter B is then determined for
consistency. Table 2 illustrates the result. Another shortcoming of Eq. (2.61)
is that it has the incorrect asymptotic limit[26] for an Einstein spectrum. It
was shown in Ref. 26 that as $\lambda \to \infty$, $T_c \sim \sqrt{A\nu_E}$. Hence at some large value
of T_c/ω_{ln}, we expect Eq. (2.61) to break down.

Table 2.   Comparison of approximate T_c values obtained using Eq. (2.61)
with numerical T_c values, using $\mu^* = 0.1$. The areas and ω_{ln} values were
obtained from the spectral functions (see Appendix C). The agreement is
reasonably good considering that the entire range of possible strong cou-
pling values for conventional materials is covered. Note that Hg has the
worst agreement due to its spectral shape (i.e. low frequency phonons). The
agreement in the case of amorphous Bi is fortuitous.

Table 2

Material	T_c(meV)	T_c (approx.)	Diff. (%)
V	0.4621	0.5107	11
Ta	0.3862	0.3785	2
Sn	0.3233	0.3371	4
Tl	0.2034	0.2016	1
$Tl_{0.9}Bi_{0.1}$	0.1983	0.2024	2
In	0.2931	0.3068	5
Nb (Butler)	0.7931	0.7315	8
Nb (Arnold)	0.7931	0.7456	6
V_3Si_1	1.4741	1.3787	6
V_3Si (Kihl.)	1.3276	1.1699	12
Nb (Rowell)	0.7931	0.8255	4
Mo	0.7586	0.8185	8
$Pb_{0.4}Tl_{0.6}$	0.3966	0.3897	2
La	0.4340	0.4486	3
V_3Ga	1.2931	1.3357	3
Nb_3Al (2)	1.2069	1.2166	1
Nb_3Ge (2)	1.7241	1.0312	6
$Pb_{0.6}Tl_{0.4}$	0.5086	0.4992	2
Pb	0.6198	0.5882	5
Nb_3Al (3)	1.6121	1.6657	3
$Pb_{0.8}Tl_{0.2}$	0.5862	0.5747	2
Hg	0.3612	0.4210	17
Nb_3Sn	1.5603	1.5864	2
$Pb_{0.9}Bi_{0.1}$	0.6595	0.6527	1
Nb_3Al (1)	1.4138	1.4725	4
Nb_3Ge (1)	1.7241	1.7647	2
$Pb_{0.8}Bi_{0.2}$	0.6853	0.6904	1
$Pb_{0.7}Bi_{0.3}$	0.7284	0.7364	1
$Pb_{0.65}Bi_{0.35}$	0.7716	0.7867	2
$Pb_{0.5}Bi_{0.5}$	0.6026	0.5944	1
Ga	0.7379	0.8413	14
$Pb_{0.75}Bi_{0.25}$	0.5957	0.6023	1
Bi	0.5267	0.5281	~0

LEAF 68 OMITTED IN PAGE NUMBERING.

FEUILLET 68 NON INCLUS DANS LA PAGINATION.

Chapter 3

High T_c Oxides

3.1 HISTORICAL INTRODUCTION

The "modern" (as of Nov., 1987) era of high T_c superconductivity began early in 1986, when J. G. Bednorz and K. A. Müller[1] succeeded in obtaining the resistivity curve displayed in Fig. 3.1, which showed an onset critical temperature of near 30 K. The sample they worked with was reported to be $Ba_x La_{5-x} Cu_5 O_{5(3-y)}$, but was in fact multi-phased and polycrystalline. Later that year several groups[2,3,4] had substituted Sr for Ba, and T_c had increased to the 40 K range. Meanwhile, the superconducting phase in the original compound was found to have the composition, $La_{2-x} Ba_x CuO_{4-y}$ with x varying from near zero to approximately 0.3 .

Inspection of the periodic table illustrates that Strontium ($A = 38$), Barium ($A = 56$) and Lanthanum ($A = 57$) form three corners of a square. The fourth corner is occupied by Yttrium ($A = 39$). Perhaps motivated by

69

Figure 3.1   Plot of resistivity vs. temperature by J.G. Bednorz and K.A. Müller for a multiphase sample of Ba-La-Cu-O obtained early in 1986. For low current densities the onset is clearly above 30 K.
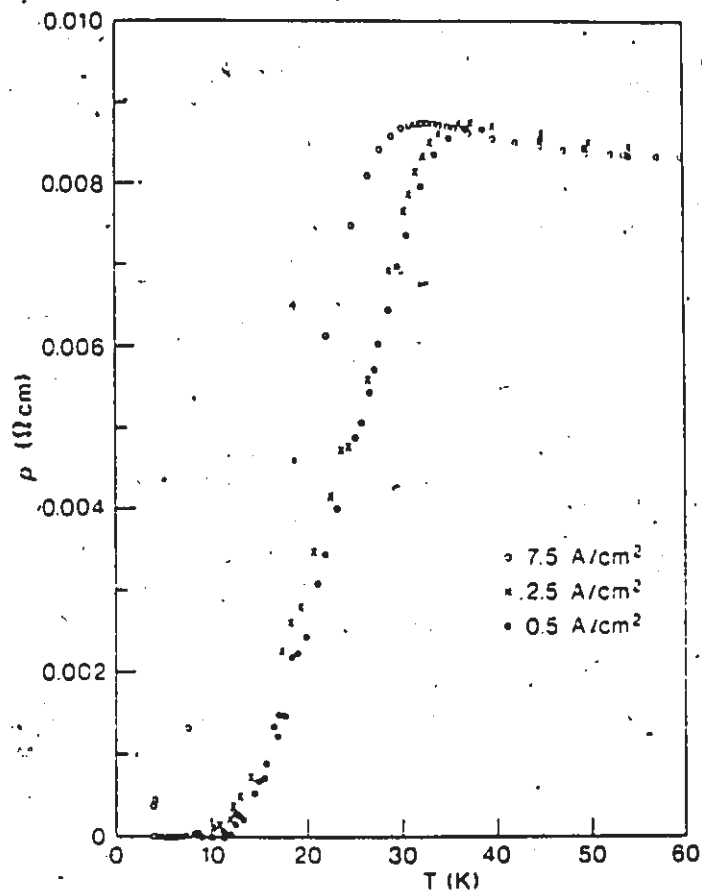
this simple observation, the Houston-Alabama group[5] suceeded in obtaining 90 K superconductivity in a mixed phase Y-Ba-Cu-O compound system in early February, 1987. (The superconducting phase was later to be identified as $YBa_2Cu_3O_{7-y}$). Even before the elements of the compound were disclosed in the 2 March issue of Physical Review Letters, reports had appeared in the People's Daily in China that $T_c \sim 100\,K$ had been observed in a Y-Ba-Cu-O system. As a result of this report, researchers in both the United States and Japan succeeded in producing the 90 K superconductor as well, in February. Once the Letter appeared on 2 March, the material was being synthesized in practically every lab in the world. This discovery has a special significance in that the liquid Nitrogen temperature barrier (77 K) had been broken, and some experiments were already being carried out without the use of liquid Helium. Since these "early" days, some published and many unpublished reports have appeared, claiming T_c 's of significantly higher value than 100 K. However, at the time of this writing, the general concensus appears to be that the maximum reproduceable T_c is $T_c \sim 100\,K$.

The "old age" era of high T_c superconductivity actually began in the mid-1960's when M. Cohen[94] suggested that superconductivity would occur in semiconducting materials. The first oxide superconductor, $SrTiO_3$ ($T_c < 1\,K$) was subsequently discovered, to be followed by truly "high T_c" superconducting oxides, $LiTi_2O_4$ [95] and $BaPbBiO_3$,[96] discovered in the mid-1970's. These compounds had $T_c \sim 13\,K$, which is rather high, considering the low carrier concentrations in these oxide superconducting materials. This latter fact motivated a great deal of interest in the oxide superconductors, culminating in the discoveries of 1986.

All of the developments described so far have been experimental. At the same time, many theoretical proposals[11] were put forth to explain the high T_c oxides. The numerous proposals can probably be classified under two general headings: BCS-like and non-BCS-like. The first category includes any theory in which the superconducting electrons are thought to pair via the exchange of some virtual boson; this boson has been idenitified in conventional materials to be the phonon. We have regarded the proposals that come under this heading as involving different mechanisms, in the sense that the boson which mediates the electron-electron attraction differs from mechanism to mechanism. Possibilities included plasmons, spin fluctuations, excitons, demons, *etc.* The second category is of course quite vague in name, but is perhaps best exemplified by the resonating valence bond (RVB) theory first proposed by Anderson[97-99] in 1973. In these theories electron-electron correlations are deemed to be so important in the normal state, that a BCS description based on quasiparticles in the normal state is inappropriate. In the RVB, for example, it is thought that a superconducting condensate occurs through a Bose condensation of charge carriers, which are bosons because of the environment they find themselves in (resonating valence bonds). The RVB theory has only recently received much attention, and so suffers the disadvantage of being in its infancy, whereas theories of the first type have been relatively well studied. In the remainder of this thesis we will discuss only theories of BCS-type.
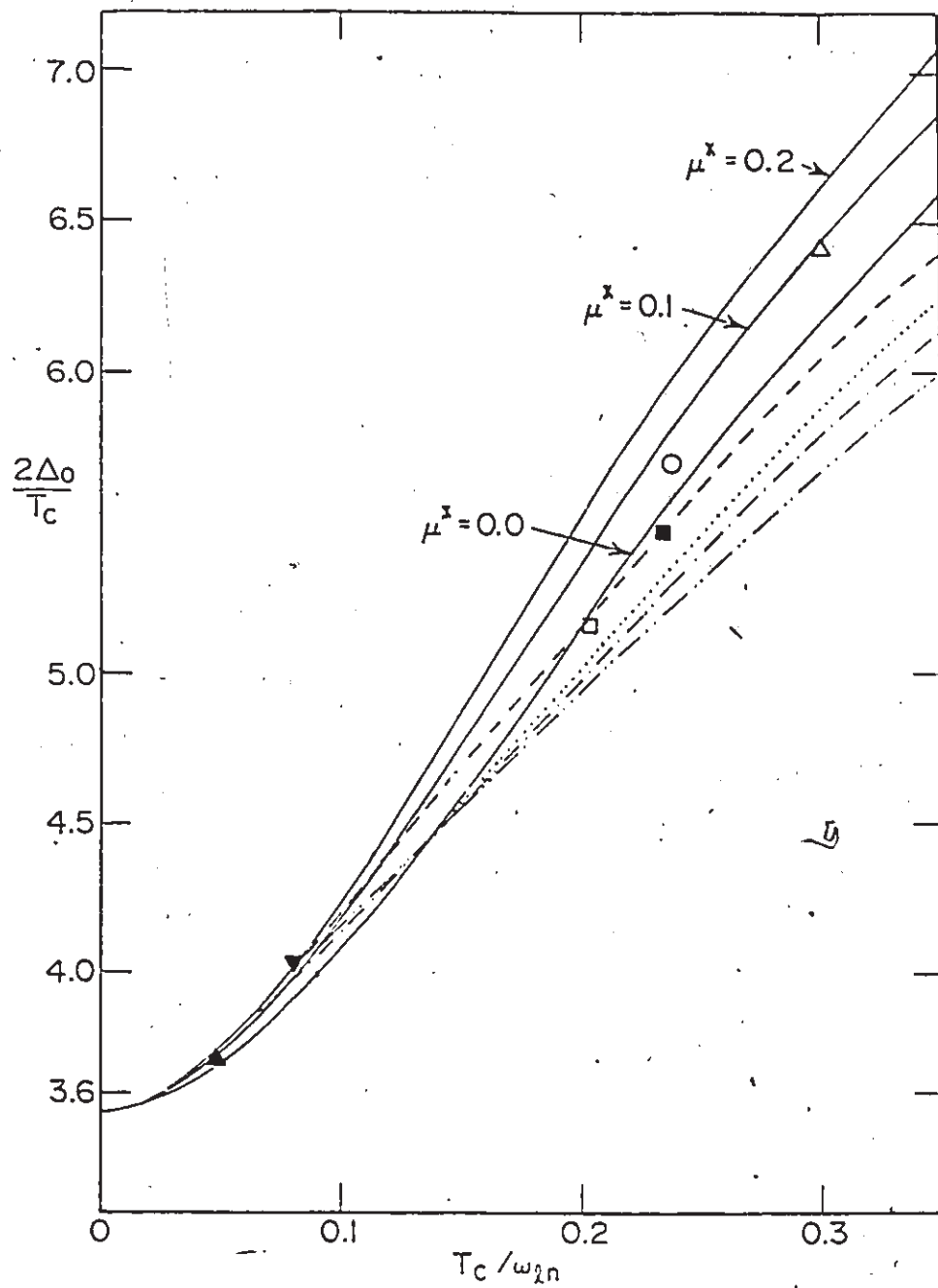
3.2   GENERAL REMARKS

Eliashberg theory is based on the calculation of the electron self-energy due to the emission and absorption of some boson (see Fig. 1.2).

Hence, Eliashberg theory in principle is applicable to all BCS-type theories. However, the infinite sum of diagrams indicated in Fig. 1.2 is only a subset of all possible diagrams. The neglect of all other diagrams ("vertex corrections") is justified by Migdal's theorem[16] which ensures that contributions from these corrections are $O\left(\frac{m}{M}\right)^{1/2}$ (or $O\left(\frac{\omega_D}{E_F}\right)$) where m is the electron mass and M is the ion mass. This approximation is extremely accurate in the case of phonon mechanism, since $\omega_D \ll E_F$. However, other boson mechanisms include "electronic" bosons whose characteristic frequency is $O(E_F)$ and hence the use of Migdal's theorem will be suspect. One can nonetheless proceed to investigate the consequences[100] of Eliashberg theory in the same spirit that resulted in BCS theory. For the time being, experiment may be able to decide on the correctness of this approach.

What is the need to introduce another mechanism? As has already been mentioned in Ch. 2, Eliashberg theory imposes no limit on the maximum attainable T_c . However, crude estimates based on the phonon mechanism have been proposed in the past[101,102] yielding $T_c^{max} \lesssim 35\,\mathrm{K}$ due to lattice instability. Hence, observation of a high T_c alone justifies the search for an alternative mechanism. At the same time one must be wary of maximum T_c arguments. They have been wrong before and they will possibly be wrong again.

The standard argument in favour of some (usually) higher frequency electronic boson mechanism uses Eq. (2.19a) for T_c . It is clear that for the same value of λ, an increase in ω_c (to $O(E_F)$) from ω_D will result in a substantial increase in T_c . Again, one must be wary with this naive argument for reasons already mentioned.

Figure 3.2 Plot of $\frac{2\Delta_o}{k_B T_c}$ vs. T_c/ω_{ln}. The solid curves are for Einstein spectra with $\mu^* = 0.0, 0.1$, and 0.2. These curves are universal, and indicate that, for given T_c/ω_{ln}, μ^* causes $\frac{2\Delta_o}{k_B T_c}$ to increase. Also shown are various scaled real spectra, with $\mu^* = 0.1$. They are universal in the sense that they represent spectra which have been scaled by an arbitrary amount along the frequency axis. Note that they form a rather tight band as a function of T_c/ω_{ln}. The materials are Pb($- - -$), Nb($\cdots$), V($- \cdot -\cdot$), and Nb$_3$Sn and Nb$_3$Al($- \cdots - \cdots$). The various symbols represent the δ-function spectra described in Table 3 as follows: $\blacktriangle$, $\lambda = .75$; $\blacktriangledown$, $\lambda = 1.0$; $\blacksquare$, $\lambda = 2.6$; $\bigcirc$, $\lambda = 2.3$; $\square$, $\lambda = 2.9$; $\triangle$, $\lambda = 4.4$.

The figure plots $\frac{2\Delta_0}{T_c}$ (vertical axis) versus $T_c/\omega_{\ell n}$ (horizontal axis). Curves are labelled $\mu^{x} = 0.2$, $\mu^{x} = 0.1$, and $\mu^{x} = 0.0$. Vertical axis values shown: 7.0, 6.5, 6.0, 5.0, 4.5, 4.0, 3.6. Horizontal axis values shown: 0, 0.1, 0.2, 0.3.

With knowledge of the value of T_c only, there is little one can determine. Fig. 2.20 illustrates this point clearly. One can obtain T_c of any magnitude simply by adjusting ω_{ln} and A independently. A system with a given T_c could then be described by parameters corresponding to any point along the universal curve in Fig. 2.20 . However, Fig. 3.2 illustrates the gap ratio $\frac{2\Delta_0}{k_B T_c}$ vs. $\frac{T_c}{\omega_{ln}}$ for a variety of spectral shapes and μ^*. This figure emphasizes what was already discussed in Ch. 2 and Ref. 46; $\frac{2\Delta_0}{k_B T_c}$ is an almost universal function of $\frac{T_c}{\omega_{ln}}$, regardless of shape. Given $\frac{2\Delta_0}{k_B T_c}$, figures (2.20) and (3.2) together provide us with the data required to determine ω_{ln} and A, the fundamental parameters characterizing $\alpha^2 F(\nu)$ (recall $\lambda \sim \frac{2A}{\omega_{ln}}$). In Table 3 we have included several model spectra consisting of Einstein spectra and the scaled Pb spectrum. Several possibilities are illustrated; the first entry, for example, would be representative of an $\alpha^2 F(\nu)$ which is comprised largely of phonons which represent the oxygen breathing modes in these oxides. The strong coupling parameter, $\frac{T_c}{\omega_{ln}}$ is then very small, and $\frac{2\Delta_0}{k_B T_c}$ (and other

Freq. of δ-fns.	Area (meV)	λ	T_c/ω_{ln}	$\frac{2\Delta_0}{k_B T_c}$
60	23.1	.75	.05	3.7
30,60	20.0	1.0	.08	4.0
10,60	22.7	2.6	.23	5.5
10,20,30	18.4	2.3	.20	5.2
10,20	19.0	2.9	.24	5.6
10	21.9	4.4	.30	6.4
Pb($\gamma = 1$)	32.3	12.4	.62	8.0
Pb($\frac{1}{3}$)	18.3	2.3	.21	5.2
Pb($\frac{1}{5}$)	18.1	1.4	.12	4.4

Table 3   Summary of model spectra used in Figs. (2.2) and (3.23).

superconducting ratios) attains a value close to its BCS value. Model spectra with even higher modes will yield BCS results, and would be representative of say, an exciton model. Models with even lower frequency phonon modes are representative of $\alpha^2F(\nu)$'s with strongly renormalized oxygen breath- ing modes, as well as spectra with acoustic modes in a more conventional frequency regime. One immediate consequence of these models is the $\frac{2\Delta_0}{k_BT_c}$ attains values ≈ 5 or higher. It is seen how an accurate measurement of $\frac{2\Delta_0}{k_BT_c}$ can decide between these two possibilities. Moreover, the area required remains more or less constant at $A \sim 20$ meV. This value is not so unreasonable, though it is unprecedented; the A15 compounds have values of $A \lesssim 13$. However the A15's are known to have large densities of states. Thus, using Eq. (2.19a) one sees that the electron-phonon coupling must be very large. These remarks have been made with respect to the 35 K superconductor. The effects become even more pronounced for the 95 K superconductor. It can be seen for example, on the basis of Fig. 3.2 that a BCS gap measurement rules out the phonon mechanism completely, since phonon modes generally cannot exceed 100 meV. A phonon mechanism would invariably require large values of $\frac{2\Delta_0}{k_BT_c}$, and an area $A \gtrsim 50$ meV would be required. The possibility of a lattice instability would have to be seriously considered.

The amount of information one can glean without a knowledge of the underlying spectral function is somewhat limited, although if one is fortunate, it may be possible to pin down the characteristic boson frequency, which is of obvious significance. In the next section we will delineate the quantitative predictions based on Weber's calculated $\alpha^2F(\nu)$ spectrum[69] and then return to further considerations based on model spectra.

3.3   PROPERTIES OF $La_{1.85}Sr_{0.15}CuO_4$

Based on the first-principles energy band results of L. Mattheiss,[103] W. Weber[69] has calculated an $\alpha^2F(\nu)$ spectrum for $La_{2-x}Sr_xCuO_4$ (LSCO) in the framework of the non-orthogonal tight binding theory of lattice dynamics developed by himself and C. M. Varma.[68] This framework is highly sophisticated and had already proven to be quite successful in describing the A15 compounds. In LSCO he found that the material bordered on a lattice instability, achieving, with $\mu^* (\omega_c = 540\,meV.) = 0.13$, a $T_c \sim 35 - 40\,K$. The spectrum is illustrated in Fig. 3.3. Prominent features are (i) a very large peak at $\omega \sim 10\,meV$, and (ii) coupled phonon modes extending out to beyond $80\,meV$. The high frequency range is due to the low oxygen mass. Using this spectrum we have calculated many superconducting properties, based on the isotropic Eliashberg equations.[104] For most properties no adjustable parameters are involved. Some properties, however, simply scale with either $N(0)$ or v_F^2 (a notable exception is $H_{c2}(T)$ with Pauli limiting, although the dependence is weak). The scaling enables us to choose values of $N(0)$ and v_F for the purpose of presentation. As experimental determinations or theoretical estimates of these quantities improve in the future, one can easily incorporate the improvements into the results we present without further numerical work. The reduced properties will remain unchanged. Calculated ratios are presented in Table 4 (see last column). There is nothing unusual about the calculated values. The various properties have values characteristic of the strong coupling regime as described in Ch. 2. Unfortunately, nature has conspired to be somewhat secretive about the high T_c oxides. Properties involving γ_0 have not been measured because γ_0 is difficult to obtain.

Figure 3.3   The electron-phonon spectral density $\alpha^2 F(\omega)$ for LSCO cal-
culated by Weber. Some of the parameters corresponding to this spectrum
are: $A = 22.04$ meV, $T_c = 3.09$ meV, $\omega_{ln} = 13.876$ meV, $\lambda = 2.606$, and
$\mu^*(\omega_c = 450$ meV$)= 0.13$.
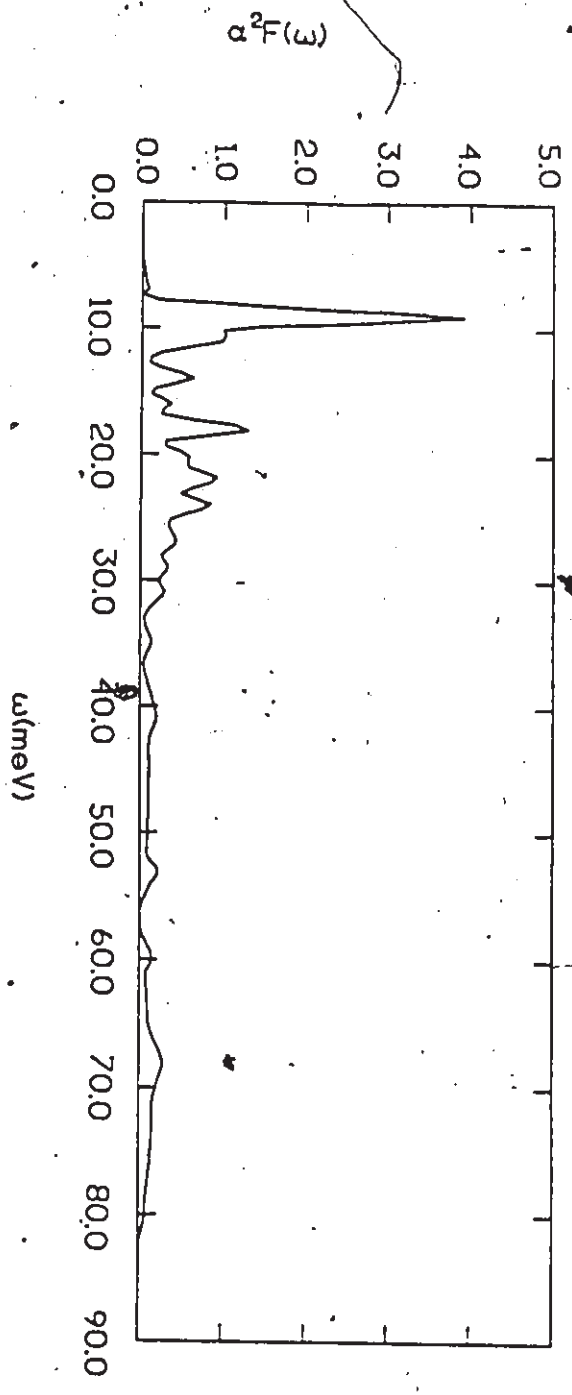
T_c is sufficiently high that the normal state specific heat is dominated by the phonon contribution. Furthermore, the critical magnetic fields are so large that at low temperatures it is impossible to force the material to become normal, and hence measure γ_0. Quantities involving upper critical magnetic fields suffer from the same difficulty; such a high field is unattainable at low temperatures. The data obtained on electromagnetic properties is insufficiently accurate for the ratios defined to be evaluated experimentally. Finally, our last hope, the gap ratio, has been measured by many groups (see Table 5). Unfortunately, there remains considerable controversy about

Property	BCS	$\delta^b = 0.50$	$\delta = 0.25$	$\delta = 0.0$
$\frac{2\Delta_0}{k_B T_c}$	3.53	4.0	4.4	5.3
β_{ox}	0.0	0.14	0.24	0.28
$\frac{\Delta C(T_c)}{\gamma T_c}$	1.43	1.7	2.1	2.8
$\frac{\gamma T_c^2}{H_c^2(0)}$	0.168	0.153	0.140	0.124
$h_c(0)$	0.576	0.55	0.52	0.48
$h_{c2}(0,0)^*$	0.727	0.77	0.81	0.88
$h_{c2}(0,100)$	0.693	0.715	0.74	0.78
$k(0,0)$	1.26	1.40	1.56	1.83
$k(0,100)$	1.20	1.30	1.42	1.63
$\frac{\xi(0,t^+=0)}{\xi(T_c,t^+=0)}$	1.33	1.28	1.24	1.21
$\frac{y_L(0)}{T_c\|y_L'(T_c)\|}$†	0.50	0.43	0.37	0.29
$\frac{y_l(0)}{T_c\|y_l'(T_c)\|}$	0.376	0.335	0.30	0.24

Table 4 Summary of theoretical results obtained for $\delta = 1.0$ (pure exciton or BCS), $\delta = 0.0$ (pure phonon) and $\delta = 0.25, 0.5$ (combined phonon-exciton).

$^b\delta \equiv \lambda_{ex}/\lambda_{tot}$

$^* y_i(T) \equiv \lambda_i^{-2}(T) \quad i = \begin{cases} l & \text{(local limit)} \\ L & \text{(London limit)} \end{cases}$

† no Pauli limiting

the experimental value of the gap in $La_{1.85}Sr_{0.15}CuO_4$.

Far-infrared measurements tend to give values of the gap ratio close to the BCS value (with one exception) whereas tunneling measurements give values which are rather higher, although some measurements now give values closer to BCS. Both types of mesaurements display somewhat anomalous features: the far-infrared measurements give considerable absorption below twice the gap edge where there should be none. Moreover, the presence of phonons obscures the analysis somewhat. The tunneling measurements tend to be quite erratic, even from measurements at different spots on the same sample. Anomalous structure is also seen in the I-V characteristic, about which we will have more to say later. The theoretical value of 5.3 obtained from Weber's spectrum would certainly be compatible with some of the tunneling measurements.

The specific heat jump, ΔC, has also been measured by several groups, and as is apparent from Table 5, there is considerable disagreement for this measurement as well. It is clear that there is considerable sample dependence in these measurements. This is also exemplified by the fact that the normal state resistivity is (anomalously) linear in temperature down to T_c although in some measurements there is an upturn before the sample goes superconducting. It should be kept in mind that almost all experimental results reported here were obtained from measurements on polycrystalline samples. There is also increasing evidence that while the superconductivity is bulk, it is by no means 100 % bulk. There seem to be both metallic and insulating components present. Moreover, the granularity of the samples varies from sample to sample, and this feature is known to affect many superconducting properties.[105-107] Nonetheless, we can proceed to investigate the consistency

of the data in the following fashion. On the basis of the results quoted in Table 5, we choose a value of $\frac{\Delta C(T_c)}{T_c} = 17$ mJ/ mole K^2. Using the calculated value $\frac{\Delta C}{\gamma T_c} = 2.8$ (see Table 4), we find $\gamma_0 = 6.1$ mJ/ mole K^2. Equation (2.55) allows us to extract the band density of states. A more useful formula to use is:

$$N(0)\left[\frac{\text{states}}{\text{eV} - \text{f.u.} - \text{spin}}\right] = \frac{0.212}{1+\lambda}\gamma\left[\frac{\text{mJ}}{\text{mole K}^2}\right].\qquad(3.1)$$

We find $N(0) = 0.36\frac{\text{states}}{\text{eV}-\text{f.u.}-\text{spin}}$. This value should correspond to the band structure density of states. We have assumed that the important electron-electron correlation effects have been included in the band structure calculation. The band structure density of states for La$_2$CuO$_4$ has been obtained by several groups.[183] There is general agreement that $N(0) \approx 0.65\frac{\text{states}}{\text{eV}-\text{f.u.}-\text{spin}}$. Freeman et al.[183b] and Papaconstantopoulis et al.[183c] have used a rigid band model to include the effect of doping. They find for La$_{1.85}$Sr$_{0.15}$CuO$_4$, $N(0) = 0.9\frac{\text{states}}{\text{eV}-\text{f.u.}-\text{spin}}$ and $N(0) = 1.1\frac{\text{states}}{\text{eV}-\text{f.u.}-\text{spin}}$ respectively. Hence there is a discrepancy of a factor of 3 for $N(0)$. It may be argued that this rules out such a large value of λ for La$_{1.85}$Sr$_{0.15}$CuO$_4$. However, as has been alluded to already, the measured value of $\frac{\Delta C}{T_c}$ may be lower than the "ideal" value due to effects of granularity, anisotropy, and a significant non-superconducting fraction. We note that Phillips et al.[179g] have attempted to account for this latter effect.

The upper critical magnetic field has also been measured near T_c by many groups. Again as Table 5 indicates there is significant variation not only from sample to sample, but also depending on whether the onset or midpoint of the resistivity drop is used. Strictly speaking the onset point should be used, but the polycrystalline samples and the possible fluctuation

Table 5   Summary of Data for LSCO

$\frac{\Delta C(T_c)}{T_c} \frac{mJ}{moleK^2}$	$\frac{2\Delta_o}{k_B T_c}$	$\mid H'_{c2}(T_c) \mid \frac{T}{K}$	$\lambda_L(0)A$	$N_B(E_F)$[*]
7.6 ± 1.8[a]	2.4[a]	$2.2 - 5.0$[a]	~ 2500[a]	0.66[a]
20 ± 5[b]	$1.6 - 2.7$[b]	1.51[b]	~ 2000[b]	0.6 (0.95[b])[b]
16.8[c]	2.5[c]	1.7[c]	~ 2650[c]	0.65[c]
8.8[d]	$2.9 - 4.5$[d]	$2.7 - 6.0$[d]		0.82[d]
$22 - 26$[e]	$5.2 - 9.1$[e]	$0.3 \parallel, 4 \perp$[e]		0.62 (1.08[†])[e]
11[f]	< 4.5[f]	1.8[f]		0.83[f]
9.9[g]	$5 - 8.7$[g]	2.13[g]		1.03[g]
10 ± 2[h]	$4.07 - 4.78$[h]	$1.3 - 4.0$[h]		
6.5[i]	$4.5 - 5.8$[i]	2[i]		
	$3 - 6$[j]	2.1 ± 0.1[j]		
	$3.5 - 4.0$[k]	2.2[k]		
	$0.7 - 2.7$[l]	$2.0 - 3.7$[l]		
	$8 - 18$[m]			
	2.6[n]			
	1.3 ± 0.2[o]			
	5[p]			
	4.7[q]			
	7 ± 2[r]			
	$2(c - axis)$[s]			

See Refs. (179-183) for columns (1-5), respectively.

*   units are: $\frac{states}{eV-Cu-atom-spin}$

♭   with doping: $x = 0.15$

†   with doping: $x = 0.15$

Table 6   Summary of Data for YBCO

$\frac{\Delta C(T_c)}{T_c}$ $\frac{mJ}{moleK^2}$	$\frac{2\Delta_o}{k_BT_c}$	$\mid H'_{c2}(T_c)\mid \frac{T}{K}$	$N_B(E_F)$ $\frac{states}{eV-Cu-atom-spin}$
18[a]	3.2 ± 0.3[a]	1.3(50%)[a]	1.5[a]
15.5[b]	3.5 ± 0.3[b]	3(10%)[a]	0.56(0.43*)(0.26†)[b]
13[c]	2.0[c]	2.5(50%)[b]	1.1(0.92 − 0.97♭)[c]
1.32[d]	3.5[d]	1.2(?)[c]	
16[e]	3.7 − 5.6[e]	2.4(?)[c]	
7[f]	1.6 − 3.4[e]	2.3 ∥, 0.46 − 0.71 ⊥[d]	
11 ± 2[g]	2.3 − 3.5[f]	4.6(10%)[e]	
23 ± 5[h]	2.5 − 4.2[g]	0.6(0%)[e]	
13[i]	1.3 ± 0.2[h]	1.25(?)[f]	
11.3[j]	3.3[i]	3.8(50%)[g]	
20[k]	3.2[j]	1.0(1%)[g]	
	11[k]	2.35(50%)[h]	
	4.5 − 6.0 ⊥[l]	0.37 ⊥ (50%)[i]	
	3.9 − 4.8 ∥[l]	1.95 ∥ (50%)[i]	
	4.8[m]	2.2(50%)[j]	
	3.8 − 4.5[n]	1.8(50%)[k]	
	10[o]	2.2 − 3.6(50%)[l]	
	13[p]	1.75(50%)[m]	
	3.9[q]	5.3(10%)[m]	
	3.2 ± 0.4[r]	3 ∥, 0.9 ⊥ (100%)[n]	
	7 − 13[s]	1.27(50%)[o]	
	3.5[t]	4.7(90%)[p]	
	5 ± 0.2[u]	1.9 ± 0.2(?)[q]	
	3.4 ± 1.5[v]	1.3(50%), 5(onset)[r]	
	4.8 ± 0.5[w]	1.9(50%)[s]	
	∼ 8[x]	2.9(50%)[t]	
	7.5[y]	5.3(90%)[t]	
	3.9[z]	3 ± 0.3(?)[u]	
	3.8[aa]		

See Refs. (184-187) for columns (1-4), respectively.

*$y = 0.1$,   †$y = 0.2$,   ♭$y = 0.5$

above T_c complicate this simple prescription. Moreover, anisotropy now plays a more significant role, as very recent measurements[181e] on single crystals indicate. We proceed nonetheless with the isotropic theory, noting that simple modifications are required to treat an anisotropic electron gas.[108]

Table 4 indicates that the reduced upper magnetic field changes very little from the clean to dirty limit, so that an estimate can be obtained for the upper critical magnetic field at $T = 0$. We find $H_{c2}(0) \approx 40$ T. Pauli limiting is an effect which takes into account the fact that in high magnetic fields there is an energy gain due to the Zeeman splitting of the up and down spin electrons, which drives the superconductor normal sooner than it would otherwise. The effect at these fields is small and amounts to a lowering of $H_{c2}(0)$ of less than 5%.

It is not possible to verify the measurements near T_c directly, since, as the line following Eq. (2.47c) indicates, the Fermi velocity v_F is required. One can of course deduce a value for v_F, by the reverse procedure. Taking $H'_{c2}(T_c) = -1.5\frac{T}{K}$ obtained by Kwok et al.,[181b] we deduce ⟩ $\langle v_F \rangle = (0.3\text{–}0.7)\times 10^6$ m/s where the range of values indicates the dependence on impurity content (clean-dirty). The measured slope can also be used to give an independent estimate of the Sommerfield γ_0, through the relation[57]

$$H'_{c2}(T_c) = -4.48 \times 10^4 \, \gamma_0 \, \rho_{\Omega\,cm} \, \eta_{H_{c2}}(T_c) \quad [\text{OeK}^{-1}] \qquad (3.2)$$

$\rho_{\Omega\,cm}$ is the residual resistivity in Ω cm. The factor $\eta_{H_{c2}}(T_c)$, first introduced by Bergmann and Rainer,[74] takes into account strong coupling effects. It remains within 30% of unity for a moderate strong coupling material and so is not an important factor in this regime. The problematic factor is $\rho_{\Omega\,cm}$. Normally, the residual resistivity is found by measuring the zero temperature

normal state resistance; in this manner, the phonon-assisted resistance is re-
moved. This is impossible, however, in the oxides; moreover, extrapolation is
difficult—the linear resistivity behaviour is not well understood, and some-
times there is a sharp rise just before T_c . In some resistivity measurements,
the extrapolation would cause $\rho(T = 0)$ to be very near to zero, which is
not understood, Kwok *et al.*[181b] used $\rho(T_c)$ in their analysis and obtained
$\gamma_0 \approx 4.9$ mJ/ mole K^2. A linear extrapolation to zero temperature gives a
resistivity of just more than half that at T_c , so that we get $\gamma_0 \approx 8$ mJ/ mole
K^2 ($\eta_{H_{c2}} \approx 1$ for LSCO[69]). This is in reasonable agreement with our previous
estimate for γ_0.

We note in passing that, using the expression given in Ch. 2, the
Ginzburg-Landau parameter, $K_1(T_c)$ can be determined from critical mag-
netic field measurements. The value obtained is $K_1(T_c) \approx 63$, indicating that
the material is strongly type-II ($\lambda \gg \xi(0)$).

The electromagnetic coherence length, $\xi(T)$ can be obtained from the
expression in Ch. 2, and the value of v_F deduced above from $H'_{c2}(T_c)$. We find
$\xi(0) = 35$ Å, in the clean limit. The dirty limit value is simply $\xi = \ell$, the mean
free path of the electron, and a lower bound would be[109] ≈ 2 Å, the Cu-O
bond length. Note that this coherence distance is not a correlation length in
the phase transition sense—it does not diverge at $T = T_c$, for instance. The
value obtained in the clean limit is significantly different from that obtained
using the BCS expression, $\xi^{BCS}(0) = \frac{v_F}{\pi \Delta_0 (1+\lambda)}$; in this case $\frac{\xi^{BCS}(0)}{\xi(0)} = 0.65$.
Note, however, the reduced quantity $\frac{\xi(T_c)}{\xi(0)} = 0.83$ which is not very different
from the BCS value of 0.75 .

We have also evaluated the London-limit penetration depth (clean
limit) $\lambda_L(T)$, and, using the values of v_F and $N(0)$ quoted above, we obtain

Figure 3.4   The temperature variation of the London penetration depth for LSCO (solid line) compared with that for Pb (dashed line). The S-shape is indicative of strong coupling. The BCS curve (not shown) is negative with a minimum value of –0.21.

$[\lambda_L(0)/\lambda_L(T)]^2-(1-t)^4$

$t=T/Tc$
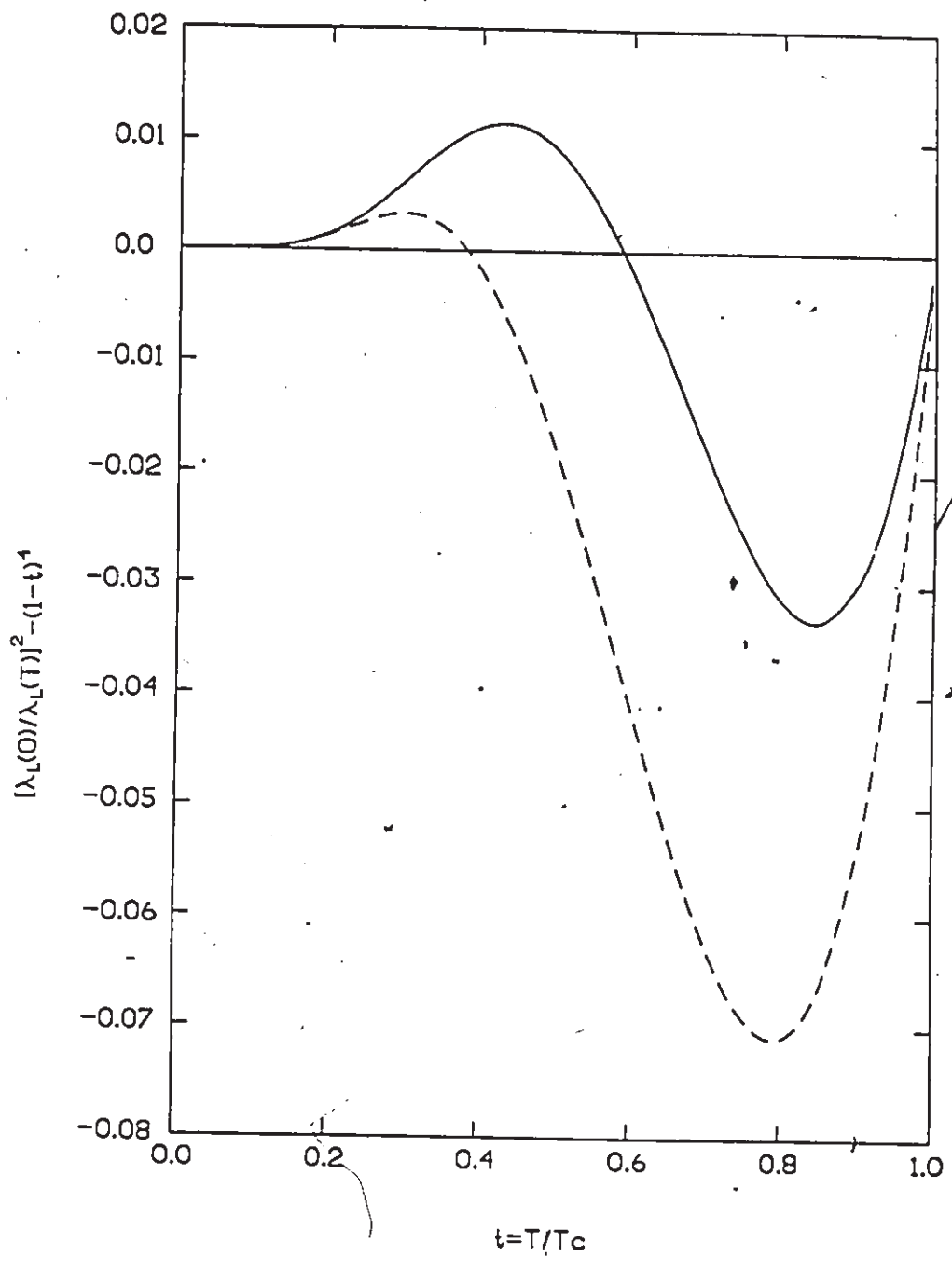
$\lambda_L(0) \sim 2950$ Å. [The BCS value would be 2700Å.] These estimates are in the right range, as Table 5 indicates. To illustrate the differences from BCS due to strong coupling most clearly, it is best to calculate the penetration depth deviation function, $D_L(t) \equiv \left(\frac{\lambda_L(0)}{\lambda_L(T)}\right)^2 - (1 - t^4)$, in analogy to the often used magnetic field deviation function. The subtracted term is the prediction of the two fluid model.[110] In BCS, both deviation functions are negative definite. $D_L(t)$ has a minimum at a value $D_L^{\min}(t) \approx -0.21$. Fig. 3.4 illustrates $D_L(t)$ for La$_{1.85}$Sr$_{0.15}$CuO$_4$ and Pb. Note that in both cases the curves are S-shaped. It is hoped that improved muon spin relaxation experiments can decide between different possibilities through such a plot.

Before closing this section, we should also mention the important isotope effect measurements which have taken place.[111,112] One group[111] finds $\beta_{ox} = 0.16 \pm 0.02$, where $\beta_i = -\frac{d\ln T_c}{d\ln M_i}$, and M_i is the ith element, in this case oxygen. The other group[112] finds a similar result, but with a much larger error margin. The naive isotope effect coefficient one expects is $\beta = 0.5$. It is normally argued that this can be reduced due to finite μ^*. In fact, when large values of λ are present to produce such high T_c 's, the reduction in β due to μ^* is very small. Another important point is that here a partial isotope effect is involved, *i.e.* only oxygen atoms are replaced by O^{18} isotopes. Hence the simple fact that $\omega_{ph} \sim M^{-\frac{1}{2}}$ no longer holds since phonon modes in general involve all the atoms in the unit cell. Rainer and Culetto[113] have analysed in detail partial isotope effects and Ashauer *et al.* [114] have found that under the assumption that phonon modes that are due to the oxygen atoms can be isolated from the rest at high frequency, a small isotope effect is not unexpected. The most rigorous manner in which to compute a theoretical estimate for β_{ox} is for Weber to recompute $\alpha^2 F(\omega)$, using O^{18} in place of

O^{16} to compute the phonon dynamics for LSCO. He has done this,[111] and finds $\beta_{ox} \approx 0.30$. Another effect that has not been mentioned so far, but has been included in Weber's calculation is that phonon frequencies are generally renormalized by the electron-phonon interaction. (In fact Weber[69] uses as a lattice instability criterion the requirement $\omega_{ph} \geq 5\,meV$.) The simple rule that $\omega_{ph} \sim M^{-\frac{1}{2}}$ applies to unrenormalized phonons. The effect of a mass change to strongly renormalized phonon frequencies will in general be quite complicated. Hence at this point it is difficult to say whether the measured isotope effect rules out the phonon mechanism. We also note that in Nb_3Sn, a well established electron-phonon superconductor, $\beta \approx 0.08$,[115] in significant disagreement with that expected from simple arguments.

The experimental data is sufficiently vague that few conclusions can be reached about the validity of Weber's $\alpha^2 F(\nu)$. Most important in this regard will be a repeat of experiments on single crystals, along with a theoretical analysis which includes anisotropy. In the ensuing sections however, we will continue our analysis based on the isotropic Eliashberg equations, in two extreme regimes, weak-coupling and very strong coupling.

3.4   VERY STRONG COUPLING REGIME: $\frac{T_c}{\omega_{\ln}} \gtrsim 1$

The tunneling experiments (see Tables 5 and 6) on both LSCO and $YBa_2Cu_3O_{7-y}$ (YBCO) indicate that the gap ratio $\frac{2\Delta_0}{k_B T_c}$ may be very large. As was mentioned in Section 3.3, $\frac{2\Delta_0}{k_B T_c}$ increases as λ or $\frac{T_c}{\omega_{\ln}}$ increases. Hence it is of interest to study the regime $\frac{T_c}{\omega_{\ln}} \approx 1$ for the high T_c oxides. Further motivation comes from the simple observation that $\frac{T_c}{\omega_{\ln}} \approx 0.22$ for LSCO. In the absence of a calculated $\alpha^2 F(\nu)$ spectrum for YBCO (Weber[116] has since produced a calculation which yields only a very low T_c) one can assume

a spectrum having the same shape as the LSCO compound, but of course with coupling strength scaled to give $T_c \sim 90\,\text{K}$. This immediately gives $\frac{T_c}{\omega_{\ln}} \approx 0.6$, and, in fact mode softening is expected, due to renormalization from increased electron-phonon coupling, so that even larger $\frac{T_c}{\omega_{\ln}}$ is expected. Of course, we have assumed that a lattice instability has not occurred first, which at present is in conflict with Weber's findings.

Unfortunately, the analytic approach used in the previous chapter can no longer be used, as there is no small parameter with which one can expand solutions away from BCS theory. Hence we have proceeded numerically,[117] using the scaling theorems developed in Ref. 43. We have taken two spectra, that of Pb and that of Weber's $\alpha^2 F(\nu)$ for LSCO, and constructed models of the form

$$\alpha^2 F(\nu) \equiv B\alpha^2 F^0(b\nu) , \qquad (3.3)$$

so that both T_c and $\omega_{\ln}$ can be adjusted independently. Here, $\alpha^2 F^0(\nu)$ refers to either of the two base spectra. In practice, only B need be adjusted so that a universal curve for a particular spectral shape can be obtained for many properties as a function of the strong coupling parameter $T_c/\omega_{\ln}$. This "universality" parallels the strict universality found in Ref. 91 for Einstein spectral functions. There it was found that

$$\frac{2\Delta_0}{k_B T_c} = g\left(\frac{T_c}{\nu_E}\right) , \qquad (3.4)$$

where g is a universal function. For a realistic spectral shape, "ν_E" is replaced by "$\omega_{\ln}$" and the same universality holds as long as the spectral shape remains the same, within the scalings implied by Eq. (3.3). Fig. (3.5) illustrates $\frac{2\Delta_0}{k_B T_c}$

Figure 3.5   The gap ratio, $\frac{2\Delta_0}{k_B T_c}$ vs. $\frac{T_c}{\omega_{ln}}$ for two spectral function shapes, that of Pb and LSCO. Note that in the very strong coupling regime, $\frac{2\Delta_0}{k_B T_c}$ continues to rise above the BCS value. The shape dependence is more pronounced in this regime; however, the qualitative feature of increasing $\frac{2\Delta_0}{k_B T_c}$ seems to be shape-independent.
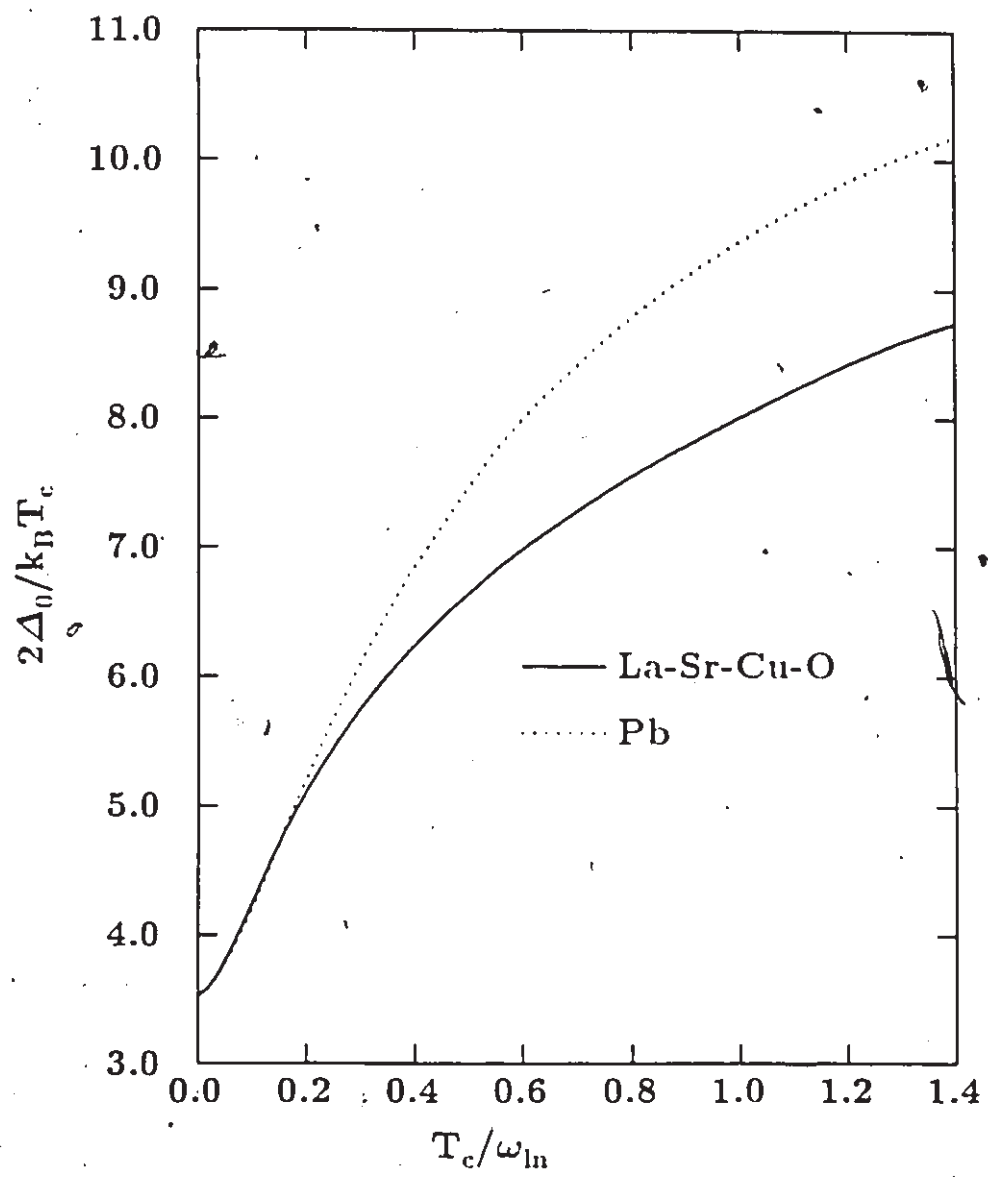
as a function of $T_c/\omega_{\ln}$ well into the very strong coupling regime. As can be seen from the figure, $\frac{2\Delta_0}{k_B T_c}$ continues to increase to values $8 \sim 10$ for $T_c \sim \omega_{\ln}$. Note that the independence on spectral shape which existed in the regime $\frac{T_c}{\omega_{\ln}} \lesssim 0.2$ (see Fig. 2.4, Fig. 3.2, and the initial portion of Fig. 3.5) no longer remains in a quantitative sense for $\frac{T_c}{\omega_{\ln}} \sim 1$. However, qualitatively the main feature is the same regardless of shape: $\frac{2\Delta_0}{k_B T_c}$ increases with increasing strong coupling. Although not apparent from this figure, we will show later on that $\frac{2\Delta_0}{k_B T_c}$ actually saturates with increasing $\frac{T_c}{\omega_{\ln}}$. The effect on almost all other properties is drastically different. Fig. (3.6) illustrates the normalized specific heat jump $f \equiv \frac{\Delta C(T_c)}{\gamma_0 T_c}$ as a function of $\frac{T_c}{\omega_{\ln}}$. Note that the enhancement due to strong coupling ceases at $\frac{T_c}{\omega_{\ln}} \sim \frac{1}{4}$. As $\frac{T_c}{\omega_{\ln}}$ increases beyond this point the normalized specific heat jump becomes lower in value, to a point where f becomes less than the BCS value, 1.43 . As was already mentioned in Ch. 2, this decrease does not represent a physical process. It occurs as a result of the normalization denominator we have used, $\gamma_0 T_c$. This denominator is often associated with the normal state electronic specific heat at T_c . However, when electron-phonon coupling becomes important, Grimvall[45] has shown that the normal state electronic specific heat becomes $C_N(T) = \gamma(T)T$, where $\gamma(T)$ is given by Eq. (2.54). For moderate electron-phonon coupling, as in Pb or Nb_3Sn, the effect at T_c is an enhancement of less than 20% and hence not so important. However, as $\frac{T_c}{\omega_{\ln}}$ approaches unity, the renormalization begins to diminish to zero, as we would expect, since at high temperatures the phonons will have no effect on the electronic specific heat. Hence, as $\frac{T_c}{\omega_{\ln}}$ increases, $\frac{\Delta C(T_c)}{\gamma(T_c)T_c}$ will saturate to a maximum value in the same manner as $\frac{2\Delta_0}{k_B T_c}$, since $\gamma(T_c)$ will reach some constant value. However, the behaviour of f will be different from the previous ratio, since as $\frac{T_c}{\omega_{\ln}}$ increases, λ increases,

Figure 3.6   Plot of $\frac{\Delta C(T_c)}{\gamma_0 T_c}$ vs. $\frac{T_c}{\omega_{1n}}$. As $\frac{T_c}{\omega_{1n}}$ increases beyond the conventional regime ($\frac{T_c}{\omega_{1n}} \sim 0.20$), the normalized jump decreases to values lower than the BCS value.
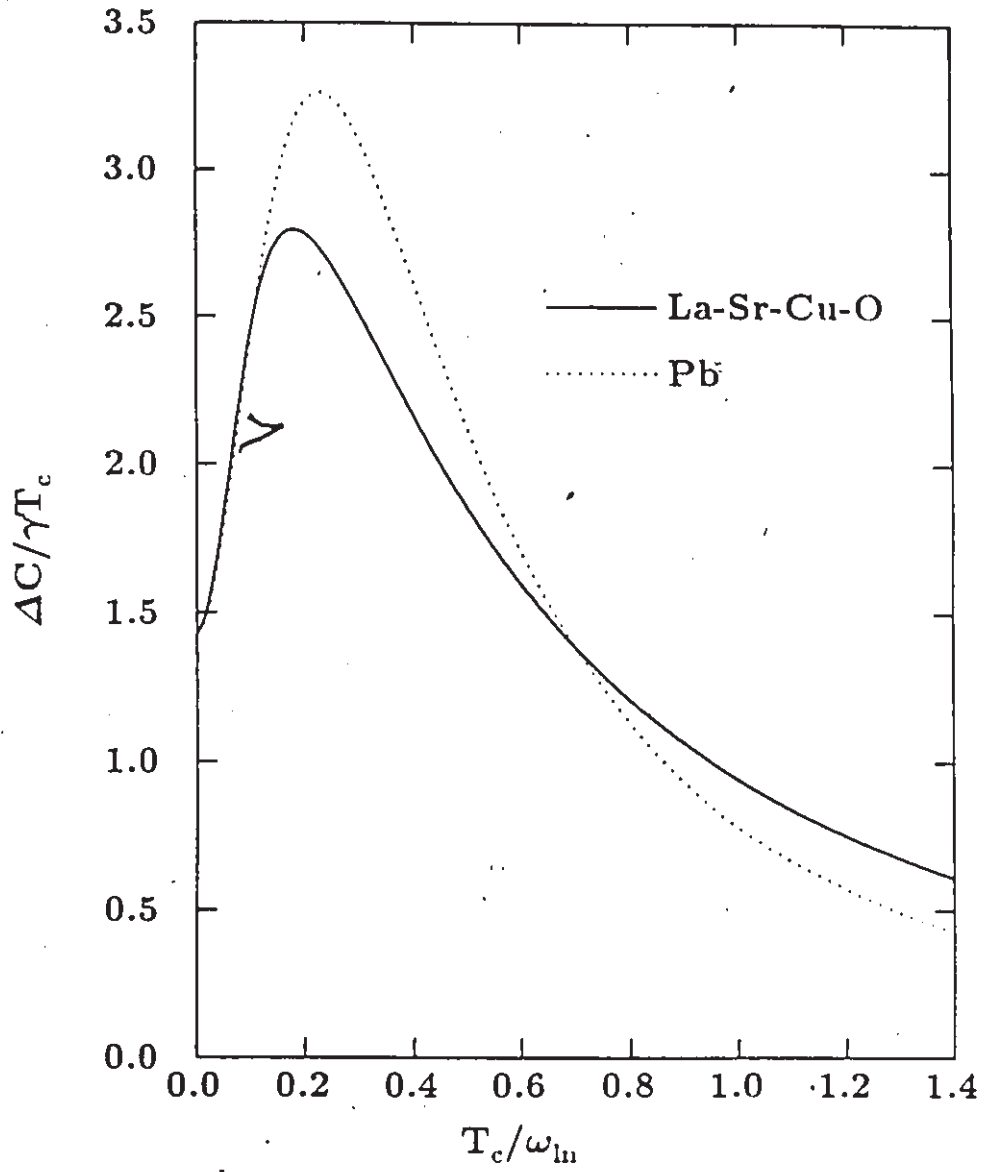
and thus γ_0 continues to increase.

It is more useful, however to use f rather than the more physical ratio, because in practice, it is very difficult to extract $\gamma(T)$ from experiment. In conventional materials, an applied magnetic field causes the sample to become normal, and the specific heat can be measured down to low temperatures. At low temperatures the phonon contribution itself becomes frozen out, as well as the renormalization to the electronic contribution. Hence, the specific heat will become linear in temperature. The conventional plot of $\frac{C}{T}$ vs. T^2 will have an intercept which is taken to be (and is) γ_0. In the high T_c materials, this procedure to extract γ_0 (never mind $\gamma(T)$!) is impossible because of the high magnetic fields required to make the sample become normal. However, attempts are made to extract γ_0 through other measurements, such as the upper critical magnetic field, through the use of Eq. (3.2). Note that it is then γ_0, and not $\gamma(T_c)$, which is obtained.

In a similar way we can study the ratio $\frac{\gamma_0 T_c^2}{H_c^2(0)}$. Here again the moderate strong coupling effect (a lowering from the BCS value of 0.168) is reversed in the very strong coupling regime, as is illustrated in Fig. (3.7). The reason is the same as before; γ_0 is used instead of $\gamma(T)$. Equation (B48) allows us to calculate $h_c(t)$, $t \ll 1$, as well in the very strong coupling limit; it will saturate to some constant value; this reflects the fact that the low temperature behaviour of the thermodynamic critical field as a function of strong coupling is qualitatively the same as the behaviour near T_c . Finally, we illustrate the thermodynamic deviation function. $D(t) \equiv \frac{H_c(T)}{H_c(0)} - (1 - t^2)$, in Fig. (3.8). The plotted points indicate the minimum and/or maximum value of the $D(t)$ curve (as a function of t) for each $\frac{T_c}{\omega_{ln}}$ value. Note that for some values of $\frac{T_c}{\omega_{ln}}$ the curve in Fig. (3.8) is double-valued, indicating that the $D(t)$

Figure 3.7   Plot of $\frac{\gamma_0 T_c^2}{H_c^2(0)}$ vs. $\frac{T_c}{\omega_{\ln}}$ in very strong coupling regime. The trend has reversed, as it did for the jump, and values above that of BCS are found in this regime.
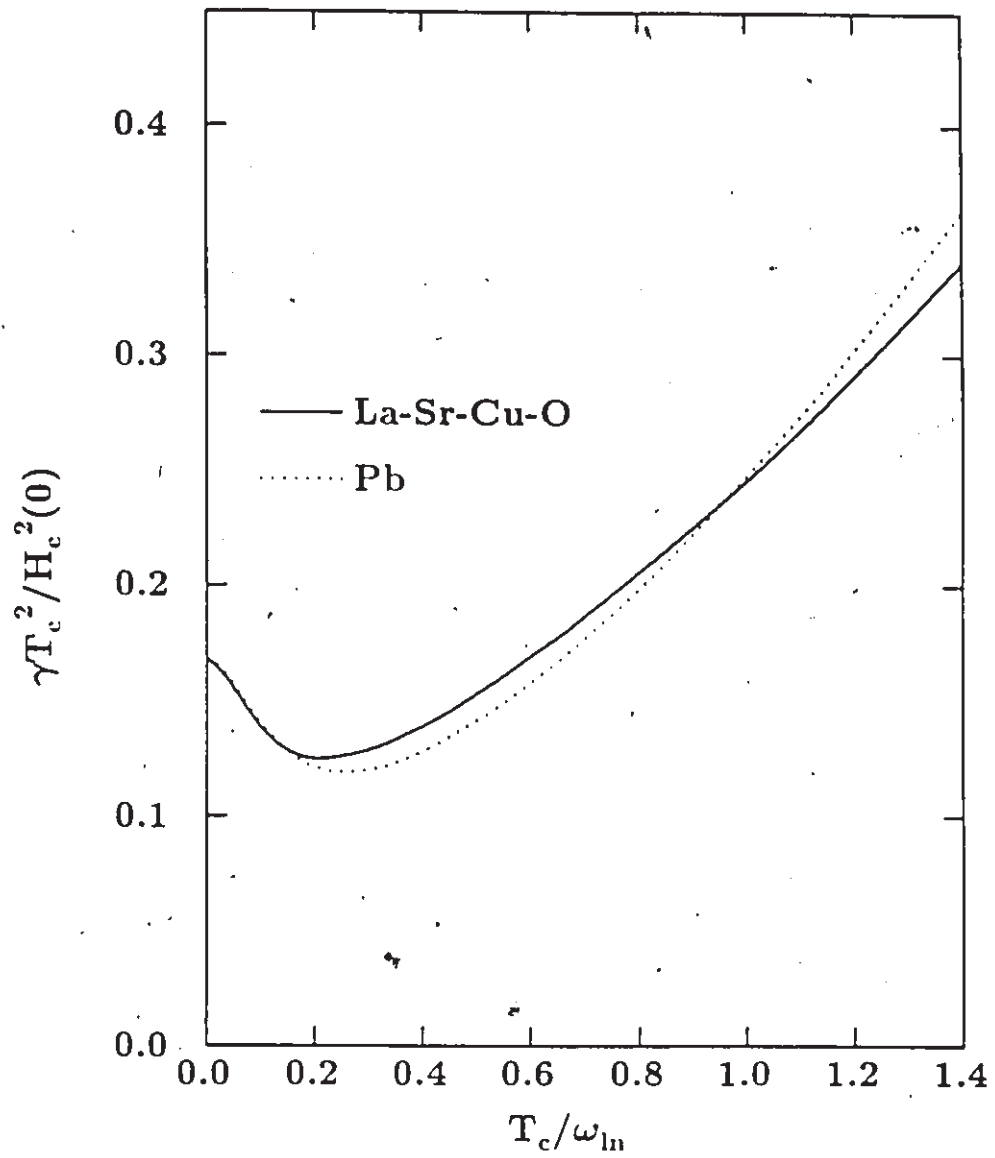
curve is S-shaped. In the BCS regime $\left(\frac{T_c}{\omega_{\ln}} \sim 0\right)$, only a minimum is present, indicating that $D(t)$ is negative definite. As is well known for strong couplers such as Pb $\left(\frac{T_c}{\omega_{\ln}} = 0.128\right)$, $D(t)$ becomes positive definite, as is shown in Fig. (3.8) (since only a maximum occurs). However, in the very strong coupling regime, the curve becomes negative definite once again, with a min-imum value which can greatly exceed (in absolute value) the minimum value found in BCS theory. This is a very strong signature for very strong coupling.

In a similar manner, the upper critical magnetic field,[118] the Ginzburg-Landau parameter $K_1(T)$,[119] and the electromagnetic properties[120] have been studied in the very strong coupling regime. We illustrate some results for $H_{c2}(T)$, referring the reader to references 119 and 120 for a further discussion of the other properties. Fig. (3.9) illustrates $\eta_{H_{c2}}(T, t^+)$ for the two spectral shapes for $T = 0$, T_c and $t^+ = 0$, $100 \, \mathrm{meV}$. The strong coupling correction parameter η is defined[31]

$$H_{c2}(T, t^+) = \eta_{H_{c2}}(T, t^+) H_{c2}^{\mathrm{BCS}}(T, t^+) . \tag{3.5}$$

Again, the moderate strong coupling trend is reversed in the very strong coupling regime, where the correction to the BCS value becomes less than unity. Note that at T_c, the curves representing the clean ($t^+ = 0$) and dirty ($t^+ = 100 \, \mathrm{meV}$) limits merge in the very strong coupling regime indicating that the result is independent of concentration of impurities. This is expected because as $\frac{T_c}{\omega_{\ln}}$ increases, the typical phonon frequency decreases, and the phonons behave more like static impurities, so that the "clean" limit calculation will actually look "dirty". At $T = 0$, this is no longer true because the phonons are frozen out so that there ought to be a difference .
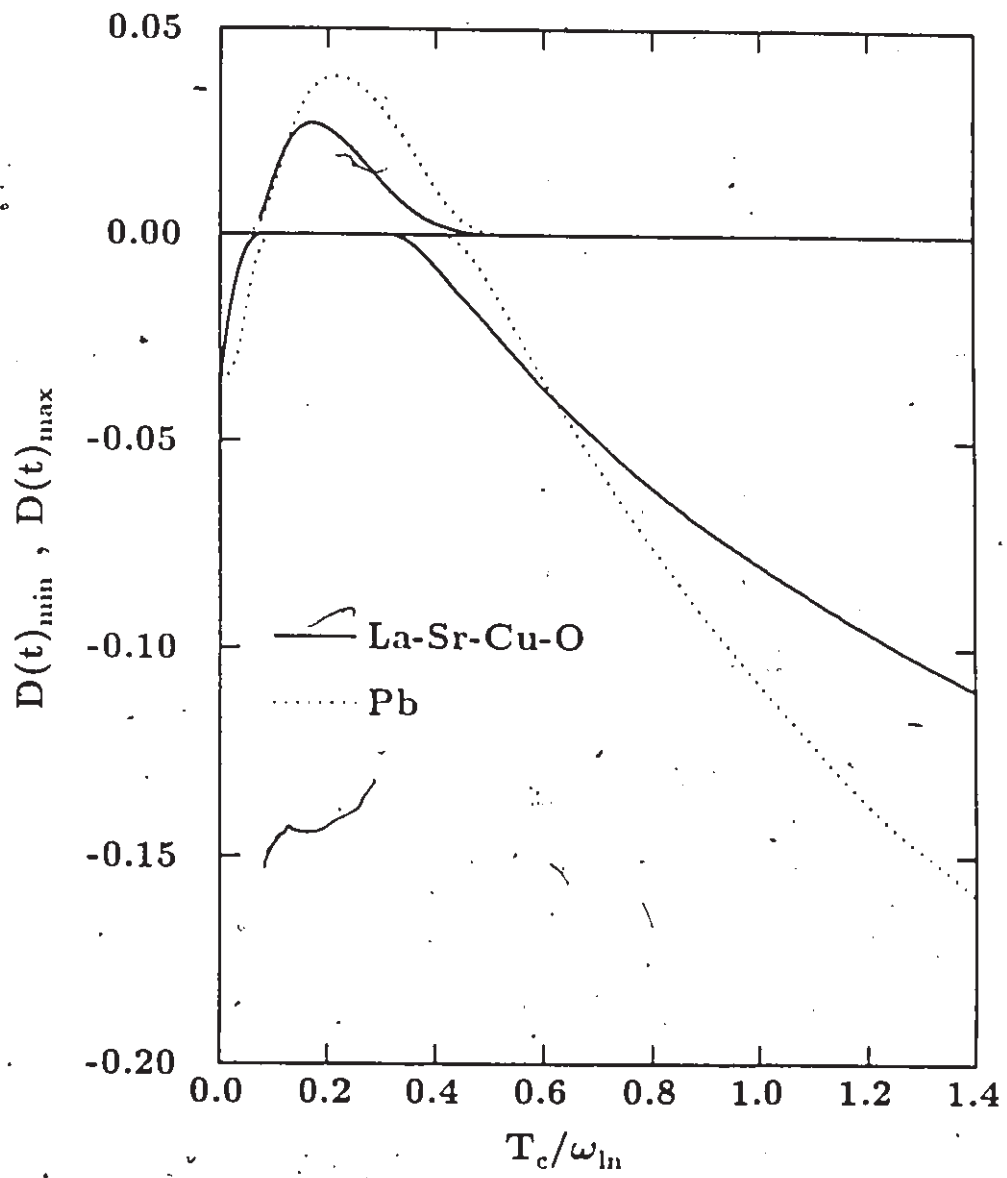
Figure 3.8   Plot of the maximum or minimum (or both when it is S-shaped) of the critical magnetic field deviation function vs. $\frac{T_c}{\omega_{\ln}}$. In the very strong coupling regime the curve becomes negative definite with minimum values which exceed the BCS value in absolute terms.
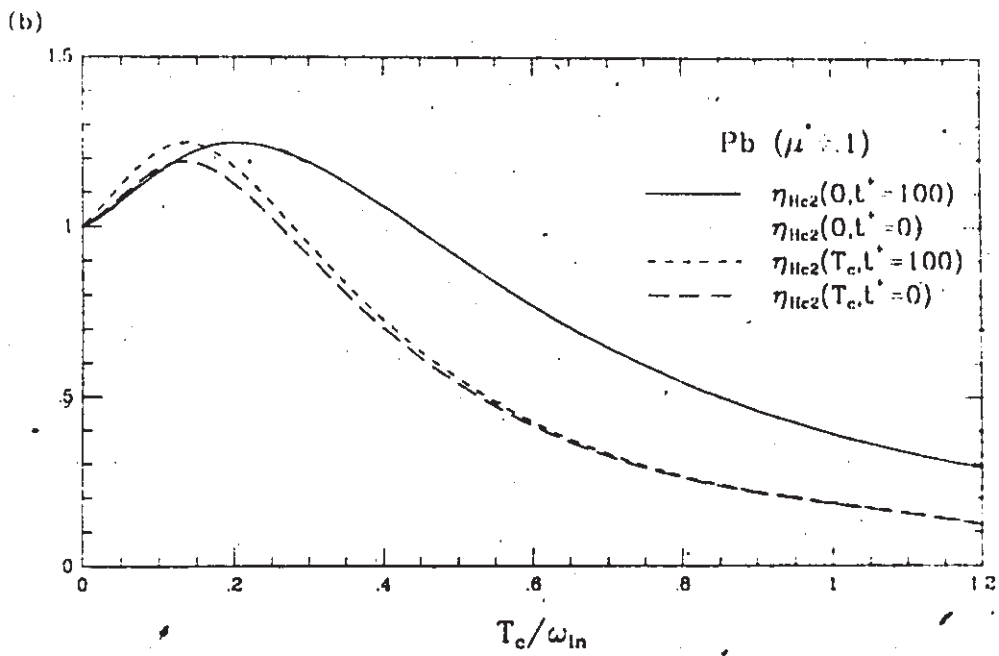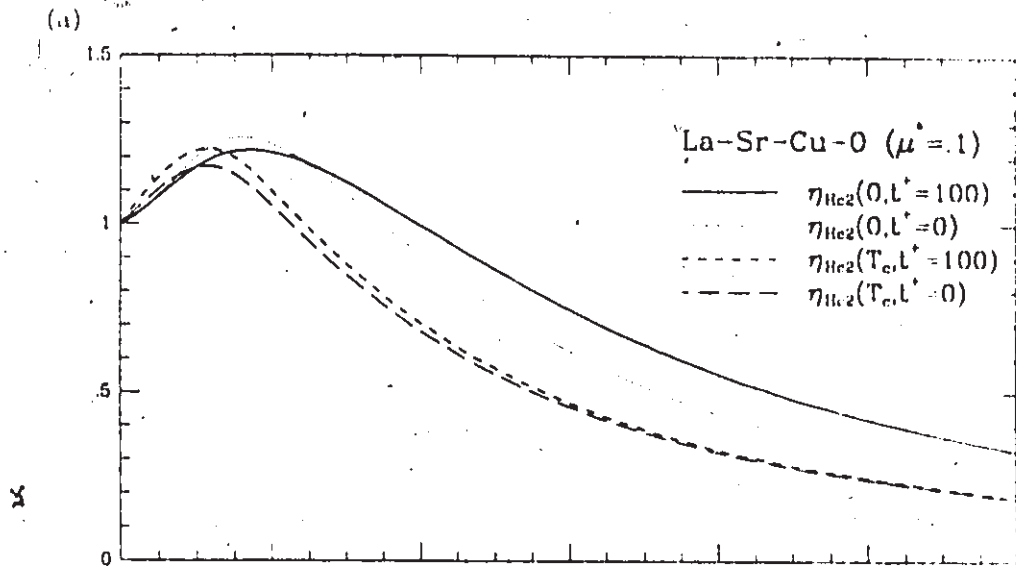
between the strong coupling corrections in the clean and dirty limits, as there is. Note, moreover, that the BCS expressions[61] exhibit a qualitative difference as $\frac{T_c}{\omega_{\ln}}$ increases.

.Another important effect of very strong coupling is exhibited in Fig. (3.10), where $h_{c2}(t, t^+)$ is plotted as a function of reduced temperature, t, for the same two impurity concentrations. It can be seen that as $\frac{T_c}{\omega_{\ln}}$ increases, the curves develop a large positive curvature, contrary to the negative curvature observed within BCS theory. The zero temperature behaviour is more clearly illustrated in Fig. (3.11), where $h_{c2}(0)$ is shown versus $\frac{T_c}{\omega_{\ln}}$ for $t^+ = 0$ and $100\,\text{meV}$. The quantitative aspects of the curves depend on the spectral shape used, as is clear from the two examples we have used. However it can be seen that generally, as $\frac{T_c}{\omega_{\ln}}$ increases, $h_{c2}(0, t^+)$ increases also. The $t^+ = 0$ curve for LSCO shows an exception to this rule, where $h_{c2}(0, t^+ = 0)$ begins to decrease slightly with increasing $\frac{T_c}{\omega_{\ln}}$. Moreover, the increase is much greater for $t^+ = 100\,\text{meV}$ than for $t^+ = 0$ when $\frac{T_c}{\omega_{\ln}} \gtrsim 1$. The inset displays this more convincingly, where $h_{c2}(0, t^+)$ is plotted versus t^+ for t^+ ranging over four orders of magnitude. When $\frac{T_c}{\omega_{\ln}}$ is large (as it is here ~ 1) the "dirty limit" is only achieved when t^+ becomes very large. This is expected on the basis of BCS theory, where it can be seen[121] that the relevant impurity parameter enters via the expression:

$$(t^+)^\bullet \equiv \frac{t^+}{2\pi T_c(1 + \lambda)} \cdot \qquad (3.6)$$

If the "dirty limit" is designated by $(t^+)^\bullet \gtrsim 10$. for example. then as $\frac{T_c}{\omega_{\ln}}$ increases. λ increases and the appropriate t^+ will also have to increase. The inset also clearly shows that in this case the difference between clean and dirty

Figure 3.9 (a) The strong coupling correction parameter, $\eta_{H_{c2}}(t^+, T)$ is displayed for $T = 0$ and $T = T_c$, and for $t^+ = 0$ and 100 meV. Note that all the correction parameters display the same qualitative trend. In the conventional strong coupling regime ($\frac{T_c}{\omega_{\ln}} \lesssim 0.2$), all the corrections are greater than one, and modest. However, in the very strong coupling regime ($\frac{T_c}{\omega_{\ln}} \approx 1$), the corrections differ substantially from unity, and are less than one. No significant qualitative difference is noticeable between $t^+ = 0$ meV. (b) The same results are displayed as in (a), but for a Pb spectrum. No qualitative change from (a) is observed, indicating that the results noted in (a) are not very model dependent.

(a)

La-Sr-Cu-O ($\mu^* = .1$)

$\eta_{Hc2}(0, t^* = 100)$
$\eta_{Hc2}(0, t^* = 0)$
$\eta_{Hc2}(T_c, t^* = 100)$
$\eta_{Hc2}(T_c, t^* = 0)$

(b)

Pb ($\mu^* = .1$)

$\eta_{Hc2}(0, t^* = 100)$
$\eta_{Hc2}(0, t^* = 0)$
$\eta_{Hc2}(T_c, t^* = 100)$
$\eta_{Hc2}(T_c, t^* = 0)$

T_c/ω_{ln}

limits is greatly enhanced over the difference obtained in the BCS limit.

One of the main results of this section is that while only one value of $\frac{T_c}{\omega_{l_a}}$ (~ 0) will produce a BCS value for $\frac{2\Delta_0}{k_B T_c}$, in general two values are possible for most other ratios. Thus, BCS type results, for example, can be achieved in two ways; (1) the conventional way, with $\frac{T_c}{\omega_{l_a}} \sim 0$, and (2) with very strong coupling, $\frac{T_c}{\omega_{l_a}} > 0.3$. However, the gap ratio measurement is critical, as its value will rule out one of these two cases.

We also note that there are additional reasons for considering the very strong coupling limit. The normal state resistivity is roughly linear as a function of temperature, which indicates[21] that the boson causing the scattering is low in frequency compared to the temperature. (Note, however, that Gurvitch and Fiory[109] have analysed the linear dependence to imply that λ must be small.) Moreover, Deutscher[122] has analysed some of the available data and has found that the Ginzburg criterion yields a broad critical region for the oxides, so that the critical behaviour should resemble that of superfluid He^4 rather than that of conventional superconductors. Some of the more recent data on specific heat,[179g] for example, is however, very mean field like. This can be recovered from Deutscher's analysis provided strong coupling effects are important, and hence would suggest indirectly that the high T_c oxides are in the strong coupling limit.
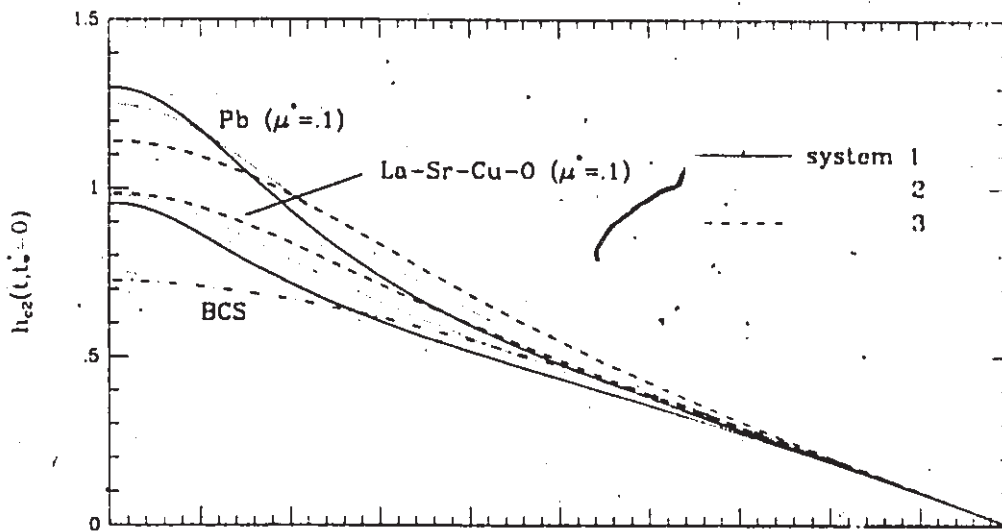
3.5   COMBINED PHONON-EXCITON MECHANISM

Exciton superconductivity was first suggested as a theoretical possibility in 1964 by Little[123] and Ginzburg.[124] The idea is very similar to that involving phonons. Fig. (1.1) still applies, except that the polarization is not due to a movement of the ions themselves, but rather to movements of
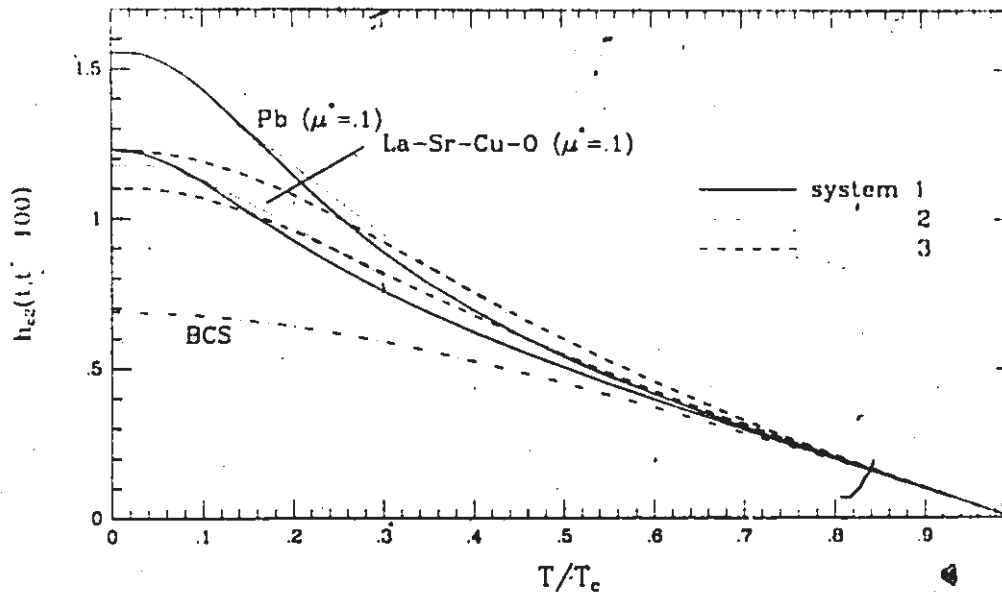
Figure 3.10   (a) The reduced upper critical magnetic field, in the clean limit, is displayed as a function of reduced temperature T/T_c. We show curves for three systems in the very strong coupling regime for both Pb and $La_{1.85}Sr_{0.15}CuO_4$. For Pb they can be characterized by $\frac{T_c}{\omega_{ln}} = 1.14$ (system 1), $\frac{T_c}{\omega_{ln}} = 0.86$ (system 2), and $\frac{T_c}{\omega_{ln}} = 0.57$ (system 3). For $La_{1.85}Sr_{0.15}CuO_4$ the scaled spectra have $\frac{T_c}{\omega_{ln}} = 1.19$ (system 1), $\frac{T_c}{\omega_{ln}} = 0.83$ (system 2), and $\frac{T_c}{\omega_{ln}} = 0.60$ (system 3). Also shown is the BCS result, for comparison. Note that in the very strong coupling regime the curves have developed a large positive curvature, a feature missing in the BCS model. Also note that for Pb the value of $h_{c2}(0, t^+ = 0)$ is still increasing as $\frac{T_c}{\omega_{ln}}$ is increasing above unity, whereas, for LSCO $h_{c2}(0, t^+ = 0)$ has attained a maximum value near $\frac{T_c}{\omega_{ln}} \approx 0.6$ and is slightly decreasing as $\frac{T_c}{\omega_{ln}}$ increases further (see Fig. 3.11). (b) The same results are displayed as in (a), but for impurity parameter $t^+ = 100$ meV.

(a)

Pb ($\mu^*=.1$)

La-Sr-Cu-O ($\mu^*=.1$)

system 1

2

3

BCS

$h_{c2}(t,t^*=0)$

(b)

Pb ($\mu^*=.1$)

La-Sr-Cu-O ($\mu^*=.1$)

system 1

2

3

BCS

$h_{c2}(t,t^*\ 100)$

T/T_c

electrons (say on the ion cores). This polarization will result in a net positively charged region of space to which a conduction electron will be attracted. Little[123] envisioned a one-dimensional geometry with conduction chains along side "exciton" chains. The two types of electrons (conduction and those that produce the excitons) are then physically separated from one another. Ginzburg considered a two-dimensional geometry with a metallic layer sandwiched between two dielectric layers. This geometry was later investigated in detail by Allender, Bray and Bardeen,[100] within the Eliashberg formalism. There are many objections to the idea of excitonic superconductivity, which have been neatly summarized be Little.[125] We will not reiterate them here, but simply note that many can be overcome under the proper conditions. Perhaps the most serious problem is that vertex corrections may become important,[126] since the ratio of the electron mass to exciton mass is no longer small. We will nonetheless proceed, following Allender et $al.$,[100] and ignore this complication.

The most compelling reason for considering excitonic superconductivity is associated with this last problem, in that the mediating boson (exciton) now has an electronic energy scale. Hence, in the simple BCS picture, T_c will be significantly enhanced (see Eq. 2.19a) because the prefactor is now $\omega_{ex} \gg \omega_D$. Theoretical work[127-131] has also suggested the possibility of excitonic superconductivity in the high T_c oxides. Several experiments have indicated that excitons may be playing a role in these materials. Far-infrared optical measurements[132-134] reveal an increased absorption at high frequencies (0.44 eV in YBCO and 0.37 eV in LSCO), which may be due to an exciton mode being present. Moreover, the presence of the increased

Figure 3.11 The reduced upper critical magnetic field at zero temperature, $h_{c2}(0)$, is shown for the scaled spectra as a function of $\frac{T_c}{\omega_{ln}}$, for impurity parameters $t^+ = 0$ and 100 meV. All curves show a modest decrease below their respective BCS values as $\frac{T_c}{\omega_{ln}}$ increases beyond BCS in the very strong coupling regime. Note that the difference between $t^+ = 0$ and 100 meV becomes much more pronounced as $\frac{T_c}{\omega_{ln}}$ increases (although a value of $\frac{T_c}{\omega_{ln}}$ exists in the intermediate strong coupling regime for which there is no difference). The striking enhancement of the difference between the clean and dirty limits in the very strong coupling limit is illustrated in the inset, where the dirty limit deviates from the clean by roughly 100%, as compared to 5% in the BCS model.
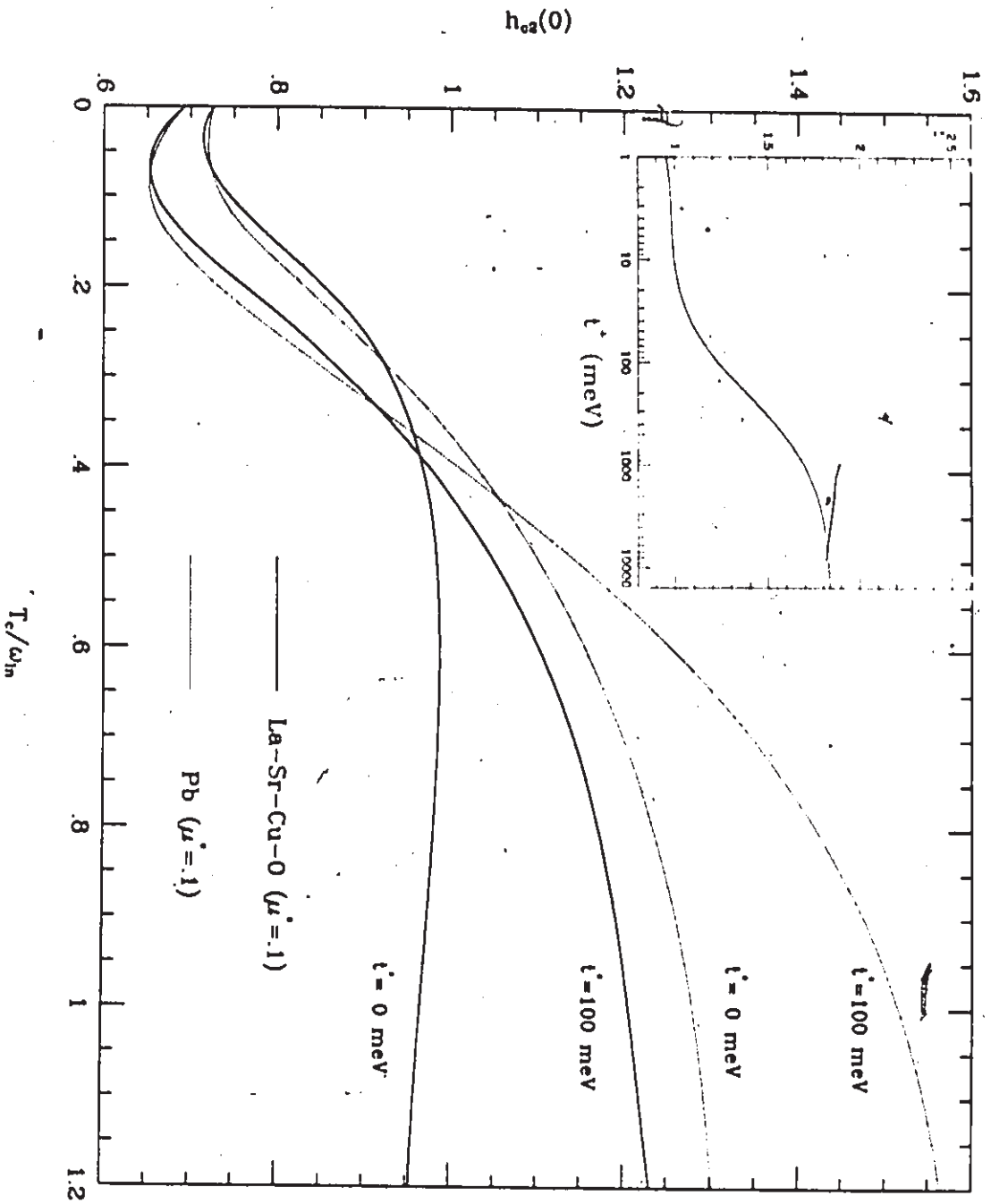
absorption has been shown[135,134] to be strongly correlated with the presence of superconductivity in the material. (The 'peak' has since disappeared in single crystal measurements.[135a] However, the significance of the anomalous "Drude-like" absorption is still controversial.[135b]) Meanwhile, most far-infrared and some tunneling measurements indicated a BCS value for the gap ratio (see Tables 5 and 6), which, as we have argued earlier, implies that the mediating boson is electronic in origin. Finally, measurements of the isotope effect have suggested that the superconductivity is not phononic in origin. Measurements were first performed[136,137] for YBCO samples with ^{16}O replaced by ^{18}O. No isotope effect was observed. A subsequent measurement[138] reported a small isotope effect of $\beta_{ox} \approx 0.05$, where $\beta_{ox} \equiv -\frac{d \ln T_c}{d \ln M_{ox}}$. The subscript "$ox$" indicates that only oxygen atoms are replaced. Measurements on LSCO samples revealed much higher isotope effects with one group reporting[111] $\beta_{ox} = 0.16 \pm 0.02$ and the other reporting[112] $0.15 < \beta < 0.35$. On the basis of Weber's calculation,[111] the expected isotope effect is $\beta_{ox} = 0.30$, so that a discrepancy exists with the first result. Note, however, as we have already mentioned, this theoretical estimate can be significantly reduced[114] if more higher frequency oxygen phonon modes are participating in the electron-phonon interaction. In the meantime, the isotope effect in BaPbBiO has been measured[139] to be $\beta_{ox} \approx 0.22$. One would like to think that the same mechanism is causing superconductivity in all three of these compounds, so we are led to investigate[140,141] a combined phonon-exciton mechanism. The case of a 96 K superconductor has been treated in Ref. 140, using the model:

$$\alpha^2 F(\nu) = \frac{1}{2}\lambda_{ph}\,\omega_{ph}\,\delta(\nu - \omega_{ph}) + \frac{1}{2}\lambda_{ex}\,\omega_{ex}\,\delta(\nu - \omega_{ex}) \qquad (3.6)$$

where $\lambda_{ph}(\lambda_{ex})$ is the electron-phonon (electron-exciton) electronic mass renormalization. The two Einstein modes have been placed at frequencies $\omega_{ph} = 8\,\mathrm{meV}$ (to simulate the phonon spectrum) and $\omega_{ex} = 500\,\mathrm{meV}$ (to simulate the exciton spectrum). The coupling strengths were then varied such that $\frac{\lambda_{ex}}{\lambda_{tot}}$ spanned the range from 0 to 1 ($\lambda_{tot} = \lambda_{ex} + \lambda_{ph}$). We will simply report briefly on the results found there. The full isotope effect, gap ratio, specific heat jump and critical magnetic field properties were calculated as a function of $\frac{\lambda_{ex}}{\lambda_{tot}}$. It was found that an isotope effect of $0 < \beta < 0.05$ was not very restrictive, *i.e.* a large range of $\frac{\lambda_{ex}}{\lambda_{tot}}$ was possible. Furthermore calculation of the various superconducting properties resulted in values very close to BCS values, and hence, would make a combined mechanism difficult to be distinguished from a pure exciton mechanism through experiments. It is noteworthy, however, that in all the properties calculated, the trend as a function of decreasing $\frac{\lambda_{ex}}{\lambda_{tot}}$ (from the "BCS" value of 1) was qualitatively similar to the trends observed in the very strong coupling regime. This indicated that while most of the T_c (about 90 K) was caused by the "exciton" peak at $\omega_{ex} = 500\,\mathrm{meV}$, the thermodynamic and critical magnetic field properties were largely affected by the phonon peak at $\omega_{ph} = 8\,\mathrm{meV}$, which, considered on its own, gives the ratio $\frac{T_c}{\omega_{ph}} \approx 1$, which is in the very strong coupling regime. Note, however, that $\frac{2\Delta_0}{k_B T_c}$ remained relatively BCS-like for the range of $\frac{\lambda_{ex}}{\lambda_{tot}}$ for which $\beta \leq 0.05$.

Because of the relatively large isotope effect observed in the LSCO compound, the effects of a combined exciton-phonon mechanism are much more interesting to study. Moreover, the detailed calculation of $\alpha^2 F(\nu)$ by Weber[69] allows for a more detailed calculation, although we follow the previous example and model the exciton mode by the same Einstein spectrum

located at $\omega_{ex} = 500\,\text{meV}$. The relative weightings of the phonon and exciton contributions are then adjusted keeping $T_c = 36\,\text{K}$. We have used $\mu^*(\omega_c = 1.53\,\text{eV}) = 0.15$. The results for the isotope effect coefficient, β_{ox} are illustrated in Fig. (3.12). Note that when only phonons are present $\left(\frac{\lambda_{ex}}{\lambda_{tot}} = 0\right)$, β_{ox} is near 0.275, whereas, when only excitons are present, the isotope coefficient approaches zero, as is expected. We have used Weber's calculated spectrum with ^{16}O replaced by ^{18}O in the planes. While there is a small added effect from replacement by ^{18}O along the chains, $(\beta_{ox}^{chain} \approx 0.03)$ we have been unable to include it in our calculations. Allowance for this will be made later on. Also note that had the isotope coefficient been measured to be near zero, the phonons could not have played a significant role, since the increase in β_{ox} from zero is relatively steep (compared to that for the 96 K superconductor —see Ref. 140). Note that the value for the pure phonon case would be slightly higher, except that there is a μ^* present. The small maximum near $\frac{\lambda_{ex}}{\lambda_{tot}} = 0$ is indicative of the fact that as λ_{ex} increases from zero it initially has the effect of representing a negative μ^* and hence tends to cancel some of the effect of the existing μ^*. The manner in which the isotope effect was calculated followed the method used by Rainer and Culleto.[113] They kept the cutoff in the Δ-channel fixed, and simply shifted the frequencies in the $\alpha^2 F(\nu)$ spectrum downwards in inverse proportion to the square root of the mass change. This method contrasts with the more complicated procedure[32,142,143] of referring the cutoff to the phonon spectrum so that μ^* acquires an artificial mass dependence through its cutoff. We have the added advantage of having Weber's more accurate calculation of the phonon frequency shifts at our disposal as well.

Figure 3.12   The isotope effect coefficient β_{ox} vs. $\frac{\lambda_{ex}}{\lambda_{tot}}$, with $\mu^* = 0.15$ for the combined phonon and exciton spectrum. This calculation uses Weber's spectral functions calculated with and without oxygen replacement in the Cu-O planes. The effect of replacement of ^{16}O by ^{18}O along the chains is very small. Note that the experimentally measured value $\beta_{ox} = 0.16 \pm 0.02$ gives rather stringent constraints on the possible value of $\frac{\lambda_{ex}}{\lambda_{tot}}$ within this model.
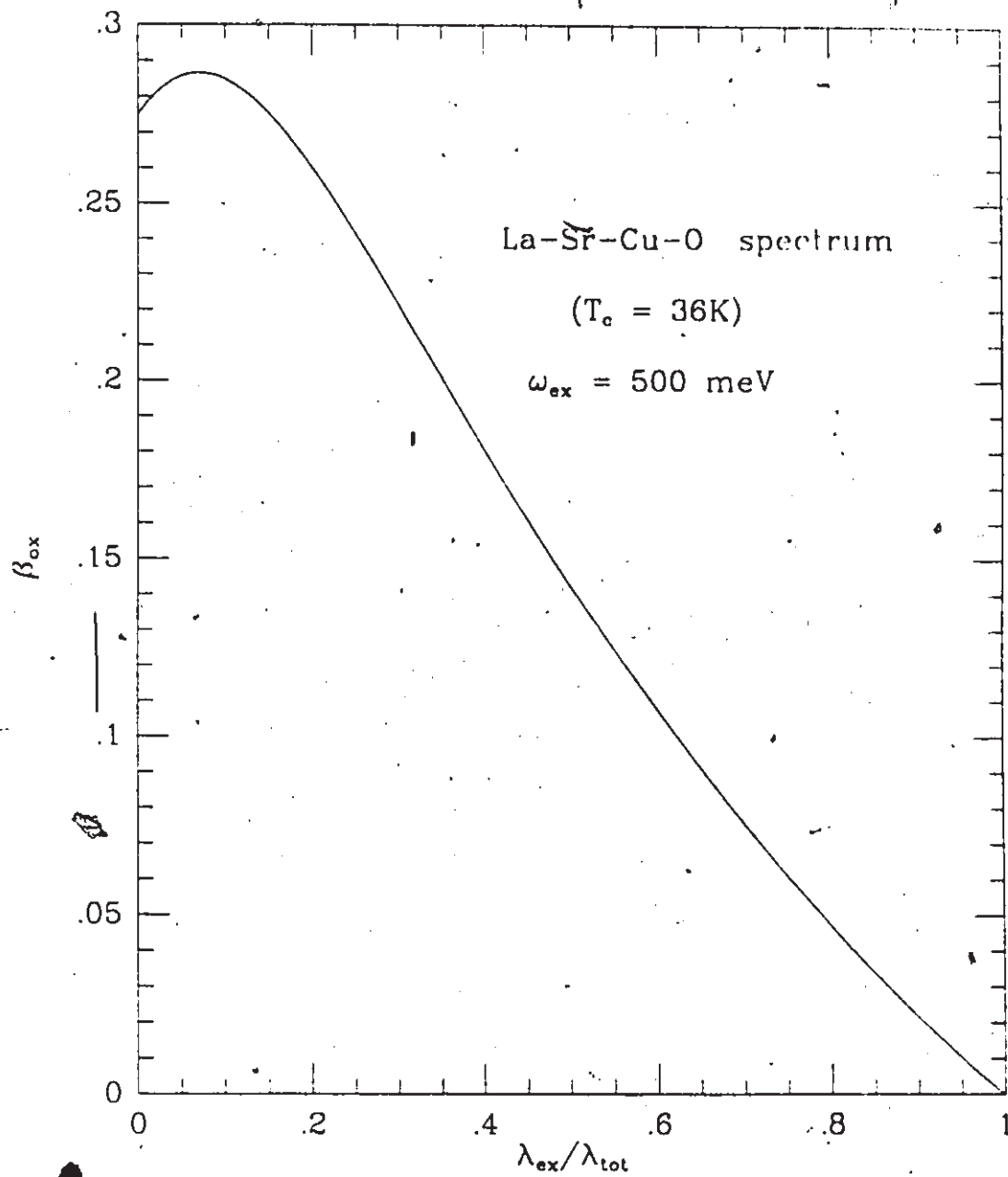
La-Sr-Cu-O spectrum

$(T_c = 36K)$

$\omega_{ex} = 500$ meV

Fig. (3.12) allows us to decide on the ratio of λ_{ph} to λ_{ex} in LSCO on the basis of the isotope effect measurement[111] alone. Taking into account the axial site oxygen isotope effect we require $\beta_{ox} \approx 0.14$ in Fig. (3.12), which determines $\frac{\lambda_{ex}}{\lambda_{tot}} \approx 0.5$. This choice will depend somewhat on our choice for μ^* and ω_{ex}, as well as the manner in which we simply scaled Weber's $\alpha^2 F(\nu)$ spectrum. However, for definiteness and for purposes of illustration we fix $\frac{\lambda_{ex}}{\lambda_{tot}} = 0.5$ and investigate other properties.

Fig. (3.13) displays the gap ratio, $\frac{2\Delta_0}{k_B T_c}$, as a function of $\frac{\lambda_{ex}}{\lambda_{tot}}$. Again in the pure phonon case, we have simply Weber's spectrum, so that the results of section 3 apply, and $\frac{2\Delta_0}{k_B T_c} = 5.3$. In the other extreme a purely excitonic mechanism implies that $\frac{T_c}{\omega_{ex}} \approx 0.006$, so that a BCS result will be achieved (see Fig. 3.2). Our choice of $\frac{\lambda_{ex}}{\lambda_{tot}}$ implies that $\frac{2\Delta_0}{k_B T_c} \approx 4$, which is certainly in the thick of things, as far as experiments go (see Table 5). Note that this and ensuing results will differ slightly from those of Ref. 141, where the choice of $\frac{\lambda_{ex}}{\lambda_{tot}} \approx 0.4$ was made based on the calculated *full* isotope effect. The normalized specific heat jump, $\frac{\Delta C(T_c)}{\gamma_0 T_c}$, is illustrated in Fig. (3.14). $\frac{\lambda_{ex}}{\lambda_{tot}} = 0.5$ implies $\frac{\Delta C(T_c)}{\gamma_0 T_c} = 1.7$. Again, here we cannot check this against experiment, but instead rely on it to determine γ_0. We use once again the experimental value $\frac{\Delta C(T_c)}{T_c} = 17 \frac{mJ}{mole\,K^2}$ (see Table 5) so that $\gamma_0 \approx 10 \frac{mJ}{mole\,K^2}$. To determine the density of states we need to know λ_{tot}. Fig. (3.15) illustrates λ_{ph} *vs.* $\frac{\lambda_{ex}}{\lambda_{tot}}$, from which λ_{tot} can be determined for $\frac{\lambda_{ex}}{\lambda_{tot}} = 0.5$. We find $\lambda_{tot} \approx 0.9$. Using Eq. (3.1), we find $N(0) = 1.12 \frac{states}{eV-fu-spin}$. This value is far more consistent with the values $0.95^{[183b]}$ and $1.08^{[183c]}$ determined through band structure calculations than the value determined directly from Weber's spectrum (0.36 in the same units), and hence lends support to the combined

Figure 3.13   Plot of $\frac{2\Delta_0}{k_B T_c}$ vs. $\frac{\lambda_{ex}}{\lambda_{tot}}$ for the combined phonon-exciton model considered in the text. A choice of $\frac{\lambda_{ex}}{\lambda_{tot}} \approx 0.5$ implies $\frac{2\Delta_0}{k_B T_c} \approx 4$ which is in better agreement with far-infrared measurements of the gap edge.

La-Sr-Cu-O spectrum

$(T_c = 36K)$

$\omega_{ex} = 500$ meV
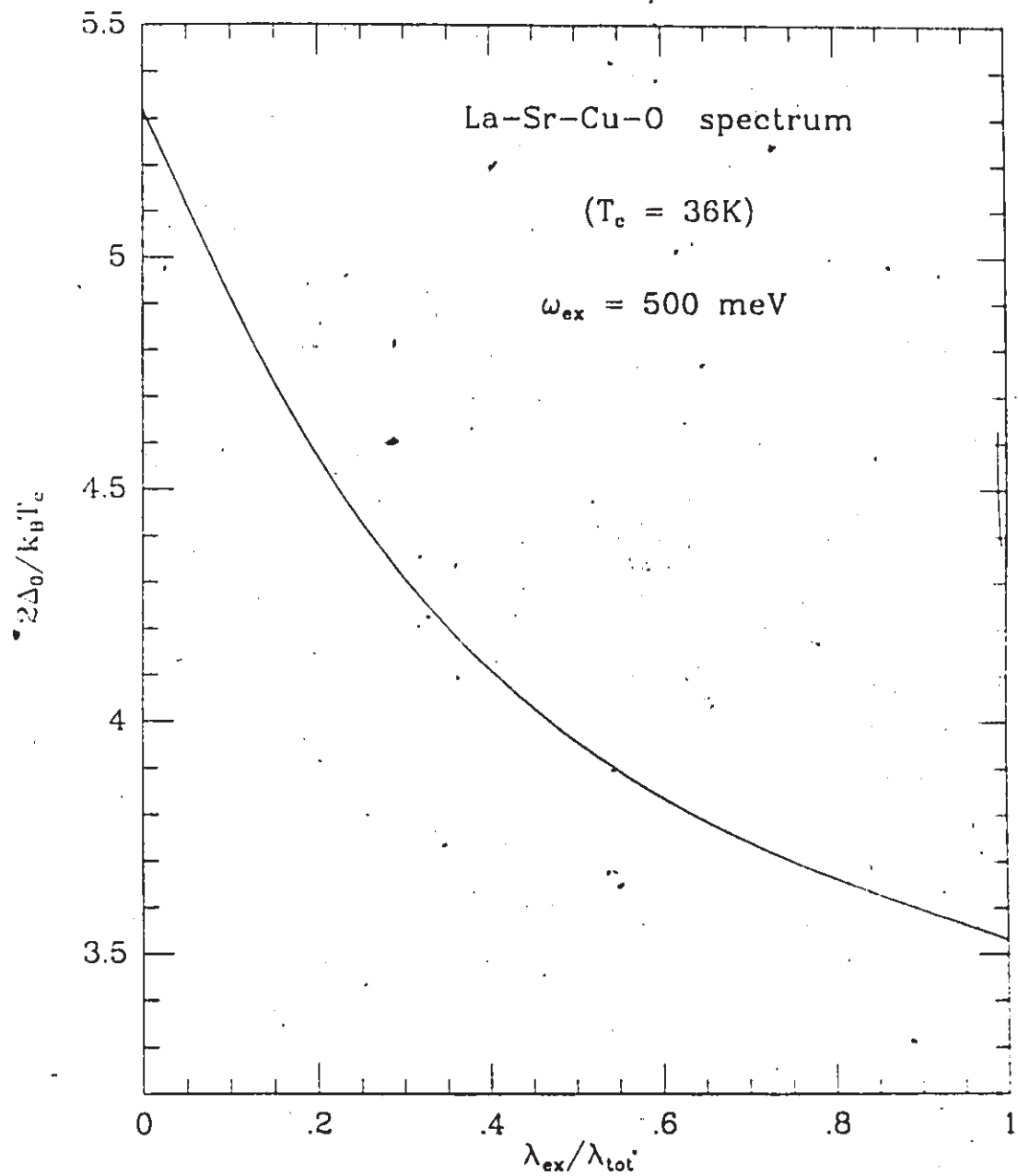
phonon-exciton model for LSCO. The degree of agreement can be varied, however, by adjustment of choice of $\frac{\lambda_{ex}}{\lambda_{tot}}$ and by variation of μ^*, not to mention the choice of the experimental value of $\frac{\Delta C(T_c)}{T_c}$. What is clear, however, is that significant improvement has been achieved over the pure phonon model.

Theoretical calculations for the reduced upper critical magnetic field $h_{c2}(0)$ are also presented in Table 4. We have ignored Pauli limiting, as it was found to play a minor role.[104] The experimentally accessible quantity is, however, $H'_{c2}(T_c)$, and various measured values are given in Table 5. Most of these have been taken on polycrystalline samples. The measurement of Hidaka et al,[181e] for example, clearly demonstrates the anisotropy of a single crystal, which we have assumed has been averaged over in the polycrystalline samples. There is a considerable variation in the slopes, which may be due to impurity dependence of the sample involved, as well as the choice of onset or midpoint, as previously mentioned.

One can write $H'_{c2}(T_c) = F[\alpha^2 F(\nu), \mu^*, t^+]/v_F^2$, where F is a functional completely determined by the model spectrum, Coulomb pseudopotential and impurity content. If we fit an average slope (say $2\frac{T}{K}$), we find an average Fermi velocity, $v_F \approx 0.14 \times 10^6$ m/s for $t^+ = 0$ and $v_F = 0.58 \times 10^6$ m/s for $t^+ = 100$ meV, a fairly dirty value. For completeness we have presented results in Table 4 for the reduced Ginzburg-Landau parameter $k(T)$, and the reduced thermodynamic critical field, $h_c(0)$.

Electromagnetic properties have been calculated for the combined phonon-exciton mechanism. In Fig. (3.16) we plot the deviation function for the London penetration depth $D_L(t) \equiv \frac{\lambda_L^2(0)}{\lambda_L^2(T)} - (1 - t^4)$, as a function of reduced temperature for the case $\frac{\lambda_{ex}}{\lambda_{tot}} = 0.5$, as well as the cases $\lambda_{ex} = 0$

Figure 3.14   Plot of $\frac{\Delta C(T_c)}{\gamma_0 T_c}$ vs. $\frac{\lambda_{ex}}{\lambda_{tot}}$ for tthe combined phonon-exciton model considered in the text.

La–Sr–Cu–O spectrum

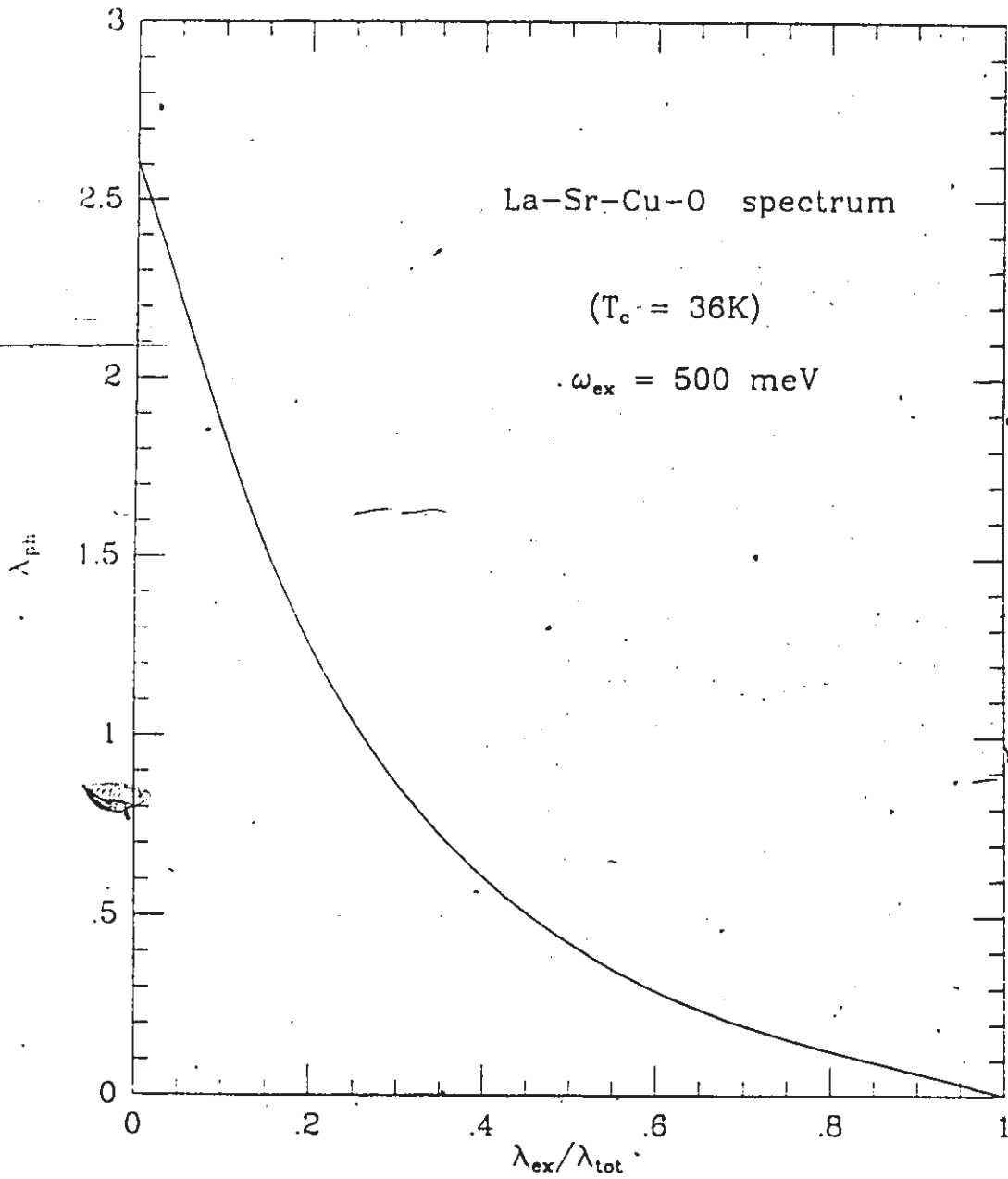$(T_c = 36K)$

$\omega_{ex} = 500$ meV
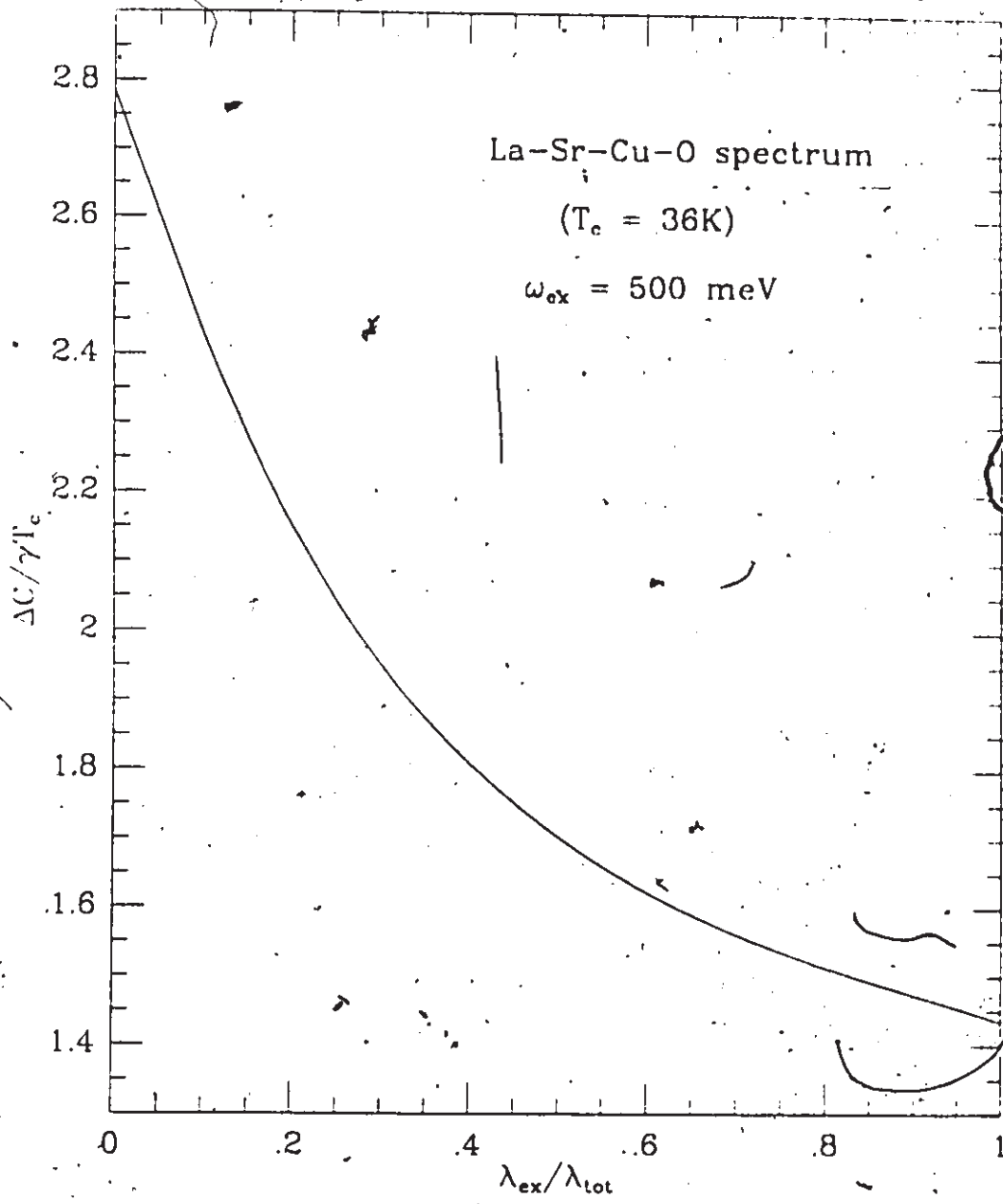
(pure phonon) and $\lambda_{ph} = 0$ (pure exciton, BCS). The differences between the three cases are quite pronounced, although these types of curves are generally not uniquely determined, as they are impurity dependent as well. However, if LSCO can be established as being in one of the impurity limits, then distinction of the three cases based on these types of curves may be possible. Using the Fermi velocity quoted above for the clean limit, and the density of states $N(0)$ quoted earlier, we find the zero temperature London penetration depth, $\lambda_L(0) = 2400$ Å. The zero temperature electromagnetic coherence length is found to be $\xi(0) = 29\text{Å}$ which is comparable to the cell size in these materials.

Finally, one very important consequence of a combined exciton-phonon model was first indicated in the work of Kus and Carbotte.[144] They found that even when the phonon coupling is relatively small, the I-V characteristic at low frequency displays a large variation when a high frequency peak is present. Tunneling measurements at higher frequencies are difficult so that such a high frequency peak (as caused, for example, by a high frequency optical phonon, or some electronic excitation) would remain undetected. Inversion procedures would then inevitably fail. This has already happened in the case of $Ba(Pb,Bi)O_3$.[145] We expect a similar problem in the case of LSCO, assuming it is described by a combined phonon-exciton model.

While the possibility of a combined phonon-exciton model looks very promising the existing experimental information is not sufficient to rule out either the pure phonon or pure "exciton" (BCS) case. In particular Schossmann et al.[104] have examined the former. Arberg et al.[146] have considered the latter case and find consistency with their experimental results.

Figure 3.15 Plot of λ_{ph} vs. $\frac{\lambda_{ex}}{\lambda_{tot}}$ for the combined phonon-exciton model considered in the text.

La-Sr-Cu-O spectrum

$(T_c = 36K)$

$\omega_{ex} = 500$ meV

Vertical axis: λ_{ph}

Horizontal axis: $\lambda_{ex}/\lambda_{tot}$

3.6   VERY STRONG COUPLING REVISITED
(i)   Asymptotic Limits

In section 4 of this chapter we discussed the possibility of the high T_c oxides being in the very strong coupling regime, $\frac{T_c}{\omega_{\ln}} \approx 1$. In this section, we pursue this possibility further, and examine the behaviour of superconducting properties in the limit $\lambda \to \infty$. This exercise, though somewhat theoretical, will help elucidate the effects of strong coupling, while at the same time will equip us with some useful limiting values.

The first work on asymptotic limits was done by Allen and Dynes.[26] They found that in the limit of $T_c \gg \nu_E$, where ν_E is the frequency at which the Einstein spectrum is located, T_c is given by:
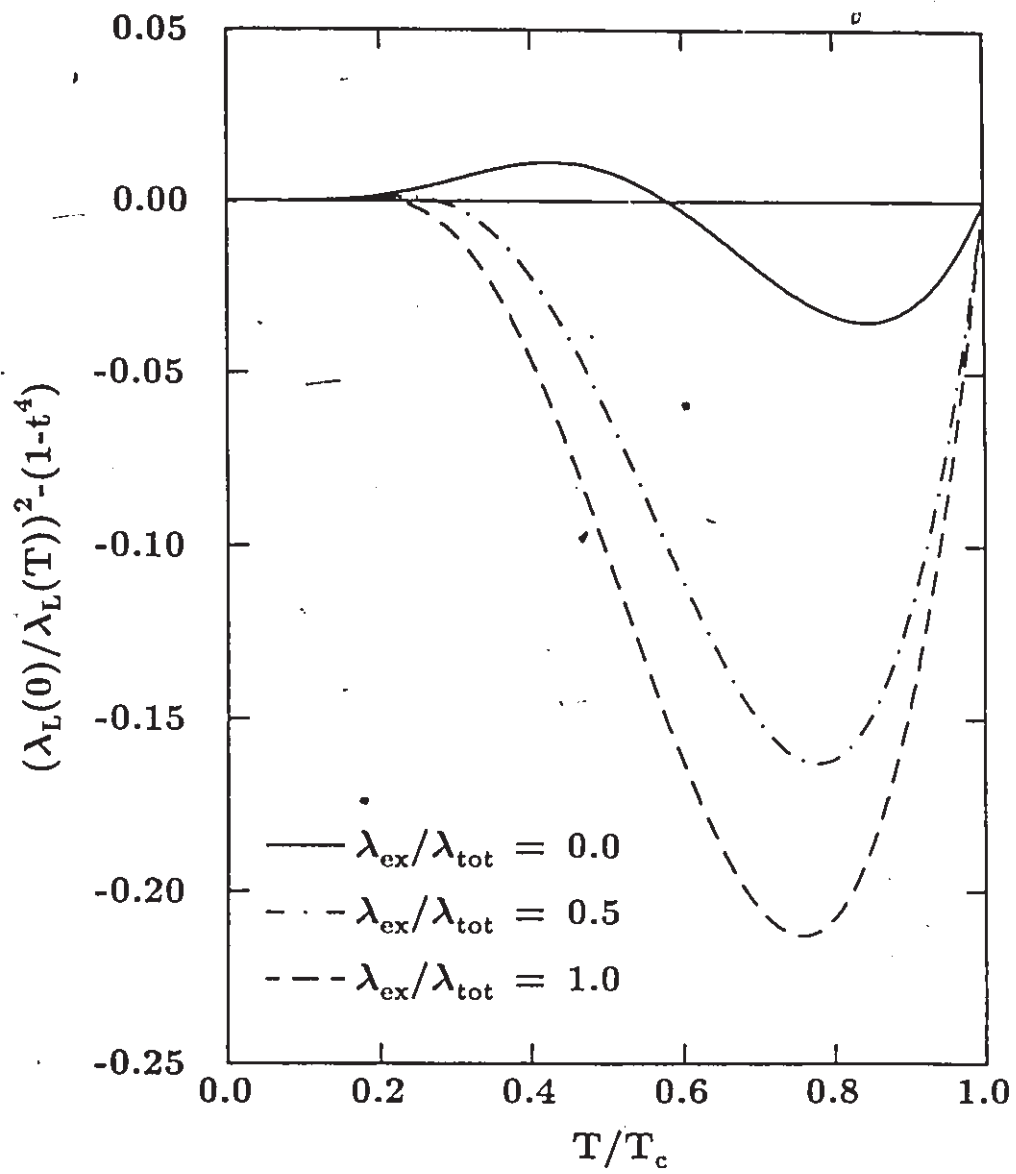
$$T_c = 0.258 \sqrt{A\nu_E} . \tag{3.7}$$

Noting that $\lambda \equiv \frac{2A}{\nu_E}$, Eq. (3.7) says two things:

1) If the Einstein frequency is held fixed, then $T_c \propto \sqrt{\lambda}$, and grows with increasing λ.

2) If the area is held fixed, then $T_c \propto \frac{1}{\sqrt{\lambda}}$, and decreases with increasing λ.

The optimum spectrum analysis for T_c described in Ch. 2 implicitly keeps A fixed while varying λ, so that the optimum λ is some number of order unity. Conversely, if ν_E is held fixed, the optimum λ will be infinity. In studying ratios such as $\frac{2\Delta_0}{k_B T_c}$ [91] and $\frac{\Delta C}{\gamma_0 T_c}$,[88] however, one finds that they depend only on λ, so that the optimum spectrum is unambiguously defined. In their search for an optimum spectrum for $\frac{2\Delta_0}{k_B T_c}$, Carbotte et al.[91] found that $\frac{2\Delta_0}{k_B T_c}$ continued to increase as λ was increased. They showed that $\frac{2\Delta_0}{k_B T_c}$ approaches a universal number in the limit $\lambda \to \infty$, since $\Delta_0 \propto \sqrt{A\nu_E}$ has the same asymptotic

Figure 3.16   Plot of $D_L(t)$ vs t for the pure phonon case, for $\frac{\lambda_{ex}}{\lambda_{tot}} = 0.5$, and for the pure exciton case, in the clean limit. Very accurate data on the penetration depth could discern these possibilities. Additional complication arises, however, due to impurity dependence.

behaviour as T_c . The proof used is not entirely rigorous, as is explained in Appendix E. However, numerical work has verified the result. Hence, the important result is that $\frac{2\Delta_0}{k_B T_c}$ could not increase indefinitely with increasing strong coupling was demonstrated. We have found $\frac{2\Delta_0}{k_B T_c}\Big|_{max} \approx 13$. It is important to note, however, that nonzero μ^* and realistic shapes tend to reduce this value, and furthermore that this maximum value is achieved only in the limit $\lambda \to \infty$. In fact, for the Einstein spectrum used in Ref. 91, $\frac{2\Delta_0}{k_B T_c} \approx 9$ for $\lambda = 20$. Such a large value of λ is most certainly beyond the physical regime for phonons; beyond this limit the exercise is more academic, unless perhaps very low frequency electronic excitations are responsible for the superconductivity .

An analytic estimate was also given in Ref. 91, and is improved upon in Appendix E. Kresin[147] has also provided an analytic estimate; he finds $\frac{2\Delta_0}{k_B T_c} \approx 13.4$, which is surprisingly close to the numerical result. On the other hand, we note that Bulaevskii et al.[92,148] claim that $\frac{2\Delta_0}{k_B T_c} \propto \sqrt{\lambda}$ and hence never reaches a maximum. While we of course discount this claim, it is to some extent irrelevant; a practical limit appears to be $\frac{2\Delta_0}{k_B T_c} \approx 10$.

Other asymptotic limits[148] follow through an analysis similar to that given in Appendix E. The free energy difference, Eq. (2.26), becomes, near T_c , for $\nu_E \to 0$,

$$\frac{\Delta F}{N(0)} = aA\,\nu_E\,(1-t)^2 \tag{3.8}$$

where a is a constant. Thus, using Eq. (2.27), we find,

$$\lim_{\lambda \to \infty} \left(\frac{\Delta C(T_c)}{\gamma_0 T_c} \right) = \frac{b}{\lambda} \,, \tag{3.9}$$

where $b = 19.82$ was determined numerically. The reduced thermodynamical critical field, $h_c(t)$, is also found to display the behaviour,
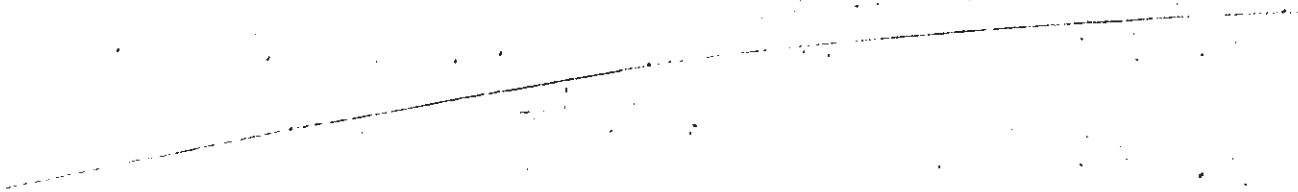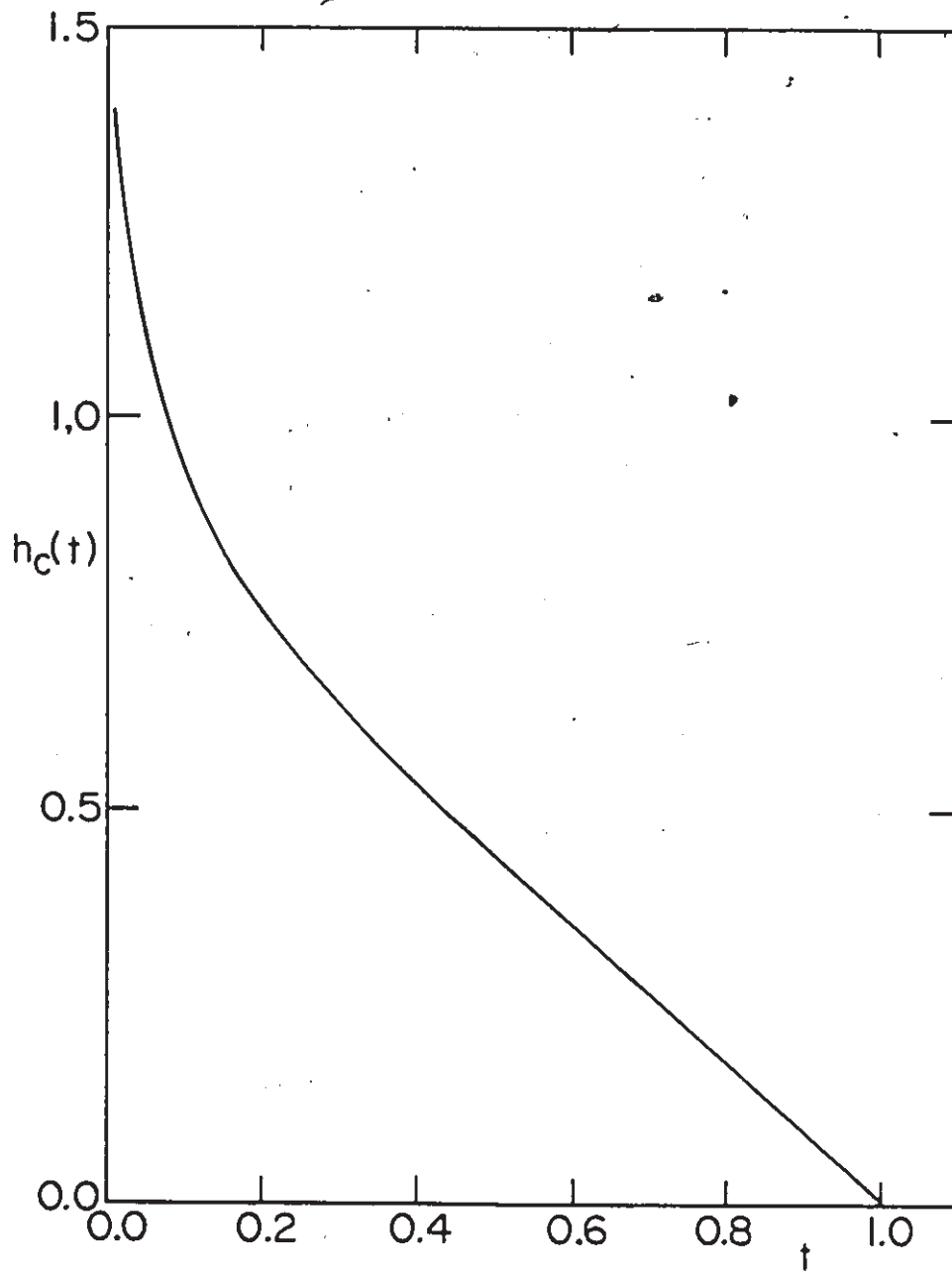
Figure 3.17 Plot of $h_c(t)$ vs. t in the limit of $\lambda \to \infty$. The curve has pronounced positive curvature with the zero temperature value unclear. We believe that it is (pathologically) infinite, reflecting a qualitative difference in scaling with λ at $T = 0$ (as compared to $T > 0$) for $h_c(T)$, which is not present, we believe, for $\Delta_0(T)$.

$$\lim_{\lambda \to \infty} h_c(t, \lambda) = g(t) \tag{3.10}$$

where $g(t)$ is a universal function of reduced temperature, and is displayed in Fig. (3.17). Our analysis here in inconclusive, however. We have been unable to extend our calculations to below $t \approx 0.01$, and it is not clear whether $g(t = 0)$ is finite or not. A theoretical analysis at $T = 0$ is prevented by the difficulty mentioned in Appendix E. Similarly, the upper critical magnetic fields have not been analysed analytically, although it is known numerically[92,148,89] that $h_{c2}(0, t^+ = 0) \to$ const., and $h_{c2}(0, t^+ \to \infty) \propto \sqrt{\lambda}$ in the asymptotic limit. Finally, the electromagnetic properties are readily studied in the asymptotic regime. From Eq. (2.39), we note that $\lim_{\lambda \to \infty} y_L(t) = \frac{a_L}{\lambda}$ for $t > 0$ and "a_L" a constant. Note, however, that $\lim_{\lambda \to \infty} y_\ell(t) = \frac{a_\ell}{\sqrt{\lambda}}$. Moreover, Eq. (2.41) yields for the coherence length, $\lim_{\lambda \to \infty} \xi(t) = \frac{a_c}{\sqrt{\lambda}}$. Note that included in these constants (a_L, a_ℓ, a_c) are *bare* masses and Fermi velocities, and not *dressed* quantities. The asymptotic behaviour will clearly differ depending on whether bare or dressed $\left(v_F^* = \frac{v_F}{1+\lambda}, \ m^* = m(1+\lambda), \ N(0)^* = N(0)(1+\lambda)\right)$ properties are used.

The coherence length lends itself to further study, analytically, since

$$\lim_{\lambda \to \infty} Z(i\omega_n) = \frac{\pi T}{\sqrt{\omega_n^2 + \Delta_n^2}} \lambda, \quad T > 0. \tag{3.11}$$

Hence,

$$\lim_{\lambda \to \infty} \xi(t) = \frac{v_F}{2\pi T} \frac{1}{\lambda}, \quad T > 0. \tag{3.12}$$

Note that in the dirty limit we found in Ch. 2 that $\xi(t) = \frac{v_F}{2\pi t^+}$, so $T\lambda$ has taken on the role of impurities, as we have already argued it should, since low frequency phonons are really like static impurities. Note that finite temperature is important, as indicated by the presence of "T" in the correspondence.

Figure 3.18   Plot of $\Re_e \Delta(\omega)$ (—) and $\Im_m \Delta(\omega)$ ($\cdots$) vs. ω produced from an Einstein spectrum with $\omega_E = 8$ meV, and $\lambda = 1$. The straight dashed line is the curve $f(\omega) = \omega$. See text for an elucidation of the features of these curves.
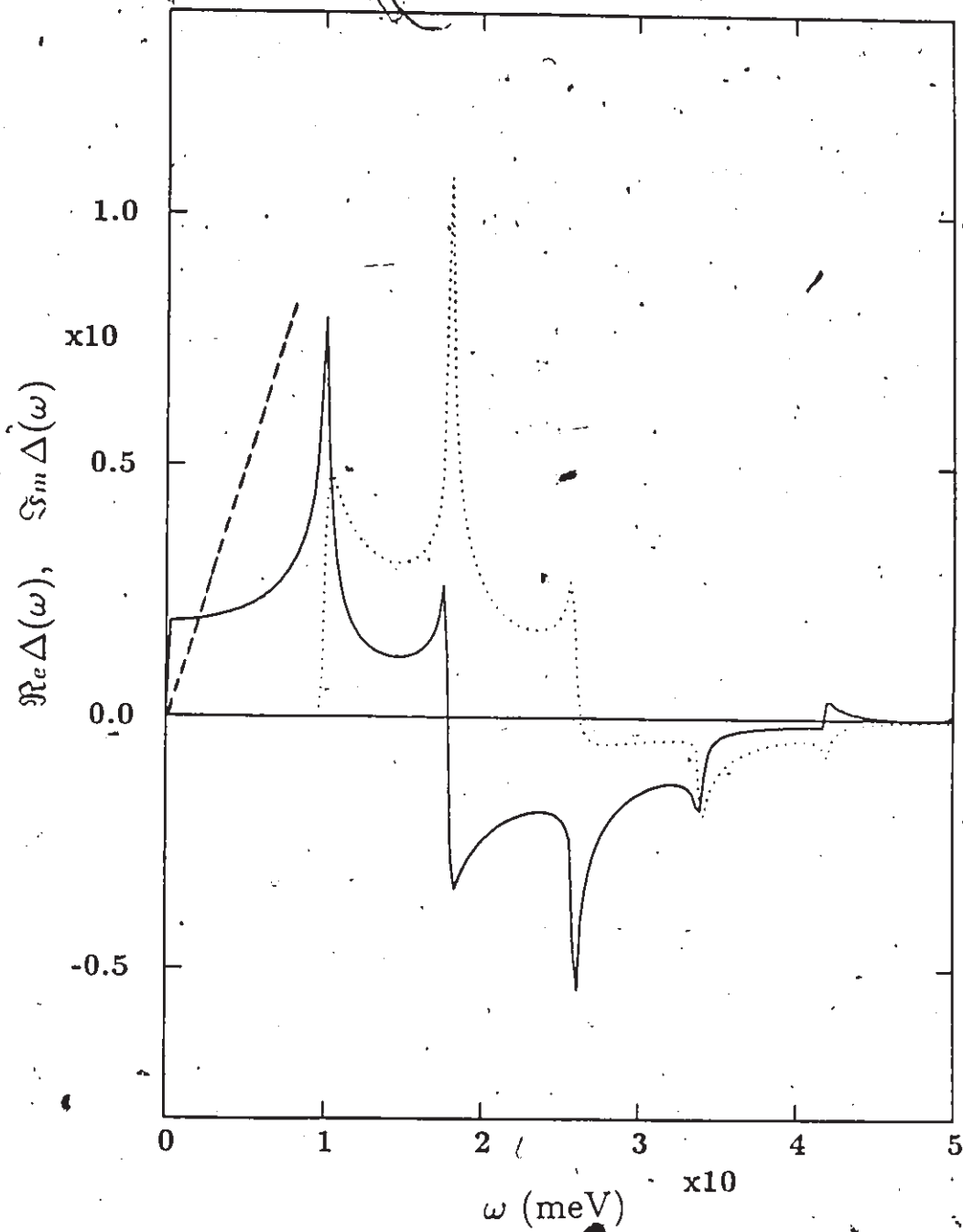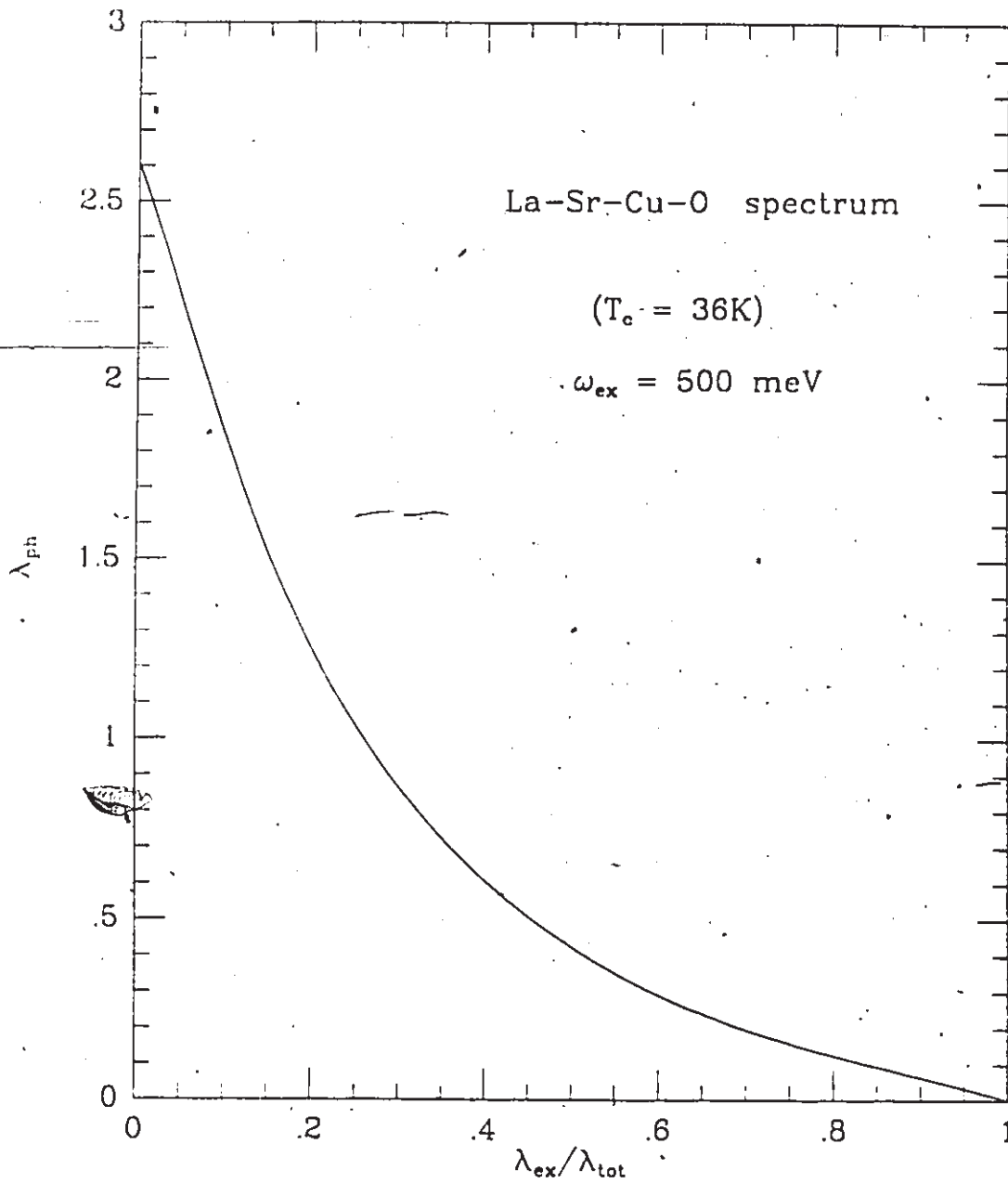
Figure 3.15 Plot of λ_{ph} vs. $\frac{\lambda_{ex}}{\lambda_{tot}}$ for the combined phonon-exciton model considered in the text.

La-Sr-Cu-O spectrum

$(T_c = 36K)$

$\omega_{ex} = 500$ meV

3.6   VERY STRONG COUPLING REVISITED
(i) Asymptotic Limits

In section 4 of this chapter we discussed the possibility of the high T_c oxides being in the very strong coupling regime, $\frac{T_c}{\omega_{\ln}} \approx 1$. In this section, we pursue this possibility further, and examine the behaviour of superconducting properties in the limit $\lambda \to \infty$. This exercise, though somewhat theoretical, will help elucidate the effects of strong coupling, while at the same time will equip us with some useful limiting values.

The first work on asymptotic limits was done by Allen and Dynes.[26] They found that in the limit of $T_c \gg \nu_E$, where ν_E is the frequency at which the Einstein spectrum is located, T_c is given by:
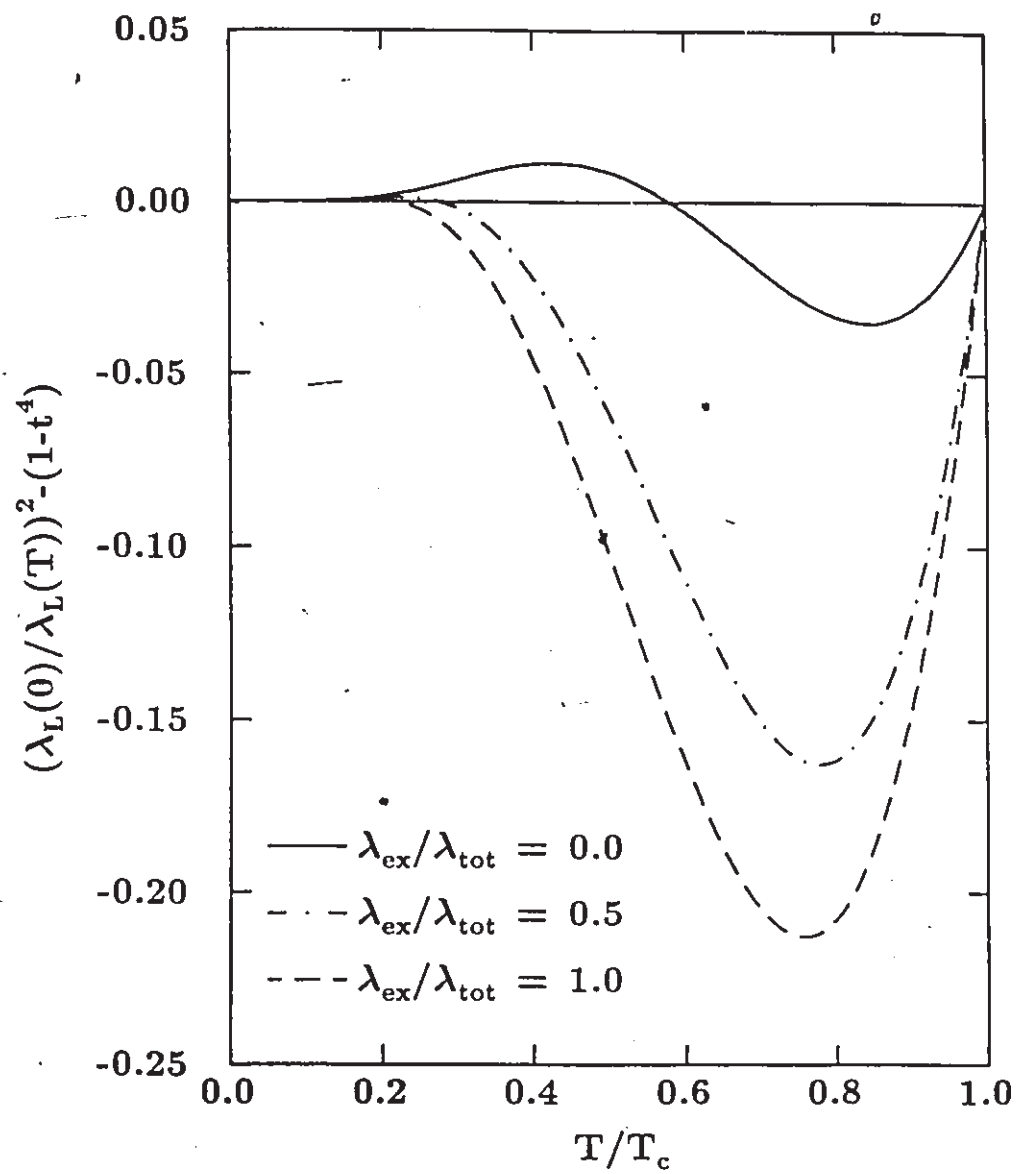
$$T_c = 0.258\sqrt{A\nu_E}\,. \qquad\qquad (3.7)$$

Noting that $\lambda \equiv \frac{2A}{\nu_E}$, Eq. (3.7) says two things:

1) If the Einstein frequency is held fixed, then $T_c \propto \sqrt{\lambda}$, and grows with increasing λ.

2) If the area is held fixed, then $T_c \propto \frac{1}{\sqrt{\lambda}}$, and decreases with increasing λ.

The optimum spectrum analysis for T_c described in Ch. 2 implicitly keeps A fixed while varying λ, so that the optimum λ is some number of order unity. Conversely, if ν_E is held fixed, the optimum λ will be infinity. In studying ratios such as $\frac{2\Delta_0}{k_B T_c}$ [91] and $\frac{\Delta C}{\gamma_0 T_c}$,[88] however, one finds that they depend only on λ, so that the optimum spectrum is unambiguously defined. In their search for an optimum spectrum for $\frac{2\Delta_0}{k_B T_c}$, Carbotte et al.[91] found that $\frac{2\Delta_0}{k_B T_c}$ continued to increase as λ was increased. They showed that $\frac{2\Delta_0}{k_B T_c}$ approaches a universal number in the limit $\lambda \to \infty$, since $\Delta_0 \propto \sqrt{A\nu_E}$ has the same asymptotic

Figure 3.16   Plot of $D_L(t)$ vs t for the pure phonon case, for $\frac{\lambda_{ex}}{\lambda_{tot}} = 0.5$, and for the pure exciton case, in the clean limit. Very accurate data on the penetration depth could discern these possibilities. Additional complication arises, however, due to impurity dependence.

behaviour as T_c . The proof used is not entirely rigorous, as is explained in Appendix E. However, numerical work has verified the result. Hence, the important result is that $\frac{2\Delta_0}{k_B T_c}$ could not increase indefinitely with increasing strong coupling was demonstrated. We have found $\frac{2\Delta_0}{k_B T_c}\Big|_{max} \approx 13$. It is important to note, however, that nonzero μ^* and realistic shapes tend to reduce this value, and furthermore that this maximum value is achieved only in the limit $\lambda \to \infty$. In fact, for the Einstein spectrum used in Ref. 91, $\frac{2\Delta_0}{k_B T_c} \approx 9$ for $\lambda = 20$. Such a large value of λ is most certainly beyond the physical regime for phonons; beyond this limit the exercise is more academic, unless perhaps very low frequency electronic excitations are responsible for the superconductivity .

An analytic estimate was also given in Ref. 91, and is improved upon in Appendix E. Kresin[147] has also provided an analytic estimate; he finds $\frac{2\Delta_0}{k_B T_c} \approx 13.4$, which is surprisingly close to the numerical result. On the other hand, we note that Bulaevskii et al.[92,148] claim that $\frac{2\Delta_0}{k_B T_c} \propto \sqrt{\lambda}$ and hence never reaches a maximum. While we of course discount this claim, it is to some extent irrelevant; a practical limit appears to be $\frac{2\Delta_0}{k_B T_c} \approx 10$.

Other asymptotic limits[148] follow through an analysis similar to that given in Appendix E. The free energy difference, Eq. (2.26), becomes, near T_c , for $\nu_E \to 0$,

$$\frac{\Delta F}{N(0)} = a A \nu_E (1 - t)^2 \tag{3.8}$$

where a is a constant. Thus, using Eq. (2.27), we find,

$$\lim_{\lambda \to \infty} \left(\frac{\Delta C(T_c)}{\gamma_0 T_c} \right) = \frac{b}{\lambda} , \tag{3.9}$$

where $b = 19.82$ was determined numerically. The reduced thermodynamical critical field, $h_c(t)$, is also found to display the behaviour,
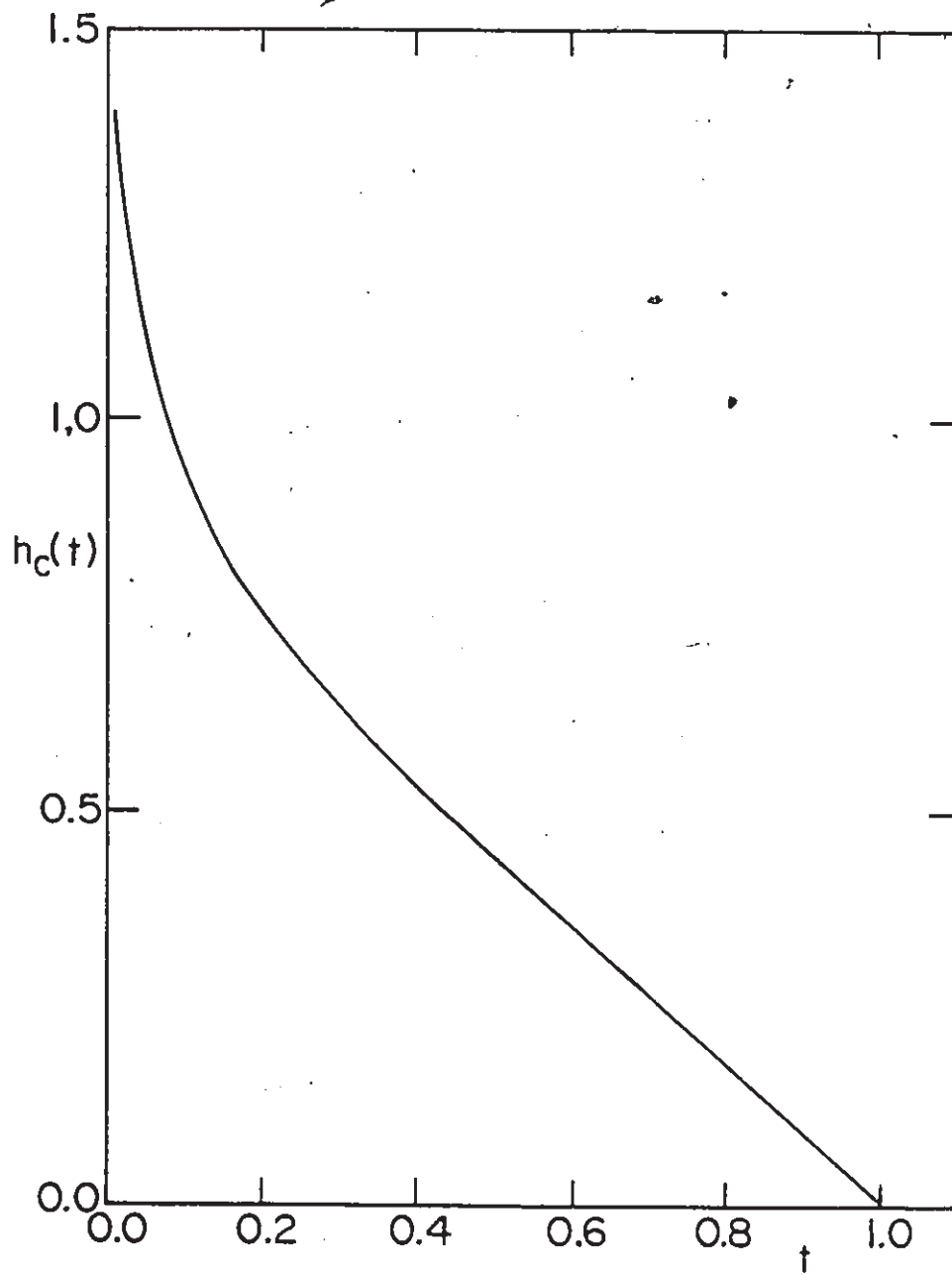
Figure 3.17   Plot of $h_c(t)$ vs. t in the limit of $\lambda \to \infty$. The curve has pronounced positive curvature with the zero temperature value unclear. We believe that it is (pathologically) infinite, reflecting a qualitative difference in scaling with λ at $T = 0$ (as compared to $T > 0$) for $h_c(T)$, which is not present, we believe, for $\Delta_0(T)$.

$$\lim_{\lambda \to \infty} h_c(t, \lambda) = g(t) \qquad (3.10)$$

where $g(t)$ is a universal function of reduced temperature, and is displayed in Fig. (3.17). Our analysis here in inconclusive, however. We have been unable to extend our calculations to below $t \approx 0.01$, and it is not clear whether $g(t = 0)$ is finite or not. A theoretical analysis at $T = 0$ is prevented by the difficulty mentioned in Appendix E. Similarly, the upper critical magnetic fields have not been analysed analytically, although it is known numerically[92,148,89] that $h_{c2}(0, t^+ = 0) \to$ const., and $h_{c2}(0, t^+ \to \infty) \propto \sqrt{\lambda}$ in the asymptotic limit. Finally, the electromagnetic properties are readily studied in the asymptotic regime. From Eq. (2.39), we note that $\lim_{\lambda \to \infty} y_L(t) = \frac{a_L}{\lambda}$ for $t > 0$ and "a_L" a constant. Note, however, that $\lim_{\lambda \to \infty} y_\ell(t) = \frac{a_\ell}{\sqrt{\lambda}}$. Moreover, Eq. (2.41) yields for the coherence length, $\lim_{\lambda \to \infty} \xi(t) = \frac{a_c}{\sqrt{\lambda}}$. Note that included in these constants (a_L, a_ℓ, a_c) are *bare* masses and Fermi velocities, and not *dressed* quantities. The asymptotic behaviour will clearly differ depending on whether bare or dressed $\left(v_F^* = \frac{v_F}{1+\lambda}, \ m^* = m(1 + \lambda), \ N(0)^* = N(0)(1 + \lambda) \right)$ properties are used.

The coherence length lends itself to further study, analytically, since

$$\lim_{\lambda \to \infty} Z(i\omega_n) = \frac{\pi T}{\sqrt{\omega_n^2 + \Delta_n^2}} \lambda , \quad T > 0 . \qquad (3.11)$$

Hence,

$$\lim_{\lambda \to \infty} \xi(t) = \frac{v_F}{2\pi T} \frac{1}{\lambda} , \quad T > 0 . \qquad (3.12)$$

Note that in the dirty limit we found in Ch. 2 that $\xi(t) = \frac{v_F}{2\pi t^+}$, so $T\lambda$ has taken on the role of impurities, as we have already argued it should, since low frequency phonons are really like static impurities. Note that finite temperature is important, as indicated by the presence of "T" in the correspondence.

Figure 3.18   Plot of $\Re_e \Delta(\omega)$ (—) and $\Im_m \Delta(\omega)$ (· · · ·) vs. ω produced from an Einstein spectrum with $\omega_E = 8$ meV, and $\lambda = 1$. The straight dashed line is the curve $f(\omega) = \omega$. See text for an elucidation of the features of these curves.

This analogue is made clear if we note that in Eqs. (2.13) and (2.14), we can include the impurity terms added later by writing $\alpha^2 F(\nu)$ as the sum of the two terms:

$$\alpha^2 F(\nu) = \alpha_{\mathrm{ph}}^2 F(\nu) + \alpha_{\mathrm{im}}^2 F(\nu) \tag{3.13a}$$

where

$$\alpha_{\mathrm{im}}^2 F(\nu) = \frac{\nu t^+ \delta(\nu)}{T} . \tag{3.13b}$$

For an Einstein spectrum, this gives exactly the correspondence suggested above. At $T = 0$, however, the situation changes dramatically. We find

$$\lim_{\lambda \to \infty} Z(i\omega) = \frac{\pi A}{\sqrt{\omega^2 + \Delta^2(\omega)}} , \quad T = 0 \tag{3.14}$$

and hence

$$\lim_{\lambda \to \infty} \xi(0) = \frac{v_F}{2\pi A} , \quad T = 0 \tag{3.15}$$

so that A has taken on the role of impurities. This is also seen by referring back to Eqs. (2.13) and (2.14) written at $T = 0$, so that

$$\alpha_{\mathrm{im}}^2 F(\nu) = t^+ \lim_{\nu \to 0} \tag{3.16}$$

will generate the impurity term when used in Eq. (3.13a). Note that here the correspondence is a little more awkward and an operator has been used. However, in both Eqs. (3.13b) and (3.16) the important requirement is that the phonon frequency is forced to zero. The qualitative difference between the $T = 0$ and $T > 0$ correspondence arises due to the fact that thermal phonons are present at $T > 0$. The low frequency expansion for the Bose function is then included in Eq. (3.13b) whereas it is not in Eq. (3.16).

This type of discontinuous behaviour exhibited by the Eliashberg equations at $T = 0$ has been noted before in other contexts. Karakosov *et al.*,[149] for example, noted that the gap function on the real axis exhibited

Figure 3.19 Plot of $\frac{N(\omega)}{N(0)}$ vs. ω for an Einstein spectrum ($\lambda = 1$, $\omega_E = 8$ meV). The peak is roughly where the gap is located. The additional peaks arise from multi-phonon scattering.
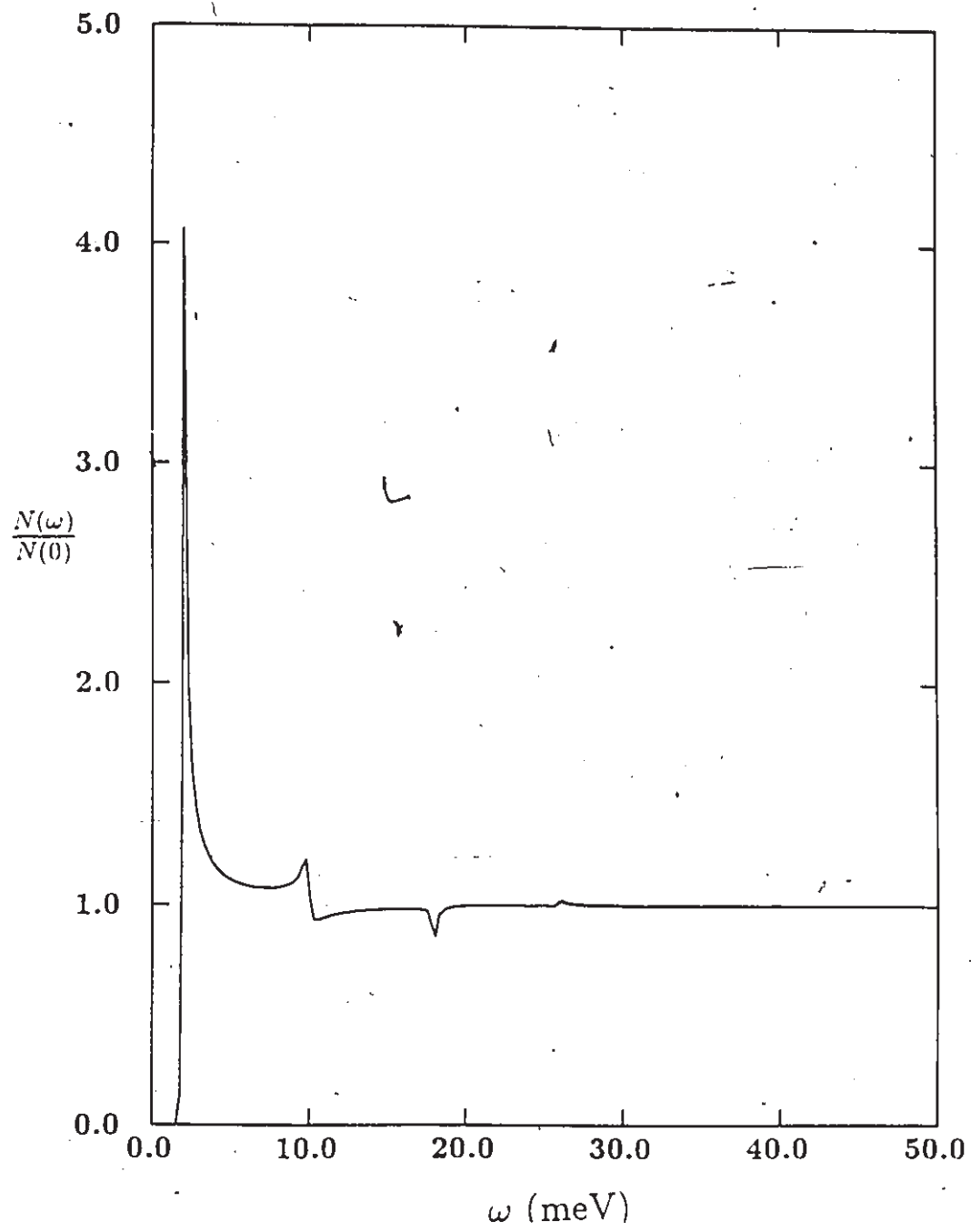
the behaviour at low frequency:

$$\Re_e \Delta(\omega) \propto \omega^2$$
$$\Im_m \Delta(\omega) \propto \omega \qquad T > 0 \qquad\qquad (3.17a)$$

but at $T = 0$, this became, for low frequnecy,

$$\Re_e \Delta(\omega) = c$$
$$\Im_m \Delta(\omega) = 0 \qquad T = 0 \qquad\qquad (3.18a)$$

where c is a positive constant and $\Im_m \Delta(\omega)$ is identically zero right up to the gap edge. At low temperatures this has little practical consequence, since, despite the frequency dependence at $\omega \to 0$, a constant value for the gap is achieved very quickly.

Finally, we wish to discuss the quasiparticle density of states, in the asymptotic regime, $\Delta_0 \ll \omega_E$, where ω_E is the frequency of an Einstein spectrum which we use, say, to model some material. Figures (3.18) and (3.19) display the gap function on the real axis, and $\frac{N(\omega)}{N(0)}$, respectively. Note several things:

i) The gap function becomes negative even though $\mu^* = 0$.

ii) The zero crossing occurs at roughly $\omega_0 \approx 2\omega_E + \Delta_0$.

iii) The gap function is relatively flat in the region in which the gap edge is defined.

iv) Although not readily apparent from these figures alone, both the gap function and $\frac{N(\omega)}{N(0)}$ contain an image of $\alpha^2 F(\nu)$, in this case, an Einstein spectrum.

v) $\frac{N(\omega)}{N(0)}$ is zero up to the gap edge, there is a square-root singularity at $\omega = \Delta_0$ and there is structure at multiples of $\omega_E (= 8\,\text{meV})$.

These images of the Einstein mode arise from multiple phonon scattering.

Figure 3.20 Same as for Fig. 3.18, but with $\lambda \to \infty$. The variables used are actually-scaled variables ($i.e.\,\bar{\Delta}(\bar{\omega}) \equiv \frac{\Delta(\omega)}{\sqrt{A\nu_E}}$, and $\bar{\omega} \equiv \frac{\omega}{\sqrt{A\nu_E}}$). The intersections of the $\Re_e\,\bar{\Delta}(\bar{\omega})$ with the line $y = \bar{\omega}$ (for $\Im_m\,\bar{\Delta}(\bar{\omega}) = 0$) define "gap edges".
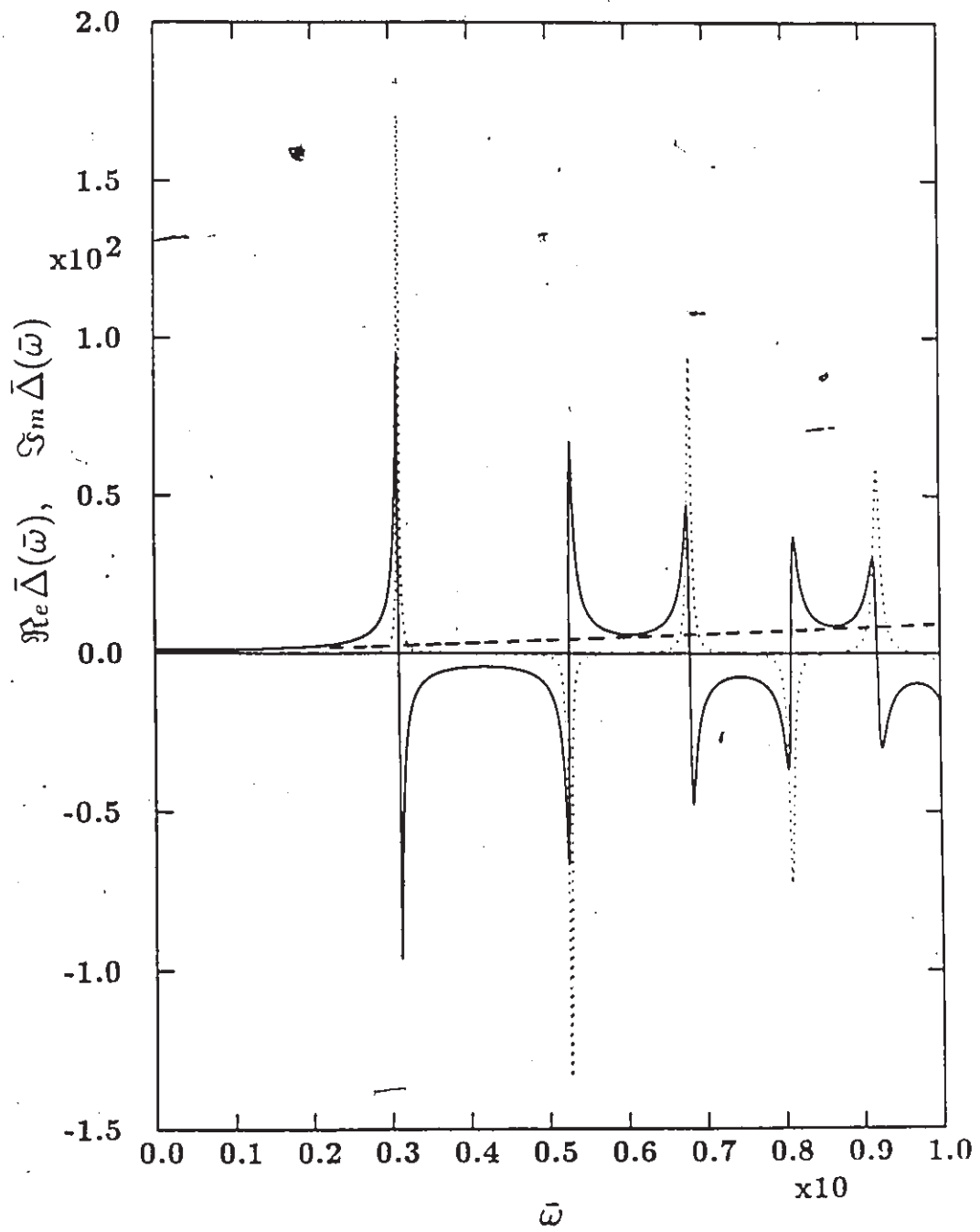
The same functions are plotted in Figures (3.20) and (3.21) for $\lambda \to \infty$ (they have been normalized to $\sqrt{A\nu_E}$, of course). Note the sharp structure which mainly reflects the fact that an Einstein spectrum has been used. However, the multiple peaks present in Fig. (3.21) are puzzling at first, since $\omega_E \to 0$, and hence they cannot be due to multiple phonon scattering. They in fact represent multiple gaps, as can be seen from Fig. (3.20). The equation, $|\Re_e \Delta(\omega)| = \omega$ is now satisfied at several points, as is shown. The zero crossing now occurs at $2\Delta_0$, and there is continued oscillation with decreasing period beyond this point. The structure in both figures is now on a scale of Δ_0, the gap edge; it has in effect taken over the previous role of ω_E. A simple explanation of this is due to Kivelson.[150] In the $\lambda \to \infty$ limit, the coherence distance becomes very small so that Cooper pairs are much more tightly bound in real space (see Eq. 3.12). Hence, there ought to be an increased density of states at $3\Delta_0$, $5\Delta_0$, *etc.*, corresponding to the fact that one or more Cooper pairs are being excited into particle-hole states as a single electron tunnels across the normal superconducting barrier. In a simple BCS picture, these excitations cost $(2n-1)\Delta_0$, $n = 2, 3, 4, \ldots$. We find peaks in the tunneling density of states at value of energy somewhat less than these multiples. This no doubt is due to life-time effects which come in as $\lambda \to \infty$ and are absent within BCS.

ii) High T_c Oxides

Some reports[180m,185p] have appeared presenting results of tunneling characteristics which display structure at $3\Delta_0$ and $5\Delta_0$. This would suggest the possibility that λ is very large in the high T_c oxides. It should be noted,

Figure 3.21 Same as for Fig. 3.19, but with $\lambda \to \infty$. Note that peaks occur because of the multiple gaps present (see Fig. 3.20) and not due to phonon scattering.
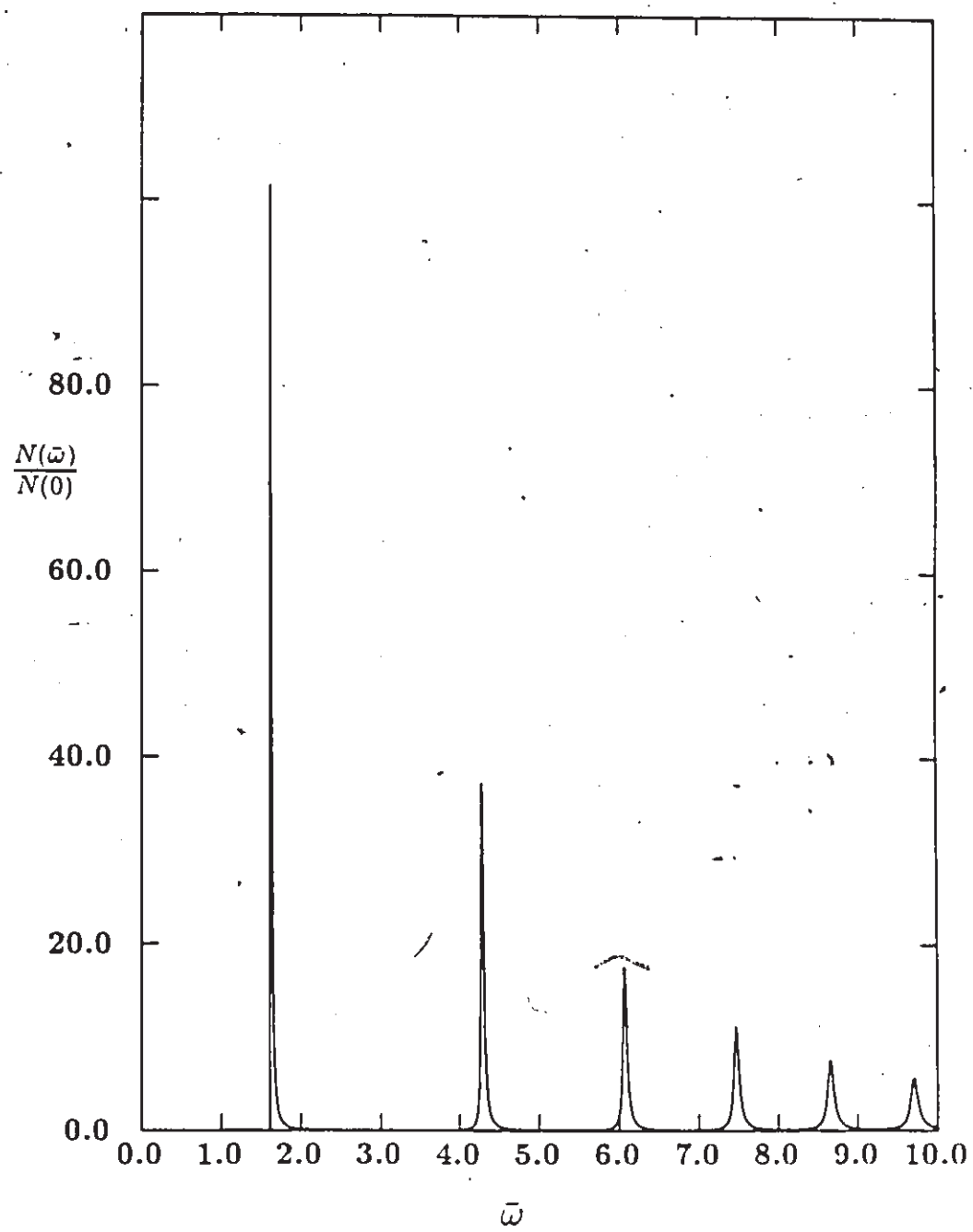
however, that this structure is expected to appear as long as $\Delta_0 \gg \omega_E$, so that this effect will appear in the very strong coupling regime (and not only when $\lambda \to \infty$) discussed earlier. Figure (3.22) illustrates an I-V characteristic for an Einstein spectrum with $\omega_E = 3\,\text{meV}$ and $\lambda = 30$. T_c was calculated to be almost $3\,\text{meV}$ so that $\frac{T_c}{\omega_{\ln}} \approx 1$. The gap edge is $14\,\text{meV}$. Multiple peaks are evident in the figure. Note that we have used $t = 0.3$ in order to smear out the artificial structure (on a scale of $\sim 3\,\text{meV}$) Einstein mode; this would in practice be smeared out by the effects of a realistic spectrum. In Table 6 we have listed some of the experimental properties of YBCO. As was the case with LSCO, there is quite a spread in measured values of $\frac{2\Delta_0}{k_B T_c}$, with the same trends as in that case; far-infrared values are BCS-like whereas tunneling values are quite high. Again, there is no frequency below which zero absorptivity is observed in any of the far-infrared measurements as is required by Mattis-Bardeen theory.[151] Similarly the tunneling measurements are not sharp and as mentioned above, anomalous structure is seen in the I-V characteristic. In light of the last result of the previous section, this structure may be interpreted as evidence for strong coupling (in the sense $\lambda \gg 1$). At this stage, however, this is somewhat speculative, since many tunneling characteristics do not display structure, and an anomalous background is unaccounted for. We will pursue this analysis in any event. For the spectrum with $\lambda = 30$ shown in Fig. (3.22), $\frac{2\Delta_0}{k_B T_c} \approx 9\text{--}10$, which agrees with some of the tunneling results. Many specific heat measurements have also been performed. the results of which are listed in Table 6. Let us consider as given an average measured value of $\frac{\Delta C(T_c)}{T_c} = 15 \frac{mJ}{\text{mole Cu} - K^2}$. Then. using theoretically

Figure 3.22 $\frac{N(\omega)}{N(0)}$ vs. ω for an Einstein spectrum with $\omega_E = 3$ meV and $\lambda = 30$ ($T_c \approx 3$ meV, $\Delta_0 \approx 14$ meV). Multiple peaks due to several "gap edges" remain even for this finite value of λ. We have used $t = 0.3$ to (artificially) smear out some of the structure (on a scale of ~ 3 meV) due to the Einstein peak. In reality this would be smeared at low temperatures due to a realistic spectral shape being used.
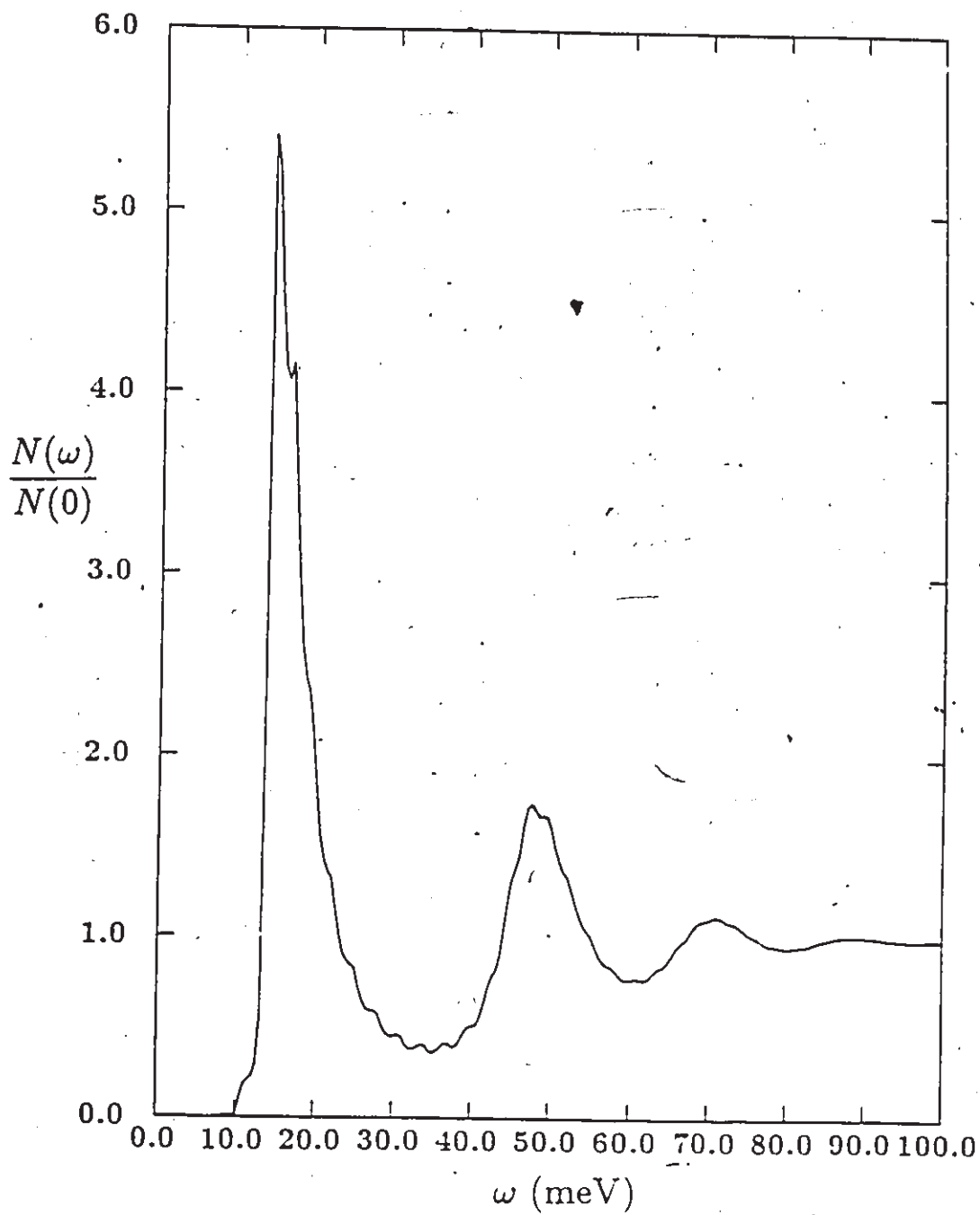
obtained $f \equiv \frac{\Delta C(T_c)}{\gamma_0 T_c}$ values we can calculate the electron density of states at the Fermi surface, $N(0)$, via Eq. (3.1). With $f = 1.43$, $N(0)(1 + \lambda) = 2.2 \frac{states}{ev-Cu-atom-spin}$. Table 6 also lists some values of $N(0)$ calculated from band structure. With $\lambda \approx 0.5$ we would obtain $N(0) \sim 1.5 \frac{states}{ev-Cu-atom-spin}$ in agreement with the upper limit of the calculated values. Higher values of λ would violate the BCS assumption (see Figs. 2.2 and 3.23). With $f = 2.8$, $N(0)(1 + \lambda) = 1.1 \frac{states}{ev-Cu-atom-spin}$. Choosing $\lambda \approx 1.5$–3.0 gives $N(0) \sim 0.28$–$0.45 \frac{states}{ev-Cu-atom-spin}$, which agrees with Massidda et al.'s[187b] values including doping. Finally, to represent the very strong coupling limit, we use the $\lambda = 30$ spectrum. Then, $f \approx 0.6$, so that $N(0)(1 + \lambda) = 5.3 \frac{states}{ev-Cu-atom-spin}$, and hence $N(0) \approx 0.2 \frac{states}{ev-Cu-atom-spin}$. This is just below the range indicated by Massidda et al.'s[187b] calculations with doping.

On the basis of the existing data, then, it is not possible to favour one or the other of these possibilities. Many uncertainties exist in the analysis itself. The bulk specific heat capacity should be used, whereas most of the measurements were performed on polcrystalline samples with as low as 25% Meissner effects at low temperatures. This would seen to indicate that only a quarter of the samples was superconducting and thus $\frac{1}{4}f$ should be used in the analysis. Moreover, Deutscher et al.[106] have noted that granularity in a sample tends to reduce the specific heat jump. Finally, anisotropy, is known to reduce the jump as well. All of these effects point toward larger γ_0 values than is obtained in this analysis, and hence larger mass renormalization, which would favour the very strong coupling limit. However, Fermi liquid effects have been ignored, and these may also play a large role in contributing to a mass renormalization. Finally, the disagreement in values for $N(0)$

Figure 3.23 (a) Plot of λ vs. $\frac{T_c}{\omega_{ln}}$; refer to Fig. 3.2 for the legend. As $\frac{T_c}{\omega_{ln}}$ increases, λ becomes more sensitive to the μ^* value. Note that large values of λ require large $\frac{T_c}{\omega_{ln}}$ values; conversely, small values of λ are tied to small values of $\frac{T_c}{\omega_{ln}}$ (BCS regime). (b) Plot of λ vs. $\frac{T_c}{\omega_{ln}}$ for scaled Pb and LSCO spectra, with $\mu^* = 0.1$.
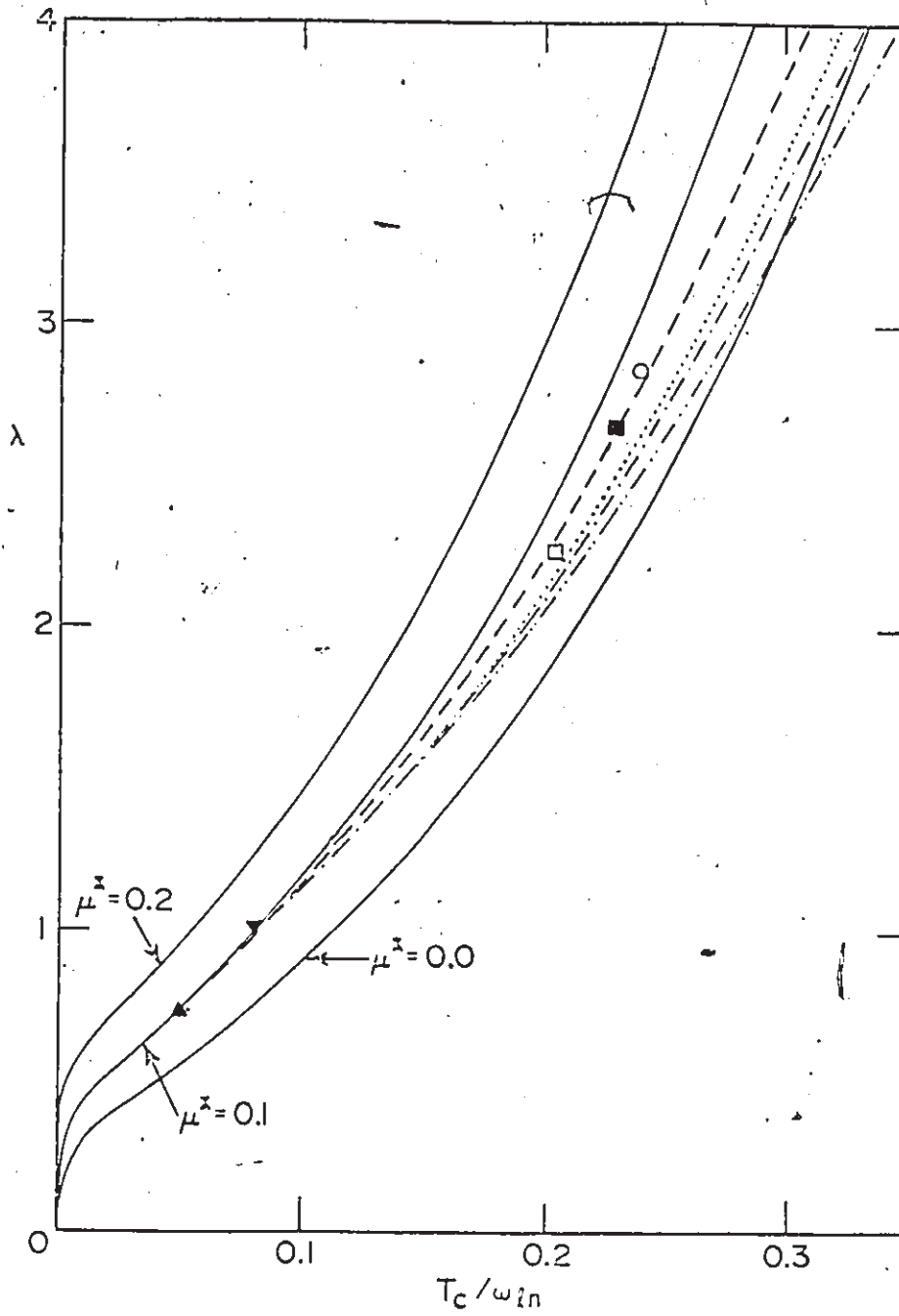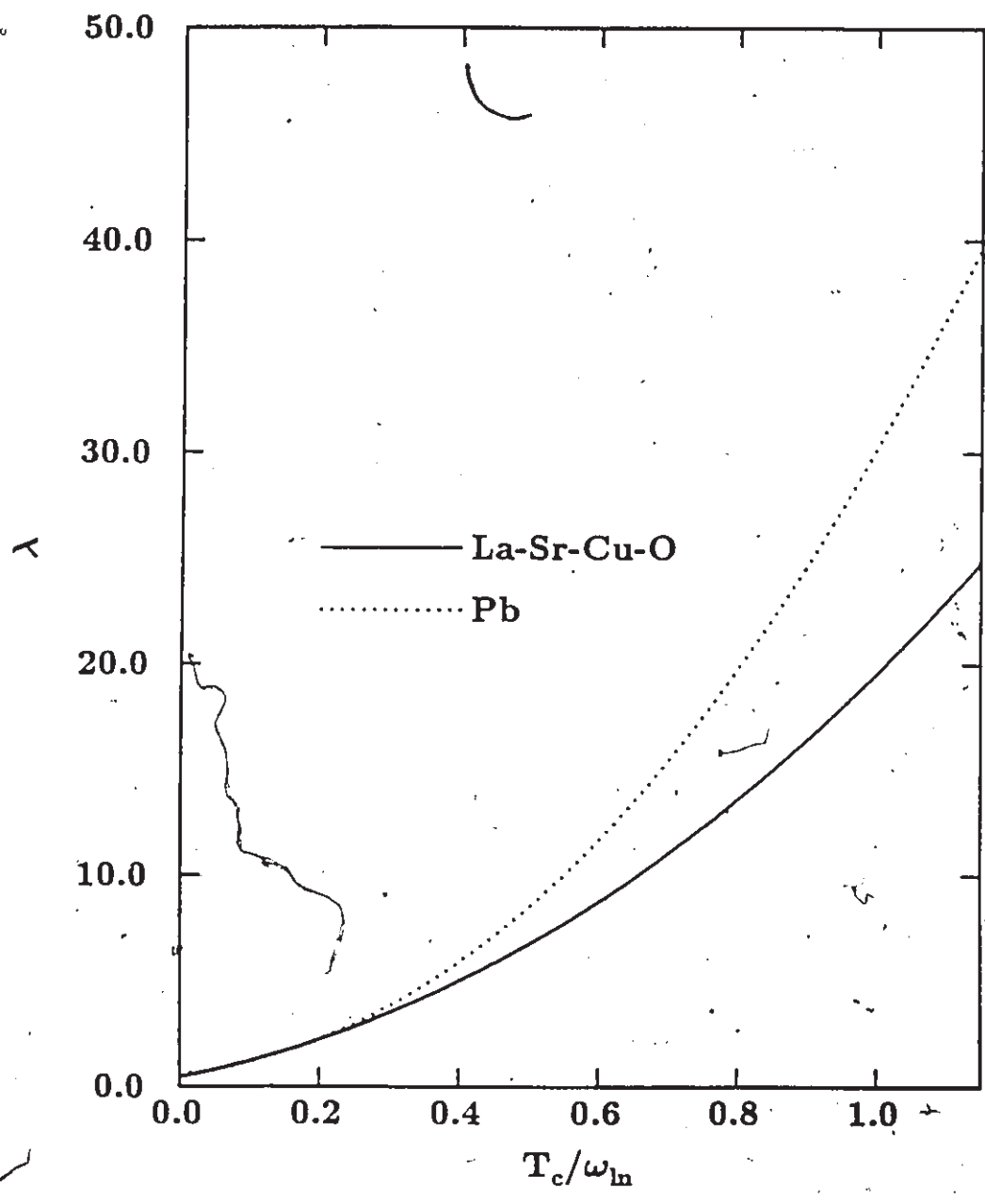
produced by band structure theorists is also disturbing, and prevents this sort of analysis from being quantitative, at this stage.

Chapter 4

Conclusions

In the first part of this thesis, we derived strong coupling corrections to BCS universal constants. It was found that a semiphenomenological approach worked quite well, so that, rather than evaluate integrals requiring detailed information about $\alpha^2 F(\nu)$ for each material, averages of the spectral moment were defined, in terms of a single parameter, T_c/ω_{ln}. Coefficients were fit on the basis of realistic spectral shapes available. A more sophisticated approach could have been used; however, this would have defeated our purpose. We wished simply to describe the trends of properties semi-quantitatively as a function of strong coupling. We found that all the corrections were of the form,

$$ax + bx^2 \ln(1/cx) \tag{4.1}$$

where $x \equiv T_c/\omega_{ln}$. In many cases the linear term was absent.

The expression (4.1) signifies the fact that a single parameter could describe quite well strong coupling properties. As an immediate consequence,

this implies that various properties are simply related to one another. Hence, our analysis allows estimates of the gap edge based on thermodynamic measurements, for example. A new T_c equation was obtained phenomenologically; its accuracy and simplicity are satisfactory in light of the regime it covers.

All known conventional materials, with the exception of amorphous materials, are found to fall in the regime where the strong coupling expansion used is valid. With the discovery of the high-T_c oxides, however, the possibility remains that their T_c/ω_{ln} values fall outside the regime described by expressions of type (4.1). On the basis of a spectral function calculated by W. Weber, we have tried to evaluate the degree of agreement with experiment. Inspection of Table 5, however, exhibits the variation in the measured properties. Moreover, the Sommerfeld constant γ_0 is critical to our analysis, and, at the same time, very difficult to measure. Disagreement by a factor of about three has been found for the density of electron states, although this can only be considered serious after some of the measurements have settled down. Single crystal measurements may provide more uniformity, although our calculations should be extended to include anisotropy. Large anisotropy in the electron gas alone could cause a significant non-constant density of states at the Fermi surface. No doubt an anisotropic electron gas will also manifest itself in an anisotropic electron-phonon interaction so that superconducting properties will also be affected by the resulting anisotropic gap.

The high T_c's observed in these materials have motivated us to explore the very strong coupling regime, in which the parameter T_c/ω_{ln} can take on values of about unity. Many signatures of this regime have been found. The gap ratio will be very large, while, at the same time, the normalized specific heat jump will be *less* than BCS. The correction to the upper critical

magnetic field will be *less* than unity. Both of these possibilities will drastically affect estimates of γ_0, based on BCS formulas. Anomalous structure is expected in the quasiparticle density of states, and it is intriguing that a few groups have observed structure of the nature we would expect. Finally the deviation functions will be quite unique, indicative of anomalous curvature in the temperature dependence of several properties.

In light of the various measured isotope effects, we have also investigated a combined phonon-exciton mechanism, where by "exciton" here, we mean some high frequency electronic excitation which mediates as electron-electron attraction. In both LSCO and YBCO, this possibility would be difficult to detect on the basis of thermodynamic and magnetic measurements alone. In the former, the effect of an added exciton mechanism is to mimick a pure phonon mechanism with a higher characteristic frequency. In the latter, the isotope effect is almost nil, so even if phonons are partially responsible, the predicted properties would be very BCS like. Nonetheless, the interesting result that values of $\frac{\Delta C(T_c)}{\gamma_0 T_c}$ below BCS could be obtained with the addition of a few low frequency phonons is surprising. It indicates that while the exciton component is most responsible for the high T_c, the phonon component is drastically affecting the thermodynamic properties. In the case of LSCO, the precision of the isotope effect measurement looks promising, but the other measurements have to settle down before a quantitative analysis as we have suggested can be taken seriously.

The most prominent effect of the combined phonon-exciton mechanism, however, was noted several years ago. Kus and Carbotte[144] found that a high frequency peak, which is not observed in tunneling, would nonetheless enhance the low frequency part, so that inversion attempts would have

the tendency to fail. At the present, however, tunneling junctions of a high
enough quality for inversion have not been fabricated.

Appendix A

Fun on the Complex Plane

We review here the variety of methods available for solution of the Eliashberg equations. The standard formulation[19,20] utilizes the Fourier series representation of the electron Green's function which is determined through Dyson's equation:

$$G^{-1}(\vec{p}, i\omega_n) = G_0^{-1}(\vec{p}, i\omega_n) - \sum(\vec{p}, i\omega_n) \qquad (A1)$$

G^{-1}, G_0^{-1} and $\sum$ are two component matrices in the Nambu[152] formalism. Self-consistency leads to the two equations written in Ch. 2, Eqs. (2.13–2.14). However the procedure was often employed[35,153–155] of analytically continuing the equations themselves to the real axis. The resulting equations are written:[19,156]

$$\Delta(\omega)Z(\omega) = -\int_{-\infty}^{\infty} d\omega' \int_0^{\infty} d\nu\, \alpha^2 F(\nu) I(\omega + i\delta, \nu, \omega') \Re_e \left(\frac{\Delta(\omega')}{\sqrt{\omega'^2 - \Delta^2(\omega')}} \right)$$

$$- 2T\mu^*(\omega_c) \int_{-\infty}^{\infty} d\omega' \Re_e \left(\frac{\Delta(\omega')}{\sqrt{\omega'^2 - \Delta^2(\omega')}} \right) \sum_{n=1}^{\infty} \frac{\omega' \theta(\omega_c - \omega_n)}{\omega'^2 + \omega_n^2} \quad (A2)$$

and)

$$Z(\omega) = 1 - \frac{1}{\omega} \int_{-\infty}^{\infty} d\omega' \int_{0}^{\infty} d\nu\, \alpha^2 F(\nu) I(\omega + i\delta, \nu, \omega') \Re_e \left(\frac{\Delta(\omega')}{\sqrt{\omega'^2 - \Delta^2(\omega')}} \right) \quad (A3)$$

where

$$I(\omega + i\delta, \nu, \omega') \doteq \frac{N(\nu) + 1 - f(\omega')}{\omega + i\delta - \nu - \omega'} + \frac{N(\nu) + f(\omega')}{\omega + i\delta + \nu - \omega'} . \quad (A4)$$

It is to be understood that "ω" always has a small positive imaginary part. The branch of the square roots must be chosen such that the real part has the same sign as ω. Note that we have adopted a model for the Coulomb self-energy which has a sharp cut-off on the imaginary axis, so that, following Leavens and Fenton,[156] we write the Coulomb part in Eq. (A2) in a non-standard way. The functions in (A4) are the standard Bose ($N(\nu)$) and Fermi ($f(\omega)$) functions. These equations can be iterated to solution at any temperature; in particular, the linearized version yields the critical temperature, T_c. Note that gap and renormalization parameters, $\Delta(\omega)$ and $Z(\omega)$, respectively, are complex, and principal value integrals are required. This makes this method of solution somewhat cumbersome, numerically.

In the early 1970's, the "imaginary axis Eliashberg equations" were first solved numerically to determine T_c [157,74] and subsequently to determine the thermodynamics.[31] As can be seen from Eqs. (2.13) and (2.14), only numerical summations are required, and all quantities involved are real, making their numerical solution relatively fast. Moreover, many superconducting properties can be determined by a direct summation of functions of these solutions.[47,42]

There are, however, disadvantages with this formulation. The physics is obscured, and, moreover several important properties cannot be determined directly from imaginary axis solutions. Most notable among these is

the gap edge, defined by Eq. (2.23), for which $\Delta(\omega)$, with ω on the real axis, is required. Transport properties[20] also require real axis solutions. Finally, tunneling inversion procedures[62] require a real axis formulation as well.

Some of these problems were alleviated a few years later by Vidberg and Serene,[158] who constructed an analytic continuation of the imaginary axis solutions using Padé approximants. That such a procedure is possible in principle was assured by a theorem of Baym and Mermin.[159] We briefly outline the methodology of this procedure, following Mitrović et al.[24] The N-point Padé approximant to a complex function $u(z)$ of the complex variable z, whose N values u_i $(i = 1, \ldots, N)$ are given at N complex points z_i $(i = 1, \ldots, N)$, is defined as a continued fraction:

$$C_N(z) = \cfrac{a_1}{1 + \cfrac{a_2(z - z_1)}{1 + \cfrac{a_3(z - z_2) \cdot}{\ddots \atop 1 + \cfrac{a_N(z - z_{N-1})}{1}}}} \qquad (A5)$$

such that

$$C_N(z_i) = u_i , \quad i = 1, \ldots, N . \qquad (A6)$$

In our case, the z_i are pure imaginary, and are in fact the Fermi Matsubara frequencies, $i\omega_n$, $n = 1, \ldots, N$. The u_i are the Matsubara gaps, $\Delta(i\omega_n)$, the renormalization function, $Z(i\omega_n)$, or any combination thereof. The coefficients a_i are given by the recursion

$$a_i = g_i(z_i) , \quad g_1(z_i) = u_i , \quad i = 1, \ldots, N \qquad (A7)$$

$$g_p(z) = \frac{g_{p-1}(z_{p-1}) - g_{p-1}(z)}{(z - z_{p-1})g_{p-1}(z)} , \quad p \geq 2 . \qquad (A8)$$

It can be shown that

$$C_N(z) = \frac{A_N(z)}{B_N(z)} , \qquad (A9)$$

where A_N and B_N are polynomials given by the recursion

$$A_{n+1}(z) = A_n(z) + (z - z_n)a_{n+1}A_{n-1}(z) , \quad n = 1,\ldots,N-1 \qquad (A10\,a)$$

$$B_{n+1}(z) = B_n(z) + (z - z_n)a_{n+1}B_{n-1}(z) , \quad n = 1,\ldots,N-1 \qquad (A10\,b)$$

and $A_0 = 0$, $A_1 = a_1$, $B_0 = B_1 = 1$. This algorithm turns out to be quite efficient numerically. However, accurate solution is required on the imaginary axis, and even then the algorithm works well only at low temperatures. Futhermore, the analytic continuation is accurate only for low frequencies. In particular, the zero temperature gap edge, Δ_0, is reproduced very accurately. The quasiparticle density of states, however, is not reproduced very well, particularly in the phonon region, so that this procedure has never been used, for example, to invert tunneling data. The Vidberg-Serene procedure has been improved upon recently, especially by Blaschke and Blocksdarf[160] and Leavens and Ritchie.[161] The latter authors, in particular, were able to perform analytic continuations near T_c for a Debye model spectrum; the accuracy requirements for the solution on the imaginary axis were extremely stringent, however.

In the remainder of this section, we outline an exact method for analytically continuing the imaginary axis solutions, which has been developed very recently.[162] We note that Eqs. (A2) and (A3) are actually valid for ω anywhere in the upper half of the complex plane. This follows from a general consideration of the analytic properties of Green's functions.[18] The integration can be performed over ω' through contour integration by noting the following:

$\omega = i\omega_n$, we recover the imaginary axis equations (2.13) and (2.14), since $f(\nu - i\omega_n) \equiv -N(\nu)$. There are many other fascinating properties of the gap and renormalization functions that one can infer from Eqs. (A11) and (A12). For example, the normal state $Z_N(\omega)$ is analytic in the upper half plane with poles in the lower half at $\omega = \pm\nu_E - i\omega_n$, $n = 1, 2, 3, \ldots$ (we are considering an Einstein spectrum to represent $\alpha^2 F(\nu)$). These poles are no longer present in the superconducting state, but have been replaced by branch cuts associated with the square root singularities at the gap edge. At finite temperature, the singularity moves off the real axis into the lower half plane, which is why the square root singularity in the quasiparticle density of states becomes smeared. At zero temperature, simplifications occur; $N(\nu) = 0$, and $F(\nu - \omega) = \theta(\omega - \nu)$, a step function. The equations are then no longer iterative but can be solved by construction from $\omega = 0$. Moreover, in the case of an Einstein spectrum, $\alpha^2 F(\nu) = A\,\delta(\nu - \nu_E)$, and, for typical spectra the solutions are such that the gap edge, $\Delta_0 < \nu_E$. This implies that the gap edge, for example, can be obtained by a single summation of imaginary axis quantities. No iteration is necessary.

For realistic spectral functions the solutions are obtained at non-zero temperature by numerical iteration. The quantities involved are complex, but there are no principal value integrations required. Moreover, the term coming from the imaginary axis acts as a forcing term, so that in general only a few iterations are required for convergence. The overall savings in time compared to direct solution of Eqs. (A2) and (A3) is about two orders of magnitude. Results are reproduced at the 1% level,[162] although it is not clear which numerical solution (that of Eqs. A2–A3 or Eqs. A11–A12) is the more accurate.

1) For a complex function f, $\Re_e(f)$ can be written $\Re_e(f) = \frac{1}{2}(f + f^*)$, where the asterisk denotes complex conjugate. Furthermore, the quantities in brackets whose real parts are required, in Eqs. (A2) and (A3), are nothing more than the energy integrated Green's functions, and these retain the property of being analytic in the lower half plane. Hence the contour of integration should be closed at $\pm\infty$ by a semicircular arc in the upper/lower half plane depending on where the Green's function is analytic.

2) This implies that contributions come from two sources only, through Eq. (A4). The first is from the denominators in Eq. (A4); the second is from the Fermi functions, which have simple poles at $\omega' = i\pi T(2n - 1)$, i.e. at the Matsubara frequencies.

Upon evaluation of the residues we obtain the two equations:

$$\Delta(\omega)Z(\omega) = \pi T \sum_{m=-\infty}^{\infty} \left[\lambda(\omega - i\omega_m) - \mu^*(\omega_c)\theta(\omega_c - |\omega_m|) \right] \frac{\Delta_m}{\sqrt{\omega_m^2 + \Delta_m^2}}$$

$$+ i\pi \int_0^\infty d\nu\, \alpha^2 F(\nu) \left\{ [N(\nu) + f(\nu - \omega)] \frac{\Delta(\omega - \nu)}{\sqrt{(\omega - \nu)^2 - \Delta^2(\omega - \nu)}} \right.$$

$$\left. + [N(\nu) + f(\nu + \omega)] \frac{\Delta(\omega + \nu)}{\sqrt{(\omega + \nu)^2 - \Delta^2(\omega + \nu)}} \right\} \qquad (A11)$$

and

$$Z(\omega) = 1 + \frac{i\pi T}{\omega} \sum_{m=-\infty}^{\infty} \lambda(\omega - i\omega_m) \frac{\omega_m}{\sqrt{\omega_m^2 + \Delta_m^2}}$$

$$+ \frac{i\pi}{\omega} \int_0^\infty d\nu\, \alpha^2 F(\nu) \left\{ [N(\nu) + f(\nu - \omega)] \frac{(\omega - \nu)}{\sqrt{(\omega - \nu)^2 - \Delta^2(\omega - \nu)}} \right.$$

$$\left. + [N(\nu) + f(\nu + \omega)] \frac{(\omega + \nu)}{\sqrt{(\omega + \nu)^2 - \Delta^2(\omega + \nu)}} \right\} . \qquad (A12)$$

Note that ω can now be interpreted as the real axis variable, "$\omega + i\delta$", or as being anywhere in the upper half of the complex plane. In particular, for

The physical processes which are occurring can be seen from Eqs. (A11) and (A12), especially if we use the identities of the type:[163]

$$N(\nu) + f(\nu + \omega) = \frac{N(\nu)[1 - f(\nu + \omega)]}{1 - f(\varphi)} .$$

(A13)

Then for example, Eq. (A12) becomes, for an Einstein spectrum,

$$Z(\omega) = 1 + \frac{i\pi T}{\omega} \sum_{m=-\infty}^{\infty} \lambda(\omega - i\omega_m) \frac{\omega_m}{\sqrt{\omega_m^2 + \Delta_m^2}}$$

$$+ \frac{i\pi A}{[1 - f(\omega)]} \left\{ [1 + N(\nu_E)][1 - f(\omega - \nu_E)] \frac{(\omega - \nu_E)}{\sqrt{(\omega - \nu_E)^2 - \Delta^2(\omega - \nu_E)}} \right.$$

$$\left. + N(\nu_E)[1 - f(\nu_E + \omega)] \frac{\omega + \nu_E}{\sqrt{(\omega + \nu_E)^2 - \Delta^2(\omega + \nu_E)}} \right\} .$$

(A14)

Clearly the last two terms correspond to quasiparticle scattering processes with the emission and absorption of a phonon, respectively.

Appendix B

Derivation of Strong Coupling Corrections

In this appendix we outline in detail the derivation of strong coupling corrections. It is divided into two sections. The first describes the derivation of thermodynamic properties. In the second section critical magnetic field properties are derived.

B.1 THERMODYNAMICS
(i) $T \sim T_c$

Eqs. (2.13) and (2.14) are expanded near T_c (small Δ_m):

$$Z_S(\omega_n)\Delta(\omega_n) = \pi T \sum_{m=-N_0+1}^{N_0} \lambda(i\omega_n - i\omega_m)\frac{\Delta_0}{|\omega_m|}\left(1 - \frac{1}{2}\frac{\Delta_0^2}{\omega_m^2} + \frac{3}{8}\frac{\Delta_0^4}{\omega_m^4}\right) \quad (B1)$$

$$Z_S(\omega_n) = Z_N(\omega_n) + \frac{\pi T}{\omega_n}\int_0^\infty 2\nu\, d\nu\, \alpha^2 F(\nu)$$

$$\times \sum_{m=-N_0+1}^{N_0} \frac{\mathrm{sgn}\,\omega_m}{\nu^2 + (\omega_m - \omega_n)^2}\left(-\frac{1}{2}\frac{\Delta_0^2}{\omega_m^2} + \frac{3}{8}\frac{\Delta_0^4}{\omega_m^4}\right). \quad (B2)$$

Here the subscript S (N) means superconducting (normal). Also, $N_0 = \frac{\omega_0}{2\pi T} + \frac{1}{2}$ enumerates the Matsubara frequencies in the sums. However, the convergence is sufficiently rapid that N_0 can be replaced by infinity. The summations are folded to the domain $[0, \infty]$. In the Z–channel (Eq. B2), this procedure results in sums like:

$$\sum_{m=1}^{\infty} \frac{1}{\omega_m^{2i-1}} \frac{1}{(\nu^2 + \omega_m^2 + \omega_n^2)^2} \left(1 + \frac{4\omega_m^2\omega_n^2}{(\nu^2 + \omega_m^2 + \omega_n^2)^2} + \cdots \right). \qquad (B3)$$

Noting that $\omega_n = \pi T(2n - 1)$, and only small n is required, one sees that terms of $O\left(\frac{T_c}{\nu}\right)^6$ have been neglected, consistent with our assumption, $T_c \ll \nu$. These terms would contribute however, in the free energy formula (Eq. 2.26), to $O\left(\frac{T_c}{\nu}\right)^2$, and hence should be retained. However, for the sake of simplicity, and since coefficients will be fitted to numerical data in the end anyways, we have dropped them. The required sums are:

$$U_i \equiv 4\pi T \sum_{m=1}^{\infty} \frac{1}{\omega_m^{2i-1}} \frac{1}{(\omega_m^2 + a_n^2)^2} \qquad (B4)$$

and

$$V_i \equiv 4\pi T \sum_{m=1}^{\infty} \frac{1}{\omega_m^{2i-1}} \frac{4\omega_m^2\omega_n^2}{(\omega_m^2 + a_n^2)^4}. \qquad (B5)$$

Here, $a_n^2 \equiv \nu^2 + \omega_n^2$, and $i = 1, 2, 3, \ldots$. In accordance with the remarks made above, only $i = 1, 2$ are required in Eq. (B4) and all i can be neglected in Eq. (B5). These are readily evaluated in terms of digamma functions:

$$U_1 \equiv \frac{2}{a_n^4} \left(\ln \frac{1.13 a_n}{k_B T} - \frac{1}{2} \right) \qquad (B5)$$

$$U_2 \equiv \frac{7}{2} \frac{\zeta(3)}{(\pi T)^2} \frac{1}{a_n^4} \qquad (B6)$$

$\zeta(3)$ is the Riemann zeta-function ($\zeta(3) \approx 1.202\cdots$). It is easy to show $V_1 = O(\frac{T}{\nu})^4$. Eq. (B2) becomes:

$$Z_S(\omega_n) - Z_N(\omega_n) = -\Delta_0^2(T) \int_0^\infty 2\nu\, d\nu\, \alpha^2 F(\nu) \frac{1}{(\nu^2 + \omega_n^2)^2} \left[\ln \frac{1.13\sqrt{\nu^2 + \omega_n^2}}{k_B T} - \frac{1}{2} \right]$$
$$+ \frac{21}{16}\Delta_0^4(T)\frac{\zeta(3)}{(\pi T)^2} \int_0^\infty 2\nu\, d\nu\, \alpha^2 F(\nu) \frac{1}{(\nu^2 + \omega_n^2)^2}. \qquad (B7)$$

At this point we also write the expansion for the Bardeen-Stephen free energy formula:

$$\frac{\Delta F}{N(0)} \equiv \frac{F_S - F_N}{N(0)} = -2\pi T \sum_{m=1}^\infty Z_N(\omega_m) \left(\frac{1}{4}\frac{\Delta_0^4}{\omega_m^3} - \frac{1}{4}\frac{\Delta_0^6}{\omega_m^5} \right)$$
$$- 2\pi T \sum_{m=1}^\infty [Z_S(m) - Z_N(m)] \left(\frac{1}{2}\frac{\Delta_0^2}{\omega_m} - \frac{1}{8}\frac{\Delta_0^4}{\omega_m^3} \right). \qquad (B8)$$

As will be seen below, the variation of $Z_N(\omega_m)$ with m is not large. In the first sum we can safely replace $Z_N(m)$ by its constant value at say, $m = 1$. However in the second sum, the first term is non-convergent with a constant value for $Z_S(m) - Z_N(m)$, and hence, the n-dependence must be retained in Eq. (B7). It will be dropped, however, in the argument of the logarithm, to facilitate the calculation. An identical expansion can be performed for $Z_N(n)$, with the result:

$$Z_N(\omega_n) = 1 + \lambda - \frac{1}{3}(\pi T)^2 [(2n-1)^2 - 1] \int_0^\infty 2\nu\, d\nu \alpha^2 F(\nu) \frac{2}{\nu^4}. \qquad (B9)$$

The constant value to be used in the first term of Eq. (B8) now depends on our choice of n. For $n = 1$, there is no strong coupling correction; $Z_N = 1 + \lambda$, which is the $\lambda^{\theta\theta}$ result. For higher value of n, a strong coupling correction results. We prefer to use the former value, since it is exact for $n = 1$. This is seen most readily from the exact equation for $Z_N(\omega_n)$:

$$Z_N(\omega_n) = 1 + \frac{\pi T}{\omega_n}\left(\lambda(0) + 2\sum_{m=1}^{n-1}\lambda(m) \right). \qquad (B10)$$

In fact, our choice for Z_N will be consistent with our use of the zero temperature Sommerfeld constant, γ_0 in the ratio $\frac{\Delta C(T_c)}{\gamma_0 T_c}$. This choice also omits strong coupling corrections arising from electron-phonon coupling at non-zero temperatures, as described by Grimvall[45] and Kresin and Zaitsev.[878]

Similar remarks apply to the Δ-channel. Eq. (B1) can be reduced to:

$$Z_S(n)\Delta_0 = \Delta_0 \int_0^\infty 2\nu \, d\nu \, \alpha^2 F(\nu) \left[P_1 + Q_1 - \tfrac{1}{2}\Delta_0^2(P_2 + Q_2) + \tfrac{3}{8}\Delta_0^4(P_3 + Q_3) \right] \quad (B11)$$

where

$$P_i \equiv \sum_{m=1}^\infty \frac{2\pi T}{\omega_m^{2i-1}} \frac{1}{\omega_m^2 + a_n^2} \quad (B12)$$

and

$$Q_i \equiv \sum_{m=1}^\infty \frac{2\pi T}{\omega_m^{2i-3}} \frac{4\omega_n^2}{(\omega_m^2 + a_n^2)^3} \quad (B13)$$

These sums are:

$$P_1 = \frac{1}{a_n^2} \ln \frac{1.13 a_n}{k_B T} - \frac{(\pi T)^2}{6 a_n^4} \quad (B14a)$$

$$P_2 = \frac{7}{4} \frac{\zeta(3)}{(\pi T)^2} \frac{1}{a_n^2} - \frac{1}{a_n^4} \ln \frac{1.13 a_n}{k_B T} \quad (B14b)$$

$$P_3 = \frac{31}{16} \frac{\zeta(5)}{(\pi T)^4} \frac{1}{a_n^2} - \frac{7}{4} \frac{\zeta(3)}{(\pi T)^2} \frac{1}{a_n^4} \quad (B14c)$$

$$Q_1 = \frac{\omega_n^2}{a_n^4} \quad (B14d)$$

$$Q_2 = Q_3 = O\left(\frac{1}{a_n^6}\right) \quad (B14e)$$

We evaluate Eq. (B11) for small n (specifically, $n = 1$) and define

$$a(T) \equiv \int_0^\infty 2\nu \, d\nu \, \alpha^2 F(\nu) \frac{1}{\nu^4} \ln \frac{1.13\nu}{k_B T} \quad (B15a)$$

and

$$b(T) \equiv \int_0^\infty 2\nu \, d\nu \, \alpha^2 F(\nu) \frac{1}{\nu^4} . \quad (B15b)$$

The gap equation (B11) becomes (using $Z_S(n = 1)$):

$$1 = F(T) + \Delta_0^2 G(T) + \Delta_0^4 J(T) \qquad (B16)$$

where,

$$F(T) = \frac{\lambda}{1+\lambda} \ln \frac{1.13\omega_{\ln}}{k_B T} - \frac{(\pi T)^2}{1+\lambda}\left(a(T) - \tfrac{4}{3}b\right) \qquad (B17a)$$

$$G(T) = \frac{-\lambda}{1+\lambda}\frac{7}{8}\frac{\zeta(3)}{(\pi T)^2} + \frac{3}{2}\frac{a(T)}{1+\lambda} + \left(\tfrac{7}{8}\zeta(3) - \tfrac{1}{2}\right)\frac{b}{1+\lambda} \qquad (B17b)$$

$$J(T) = \frac{\lambda}{1+\lambda}\frac{93}{128}\frac{\zeta(5)}{(\pi T)^4} - \frac{93}{128}\frac{\zeta(5)}{(\pi T)^2}\frac{b}{1+\lambda} - \frac{63}{32}\frac{\zeta(3)}{(\pi T)^2}\frac{b}{1+\lambda}. \qquad (B17c)$$

The T_c equation is given by $1 = F(T_c)$, with the result:

$$T_c = 1.13\omega_{\ln}\exp\left[-\left(\frac{1+\lambda}{\lambda}\right)\right]\left(1 - \frac{(\pi T_c)^2}{\lambda}\left(a(T_c) - \tfrac{4}{3}b\right)\right). \qquad (B18)$$

This is not an accurate T_c equation, but will prove useful later. The gap parameter (near T_c) is obtained from Eq. (B16):

$$\Delta_0^2(T) = -\frac{F'}{G}(T - T_c)\left(1 + \left(\frac{1}{2}\frac{F''}{F'} - \frac{G'}{G} + \frac{F'J}{G^2}\right)(T - T_c)\right) \qquad (B19)$$

where it is understood that the derivatives are with respect to temperature, and the functions are all evaluated at T_c. Eq. (B19), along with Eq. (B7), are to be substituted into Eq. (B8). Summations in the second term are required, but of the form encountered previously (U_1). The result is:

$$\frac{\Delta F}{N(0)} = \frac{1}{2}\frac{(1+\lambda)^2}{\lambda}\left(\Delta_0^4 K(T) + \tfrac{4}{3}\Delta_0^6 L(T)\right) \qquad (B20)$$

where

$$K(T) = G_0(T) - \frac{TF_0'(T)}{1+\lambda}\left(c(T) - a(T) + \tfrac{b}{4}\right) \qquad (B21a)$$

and

$$L(T) = J_0(T) + \frac{3}{2}\frac{G_0(T)}{1+\lambda}\left(a(T) - \tfrac{b}{2}\right) \qquad (B21b)$$

A new strong coupling correction, defined by

$$c(T) = \int_0^\infty 2\nu\, d\nu\, \alpha^2 F(\nu) \frac{1}{\nu^4} \ln^2 \frac{1.13\nu}{k_B T} \qquad (B22)$$

is required. The "0" subscripts in Eqs. (B21) signify that the strong coupling corrections in Eqs. (B17) have been dropped. The specific heat difference near T_c, is given by the thermodynamic formula:

$$\Delta C(T) = -T\frac{d^2 \Delta F}{dT^2}. \qquad (B23)$$

So that after some tedious algebra, one obtains:

$$\frac{\Delta C(T)}{\gamma_0 T_c} = f + (1 - t)g. \qquad (B24)$$

To simplify the formulas for f and g, we write

$$a(T_c) = \frac{\alpha_1}{\omega_{\ln}^2} \int_0^\infty 2\nu\, d\nu\, \alpha^2 F(\nu) \frac{1}{\nu^2} \ln \frac{1.13\nu}{k_B T_c} = \frac{\alpha_1}{\omega_{\ln}^2} \lambda \ln \frac{1.13\omega_{\ln}}{k_B T_c}. \qquad (B25)$$

The first equality follows for a given spectrum from the mean value theorem of calculus; α_1 can be chosen to compensate for the averaging. The second equality follows from the definition of $\omega_{\ln}$ (Eq. 2.3). Similarly,

$$b = \frac{\alpha_2}{\omega_{\ln}^2} \lambda \qquad (B26)$$

and

$$c(T_c) = \frac{\alpha_3}{\omega_{\ln}^2} \lambda \ln \frac{1.13\omega_{\ln}}{k_B T_c} \ln \frac{1.13\omega_{\ln}}{\beta_3 k_B T_c}. \qquad (B27)$$

In Eq. (B27), the weak coupling T_c equation can be used:

$$\ln \frac{1.13\omega_{\ln}}{k_B T_c} = \frac{1+\lambda}{\lambda}. \qquad (B28)$$

The result is an equation of the form:

$$f = 1.43\left\{1 + \left(\frac{\pi T_c}{\omega_{\ln}}\right)^2 \left[z_1 \ln \frac{1.13\omega_{\ln}}{k_B T_c} - z_2 - \frac{z_3}{\ln \frac{1.13\omega_{\ln}}{k_B T_c}}\right]\right\}. \qquad (B29)$$

Note that for a δ-function spectrum, the α_i, $\beta_3 \equiv 1$, and in fact we expect that even for realistic spectra, $\alpha_i \approx \beta_3 \approx 1$. With this approximation, $z_1 \approx 5.9$, $z_2 \approx 5.3$, and $z_3 \approx 0.2$. Hence, we drop the last term in Eq. (B29). Eq. (B29) becomes:

$$f \equiv \frac{\Delta C(T_c)}{\gamma_0 T_c} = 1.43 \left(1 + a_1 \left(\frac{T_c}{\omega_{\ln}} \right)^2 \ln \left(\frac{\omega_{\ln}}{b_1 T_c} \right) \right) \qquad (B30)$$

where

$$a_1 = \pi^2 \left[\left(4 + \frac{24}{7\zeta(3)} \right) \alpha_1 - \frac{8}{7\zeta(3)} \alpha_3 \right] \qquad (B31a)$$

$$b_1 = \frac{1}{1.13} \exp \left[\frac{\frac{16}{3}\alpha_2 + \frac{8}{7\zeta(3)}\alpha_2 - \frac{8}{7\zeta(3)}\alpha_3 \ln \beta_3 - \frac{8}{7\zeta(3)}\alpha_1}{\left(4 + \frac{24}{7\zeta(3)} \right)\alpha_1 - \frac{8}{7\zeta(3)}\alpha_3} \right] \qquad (B31b)$$

Eqs. (B31) are not used to determine a_1 and b_1. Rather, they are fit to numerical data as described in Ch. 2. The result is $a_1 = 53$ and $b_1 = 3$. Note that for $\alpha_i = \beta_3 = 1$, Eqns. (B31) yield $a_1 = 58$ and $b_1 = 2$, remarkably close to the accurate fit. Similarly, for g we obtain:

$$g = -3.77 \left(1 + a_2 \left(\frac{T_c}{\omega_{\ln}} \right)^2 \ln \left(\frac{\omega_{\ln}}{b_2 T_c} \right) \right) \qquad (B32)$$

where a_2 and b_2 are functions of α_i and β_3. The fitted values are $a_2 = 117$ and $b_2 = 2.9$, whereas our estimates would be (fortuitously) $a_2 = 117$ and $b_2 = 3.1$.

(ii) $T = 0$

At zero temperature the Eliashberg equations are modified according to the prescription (2.18). The equation for $Z_S(\omega)$ is folded to the domain $[0, \infty]$, with result that it can be written:

$$Z_S(\omega) = 1 + 4 \int_0^\infty \nu \, d\nu \, \alpha^2 F(\nu) [A_1 + A_2] \qquad (B33)$$

where

$$A_1 = \int_0^\infty d\omega' \frac{\omega'^2}{\sqrt{\omega'^2 + \Delta_0^2}} \frac{1}{(\omega'^2 + a_0^2)^2} \qquad (B34a)$$

and

$$A_2 = \int_0^\infty d\omega' \frac{4\omega^2\omega'^2}{\sqrt{\omega'^2 + \Delta_0^2}} \frac{1}{(\omega'^2 + a_0^2)^4}. \tag{B34b}$$

Here again $a_0^2 \equiv \omega^2 + \nu^2$. The results are

$$A_1 = \frac{1}{2a_0^2} - \frac{\Delta_0^4}{2a_0^4}\left(\ln\frac{2a_0}{\Delta_0} - 1\right) \tag{B35a}$$

and

$$A_2 = \frac{1}{3}\frac{\omega^2}{a_0^4}. \tag{B35b}$$

Other contributions are of higher order. The net result is

$$Z_S(\omega) = Z_N(\omega) + \Delta_0^2 \int_0^\infty \frac{2\nu\,d\nu\,\alpha^2 F(\nu)}{(\nu^2 + \omega^2)^2}\left(1 - \ln\frac{2\sqrt{\nu^2 + \omega^2}}{\Delta_0}\right) \tag{B36}$$

$Z_N(\omega)$ can be evaluated exactly:

$$Z_N(\omega) = 1 + \frac{1}{\omega}\int_0^\infty 2\,d\nu\,\alpha^2 F(\nu)\tan^{-1}\left(\frac{\omega}{\nu}\right). \tag{B37}$$

Recall that we have used a constant model for $\Delta(\omega)$ and $Z_S(\omega)$. Hence it should not matter at what frequency we evaluate Eq. (B37), as long as it is small. However there is a dependence, and once again we will choose $\omega = 0$. Then $Z_N(0) = 1 + \lambda$, and there is no strong coupling correction. This is again consistent with use of the Sommerfeld γ_0 in the ratio $\frac{\gamma_0 T_c^2}{H_c^2(0)}$, for example. Note, moreover, that for evaluation of the free energy difference, the ω-dependence for $Z_S(\omega) - Z_N(\omega)$ must be retained in Eq. (B36) (except in the logarithm, once again). One can argue that a more appropriate frequency at which to evaluate $Z_N(\omega)$ (and subsequently $\Delta(\omega)$) is Δ_0, the gap edge, since this defines the gap edge. However, it must be kept in mind that this calculation is on the imaginary axis, so that corrections proportional to ω^2 actually have the opposite sign from the correction on the real axis (since $\omega^2 = -(i\omega)^2$). Hence it is more accurate to evaluate at $\omega = 0$.

The gap channel is treated similarly, with the result

$$Z_S(0)\Delta_0 = \Delta_0 \int_0^\infty 2\nu \, d\nu \, \alpha^2 F(\nu)(A_3 + A_4) \qquad (B38)$$

where

$$A_3 = \int_0^\infty \frac{d\omega'}{\sqrt{\omega'^2 + \Delta_0^2}} \frac{1}{\omega'^2 + a_0^2} \qquad (B39a)$$

and

$$A_4 = \int_0^\infty \frac{d\omega'}{\sqrt{\omega'^2 + \Delta_0^2}} \frac{4\omega^2_n \omega'^2}{(\omega'^2 + a_0^2)^3} \cdot \qquad (B39b)$$

Evaluation of these integrals is straightforward. Combining with Eq. (B36) evaluated at $\omega = 0$, we obtain

$$\Delta_0 = 2\omega_{\ln} \exp\left[-\left(\frac{1+\lambda}{\lambda}\right)\right]\left(1 + \frac{3}{2}\frac{\Delta_0^2}{\lambda}(a - \tfrac{5}{6}b)\right). \qquad (B40)$$

Here, a and b are the same functions (within BCS) as in the previous section (evaluated at $T = T_c$). Combining Eq. (B18) with (B40), we obtain

$$\frac{2\Delta_0}{k_B T_c} = 3.53\left(1 + a_3\left(\frac{T_c}{\omega_{\ln}}\right)^2 \ln\left(\frac{\omega_{\ln}}{b_3 T_c}\right)\right) \qquad (B41)$$

where

$$a_3 = \left(\tfrac{3}{8}(3.53)^2 + \pi^2\right)\alpha_1 \qquad (B42a)$$

and

$$b_3 = \frac{1}{1.13}\exp\left[\left\{\frac{\frac{5}{16}(3.53)^2 + \frac{4}{3}\pi^2}{\frac{3}{8}(3.53)^2 + \pi^2}\right\}\frac{\alpha_2}{\alpha_1}\right]. \qquad (B42b)$$

The values first fit by Mitrović et al.[24] are $a_3 = 12.5$ and $b_3 = 2$. The values we would obtain by setting $\alpha_i \approx 1$ are $a_3 = 14.5$ and $b_3 = 2.9$, which again are not much different from the best fit.

The free energy difference at $T = 0$ within the model (2.25) is written

$$\frac{\Delta F}{N(0)} = -\int_0^\infty d\omega \left(Z_N(\omega)\left(\sqrt{\omega^2 + \Delta_0^2} + \frac{\omega^2}{\sqrt{\omega^2 + \Delta_0^2}} - 2\omega\right)\right.$$
$$\left. + (Z_S(\omega) - Z_N(\omega))\left(\sqrt{\omega^2 + \Delta_0^2} - \omega\right)\right). \qquad (B43)$$

In the first term, $Z_N(\omega) = 1 + \lambda$ is used. In the second, Eq. (B36) must be used to retain convergence. The integrals are easily performed with the result:

$$\frac{\Delta F}{N(0)} = -\frac{1}{2}(1 + \lambda)\Delta_0^2 \left(1 - \frac{\Delta_0^2}{1 + \lambda}(c - a)\right) . \qquad (B44)$$

Then, using Eq. (2.28), and $\gamma_0 = \frac{2}{3}\pi^2 N(0)(1 + \lambda)$, along with Eq. (B41), we obtain

$$\frac{\gamma T_c^2}{H_c^2(0)} = 0.168 \left(1 - a_4 \left(\frac{T_c}{\omega_{\ln}}\right)^2 \ln\left(\frac{\omega_{\ln}}{b_4 T_c}\right)\right) \qquad (B45)$$

where

$$a_4 = 29\alpha_1 - 3.1\alpha_3 \qquad (B46a)$$

$$b_4 = \frac{1}{1.13} \exp\left(\frac{34.1\alpha_2 - 3.1\alpha_1 - 3.1\alpha_3 \ln \beta_3}{2.9\alpha_1 - 3.1\alpha_3}\right) . \qquad (B46b)$$

The fits to numerical data give $a_4 = 12.2$, $b_4 = 3$; the estimates are $a_4 = 26$, $b_4 = 2.9$, in error by a (more realistic) factor of 2. The ingredients are also present to calculate the reduced thermodynamic critical field, $h_c(0) \equiv \frac{H_c(0)}{T_c|H_c'(T_c)|}$. We obtain an expression:

$$h_c(0) = 0.576 \left(1 - a_5 \left(\frac{T_c}{\omega_{\ln}}\right)^2 \ln\left(\frac{\omega_{\ln}}{b_5 T_c}\right)\right) \qquad (B47)$$

with a fit $a_5 = 13.4$ and $b_5 = 3.5$. Note that the properties $\frac{\Delta C}{\gamma_0 T_c}$, $\frac{\gamma T_c^2}{H_c^2(0)}$ and $h_c(0)$ are not independent. Rutgers relation provides the thermodynamic identity:

$$h_c(0) = \left(4\pi \frac{\gamma T_c^2}{H_c^2(0)} \frac{\Delta C}{\gamma_0 T_c}\right)^{-\frac{1}{2}} . \qquad (B48)$$

Our choices for the various coefficients do not satisfy Eq. (B48) exactly to $O\left(\frac{T_c}{\omega_{\ln}}\right)^2$. Hence, when manipulating the final expressions (Eqs. B30, B41, B45, B47), all terms should be retained.

B.2 UPPER CRITICAL MAGNETIC FIELD (DIRTY LIMIT)

(i) $T \sim T_c$.

We use the same model as in part 1. Moreover, near T_c, $\rho(T)$ is very small. A folding of the summation in Eq. (2.48) to positive m, gives the expression:

$$(1+\lambda)\Delta_0 = \Delta_0 \int_0^\infty 2\nu \, d\nu \, \alpha^2 F(\nu) \left\{ P_1 + Q_1 - \frac{\rho(T)}{1+\lambda}(P_2 + Q_2) \right\} \qquad (B49)$$

where

$$P_i \equiv \sum_{m=1}^\infty \frac{2\pi T}{\omega_m^i} \frac{1}{\omega_m^2 + a_n^2} \qquad (B50a)$$

and

$$Q_i \equiv \sum_{m=1}^\infty \frac{2\pi T}{\omega_m^{i-2}} \frac{4\omega_n^2}{(\omega_m^2 + a_n^2)^3} . \qquad (B50b)$$

These are evaluated in terms of digamma functions, and expanded in powers of $\left(\frac{T}{\nu}\right)^2$. The result is:

$$P_1 = \frac{1}{\nu^2} \ln \frac{1.13\nu}{k_B T} - \frac{(\pi T)^2}{\nu^4} \left(\ln \frac{1.13\nu}{k_B T} - \frac{1}{3} \right) \qquad (B51a)$$

$$P_2 = \frac{\pi}{4T} \left(\frac{1}{\nu^2} - \frac{2T}{\nu^3} - \frac{(\pi T)^2}{\nu^4} \right) \qquad (B51b)$$

$$Q_1 = \frac{(\pi T)^2}{\nu^4} . \qquad (B51c)$$

Using similar definitions as in part 1 of this appendix, we obtain

$$1 = F(T) + \frac{\rho(T)}{2\pi T(1+\lambda)} G(T) \qquad (B52)$$

where $F(T)$ is given by Eq. (B17a), and $G(T)$ is defined:

$$G(T) \equiv -\frac{\pi^2}{2} \left(\frac{\lambda}{1+\lambda} - 2T \frac{d}{1+\lambda} - (\pi T)^2 \frac{b}{1+\lambda} \right) . \qquad (B53)$$

A new moment is required, $d \equiv \int_0^\infty 2\frac{d\nu}{\nu} \alpha^2 F(\nu)$, and will lead to a strong coupling term which is linear in $\frac{T_c}{\omega_{\ln}}$. The derivative $\rho'(T_c)$ is easily obtained from Eq. (B52). The result is:

$$T_c |\rho'(T_c)| = \frac{4T_c}{\pi}(1+\lambda)\left(1 + 2\frac{T_c}{\lambda}d + 4\frac{T_c^2}{\lambda^2}d^2 + \frac{(\pi T_c)^2}{\lambda}\left(2a(T_c) - \tfrac{8}{3}b\right)\right) . \quad (B54)$$

(ii) $T = 0$.

The same prescription is used as before; the limit $\omega \to 0$ is used, with the result:

$$(1+\lambda)\Delta_0 = \Delta_0 \int_0^\infty 2\nu \, d\nu \, \alpha^2 F(\nu) I(\nu, \bar{\rho}) . \quad (B55)$$

where

$$I(\nu, \bar{\rho}) \equiv \int_0^\infty d\omega' \frac{1}{\omega'^2 + \nu^2} \frac{1}{\omega' + \bar{\rho}(0)}$$

$$= \frac{1}{\nu^2} \ln \frac{\nu}{\bar{\rho}(0)} + \frac{\pi}{2} \frac{\bar{\rho}(0)}{\nu^3} - \frac{\bar{\rho}^2(0)}{\nu^4} \ln \frac{\nu}{\bar{\rho}(0)} \quad (B56)$$

and $\bar{\rho}(0) \equiv \frac{\rho(0)}{1+\lambda}$. Using the T_c equation (B18), we easily obtain:

$$\rho(0) = \frac{\pi T_c}{2e^\gamma}(1+\lambda)\left\{1 + \frac{\pi}{4e^\gamma}\frac{\pi T_c}{\lambda}d + \frac{3}{2}\left(\frac{\pi}{4e^\gamma}\right)^2\left(\frac{\pi T_c}{\lambda}\right)^2 d^2 + \frac{(\pi T_c)^2}{\lambda}\left(\frac{4e^{2\gamma}-1}{4e^{2\gamma}}a(T_c) - \frac{4}{3}b\right)\right\}$$

$$(B57)$$

where $\gamma \approx 0.577\ldots$ is Euler's constant. Eqs. (B54) and (B57) are readily combined; using (B25) and (B26) along with $d \equiv \alpha_4 \frac{\lambda}{\omega_{\ln}}$, we obtain an equation of the form:

$$h_{c2}(0, \infty) = 0.693\left(1 - a_1\frac{T_c}{\omega_{\ln}} - a_2\left(\frac{T_c}{\omega_{\ln}}\right)^2 \ln \frac{\omega_{\ln}}{b_1 T_c}\right) . \quad (B58)$$

An Einstein model gives $a_1 = 0.61$, $a_2 = 11.3$ and $b_1 = 3.7$. The fitted parameters are considerably different as indicated in Ch. 2.

B.3 UPPER CRITICAL MAGNETIC FIELD
(CLEAN LIMIT)

(i) $T \sim T_c$.

Near T_c similar expansions as in the dirty limit apply since $\alpha(T)$ is small. We obtain the equation:

$$1 + \lambda = \int_0^\infty 2\nu \, d\nu \, \alpha^2 F(\nu) \left[P_1 + Q_1 - \tfrac{1}{3}\tilde{\alpha}(T)(P_2 + Q_2) \right] \qquad (B59)$$

where the P_i and Q_i are the same as those defined by Eqs. (B12-B13). Using Eqs. (B14) we obtain:

$$1 = F(T) + \tilde{\alpha}(T)G(T) \qquad (B60)$$

where now

$$G(T) \equiv -\frac{7}{12}\frac{\zeta(3)}{(\pi T)^2}\frac{\lambda}{1+\lambda} + \frac{7}{12}\zeta(3)\frac{b}{1+\lambda} + \frac{1}{3}\frac{a(T)}{1+\lambda} \qquad (B61)$$

and $\tilde{\alpha}(T) \equiv \frac{\alpha(T)}{(1+\lambda)^2}$. We find:

$$T_c \left| \tilde{\alpha}'(T_c) \right| = \frac{12}{7\zeta(3)}(\pi T_c)^2 \left\{ 1 + \frac{(\pi T_c)^2}{\lambda}\left[\left(2 + \frac{4}{7\zeta(3)}\right)a(T_c) - \frac{8}{3}b \right] \right\} . \qquad (B62)$$

(ii) $T = 0$.

In the limit $\omega \to 0$ we find:

$$1 + \lambda = \frac{2}{\sqrt{\tilde{\alpha}(0)}} \int_0^\infty 2\nu \, d\nu \, \alpha^2 F(\nu) I(\nu, \tilde{\alpha}(0)) \qquad (B63)$$

where

$$I(\nu, \tilde{\alpha}(0)) = \int_0^\infty \frac{d\omega}{\omega^2 + \nu^2} \int_0^\infty dq \, e^{-q^2} \tan^{-1}\left(\frac{\sqrt{\tilde{\alpha}(0)}q}{\omega} \right) . \qquad (B64)$$

I have been unable to compute this double integral. However, as was done in Ref. 61, we use the approximation $\chi(\omega) = \frac{1}{1+\lambda}\frac{1}{\omega+c}$, which was found to be quite accurate. Here, the constant c will contain strong coupling corrections

and is given by $c = \sqrt{\bar{\alpha}(0)}e^{-\frac{7}{2}-1}$. Within BCS, $c^{BCS} = \frac{\pi}{2}e^{-\gamma}T_c$. The integral is now elementary. We obtain:

$$\bar{\alpha}(0) = \left(\frac{\pi}{2}\right)^2 e^{-\gamma+2}T_c^2\left[1 + \frac{\pi^2}{2}e^{-\gamma}T_c\frac{d}{\lambda} + \frac{\pi^2}{4}e^{-2\gamma}\left(\pi T_c\frac{d}{\lambda}\right)^2\right.$$

$$\left. + \frac{2(\pi T_c)^2}{\lambda}\left(\left(1 - \frac{e^{-2\gamma}}{4}\right)a(T_c) - \frac{4}{3}b\right)\right] . \tag{B65}$$

Hence, $h_{c2}(0,0)$ is of the form:

$$h_{c2}(0,0) = 0.727\left(1 + a_1\frac{T_c}{\omega_{\ln}} - a_2\left(\frac{T_c}{\omega_{\ln}}\right)^2\ln\frac{\omega_{\ln}}{b_2 T_c}\right) . \tag{B66}$$

An Einstein model gives $a_1 = 2.8$, $a_2 = 6.25$ and $b_2 = 3$. The parameters determined through a fit to numerical data are very different: $a_1 = 0$, $a_2 = 2.7$ and $b_2 = 20$. We have found that the linear term is not required.

Appendix C

Spectral Function Sources

We tabulate here the sources for the $\alpha^2 F(\nu)$ spectra used in our calculations. Most of the spectra come from a tabulation of Rowell, McMillan and Dynes.

1) Al comes from a theoretical calculation of Leung et al.[65] However, in Table 1, BCS values have been used.

2) Several sources are available for Nb. Nb(R) comes from Robinson and Rowell through private communication. Nb(A) comes from L. Wolf et al. [164] These have been measured through tunneling. A theoretical calculation (Nb(B)) comes from Butler et al.[67]

3) V has been obtained through tunneling by Zasadzinski et al.[165]

4) Amorphous Bi and Ga have been obtained through tunneling by Chen et al.[166]

5) La is from Lou and Tomasch[167] (tunneling).

6) Mo is from Kimhi and Geballe[168] (tunneling).

7) Nb_3Sn has been obtained from Shen[169] through tunneling.

8) V_3Si (Kihl.) has been obtained through tunneling by Kihlstrom.[170] We have scaled it to give $\lambda = 1$ and used $T_c = 16.4$ K (rather than 15.4 K as measured by Kihlstrom), which is in better agreement with the single crystal T_c value.

9) V_3Si-1 was obtained from scaling $G(\Omega)$ obtained through inelastic neutron scattering, such that $\lambda = 1$, by Schweiss et al. .[171]

10) Nb_3Al has three possibilities; two of them ((1) and (2)) were obtained from tunneling measurements by Kwo and Geballe;[172] the third (3) is a phonon spectrum obtained by Schweiss et al. [171] and scaled to give $\lambda = 1.7$.

11) Nb_3Ge (1) was obtained through tunneling by Geerk et al. [173] whereas Nb_3Ge (2) was from neutron scattering data obtained by Müller et al. [174] to give $\lambda = 1.6$. μ^* has been fitted to give $T_c = 20$ K.

12) V_3Ga has been obtained by tunneling by Zasadzinski et al. [175]

13) Finally, the spectra by Weber[69,116] have been obtained by theoretical calculation.

Appendix D

Functional Derivative of the Specific Heat Jump

We outline the procedure for calculating functional derivatives of the specific heat jump, ΔC. The specific heat difference is given by $\Delta C = -T\frac{d^2\Delta F}{dT^2}$, so that the free energy difference is required. However, the Bardeen-Stephen[42] formula (Eq. 2.26) is cumbersome, since, for complete solution of $\delta\Delta F$, we require $\delta\Delta_n$ and δZ_n, which in turn require inversion of an infinite matrix. Rainer and Bergmann[31] circumvented this difficulty by noting that the Wada formula for the free energy,[176] given by:

$$\frac{\Delta F}{N(0)} = -2\pi T \sum_{n=-\infty}^{\infty} \omega_n \left[\frac{\omega_n}{\sqrt{\Delta_n^2 + \omega_n^2}} - \text{sgn}\,\omega_n \right]$$

$$- (\pi T)^2 \sum_{n=-\infty}^{\infty} \sum_{m=-\infty}^{\infty} \left\{ \left[\frac{\omega_n}{\sqrt{\Delta_n^2 + \omega_n^2}} \frac{\omega_m}{\sqrt{\Delta_m^2 + \omega_m^2}} - \text{sgn}\,(\omega_n\omega_m) \right] \lambda(i\omega_n - i\omega_m) \right.$$

$$\left. + \frac{\Delta_n}{\sqrt{\Delta_n^2 + \omega_n^2}} \frac{\Delta_m}{\sqrt{\Delta_m^2 + \omega_m^2}} \left[\lambda(i\omega_n - i\omega_m) - \mu^* \right] \right\} \qquad (D1)$$

is stationary with respect to variations in Δ_n, given the Eliashberg Eqs. (2.13-2.14). Hence, the functional derivative of the free energy difference is given simply by considering the explicit $\alpha^2 F(\nu)$ dependence contained within $\lambda(i\omega_n - i\omega_m)$. However, the free energy also depends on temperature. Temperature is an externally controlled parameter, and hence has no dependence on $\alpha^2 F(\nu)$,except that the temperature is always referred to T_c, for example, in the specific heat jump, $\Delta C(T)\,|_{T_c}$. It then becomes important as to what the order of operations is,*i.e.*is T evaluated at T_c, and then the functional derivative taken, or vice-versa? It is clear that if one wishes to have

$$\left[\frac{\delta}{\delta\alpha^2 F(\Omega)}\left(\frac{\Delta C(T)}{\gamma T_c}\right)\right]\Bigg|_{T_c} = \frac{\delta}{\delta\alpha^2 F(\Omega)}\frac{\Delta C(T_c)}{\gamma T_c} \qquad (D2)$$

then it is necessary that $T = tT_c$, and we impose the commutation property, $[t,\delta] = 0$ (and not $[T,\delta] = 0$). Let us define[84]

$$I \equiv \frac{1}{\gamma}\frac{\delta}{\delta\,\alpha^2 F(\Omega)}\left(\frac{\Delta C(T)}{T_c}\right). \qquad (D3)$$

Then

$$I = -\frac{1}{\gamma}\frac{\delta}{\delta\,\alpha^2 F(\Omega)}\left(\frac{t}{T_c^2}\frac{d^2\Delta F}{dt^2}\right) \qquad (D4)$$

$$= -\frac{2}{T_c}\frac{\Delta C(t)}{\gamma T_c}\frac{\delta T_c}{\delta\alpha^2 F(\Omega)} - \frac{t}{\gamma T_c^2}\frac{d^2}{dt^2}\frac{\delta\Delta F}{\delta\alpha^2 F(\Omega)}. \qquad (D5)$$

In evaluating the last term in Eq. (D5), we must consider the T dependence of ΔF:

$$\frac{\delta\Delta F}{\delta\,\alpha^2 F(\Omega)} = \frac{\bar{\delta}\,\Delta F}{\bar{\delta}\,\alpha^2 F(\Omega)} + \frac{T}{T_c}\frac{\partial\Delta F}{\partial T}\frac{\delta T_c}{\delta\,\alpha^2 F(\Omega)}. \qquad (D6)$$

The first term is given by Rainer and Bergmann;[31] the second term is easily evaluated. We have used "$\bar{\delta}$" to mean "partial functional derivative"; it

differentiates only explicit $\alpha^2 F(\Omega)$ dependence. The final expresion is:

$$
I = \frac{T}{\gamma T_c} \frac{d^2}{dT^2} (\pi T)^2 \sum_{n=-\infty}^{\infty} \sum_{m=-\infty}^{\infty} \left\{ \left[\frac{\omega_n \omega_m + \Delta_n \Delta_m}{\sqrt{\omega_n^2 + \Delta_n^2} \sqrt{\omega_m^2 + \Delta_m^2}} - \operatorname{sgn}(\omega_n \omega_m) \right] \right.
$$

$$
\left. \times \left(\frac{2\Omega}{\Omega^2 + (\omega_n - \omega_m)^2} + \frac{T}{T_c} \frac{\partial \lambda(i\omega_n - i\omega_m)}{\partial T} \frac{\delta T_c}{\delta \alpha^2 F(\Omega)} \right) \right\} \qquad (D6)
$$

The term inside the curly brackets can be evaluated from a single solution of the Eliashberg equations along with the solution of $\frac{\delta T_c}{\delta \alpha^2 F(\Omega)}$.[74] The tempera-ture derivative is then performed numerically, using a fitting routine.

We note in passing that the same method is possible when considering the functional derivative with respect to the free electron density of states, $N(\epsilon)$, using the generalization of Eliashberg theory with non-constant density of states.

Appendix E

Asymptotic Limits

We present here some results concerning asymptotic limits. We begin by combining Eqs. (2.13) and (2.14) into a single equation:

$$\Delta(i\omega_n) = \pi T \sum_{m(\neq n)} \lambda(i\omega_m - i\omega_n) \left[\frac{\Delta(i\omega_m) - \frac{\omega_m}{\omega_n}\Delta(i\omega_n)}{\sqrt{\omega_m^2 + \Delta^2(i\omega_m)}} \right], \qquad (E1)$$

where we have noted that the term $m = n$ does not enter the sum because the term in the large parentheses is zero. Thus we can take the limit $\nu_E \to 0\,(\nu_E \ll 2\pi T)$ so that

$$\lambda(i\omega_m - i\omega_n) = \frac{2A\nu_E}{(\omega_n - \omega_m)^2} \qquad .(E2)$$

and scale the entire equation by $\sqrt{A\nu_E}$. We obtain

$$\bar{\Delta}_n = \pi t\,\bar{T}_c \sum_{m \neq n} \frac{2}{(\bar{\omega}_n - \bar{\omega}_m)^2} \left[\frac{\bar{\Delta}_m - \frac{\bar{\omega}_m}{\bar{\omega}_n}\bar{\Delta}_n}{\sqrt{\bar{\omega}_m^2 + \bar{\Delta}_m^2}} \right], \qquad (E3)$$

where $\bar{Q} \equiv Q/\sqrt{A\nu_E}$, and we have written $T \equiv t\,T_c$. Once we fix t, this is an equation with no material parameters, so that $\bar{\Delta}_n = f(t, i\bar{\omega}_n)$, where f is independent of material parameters. This implies that the analytic continuation

satisfies

$$\Delta(t,\omega) = \sqrt{A\nu_E}\, f\left(t, \frac{\omega}{\sqrt{A\nu_E}}\right). \tag{E4}$$

Defining the temperature gap edge through

$$\Re_e\left[\Delta(t,\Delta_0(t))\right] = \Delta_0(t) \tag{E5}$$

it then follows that $\Delta_0(t) = \sqrt{A\nu_E}\, g(t)$, where $g(t)$ is some universal function of t. Hence, $\frac{2\Delta_0(t)}{k_B T_c} = $ constant, provided that $T \gg \nu_E$, i.e., $t \gg \sqrt{\nu_E}$. How can zero temperature be achieved with this restriction? The point is that we want to achieve zero temperature *behaviour*, which does not necessarily entail solving $T = 0$ equations. This is standard procedure for conventional materials, where, utilizing the imaginary axis equations, we actually solve at $t = 0.1$, and call this our zero temperature solution. This is justified by the fact that the gap edge, for example, does not change (to $\sim 6 - 7$ significant digits) when we use $t = 0.05$, or $t = 0.025$. The reason for this is of course, well understood: the presence of a gap causes exponential behaviour. Simple Boltzmann factors like $e^{-\beta\epsilon}$ become $e^{-\beta E}$ in BCS theory, where $E^2 = \epsilon^2 + \Delta^2$. Hence, even as $\epsilon \to 0$, $e^{-\Delta_0/T}$ remains. For example, in BCS theory, the low temperature behaviour of the gap is given by[177]

$$\Delta(T) \approx \Delta_0 - (2\pi\Delta_0 T)^{1/2} e^{-\Delta_0/T}, \tag{E6}$$

where Δ_0 is the zero temperature gap. Thus, when $T \ll \Delta_0$, the second term in Eq. (E6) switches off very quickly, and zero temperature behaviour is achieved. Within BCS, $\frac{2\Delta_0}{k_B T_c} = 3.53$ so that the term is governed by the factor $e^{-1.75/t}$, to be compared with unity (the first term). At $t = 0.1$, this is already eight orders of magnitude smaller than unity, so zero temperature behaviour has been achieved at even higher temperature.

The analysis in Ref. 91 assumed this would be the case in the strong coupling limit as well, without proof. If it is, then $T = 0$ behaviour will be achieved for the case when $e^{-a/t}$ is small, or $t \approx 0.1a$, where a is some number. Then the conditions $T \gg \nu_E$ and yet $T \approx 0$ (behaviour-wise) can be simultaneously achieved, so that the proof will be applicable to the zero temperature ratio, $\frac{2\Delta_0}{k_B T_c}$. Clearly then, the important issue is the low temperature behaviour of the universal function, $g(t)$, or equivalently, $f(t, i\bar{\omega}_n)$. We have proceeded numerically to investigate this function.

Eq. (E3) was solved numerically in scaled form.[93] In fact for $t = 1$, $\tilde{T}_c$ can be determined in seconds; $T_c = 0.2584\sqrt{A\nu_E}$, in agreement with Allen and Dynes'[26] result. For low t, Eq. (E3) was solved for $\bar{\Delta}_n$, for $n = 1, 2, \ldots N_o$. As t is lowered, the number of Matsubara frequencies increases since the temperature mesh becomes finer, and the $\bar{\Delta}_n$ tend to increase with decreasing temperature, as is expected, since the $\bar{\Delta}_n$ are order parameters. We found that at $t \approx 0.01$, the size of the gaps is no longer changing. The effect of lowering the temperature, then, is to fill in gap values at more Matsubara frequencies. Hence, we are assured that zero temperature behaviour has been achieved, as far as the imaginary axis calculations go, where now the solution is a continuous curve ($i\omega_n \rightarrow i\omega$).

It remains to analytically continue $\Delta(i\omega)$ and $Z(i\omega)$ to the real axis. Here we can distinguish between very low temperatures and zero temperature, which is necessary, since it is known that there is a qualitative difference in the solutions[149] (say, at $\omega = 0$). Inspection of Eqs. (A11) and (A12) reveals that this occurs in two places. The first is in the summations, which are integrals at $T = 0$. The behaviour for $\omega \lesssim \pi T$ will depend strongly on whether $T = 0$ or $T > 0$. However, this frequency region is unimportant. The second

is in the Bose and Fermi factors. In particular, for $T = 0$, $N(\nu) = 0$. However, for $T > 0$, in the asymptotic limit, $\lim_{\nu \to 0} N(\nu) = T/\nu$ and hence we get an infinity. Since we are interested in zero temperature, we put $N(\nu) = 0$, and $f(x) = \theta(-x)$, the unit step function. These conditions represent the freezing out of thermal phonons, and the sharpening of the distribution of electron states, respectively. Eqs. (A11) and (A12) are then scaled according to

$$\bar{\Delta}(\bar{\omega})Z(\bar{\omega}) = \pi \bar{T} \sum_{m=-\infty}^{\infty} \frac{2}{(\bar{\omega} - i\bar{\omega}_m)^2} \frac{\bar{\Delta}_m}{\sqrt{\bar{\omega}_m^2 + \bar{\Delta}_m^2}}$$

$$+ i\pi \sqrt{\frac{A}{\nu_E}} \frac{\bar{\Delta}(\bar{\omega} - \bar{\nu}_E)}{\sqrt{(\bar{\omega} - \bar{\nu}_E)^2 - \bar{\Delta}^2(\bar{\omega} - \bar{\nu}_E)}} \quad (E7)$$

$$Z(\bar{\omega}) = 1 + i\frac{\pi \bar{T}}{\bar{\omega}} \cdot \sum_{m=-\infty}^{\infty} \frac{2}{(\bar{\omega} - i\bar{\omega}_m)^2} \frac{\bar{\omega}_m}{\sqrt{\bar{\omega}_m^2 + \bar{\Delta}_m^2}}$$

$$+ i\pi \sqrt{\frac{A}{\nu_E}} \frac{\bar{\omega} - \bar{\nu}_E}{\sqrt{(\bar{\omega} - \bar{\nu}_E)^2 - \bar{\Delta}^2(\bar{\omega} - \bar{\nu}_E)}} \quad (E8)$$

These equations do not obey exact scaling laws. This is expected since we have found $\lim_{\lambda \to \infty} Z(\bar{\omega}) \propto \sqrt{\lambda}$ as Eqs. (E7) and (E8) indicate. Hence, we have solved Eqs. (E7) and (E8) numerically, using progressively smaller values of $\bar{\nu}_E \equiv \sqrt{\frac{\nu_E}{A}}$. The dependence on $\bar{\nu}_E$ is linear at small $\bar{\nu}_E$, and hence the $\nu_E \to 0$ behaviour can be extrapolated. We find, in this manner, $\frac{2\Delta_0}{k_B T_c}\Big|_{\text{max}} \approx 12.8$. Note, that as an added bonus, we can combine (E7) and (E8) and expand for small ν_E. We find

$$\bar{\Delta}(\bar{\omega}) = \bar{\Delta}_{in}(\bar{\omega}) + \frac{i\pi}{\bar{\omega}} \frac{\bar{\Delta}(\bar{\omega}) - \bar{\omega}\bar{\Delta}'(\bar{\omega})}{\sqrt{\bar{\omega}^2 - \bar{\Delta}^2(\bar{\omega})}} \quad (E9)$$

where $\bar{\Delta}_{in}(\bar{\omega}) \equiv [\bar{\Delta}(\bar{\omega})Z(\bar{\omega})]_{in}/Z_{in}(\bar{\omega})$, and the subscript "$in$" refers to the two terms in Eqs. (E7) and (E8) which involve summations. Now at the gap edge, $\bar{\omega} = \bar{\Delta}(\bar{\omega}) = \bar{\Delta}_0$, so that for Eq. (E9) to remain finite, we require $\Delta'(\omega = \Delta_0) = 1$. This gap derivative has been studied in detail by Coombes

and Carbotte.[178] It is zero in the BCS limit, and increases for conventional strong couplers in a regular way.[178] Here we find that in the very strong coupling limit, it continues to increase to unity. This dependence is verified by numerical calculation.

To obtain an estimate of the gap ratio in the strong coupling limit, we use a square well model for the gap, but with a cutoff $\omega_c = 2\Delta_0$ rather than ω_E ($\omega_c = \Delta_0$ was used in Ref. 91) as suggested by Fig. (3.18):

$$\Delta(\omega) = \begin{cases} \Delta_0 & \text{for} \quad \omega < 2\Delta_0 \\ 0 & \text{for} \quad \omega > 2\Delta_0 \end{cases} \quad . \tag{E10}$$

For small ω, $Z(\omega)$ can be evaluated in the limit as $\nu_E \to 0$:

$$Z(\omega \sim 0) = 1 + 2A \frac{d}{d\nu_E}\left(\nu_E^2 \, J(\nu_E)\right) + \frac{A\nu_E}{2\Delta_0^2} \tag{E11}$$

and the gap equation reduces to:

$$Z(\omega \sim 0)\Delta_0 = 2A\nu_E \, \Delta_0 J(\nu_E) \tag{E12}$$

where

$$J(\nu_E) = \int_0^{2\Delta_0} \frac{d\omega'}{\omega'^2 + \nu_E^2} \frac{1}{\sqrt{\omega'^2 + \Delta_0^2}}$$

$$\approx \frac{1}{\nu_E \Delta}\left\{\frac{\pi}{2} - \frac{\sqrt{5}}{2}\frac{\nu_E}{\Delta}\right\} . \tag{E13}$$

Combining Eqs. (E11) and (E12) results in $\Delta_0 \sim 1.3\sqrt{A\nu_E}$ so that $\frac{2\Delta_0}{k_B T_c} \approx 10.2$. This is in fair agreement with our numerical limit considering the crudeness of our model. Note in particular that we have $\Delta'(\omega = \Delta_0) = 0$ and not unity as is the case in the exact calculation.

Bibliography

1. J.G. Bednorz and K.A. Müller, *Z. Phys. B* **64**, 189 (1986).

2. C.W. Chu, P.H. Hor, R.L. Meng, L. Gao, Z.J. Huang, and Y.Q. Wang, *Phys. Rev. Lett.* **58**, 405 (1987).

3. R.J. Cava, R.B. Van Dover, B. Batlogg, and E.A. Rietman, *Phys. Rev. Lett.* **58**, 408 (1987).

4. S. Uchida, H. Takagi, K. Kitazawa, and S. Tanaka, *Jpn. J. Appl. Phys.* **26**, L1 (1987).

5. M.K. Wu, J.R. Ashburn, C.J. Torng, P.H. Hor, R.L. Meng, L. Gao, Z.J. Huang, Y.Q. Wang, and C.W. Chu, *Phys. Rev. Lett.* **58**, 908 (1987).

6. S.R. Ovishinsky, R.T. Young, D.D. Allred, G. DeMaggio, and G.A. Van der Leeden, *Phys. Rev. Lett.* **58**, 2579 (1987).

7. J.T. Chen, L.E. Wenger, C.J. McEwan, and E.M Logothetis, *Phys. Rev. Lett.* **58**, 1972 (1987).

8. C.Y. Huang, L.J. Dries, P.H. Hor, R.L. Meng, C.W. Chu, and R.B. Frankel, *Nature* **328**, 403 (1987).

9. University of Maryland, High T_c News, Sept. 1, 1987.

10. Various rumours.

11. See, for example, Novel Superconductivity, edited by S.A. Wolf and V.Z. Kresin [Plenum, New York, 1987].

12. J. Bardeen, L.N. Cooper, J.R. Schreiffer, *Phys. Rev.* **108**, 1175 (1957).

13. See, for example, N.W. Ashcroft and N.D. Mermin, <u>Solid State Physics</u>, Holt, Rinehart and Winston, Philadelphia, 1976.

14. J.R. Schreiffer, <u>Theory of Superconductivity</u>, Benjamin, New York, 1964.

15. G.M. Eliashberg, *Zh. Eksp. Teor. Fiz.* **38**, 966 (1960); *Sov. Phys.-JETP* **11**, 696 (1960).

16. A.B. Migdal, *Zh. Eksp. Teor. Fiz.* **34**, 1438 (1958); *Sov. Phys.-JETP* **34**, 996 (1958).

17. A.A. Abrikosov, L.P. Gor'kov and I.E. Dzyaloshinskii, <u>Methods of Quantum Field Theory in Statistical Physics</u>, Prentice Hall, Englewood Cliffs, 1963.

18. G. Rickayzen, <u>Green's Functions and Condensed Matter</u>, Academic Press, Toronto, 1980.

19. P.B. Allen and B. Mitrović, in <u>Solid State Physics</u>, edited by H. Ehrenreich, F. Seitz, and D. Turnbull (Academic, New York, 1982), Vol. 37, p.1.

20. D. J. Scalapino, in <u>Superconductivity</u>, edited by R.D. Parks (Marcel Dekker, Inc., New York, 1969), Vol. 1, p.449.

21. G. Grimvall, <u>The Electron-Phonon Interaction in Metals</u>, North-Holland, New York, 1981.

22. O.V. Dolgov and E.G. Maksimov, *Usp. Fiz. Nauk* **138**, 95 (1982); *Sov. Phys. Usp.* **25**, 688 (1982).

23. J. M. Daams and J.P. Carbotte, *J. Low Temp. Phys.* **43**, 263 (1981).

24. B. Mitrović, H.G. Zarate, and J.P. Carbotte, *Phys. Rev. B* **29**, 184 (1984).

25. H. Wu, Z. Weng, G. Ji and Z. Zhou, *J. Phys. Chem. Solids* **48**, 395 (1987).

26. P.B. Allen and R.C. Dynes, *Phys. Rev. B* **12**, 905 (1975).

27. C.R. Leavens, *Solid State Comm.* **17**, 1499 (1975).

28. C.R. Leavens, *J. Phys.* F **7**, 1911 (1977).

29. C.R. Leavens and J.P. Carbotte, *J. Low Temp. Phys.* **14**, 195 (1974).

30. J.C. Swihart, *Phys. Rev.* **116**, 346 (1959); *IBM J. Research Develop.* **6**, 14 (1962); *Phys. Rev.* **131**, 73 (1963). See also D.J. Thouless, *Phys. Rev.* **117**, 1256 (1960).

31. D. Rainer and G. Bergmann, *J. Low Temp. Phys.* **14**, 501 (1974).

32. P. Morel and P.W. Anderson, *Phys. Rev.* **125**, 1263 (1962).

33. P.J. Williams, Master's Thesis, McMaster University, 1987 (unpublished).

34. See R. Meservey and B.B. Schwartz, in <u>Superconductivity</u>, edited by R.D. Parks (Marcel Dekker, Inc., New York, 1969), Vol. 1, p.117.

35. J.R. Schreiffer, D.J. Scalapino, and J.W. Wilkins, *Phys. Rev. Lett.* **10**, 336 (1963).

36. B.T. Geilikman and V.Z. Kresin, *Fiz. Tverd. Tela (Leningrad)* **1**, 3294 (1965). [*Sov. Phys.-Solid State* **7**, 2659 (1966).]

37. H.J. Vidberg and J.W. Serene, *J. Low Temp. Phys.* **29**, 179 (1977).

38. B.T. Geilikman, V.Z. Kresin and N.F. Masharov, *J. Low Temp. Phys.* **18**, 241 (1975).

39. F. Marsiglio and J.P. Carbotte, *Phys. Rev.* B **33**, 6141 (1986).

40. N.F. Masharov, *Fiz. Tverd. Tela* **16**, 2342 (1974). [*Sov. Phys.-Solid State* **16**, 1524 (1975).]

41. V.Z. Kresin and V.P. Parkhomenko, *Fiz. Tverd. Tela (Leningrad)* **16**, 3363 (1974). [*Sov. Phys.-Solid State* **16**, 2180 (1975).].

42. J. Bardeen and M. Stephen, *Phys. Rev.* **136**, A1485 (1964).

43. J.M. Coombes and J.P. Carbotte, *J. Low Temp. Phys.* **63**, 431 (1986).

44. J.M. Coombes and J.P. Carbotte, submitted to *Phys. Rev. B*.

45. G. Grimvall, *J. Phys. Chem. Solids* **29**, 1221 (1968).; *Phys. Kondens. Mater.* **9**, 283 (1969)..

46. F. Marsiglio and J.P. Carbotte, *Solid State Comm.* **63**, 419 (1987).

47. S.B. Nam, *Phys. Rev. B* **156**, 470 (1967); *Phys. Rev. B* **156**, 487 (1967).

48. J.W. Blezius and J.P. Carbotte, *Phys. Rev. B* **33**, 3509 (1986). See also J.W. Blezius, Ph.D thesis, McMaster University, 1987 (unpublished).

49. G.E. Reuter and E.H. Sondheimer, *Proc. Roy. Soc. (London)* **A195**, 336 (1948).

50. T.R Lemberger, D.M. Ginsberg and G. Rickayzen, *Phys. Rev. B* **18**, 6057 (1978).

51. P.W. Anderson, *J. Phys. Chem. Solids* **11**, 26 (1959).

52. V.L. Ginzburg and L.D. Landau, *Zh. Eksp. Teor. Fiz.* **20**, 1064 (1950).

53. A.A. Abrikosov, *Zh. Eksp. Teor. Fiz.* **32**, 1442 (1957); *Sov. Phys.-JETP* **5**, 1174 (1957).]

54. L.P. Gor'kov, *Zh. Eksp. Teor. Fiz.* **36**, 1918 (1959); *Sov. Phys.-JETP* **9**, 1364 (1959).

55. E. Helfand and N.R. Werthamer, *Phys. Rev. Lett.* **13**, 686 (1964).

56. E. Helfand and N.R. Werthamer, *Phys. Rev.* **147**, 288 (1966).

57. N.R. Werthamer, E. Helfand and P.C. Hohenberg, *Phys. Rev.* **147**, 295 (1966).

58. N.R. Werthamer and W.L. McMillan, *Phys. Rev.* **158**, 415 (1967).

59. M. Schossmann and E. Schachinger, *Phys. Rev. •B* **33**, 6123 (1986). See also M. Schossmann, Ph.D thesis, Technical University of Graz, 1984.

60. K. Maki, in Superconductivity, edited by R.D. Parks (Marcel Dekker, Inc., New York, 1969), Vol. 2, p.1035.

61. F. Marsiglio, M. Schossmann, E. Schachinger, and J.P. Carbotte, *Phys. Rev. B* **35**, 3226 (1987).

62. W.L. McMillan and J.M. Rowell, in Superconductivity, edited by R.D. Parks (Marcel Dekker, Inc., New York, 1969), Vol. 1, p.561.

63. E.L. Wolf and G.B. Arnold, *Phys. Reports* **91**, 32 (1982).

64. J.P. Carbotte and R.C. Dynes, *Phys. Rev.* **172**, 476 (1968).

65. H.K. Leung, J.P. Carbotte, D.W. Taylor and C.R. Leavens, *J. Low Temp. Phys.* **24**, 2534 (1976).

66. P.G. Tomlinson and J.P. Carbotte, *Can. J. Phys.* **55**, 751 (1977).

67. W.H. Butler, H.G. Smith and N. Wakabayashi, *Phys. Rev. Lett.* **39**, 1004 (1977).

68. C.M. Varma and W. Weber, *Phys. Rev. B* **19**, 6142 (1979).

69. W. Weber, *Phys. Rev. Lett.* **58**, 1371 (1987). See also W. Weber, *Phys. Rev. Lett.* **58**, 2154(E) (1987).

70. A.M. Toxen, *Phys. Rev. Lett.* **15**, 462 (1965).

71. H.Padamsee, J.E. Neighbour, and C.A. Shiffman, *J. Low Temp. Phys.* **12**, 387 (1973).

72. G.R. Stewart, *Solid State Comm.* **30**, 415 (1979).

73. F. Marsiglio, J.M. Coombes and J.P. Carbotte, *Phys. Rev. B* **35**, 3219 (1987).

74. G. Bergmann and D. Rainer, *Z. Physik* **263**, 59 (1973).

75. J.M. Daams and J.P. Carbotte, *Can. J. Phys.* **56**, 1248 (1978).

76. B. Mitrović, C.R. Leavens and J.P. Carbotte, *Phys. Rev. B* **21**, 5048 (1980).

77. E. Schachinger, J.M. Daams and J.P. Carbotte, *Phys. Rev. B* **22**, 3194 (1980).

78. J.M. Daams and J.P. Carbotte, *Solid State Comm.* **33**, 585 (1980).

79. J.M. Daams, E. Schachinger and J.P. Carbotte, *J. Low Temp. Phys.* **42**, 69 (1981).

80. B. Mitrović and J.P. Carbotte, *Solid State Comm.* **37**, 1009 (1981).

81. M. Ashraf and J.P. Carbotte, *Solid State Comm.* **46**, 63 (1983).

82. M. Whitmore, *J. Low Temp. Phys.* **56**, 129 (1984).

83. F. Marsiglio and J.P. Carbotte, *Phys. Rev. B* **31**, 4192 (1985).

84. F. Marsiglio, J.P. Carbotte and E. Schachinger, *J. Low Temp. Phys.* **65**, 305 (1986).

85. J.M. Coombes and J.P. Carbotte, *Phys. Rev. B* **35**, 6643 (1987).

86. S. Sachdev, A.J. Millis and C.M. Varma (preprint).

87. V. Z. Kresin and G.O. Zaitsev, *Zh. Eksp. Teor. Fiz.* **74**, 1886 (1978).; *Sov. Phys.-JETP* **47**, 983 (1978)..

88. J.W. Blezius and J.P. Carbotte, *Phys. Rev. B* **36**, 3622 (1987).

89. M. Schossmann, E. Schachinger and J.P. Carbotte (submitted to *Phys. Rev. B*).

90. R. Akis, E. Schachinger, F. Marsiglio and J.P. Carbotte (submitted to *Phys. Rev. B*).

91. J.P. Carbotte, F. Marsiglio and B. Mitrović, *Phys. Rev. B* **33**, 6135 (1986).

92. L.N. Bulaevskii, O.V. Dolgov and M.O. Ptitsyn (preprint).

93. P.J. Williams has suggested a trick that has allowed us to do this. See Appendix E for details.

94. M.L. Cohen, *Phys. Rev.* **134**, A511 (1964).

95. D.C. Johnston, H. Prakash, W.H. Zachariasen and R. Viswanathan, *Mat. Res. Bull.* **8**, 777 (1973).

96. A.W. Sleight, J.L. Gillson and P.E. Bierstedt, *Solid State Comm.* **17**, 27 (1975).

97. P.W. Anderson, *Mater. Res. Bull.* **8**, 153 (1973).

98. P.W. Anderson, *Science* **235**, 1196 (1987).

99. P.W. Anderson, G. Baskaran, Z. Zou, and T. Hsu, *Phys. Rev. Lett.* **58**, 2790 (1987).

100. D. Allender, J. Bray and J. Bardeen, *Phys. Rev. B* **7**, 1020 (1973).

101. C.M. Varma, in Superconductivity in d- and f- Band Metals, edited by W. Buckel and W. Weber (Kernforschungszentrum Karlsruhe, Karlsruhe, West Germany, 1982) p.603.

102. M. Cohen and P.W. Anderson, in <u>Superconductivity in d- and f-Band Metals</u>, edited by D.H. Douglass (AIP, New York, 1972) p.17.

103. L.F. Mattheiss, *Phys. Rev. Lett.* **58**, 1028 (1987).

104. M. Schossmann, F. Marsiglio and J.P. Carbotte, *Phys. Rev. B* **36**, 3627 (1987).

105. R.L. Filler, P. Lindenfeld, T. Worthington and G. Deutscher, *Phys. Rev. B* **21**, 5031 (1980).

106. G. Deutscher, O. Entin-Wohlman, S. Fishman and Y. Shapira, *Phys. Rev. B* **21**, 5041 (1980).

107. C. Ebner and D. Stroud, *Phys. Rev. B* **31**, 165 (1985).

108. H. Teichler in <u>Anisotropy Effects in Superconductors</u>, edited by H.W. Weber (Plenum, New York, 1977) p.7.

109. M. Gurvitch and A.T. Fiory, *Phys. Rev. Lett.* **59**, 1337 (1987).

110. B.S. Chandrasekhar, in <u>Superconductivity</u>, edited by R.D. Parks (Marcel Dekker, Inc., New York, 1969), Vol. 1, p.1.

111. B. Batlogg, G. Kourouklis, W. Weber, R.J. Cava, A. Jayaraman, A.E. White, K.T. Short, L.W. Rupp, and E.A. Rietman, *Phys. Rev. Lett.* **59**, 912 (1987).

112. T.A. Faltens, W.K. Ham, S.W. Keller, K.J. Leary, J.N. Michaels, A.M. Stacy, H. zur Loye, D.E. Morris, T.W. Barbee,III, L.C. Bourne, M.L. Cohen, S. Hoen, and A. Zettl, *Phys. Rev. Lett.* **59**, 915 (1987).

113. D. Rainer and F.J. Culetto, *Phys. Rev. B* **19**, 2540 (1979).

114. E. Ashauer, W. Lee, D. Rainer, and J. Rammer (preprint).

115. C. Kittel, Introduction to Solid State Physics, John Wiley and Sons, Inc., Toronto, 1986.

116. W. Weber, private communication.

117. F. Marsiglio, R. Akis and J.P. Carbotte, *Phys. Rev. B* **36**, 5245 (1987).

118. F. Marsiglio and J.P. Carbotte, *Phys. Rev. B* **36**, 3633 (1987).

119. F. Marsiglio and J.P. Carbotte, to be published in *Solid State Comm.*.

120. J.W. Blezius, R. Akis, F. Marsiglio and J.P. Carbotte, submitted to *Phys. Rev. B*.

121. E. Schachinger, H.G. Zarate, M. Schossmann and J.P. Carbotte, *J. Low Temp. Phys.* **63**, 1 (1986).

122. G. Deutscher, in Novel Superconductivity, edited by S.A. Wolf and V.Z. Kresin [Plenum, New York, 1987], p. 293.

123. W.A. Little, *Phys. Rev.* **134**. A1416 (1964).

124. V.L. Ginzburg, *Zh. Eksp. Teor. Fiz.* **47**. 2318 (1964). *Sov. Phys.-JETP* **20**, 1549 (1965).

125. W.A. Little, in Novel Superconductivity, edited by S.A. Wolf and V.Z. Kresin [Plenum, New York, 1987], p. 341.

126. M. Grabowski and L.J. Sham, *Phys. Rev. B* **29**. 6132 (1984).

127. C.M. Varma, S. Schmitt-Rink and E. Abrahams. *Solid State Comm.* **3**, 3 (1987).

128. J. Yu. S. Massidda. A.J. Freeman and D.D. Koeling. *Phys. Lett.* **A122**. 203 (1987).

129. C.F. Gallo, L.R. Whitney and P.J. Walsh, in <u>Novel Superconductivity</u>, edited by S.A. Wolf and V.Z. Kresin [Plenum, New York, 1987], p. 385.

130. W.A. Harrison (preprint).

131. B.A. Richert and R.E. Allen (preprint).

132. J. Orenstein *et al.*, *Phys. Rev. B* **36**, 729 (1987).

133. S.L. Herr *et al.*, *Phys. Rev. B* **36**, 733 (1987).

134. K. Kamarás *et al.*, *Phys. Rev. Lett.* **59**, 919 (1987).

135. S. Etemad, D.E. Aspnes, M.K. Kelly, R. Thompson, J.M. Tarascon and G.W. Hull, *Phys. Rev. B* **37**, 3396 (1987).

135a. I. Bozovic *et al.*, *Phys. Rev. Lett.* **59**, 2219 (1987).

135b. S. Etemad, T. Timusk *et al.* (preprint). It was definitively established at the Materials and Mechanisms conference (March, 1988) that a mid-infrared absorption does indeed exist in the oxides.

136. B. Batlogg, R.J. Cava, A. Jayaraman, R.B. van Dover, G.A. Kourouklis, S. Sunshine, D.W. Murphy, L.W. Rupp, H.S. Chen, A. White, K.T. Short, A.M. Mujsce, and E.A. Reitman, *Phys. Rev. Lett.* **58**, 2333 (1987).

137. L.C. Bourne, M.F. Crommie, A. Zettl, H. zur Loye, S.W. Keller, K.L. Leary, A.M. Stacy, K.J. Chang, M.L. Cohen and D.E. Morris, *Phys. Rev. Lett.* **58**, 2337 (1987).

138. K.J. Leary, H. zur Loye, S.W. Keller, T.A. Faltens, W.K. Ham, J.N. Michaels and A.M. Stacy, *Phys. Rev. Lett.* **59**, 1236 (1987).

139. B. Batlogg, private communication.

140. F. Marsiglio and J.P. Carbotte, *Phys. Rev. B* **36**, 3937 (1987).

141. F. Marsiglio, R. Akis and J.P. Carbotte, *Solid State Comm.* **64**, 905 (1987).

142. W.L. McMillan, *Phys. Rev.* **167**, 331 (1968).

143. C.R. Leavens, *Solid State Comm.* **15**, 1329 (1974).

144. F.W. Kus and J.P. Carbotte, *Solid State Comm.* **29**, 715 (1979).

145. B. Batlogg, J.P. Remeika, R.C. Dynes, H. Barz, A.S. Cooper, and J.P. Garno, in Superconductivity in d- and f- Band Metals, edited by W. Buckel and W. Weber (Kernforschungszentrum Karlsruhe, Karlsruhe, West-Germany, 1982) p.401.

146. P.N. Arberg, F.S. Razavi, F.P. Koffyberg and B. Mitrović, submitted to *Solid State Comm.*

147. V.Z. Kresin, *Solid State Comm.* **63**, 725 (1987).

148. L.N. Bulaevskii and O.V. Dolgov, *Pisma Zh. Eksp. Teor. Fiz.* **45**, 413 (1987); *JETP Lett.* **45**, 526 (1987).

149. A.E. Karakosov, E.G. Maksimov and S.A. Mashkov, *Zh. Eksp. Teor. Fiz.* **68**, 1937 (1975); *Sov. Phys.-JETP* **41**, 971 (1976).

150. S. Kivelson, private communication.

151. D.C. Mattis and J. Bardeen, *Phys. Rev.* **111**, 412 (1958).

152. Y. Nambu, *Phys. Rev.* **117**, 648 (1960).

153. V. Ambegaokar and L. Tewordt, *Phys. Rev.* **134**, A805 (1964).

154. D.J. Scalapino, J.R. Schreiffer and J.W. Wilkins, *Phys. Rev.* **148**, 263 (1966).

155. D.J. Scalapino, Y. Wada and J.C. Swihart, *Phys. Rev. Lett.* **14**, 102 (1965).

156. C.R. Leavens and E.W. Fenton, *Solid State Comm.* **33**, 597 (1980).

157. C.S. Owen and D.J. Scalapino, *Physica* , 55, 691 (1971).

158. H.J. Vidberg and J. Serene, *J. Low Temp. Phys.* **29**, 179 (1977).

159. G. Baym and D. Mermin, *J. Math. Phys.* **2**, 232 (1961).

160. R. Blaschke and R. Blocksdarf, *Z. Physik* **B49**, 99 (1982).

161. C.R. Leavens and D.S. Ritchie, *Solid State Comm.* **53**, 137 (1985).

162. F. Marsiglio, M. Schossmann and J.P. Carbotte, submitted to *Phys. Rev. B.*

163. S.B. Kaplan, C.C. Chi, D.N. Landenberg, J.J. Chang, S. Jafarey, and D.J. Scalapino, *Phys. Rev. B* **14**, 4854 (1976).

164. G.B. Arnold, J. Zasadzinski, J.W. Osmun and E.L. Wolf, *J. Low Temp. Phys.* **40**, 225 (1980).

165. J. Zasadzinski, D.M. Burnell, E.L. Wolf and G.B. Arnold, *Phys. Rev. B* **25**, 1662 (1982).

166. T.T. Chen, J.T. Chen, J.D. Leslie, and H.J.T. Smith, *Phys. Rev. Lett.* **22**, 526 (1969).

167. L.F. Lou and W.J. Tomasch, in <u>Low Temperature Physics-LT 13</u>, edited by K.D. Timmerhaus, W.J. O'Sullivan, and E.F. Hammel (Plenum Press, New York, 1972), p. 599.

168. D.B. Kimhi and T.H. Geballe, *Phys. Rev. Lett.* **45**, 1039 (1980).

169. L.Y. Shen, *Phys. Rev. Lett.* **29**, 1082 (1972).

170. K.E. Kihlstrom, *Phys. Rev. B* **32**, 2891 (1985).

171. B.P. Schweiss, B. Renker, E. Schneider and W. Reichardt, in <u>Superconductivity in d- and f-Band Metals</u>, edited by D.H. Douglass (AIP, New York, 1972).

172. J. Kwo and T.H. Geballe, *Phys. Rev. B* **23**, 3230 (1981).

173. J. Geerk, J.M. Rowell, P.H. Schmidt, F. Wuchner and W. Schaver, in <u>Super-conductivity in d- and f- Band Metals</u>, edited by W. Buckel and W. Weber (Kernforschungszentrum Karlsruhe, Karlsruhe, West Germany, 1982).

174. P. Muller, N. Nucker, W. Reichardt and A. Muller in <u>Superconductivity in d-and f- Band Metals</u>, edited by W. Buckel and W. Weber (Kernforschungszentrum Karlsruhe, Karlsruhe, West Germany, 1982).

175. J. Zasadzinski, W.K. Schubert, E.L. Wolf and G.B. Arnold in <u>Superconductivity in d- and f- Band Metals</u>, edited by H. Suhl and M.B. Maple (Academic Press, New York, 1980).

176. Y. Wada, *Phys. Rev.* **135**, A1481 (1964).

177. A.L. Fetter and J.D. Walecka, <u>Quantum Theory of Many-Particle Systems</u>, McGraw-Hill, Toronto, 1971.

178. J.M. Coombes, Ph.D thesis, McMaster University, 1987 (unpublished).

179. The following references have measured values of the specific heat jump for LSCO.

   a B. Batlogg *et al.* , *Phys. Rev. B* **35**, 5340 (1987).

   b B.D. Dunlap *et al.* , *Phys. Rev. B* **35**, 7210 (1987).

   c M. Decroux *et al.* , *Europhys. Lett.* **3**, 1035 (1987).

   d D. Finnemore *et al.* , *Phys. Rev. B* **35**, 5319 (1987).

   e K. Kitazawa *et al.* , *Jpn. J. Appl. Phys.* **26**, L751 (1987).

   f S. Uchida *et al.* , in <u>Novel Superconductivity</u>, edited by S.A. Wolf and V.Z. Kresin [Plenum, New York, 1987], p. 855.

g N.E. Phillips *et al.* , in <u>Novel Superconductivity</u>, edited by S.A. Wolf and V.Z. Kresin [Plenum, New York, 1987], p. 739.

h A.P. Ramirez *et al.* , *Phys. Rev. B* **35**, 8833 (1987).

i L.C. Bourne *et al.* , *Phys. Rev. B* **35**, 8785 (1987).

180. The following references contain measured values of the gap ratio for LSCO.

a U. Walter *et al.*, *Phys. Rev. B* **35**, 5327 (1987).

b P.E. Sulewski *et al.* , *Phys. Rev. B* **35**, 5330 (1987).

c Z. Schlesinger *et al.* , *Phys. Rev. B* **35**, 5334 (1987).

d D.A. Bonn *et al.* , *Phys. Rev. B* **35**, 8843 (1987).

e M.E. Hawley *et al.* , *Phys. Rev. B* **35**, 7224 (1987).

f J.R. Kirtley *et al.* , *Phys. Rev. B* **35**, 7216 (1987).

g S. Pan *et al.* , *Phys. Rev. B* **35**, 7220 (1987).

h T. Ekino *et al.* , *Solid State Comm.* **62**, 535 (1987).

i J. Moreland *et al.* , *Cryogenics* **27**, 227 (1987).

j P. Leiderer *et al.* , *Z. Phys. B* **67**, 25 (1987).

k P.J.M. van Bentum *et al.* , *Phys. Rev. B* **36**, 841 (1987).

l L. Degiorgi *et al.* , *Solid State Comm.* **64**, 873 (1987).

m M. Naito *et al.* , *Phys. Rev. B* **35**, 7228 (1987).

n P.E. Sulewski *et al.* , *Phys. Rev. B* **36**, 5735 (1987).

o M. Lee *et al.* , *Phys. Rev. B* **36**, 2378 (1987).

p N.V. Zavaritsky *et al.* , in <u>Novel Superconductivity</u>, edited by S.A. Wolf and V.Z. Kresin [Plenum, New York, 1987], p. 871.

q M. Sato *et al.* , in <u>Novel Superconductivity</u>, edited by S.A. Wolf and V.Z. Kresin [Plenum, New York, 1987], p. 927.

r S. Pan *et al.* , in <u>Novel Superconductivity</u>, edited by S.A. Wolf and V.Z. Kresin [Plenum, New York, 1987], p. 1029.

s Z. Schlesinger *et al.* , *Phys. Rev. B* **36**, 5275 (1987).

181. The following references contain measured values of the slope of the upper critical field near T_c for LSCO.

a T.P. Orlando *et al.* , *Phys. Rev. B* **35**, 5347 (1987).

b W.K.Kwok *et al.* , *Phys. Rev. B* **35**, 5343 (1987).

c K. Okuda *et al.* , *Jpn. J. Appl. Phys.* **26**, L822 (1987).

d N. Kobayashi *et al.* , *Jpn. J. Appl. Phys.* **26**, L757 (1987).

e Y. Hidaka *et al.* , *Jpn. J. Appl. Phys.* **26**, L377 (1987).

f K. Nakao *et al.* , *Jpn. J. Appl. Phys.* **26**, L413 (1987).

g D.W. Capone II *et al.* , *Applied Phys. Lett.* **9**, 543 (1987).

h Osofsky *et al.* , in <u>Novel Superconductivity</u>, edited by S.A. Wolf and V.Z. Kresin [Plenum, New York, 1987], p.807.

i N.V. Zavaritsky *et al.* , in <u>Novel Superconductivity</u>, edited by S.A. Wolf and V.Z. Kresin [Plenum, New York, 1987], p.871.

j A.I. Braginski *et al.* , in <u>Novel Superconductivity</u>, edited by S.A. Wolf and V.Z. Kresin [Plenum, New York, 1987], p. 935.

k P.J.M. van Bentum *et al.* , *Phys. Rev. B* **36**, 5279 (1987).

l B. Renker *et al.* , *Z. Phys. B* **67**, 1 (1987).

182. The following references contain estimates of the penetration depth for LSCO through muon spin relaxation measurements.

   a G. Aeppli et al. , *Phys. Rev. B* **35**, 7129 (1987).

   b W.J. Kossler et al. , *Phys. Rev. B* **35**, 7133 (1987).

   c F.N. Gygax et al. , *Europhys. Lett.* **4**, 473 (1987).

183. The following references contain band structure calculations for LSCO and also contain estimates for the electron density of states at the Fermi level.

   a L.F. Mattheiss, *Phys. Rev. Lett.* **58**, 1028 (1987).

   b A.J. Freeman et al. , *Phys. Rev. B* **36**, 7111 (1987).

   c W.M. Temmerman et al. , *J. Phys. F* **17**, L135 (1987).

   d K. Takegahara et al. , *Jpn. J. Appl. Phys.* **26**, L352 (1987).

   e D.A. Papaconstantopoulis et al. , Proceedings of the 18th International Conference on Low Temperature Physics, *Jpn. J. Appl. Phys.* **26**(Suppl.), 1091 (1987).

   f T. Fujiwara et al. , *Jpn. J. Appl. Phys.* **26**, L716 (1987).

   g T. Oguchi et al. , *Jpn. J. Appl. Phys.* **26**, L417 (1987).

184. The following references contain measurements of the specific heat jump for YBCO.

   a M.V. Nevitt et al. , *Phys. Rev. B* **36**, 2398 (1987).

   b S.E. Inderhees et al. , *Phys. Rev. B* **36**, 2401 (1987).

   c N.E. Phillips et al. , (preprint).

   d C. Zhaojia et al. , *Solid State Comm.* **64**, 685 (1987).

e J.C. van Miltenburg *et al.* , *Physica* **3**, 3 (1987).

f K. Kitazawa *et al.* , *Jpn. J. Appl. Phys.* **26**, L748 (1987).

g F. Li *et al.* , *Solid State Comm.* **64**, 209 (1987).

h C. Ayache *et al.* , *Solid State Comm.* **64**, 247 (1987).

i A. Junod *et al.* , *Europhys. Lett.* **4**, 247 (1987).

j D.K. Finnemore *et al.* , (preprint).

k O. Beckman *et al.* , *Phys. Lett.* **125**, A425 (1987).

185. ' The following references contain measurements of the gap ratio for YBCO.

a A. Wittlin *et al.* (preprint).

b L. Genzel *et al.* , *Solid State Comm.* **63**, 843 (1987).

c X. Wang *et al.* (preprint).

d G.A. Thomas *et al.* , LT18 proceedings, p.1001.

e J.R. Kirtley *et al.* , *Phys. Rev. B* **35**, 8846 (1987).

f G.A. Thomas *et al.* , *Phys. Rev. B* **36**, 846 (1987).

g J.M. Wrobel *et al.* , *Phys. Rev. B* **36**, 2368 (1987).

h M. Lee *et al.* , *Phys. Rev. B* **36**, 2378 (1987).

i T.H.H. Vuong *et al.* , *Solid State Comm.* **63**, 525 (1987).

j D.A. Bonn *et al.* , *Phys. Rev. Lett.* **58**, 2249 (1987).

k K.W. Ng *et al.* , LT18 proceedings, p.993.

l J.R. Kirtley *et al.* , LT18 proceedings, p.997.

m J. Moreland *et al.* , *Phys. Rev. B* **35**, 8856 (1987).

n T. Ekino and J. Akimitsu, *Jpn. J. Appl. Phys.* **26**, L452 (1987).

o I. Iguchi *et al.* , *Jpn. J. Appl. Phys.* **26**, L645 (1987).

p M.D. Kirk *et al.* , *Phys. Rev. B* **35**, 8850 (1987).

q M.F. Crommie *et al.* , *Phys. Rev. B* **35**, 8853 (1987).

r P.J.M. vanBentum *et al.* , *Phys. Rev. B* **36**, 843 (1987).

s R. Escdero *et al.* , *Phys. Rev. B* **36**, 3910 (1987).

t G.A. Thomas *et al.* , *Phys. Rev. B* **36**, 846 (1987).

u E. Polturak *et al.* , *Phys. Rev. B* **36**, 5586 (1987).

v K.B. Lyons *et al.* , *Phys. Rev. B* **36**, 5592 (1987).

w A. Barone *et al.* , *Phys. Rev. B* **36**, 7121 (1987).

x Z. Schlesinger *et al.* , *Phys. Rev. Lett.* **59**, 1958 (1987).

y N.V. Zavaritsky *et al.* , in Novel Superconductivity, edited by S.A. Wolf and
   V.Z. Kresin [Plenum, New York, 1987], p.871.

z N.A. Tulina *et al.* , in Novel Superconductivity, edited by S.A. Wolf and V.Z.
   Kresin [Plenum, New York, 1987], p.889.

aa A.V. Bazhenov *et al.* , in Novel Superconductivity, edited by S.A. Wolf and
    V.Z. Kresin [Plenum, New York, 1987], p.893.

186. The following references contain measurements of the slope of the upper
      critical magnetic field near T_c for YBCO.

a M.K. Wu *et al.* , *Phys. Rev. Lett.* **58**, 908 (1987).

b A.P. Ramirez *et al.* , in Novel Superconductivity, edited by S.A. Wolf and
   V.Z. Kresin [Plenum, New York, 1987], p. 689.

c Y. Muto *et al.* in <u>Novel Superconductivity</u>, edited by S.A. Wolf and V.Z. Kresin [Plenum, New York, 1987], p.787

d T.K. Worthington *et al.* , *Phys. Rev. Lett.* **59**, 1160 (1987).

e A. Junod *et al.* , LT18 proceedings, p. 1021.

f S.N. Song *et al.* , LT18 proceedings, p. 1039.

g K. Takita *et al.* , LT18 proceedings, p.1043.

h K. Okuda *et al.* , LT18 proceedings, p.1172.

i Y. Hidaka *et al.* , LT18 proceedings, p.1133.

j I. Apfelstedt *et al.* , LT18 proceedings, p.1181.

k K. Nakao *et al.* , LT18 proceedings, p.1187.

l W.W. Fuller *et al.* , LT18 proceedings, p.1189.

m W. Schinder *et al.* , LT18 proceedings, p.1199.

n Y. Iye *et al.* , *Jpn. J. Appl. Phys.* **26**, L1057 (1987).

o T. Takabatake *et al.* , *Jpn. J. Appl. Phys.* **26**, L978 (1987).

p J.C. Ousset *et al.* , *Europhys. Lett.* **4**, 743 (1987).

q A.I. Braginski, in <u>Novel Superconductivity</u>, edited by S.A. Wolf and V.Z. Kresin [Plenum, New York, 1987], p. 935.

r T.P. Orlando *et al.* , *Phys. Rev. B* **35**, 7249 (1987).

s A.J. Panson *et al.* , *Phys. Rev. B* **35**, 8774 (1987).

t T.P. Orlando *et al.* , *Phys. Rev. B* **36**, 2394 (1987).

u O. Laborde *et al.* , *Solid State Comm.* **63**, 877 (1987).

187. The following references contain band structure calculations for YBCO and also contain estimates for the electron density of states at the Fermi level.

a L.F. Mattheiss and R. Hamann, *Solid State Comm.* **63**, 395 (1987).

b Massidda *et al.* , *Phys. Lett.* **A122**, 198 (1987).

c F. Herman *et al.* , *Phys. Rev. B* **36**, 6912 (1987).